Universidad Autónoma de Madrid

Programa de Doctorado en Biociencias Moleculares

Generation and Characterization of a New Conditional Mouse Model of Hutchinson-Gilford Progeria Syndrome to Assess Disease Progression upon Progerin Suppression and Lamin A Restoration

Doctoral Thesis

AMANDA SÁNCHEZ LÓPEZ

Madrid, 2019

Universidad Autónoma de Madrid

Departamento de Bioquímica

Facultad de Medicina

Amanda Sánchez López, M.Sc. in Molecular Biomedicine

Doctoral Thesis: *Generation and Characterization of a New Conditional Mouse Model of Hutchinson-Gilford Progeria Syndrome to Assess Disease Progression upon Progerin Suppression and Lamin A Restoration.*

Thesis directors:

Vicente Andrés García, PhD.

Lara del Campo Milán, PhD**.**

Centro Nacional de Investigaciones Cardiovasculares (CNIC)

D. Vicente Andrés García, Doctor en Biología por la Universidad de Barcelona, y **D.ª Lara del Campo Milán**, Doctora en Biología por la Universidad Autónoma de Madrid

CERTIFICAN:

Que D.ª **Amanda Sánchez López**, graduada en Biotecnología por la Universidad Francisco de Vitoria ha realizado bajo su dirección el trabajo de Tesis Doctoral que lleva por título:

"Generation and Characterization of a New Conditional Mouse Model of Hutchinson-Gilford Progeria Syndrome to Assess Disease Progression upon Progerin Suppression and Lamin A Restoration".

Revisado el presente trabajo, expresan su conformidad para la presentación del mismo por considerar que reúne los requisitos necesarios para ser sometido a discusión ante el Tribunal correspondiente, para optar al grado de Doctora por la Universidad Autónoma de Madrid.

En Madrid, a 30 de junio de 2019

Dr. Vicente Andrés García

Dra. Lara del Campo Milán

Some people WANT it to happen,

some WISH it would happen,

others MAKE it happen.

- Michael Jordan

AGRADECIMIENTOS

Hay muchísimas personas que me han aportado algo en este camino, a todas ellas muchísimas gracias porque esta tesis es como es gracias a vosotros.

En primer lugar, me gustaría agradecer a **Vicente Andrés** el haberme dado la oportunidad de hacer el doctorado en su laboratorio. Todavía recuerdo la primera charla en la que te oí hablar sobre la progeria y lo que hacíais en el labo. Después de eso no tuve ninguna duda de que era el campo donde quería hacer la tesis doctoral y fui a buscarte a la cafetería del CNIC para hablar de ello. Muchas gracias por la confianza que depositaste y depositas en mí, por tu ayuda y por la libertad que me has brindado para diseñar y hacer experimentos, así como por la libertad con la que puedo discutir contigo ideas infinitamente. Por supuesto, también agradecerte tu gran ayuda y consejos para escribir de forma científica.

Lara, ¿qué más puedo decir? Hemos trabajado mucho tiempo juntas y nos ha dado tiempo a pasar por muchas cosas. Muchas gracias por tu apoyo, por estar ahí en las risas, en los llantos, en los agobios, en los momentos de subidón… Gracias por todo el tiempo que has dedicado y por enseñarme todo lo que me has enseñado. Ya te lo dije y te lo vuelvo a decir, eres una crack en vascular, espero poder llegar algún día a tu nivel de conocimiento (tendré suerte si consigo llegar al nivel de tus rodillas).

También quería dar las gracias a los miembros de mi comité de tesis, **Rui Benedito** y **Cristina Murga.** Gracias por escuchar y los consejos que me habéis dado tanto a nivel personal como a nivel profesional. También daros las gracias por vuestras preguntas, que han estimulado a que siguiera mejorando el trabajo.

A **Mª Isabel Sánchez**, mi tutora de la UAM. Siempre he agradecido mucho que cada vez que nos hemos visto hayas mostrado interés sincero en mi trabajo. Gracias también por haber hecho fácil todos los trámites burocráticos que había que hacer durante las tutelas.

I would like to thank **Steve Jackson** for giving me the opportunity to develop part of my thesis during a short stay at the Gurdon Institute. Thank you for opening the door of your lab and for making me feel at home. Thank you Rimma for not only your help but also for the bike and our badminton matches; I really enjoyed them. Julia, Yaron, Linda, Mukerrem, Kate, Matylda, Fabio, Ramsay, Harveer… thank you for all your help with any doubt and anything that I needed. Thank you Gabi for your time listening to my project with mice and giving me really good suggestions. Of course, thanks to Paco, Israel and Josep, the Spanish guys. La verdad es que me lo pasé genial con vosotros, siempre es agradable poder hablar en español de vez en cuando en el laboratorio. Me encantó ver como manteníais las buenas costumbres españolas de comer a las 15:00!! Gracias de veras por vuestra ayuda y por contar conmigo cuando hacíais algún plan. Last but not least, thank you **Delphine.** Thank you for accepting to be my supervisor during my short stay. Thank you for valuing my work and giving me great suggestions. Thank you for all the time you spend with me in the lab. I really cannot adequately express my gratitude and admiration for your

work. In addition, I will not forget your help with bureaucracy at the beginning and your inestimable help with my search for accommodation.

También me gustaría tener unas palabras con mis **compañeros del labo** de Vicente. Quisiera empezar por los antiguos miembros. Pedro, te agradezco mucho todo tu apoyo en lo personal y también en los primeros meses en el laboratorio, siempre dispuesto a enseñarme lo que fuera sin ponerme ningún problema. Magda, no me olvidaré de todo el tiempo que has dedicado en escucharme, apoyarme y ayudarme aun cuando siempre estabas hasta arriba de trabajo. Ricardo, Jose y Cristina R, gracias por el tiempo compartido en el CNIC.

No quiero olvidarme de los estudiantes que han "pasado por mis manos". Gracias a Javier, a Claudia, a Carlos, María Pía y a Raquel. No solo por su trabajo, sino también por enseñarme a mí a cómo ser mejor "profe". Especialmente Raquel, muchas gracias por toda la ayuda, llegaste en un pico importante de trabajo y tu ayuda fue inestimable. No me extraña que ahora estés donde estás porque tenías y tienes muchísimo potencial y llegarás muy lejos independientemente de lo que hagas (si no te autodestruyes antes). Muchas gracias por los momentos juntas, por las risas y nuestras tonterías y las que queden.

Con respecto a mis compañeros que siguen dando el callo en el laboratorio. Mª Jesús, siempre estás más que dispuesta a echar un cable cuando lo he necesitado. Muchas gracias no solo por el genotipado, sino por otras múltiples cosas en las que me has ayudado y que yo sola me habría vuelto loca. También gracias por enseñarme a usar el microtomo y a hacer cortes dignos. Gracias Cristina, gracias por toda tu ayuda, si esta tesis la he podido hacer en parte es gracias a ti. Además, no es solo que lo haces todo de maravilla, sino el estar siempre dispuesta y poder trabajar bien contigo. Elba, lo mismo, gracias por tu ayuda y por los momentos que hemos compartido. Yaazan, muchas gracias por tus interminables monólogos hablando sobre innumerables cosas sin parar. En serio, gracias por los detalles que has tenido, por tu ayuda y por intentar encontrar siempre el hueco, no solo para ayudarme a mí, sino a todos. Rosa C., muchas gracias por tu alegría y tu buen rollo, aun en momentos malos siempre tienes una sonrisa en la boca y da gusto hablar contigo. Pilar, gracias por tus consejos con las inmunos y estar siempre dispuesta a ayudar, he aprendido mucho de ti.

Alberto, Ana, Rosa N. y Victor. Podría rellenar muchas hojas en realidad, pero trataré de ser breve porque sino... Muchas gracias por el apoyo y todas las discusiones científicas que hemos tenido que han aportado un gran valor a esta tesis. Infinitas gracias por el tiempo dedicado y por la paciencia para escuchar y/o explicarme cosas mientras yo tomaba notas como en la uni. Además de los momentos de relax de tomar café, comidas y salidas, "esta es mi cara", chistes sin gracia, risas, expresiones extrañas nunca jamás oídas, acentos, pestañeos mariposa, momentos "abuelo" y las conversaciones sobre cualquier cosa (Alberto, nunca dejes de ser la enciclopedia que eres). Ha sido muy guay ver cómo hemos ido evolucionando. No os podéis quejar, sobre todo Ana, de lo bien que he tratado vuestro sitio, ¡¡respetando los espacios!! (Aunque es verdad que con los demás lo he tenido más fácil, sino, puede que tuviera un serio problema). Gracias también a Marta, ¡¡Mucho ánimo con el camino que acabas de empezar!!

José María, nunca me olvidaré de tu charla en la fiesta de Navidad de mi primer año en el CNIC. Gracias por escuchar mis ideas y darme tu opinión en todo lo que has podido, siempre la he valorado. Álvaro (el nuevo), cuatro años uno al lado de otro. Casi siempre eras el primero del labo en enterarte de si algo me había salido bien o no y al que he dado la chapa contando las infinitas posibilidades que se me pasaban por la cabeza cuando hacía algún experimento o quería hacer alguno. Gracias por la estabilidad que me has dado en los momentos (sobre todo los primeros) en los que he sido más pesimista de lo que correspondía y ayudarme a ver todo lo que he hecho. También por las risas y las bromas que hacemos prácticamente todos los días (salvo que te escondas en tu cueva) y que siempre alegran y la paciencia, sobre todo últimamente con mi inexplicable e innecesario interés en saber todo sobre los canales iónicos. Iñaki, llevas relativamente poco aquí y tampoco te has librado de mí. Gracias también por escucharme mis idas de olla y no tan idas de olla y darme tus puntos de vista tanto a nivel profesional como a nivel personal, tan útiles siempre. Bea, qué haríamos en el labo sin ti. Muchas gracias por haber sacado siempre 5 minutitos reales para resolverme cualquier duda que he podido tener durante estos 5 años.

Quisiera también agradecer a otras muchas personas, dentro del CNIC pero fuera del laboratorio de Vicente Andrés, toda la ayuda prestada. Espero no olvidarme de nadie, pero es que sois tantos…

En primer lugar, quería agradecer a la **Unidad de Transgénesis** del CNIC su ayuda en la generación del modelo de ratón. ¡Lo conseguimos! Gracias no solo por vuestro fundamental trabajo con la preparación de los zigotos y las microinyecciones que ha hecho posible que exista esta tesis, sino también por las horas de conversaciones, consejos y ayuda.

Gracias a la **Unidad de Genómica.** Puede que ni os acordéis, pero el tiempo que dedicasteis a resolverme mis dudas para mí fue muy valioso. Cada uno de los pasos que he ido consiguiendo ha sido gracias a tener gente a mi alrededor que ha podido ofrecerme su ayuda y opinión.

Gracias a la **Unidad de Microscopía.** Gracias Elvira y Verónica por enseñarme a usar los microscopios. Gracias Verónica por los macros que hemos discutido, por enseñarme junto con tus compañeros a hacerlos y por tu amabilidad y efectividad siempre. Transmites una tranquilidad, una serenidad… y haces que todo parezca fácil.

Gracias a la **Unidad de Imagen.** Gracias a Manuel Desco, Yeny, a Izaskun, a Lorena C., a Iria y a Daniel C. por vuestra ayuda con los CT y MRI. Pero especialmente gracias a Lorena F. y Ana Vanesa por las ecos, sobre todo cuando estábamos mirando todo el tema del Flow Mediated Dilation, intentando poner la cuerdecita, buscando la femoral… ¡Madre mía!, y por el Pulse Wave Velocity… Gracias por enseñarme a usar el ecógrafo y a encontrar las partes del ratón.

Gracias a la **Unidad de Vectores Virales.** Gracias a Juan Bernal por dejar de hacer tus cosas y sentarse conmigo a explicarme y a darme su punto de vista. Ha sido muy muy positivo. Gracias a Daniel Martín por explicarme como se purifican los virus y hacerme hasta un esquemita, y por las facilidades que me has puesto para generar los virus y los mapas. Aunque fuera de la unidad,

gracias Andrés por toda tu ayuda con los virus. Da gusto trabajar contigo, siempre súper optimista y con un "sin problema" como respuesta. Vaya máquina estás hecho. Y gracias María, tu ayuda siempre ha sido siempre más que bien recibida.

Gracias a la **Unidad de Histología.** Gracias a Antonio de Molina por dedicar tiempo para explicarme la anatomía del ratón en condiciones, siempre muy claro, a tu disposición y siempre tan amable. Gracias a Roisin, a Pedro, a Brenda y a Ana Isabel, gracias por vuestro incalculable trabajo. ¡¡De verdad que a veces cuando subía bloques para sus cortes sufría!!

También quería darle las gracias a Alicia y a Juan Carlos de informática por las diversas ocasiones en las que han tenido que ayudarme con algún problemilla con el ordenador.

Gracias a Daniel Jiménez por sentarte a mi lado y ayudarme con el análisis de los MEFs y por explicarme tan bien las cosas y siempre con una sonrisa. También por la macro que nos diseñaste para analizar la ondulación de la elastina, muy chula oye.

Por supuesto no puedo olvidarme de los **técnicos del pool** de animalario. Muchas gracias por la labor que hacéis gestionando las colonias y haciendo que todo funcione perfectamente. Muchas gracias a Virginia, que durante mis primeros meses estuvo gestionando los animalillos a mi nombre. ¿Y qué te voy a decir a ti Eva? ¡Has visto nacer y crecer a mi nueva línea de ratón! Sobre todo crecer y crecer y crecer... Y junto con otras 7-8 líneas mínimo más. ¡Madre mía! Muchísimas gracias por todo el trabajo, por atender a las múltiples peticiones que casi todas las semanas ponía. Y por supuesto muchas gracias por seguir a mis animalillos cuando yo no he podido y por todas y cada una de las cosas que he podido necesitar.

Gracias a Ana Ricote y a Marta G. Camacho por vuestra ayuda con los ECGs, siempre súper amables y con una sonrisa. Gracias también a Santiago por las dudas que he podido tener de gestión, así como a Rubén A. por su ayuda con los animales que han estado enfermos y hemos tratado de averiguar qué es lo que estaba pasando. Mil gracias.

Gracias a Raúl Torres por su ayuda inicial con CRISPR-Cas9, la considero realmente muy importante y valiosa con la que pude aprender muchísimo. También a Marcos S. por los consejos y referencias.

Mariajo y Sergio M., del grupo de Miguel Manzanares, muchas gracias por vuestra ayuda con los blastocistos y dejarme tantos para poder hacer pruebas fundamentales para el desarrollo de mi tesis.

Maria Villalba, gracias por sacar tiempo para explicarme algunas de las patologías del corazón y además tan claramente y tan dispuesta.

Gracias Esther por dejarme un hueco en tu laboratorio de microbiología. Anda que no nos hemos contado historietas mientras yo hacía necropsias y tú estabas con el ordenador. Me lo he pasado muy bien y me he divertido mucho.

Gracias a Eduardo Oliver, por el tiempo que has dedicado a escucharme y asesorarme sobre todo a nivel personal. Te lo agradezco un montón.

Por supuesto, gracias a Ana Briones por toda su ayuda con los experimentos de miógrafo de presión. Agradezco un montón que siempre hayas estado tan dispuesta y hayas puesto tantas facilidades.

Eeva, Eduardo, Anabel, Cristina Giménez, Ana G., muchas gracias por toda la gestión que habéis hecho, así como por vuestra ayuda en el papeleo del doctorado. Gracias Cristina por el tema de las becas y explicarme ordenadamente en su momento todo el papeleo que necesitaba hacer para cumplir con todos los plazos, fue muy útil porque hiciste que desde entonces fuera fácil.

Muchas gracias a todos los compañeros del PhDay con los que hemos organizado una iniciativa tan chula y que cada vez lo es más por el trabajo duro y la genialidad de todos los que están con ello. Gracias también a todos mis compis de promoción, que entrado prácticamente a la vez y que ya estamos saliendo, Laura, Raquel, Fran, Dani, Paula, Noelia, Jose Ángel, Maruchi… Y gracias a Fede, por nuestras quedadas y conversaciones tan inspiradoras y que te hacen ver que hay miles de posibilidades en la vida. Estoy segura de que va a haber muchas más.

Muchas gracias a Javi Mateos, llevas aquí desde que el CNIC empezó y nos vas a despedir a todos. Gracias no solo por la ayuda técnica y logística de todos estos años, sino también por todos los cafés y comidas compartidas, por las barbacoas y las paellas, por tu labia y las conversaciones siempre tan divertidas y que casi siempre terminan en lo mismo. Sé que puedo contar contigo.

Finalmente, dar las gracias al grupo de Marta Cortés. Gracias a Ana por sus historietas de la vieja del visillo. Gracias a Carlos, gracias de veras por los buenos ratos y risas y momentos compartidos. Espero que siga habiéndolos. Y por supuesto, muchas gracias a Raquel y a Irene. Sois grandes trabajadoras y mejores personas. Muchas gracias por vuestra amistad, por compartir conmigo no solo los momentos buenos, risas e historietas, sino también los momentos malos, por escucharme y apoyarme. Por todos los momentos. He tenido mucha suerte en conoceros realmente y estoy segura de que seguiremos teniendo una bonita amistad.

A continuación, quería dar las gracias a todas aquellas otras personas que han estado presentes en mi vida y que han permitido que yo esté aquí.

Quisiera primero dar las gracias en particular a un profe de mi cole, a Juan Carlos del Valle, fue el primero que hizo que el mundo de la biología y la salud me encantara y sin duda fue de las primeras influencias (quitando la estupenda serie de "Erase una vez la vida") que dirigieron mi vida hacia la investigación.

Además, también quería dar las gracias a mis profes de la universidad, Maite, Cruz, Javier C., Javier G., Javier S., Julián, Ana B, Susana, Noelia, Elvira, Raquel y a todos los demás. Es también gracias a vosotros he llegado hasta aquí. Es increíble la cantidad de cosas que se aprenden y enseñan y no te das cuenta hasta que no miras atrás.

Por supuesto también a Juan C. Cigudosa, a Sara, Sandra, Rocio, July, Ana, Alba, Miriam, Carmen… y a todos los demás miembros del labo de citogenética molecular del CNIO donde

tuve la oportunidad de hacer mis prácticas de investigación, donde aprendí tanto, me lo pasé tan bien y me hizo decantarme por la realización de la tesis doctoral.

No me puedo olvidar de Irene e Isabel, gracias a las dos de todo corazón. Habéis conseguido muchas cosas, algo de lo que siempre estaré eternamente agradecida.

Gracias a Black Thunders Derby Dames! Sois un ejemplo de constancia, trabajo duro, compromiso y sobre todo de sentimiento de equipo. Es genial poder pertenecer al equipo y practicar un deporte que me encanta donde no solo hay ganas de superación, sino que también prima el buen rollo y el compañerismo por encima de todo.

Alicia, gracias por los momentos compartidos en el teatro musical, me lo pasé estupendamente, y gracias por seguir ahí y contar contigo. Patri, nos conocemos desde hace infinitos años, a pesar de la distancia y de no poder vernos con frecuencia ahí seguimos, cuando nos volvemos a ver es como si el tiempo no hubiera pasado, y eso no es fácil de conseguir ¡gracias! Quiero también dar las gracias a David y Mercedes, gracias por las tardes de cine, cenas y risas, gracias por las vacaciones de verano y por vuestra amistad. Por supuesto, Susana, compañera de batallas en la uni, la vida nos ha llevado por diferentes caminos, pero sé que siempre puedo y podré contar contigo para cualquier cosa. Gracias por tu amistad.

Gracias a Fernando, Natalia, Sergio, Rosalía, Diego, Jhon, Laura y Pablo. Está siendo genial trabajar con vosotros en la asociación, creo que hacemos un gran equipo y que pueden salir muchas cosas chulas. Lo mejor sobre todo es la sensación de grupo, compromiso, piña y poder contar con vosotros para tantas cosas.

Arturo, muchas gracias por tu amistad. No sabemos muy bien ninguno como empezó todo, pero el caso es que empezó, ¡y aquí seguimos! Gracias por poder hablar contigo de prácticamente todo y por tener la misma confianza conmigo.

Noelia, mi compañera de guerra, anda que no habremos pasado horas y horas en la biblioteca… llamadas de agobio, de dudas y por supuesto de alegrías. Muchas gracias ser mi amiga, por todos esos momentos y los muchos que nos quedan, por estar ahí siempre y poder contarte cualquier cosa. Raquel, gracias también por tu amistad, por poder confiar en ti y por decirme siempre lo que piensas. Sois de lo mejorcito que hay y tengo suerte de teneros. Ya veremos qué pasa con la vida, pero ya sabemos que hay cosas que no cambiarán.

Y que pasa con los búhos!!! Mis amigas de Cambridge, pero que no son de Cambridge, que son españolas jajaj. Eva, Carolina y Laura. Nunca me habría imaginado que la estancia en Cambridge me fuera a regalar tres amigazas como vosotras. Vaya grupito majo y fuerte que hemos conseguido hacer. Sois geniales. Muchas gracias por todos los increíbles y felices momentos que hemos vivido. Sé que siempre vamos a estar unidas. ¿Qué somos? ¡Búhos! ¿Qué somos? ¡Búhos! ¿Qué somos? ¡¡¡¡Búhos, búhos, búhos!!!! Jajaj que payasas.

Ángela, en realidad no hay mucho que pueda decir aquí que no te haya dicho ya, así que seré breve. Son muchos años lo que llevamos juntas por los que hemos pasado por muchas cosas. Nos hemos visto crecer y evolucionar. Nos hemos peleado y nos hemos reconciliado, hemos

reído y hemos llorado. Da igual donde estemos, el tiempo que pase ni lo que pueda ocurrir, siempre vamos a estar la una para la otra. Para lo que sea. Gracias.

Gracias a Peka, Marta, Javi, Gema, Juanjo, Erika, Paco, Patricia, Andrea, Víctor, Laura, Adrián, Nalaya y Naiara. Gracias por todo el tiempo que hemos compartido y por ser una más.

Gracias a Dª. Beatriz, a Ana y a Andrés, por lo bien que me habéis tratado siempre, por aceptarme y ayudarme siempre en cualquier cosa que haya podido pedir de forma siempre tan sincera y sin esperar nada a cambio.

Gracias a mis tíos y primos, gracias a mis cuatro abuelos que siempre se han preocupado por mí y me han dado infinito cariño. Por supuesto, gracias a mis padres y a mi hermana Eva. Gracias por todo lo que habéis hecho por mí. Gracias por la educación recibida, no solo por el cole y la universidad, sino también por los valores que me habéis enseñado casi sin vosotros saberlo creo yo. Por haberme apoyado en mis decisiones y dejarme y ayudarme a hacer siempre lo que he querido. Y gracias a Eva también, porque al final da lo mismo todas las peleíllas propias de hermanas que hayamos podido tener. Gracias por los buenos momentos y las risas y las patatas jajaja (durará siempre, que le vamos a hacer) y por los que quedan.

Para terminar, Jose, mi compañero de viaje. Creo que puedes ser el ingeniero que más sepa de progeria y biología molecular del mundo. Seré breve, porque ya lo sabes todo. Hemos compartido infinidad de cosas… hemos crecido y evolucionado juntos. Gran parte de nuestra personalidad la hemos madurado estando el uno al lado del otro. Parte de lo que soy y de lo que quiero llegar a ser es gracias a ti. Gracias por hacerme mejor persona, por ser un modelo a seguir, por estar a mi lado, por las conversaciones y los silencios, por todas las miradas, sonrisas, detalles, diversión, hiperconfianza, apoyo, compresión… Gracias por ser mi pasado, presente y futuro.

La persona que empezó esta tesis no es la misma que la termina. Muchas gracias a todos por acompañarme durante todo este tiempo.

SUMMARY

Hutchinson-Gilford progeria syndrome (HGPS) is a rare fatal genetic disorder characterized by accelerated aging and premature death at an average age of 14.6 years. "Classical" HGPS is caused by a heterozygous *de novo* c.1824 C>T dominant synonymous point mutation in the *LMNA* gene, which encodes for lamin A and C. This mutation promotes the expression of a mutant protein called progerin, an aberrant form of prelamin A that cannot undergo complete maturation. Progerin remains permanently farnesylated and firmly anchored to the inner nuclear membrane, affecting many cellular processes in a dominant-negative manner.

HGPS patients appear normal at birth but develop symptoms of the disease typically during the first and second year of life. Taking into account that there is still no definitive cure for HGPS and that patients are diagnosed when symptoms are already present, it is critically important to ascertain whether the damage caused by progerin expression is reversible or if disease progression can be slowed down or halted upon progerin suppression. It is also necessary to investigate the relative contribution of systemic and tissue-specific factors to the development of HGPS to assess the effectiveness of potential future therapies designed to suppress progerin expression in specific tissues, which, if proven effective, would likely be less challenging than whole-body progerin suppression.

In order to address these questions, in this Doctoral Thesis we use the CRISPR-Cas9 system to generate *Lmna*^{HGPSrev} mice, the first "reversible" mouse model of progeria which expresses progerin ubiquitously and allows a controlled spatio-temporal suppression of progerin expression with concomitant restoration of lamin A expression upon activation of the Cre recombinase. We demonstrate that *Lmna*$^{HGPSrev/HGPSrev}$ mice recapitulate the main features of human HGPS, including failure to thrive, cardiovascular alterations and premature death. Moreover, we show that Cre activation upon tamoxifen treatment starting at an advanced stage of the disease in *Lmna*$^{HGPSrev/HGPSrev}$ *Ubc-CreERT*$^{tg/+}$ progeroid mice prolongs their life span. Finally, we show that gene therapy with adeno-associated virus overexpressing Cre ameliorates postnatal growth of adult *Lmna*$^{HGPSrev/HGPSrev}$ mice with initial symptoms of HGPS at the initiation of the therapy. These studies with the *Lmna*^{HGPSrev} mouse model, and future studies beyond the scope of the present Doctoral Thesis, will shed significant light on the cellular and molecular mechanisms of HGPS and pave the way to developing more efficient therapies.

RESUMEN

El Síndrome de Progeria de Hutchinson-Gilford (HGPS, por sus siglas en inglés) es un trastorno genético fatal extremadamente raro caracterizado por envejecimiento acelerado y muerte prematura a una edad promedio de 14,6 años. El HGPS "clásico" está causado por una mutación *de novo* c.1824 C>T en el exón 11 del gen *LMNA*, que codifica las laminas A y C. Se trata de una mutación que, a pesar de ser sinónima, promueve la expresión de progerina, una forma anómala de prelamina A que no puede madurar correctamente, permaneciendo farnesilada y unida a la membrana nuclear interna, afectando muchos procesos celulares de manera dominante-negativa.

Los pacientes con HGPS tienen un aspecto normal al nacer, pero desarrollan síntomas de la enfermedad típicamente durante el primer y segundo año de vida. Teniendo en cuenta que no existe una cura definitiva para HGPS y que los pacientes son diagnosticados cuando los síntomas están ya presentes, es crítico determinar si el daño causado por la progerina es reversible o si la progresión de HGPS puede disminuir o detenerse mediante la supresión de la expresión de esta proteína. También es necesario investigar la contribución relativa de factores sistémicos y específicos de tejido al desarrollo de HGPS, para evaluar la efectividad de posibles terapias futuras diseñadas para suprimir la expresión de progerina en tejidos específicos, lo que sería más sencillo que la supresión de progerina en todo el cuerpo.

Para abordar estas preguntas, en esta Tesis Doctoral utilizamos el sistema CRISPR-Cas9 para generar ratones *Lmna*^{HGPSrev}, el primer modelo de progeria "reversible" con expresión ubicua de progerina que puede suprimirse de manera controlada espacio-temporalmente tras la activación de la recombinasa Cre, que además permite el restablecimiento de la expresión de la lamina A. Hemos demostrado que los ratones *Lmna*$^{HGPSrev/HGPSrev}$ recapitulan las características principales de HGPS en humanos, incluyendo alteraciones en el desarrollo, problemas cardiovasculares y muerte prematura. Además, mostramos que el tratamiento de estos ratones progeroides mediante la activación de la Cre con tamoxifeno en una etapa avanzada de la enfermedad aumenta su supervivencia. Finalmente, la terapia génica con virus adeno-asociados que sobreexpresan Cre mejora el crecimiento postnatal de ratones progéricos adultos con síntomas iniciales de HGPS. Estos y futuros estudios con ratones *Lmna*$^{HGPSrev/HGPSrev}$ más allá del alcance de la presente Tesis Doctoral, arrojarán información importante sobre los mecanismos celulares y moleculares de HGPS y facilitarán el camino para desarrollar terapias más eficientes.

INDEX

ABBREVIATIONS

- **AAV:** Adeno-Associated virus
- **BAC:** Bacterial artificial chromosome
- **CO:** Cardiac output
- **CRISPR-Cas9:** Clustered regularly interspaced short palindromic repeat/CRISPR-associated 9 system
- **crRNA:** CRISPR-RNA
- **CVD:** Cardiovascular disease
- **DSB:** Double strand break
- **E/A:** Early / late diastolic velocity peak wave
- **ECG:** Electrocardiogram / Electrocardiography
- **ECM:** Extracellular matrix
- **EF:** Ejection fraction
- **FT:** Farnesyltransferase
- **FTIs:** Farnesyltransferase inhibitors
- **GFP:** Green fluorescent protein
- **HDL:** High-density lipoprotein
- **HDR:** Homologous direct repair
- **HGPS:** Hutchinson-Gilford progeria syndrome
- **HM:** Homozygous
- **HT:** Heterozygous
- **H&E:** Hematoxylin and Eosin
- **IC:** Internal circumference
- **ICMT:** Isoprenylsysteine carboxyl methyltransferase
- **ID:** Internal diameter
- **INM:** Inner nuclear membrane
- **IVRT:** Isovolumetric relaxation time

- **IVS:** Intraventricular septum
- **LB:** Luria-Bertani
- **LDL:** Low-density lipoprotein
- **LV:** Left ventricle / ventricular
- **MEFs:** Mouse embryonic fibroblasts
- **MV:** Mitral valve
- **NE:** Nuclear envelope
- **NHEJ:** Non-homologous end joining
- **NPCs:** Nuclear pore complexes
- **ONM:** Outer nuclear membrane
- **PAM:** Protospacer adjacent motif
- **PAT:** Pulmonary artery acceleration time
- **PCR:** Polymerase chain reaction
- **PET:** Pulmonary artery ejection time
- **PW:** Posterior wall
- **sgRNA:** Single-guide RNA
- **SMA:** Smooth muscle actin
- **SV:** Stroke volume
- **TAPSE:** Tricuspid annular plane systolic excursion
- **tracrRNA:** Trans-activating crRNA
- **VSMCs:** Vascular smooth muscle cells
- **WT:** Wild-type

INTRODUCTION

1. INTRODUCTION

1.1. Nuclear Envelope and Lamins

The nuclear envelope (NE) is the structure in eukaryotic cells that encloses the genetic material and separates nuclear from cytoplasmic functions. The major structural components of the NE are the inner nuclear membrane (INM), the outer nuclear membrane (ONM), the nuclear pore complexes (NPCs) and the nuclear lamina (Dechat *et al.*, 2008; Hetzer, 2010). The nuclear lamina is a complex meshwork of proteins associated with the INM, the NPCs and chromatin. The main components of the nuclear lamina are the lamins, type V intermediate filaments that can be also found at lower concentrations within the nucleosplasm. Lamins are classified in A-type and B-type lamins based on their sequence, features and properties. In most vertebrates there are two major A-type lamins (lamin A and lamin C) coded by the *LMNA* gene by alternative splicing, and two major B-type lamins called lamin B1 and lamin B2 that are coded by *LMNB1* and *LMNB2,* respectively. B-type lamins are expressed in all types of cells, while A-type lamins are mainly expressed in differentiated cells. Other minor isoforms of lamins expressed at much lower levels include lamins AΔ10, lamin C2 and lamin B3 (Dechat *et al.*, 2008, 2010).

Lamins play a fundamental role in the maintenance of nuclear shape and stability. In addition to this structural role, it has become increasingly evident that lamins play a key role in the regulation of other fundamental functions, such as cytoskeleton organization, cell proliferation, differentiation and migration, DNA repair, gene expression and organization and epigenetic regulation of chromatin (Broers *et al.*, 2006; Andrés and González-Granado, 2009; Dechat *et al.*, 2010; Dorado and Andrés, 2017). It is therefore not surprising that more than 400 mutations in the *LMNA* gene have been associated to different human diseases (Broers *et al.*, 2006) (http://www.umd.be/*LMNA*/). The discovery of these diseases, collectively called laminopathies, resulted in an increasing interest in the study of lamins. Laminopathies include familial partial lipodystrophy, dilated cardiomyopathy, congenital muscular dystrophy and progeroid syndromes, such as Atypical Werner Syndrome, Restrictive Dermopathy and Hutchinson-Gilford Progeria Syndrome (HGPS) (Cohen, Hernandez and Stewart, 2008; Dechat *et al.*, 2008; Hamczyk, del Campo and Andrés, 2018).

1.2. Hutchinson- Gilford Progeria Syndrome

HGPS (OMIM 176670) is one of the most severe laminopathies. It is an autosomal dominant ultrarare genetic disease with an overall estimated prevalence of 1 in 20 million people, therefore it is estimated that around 350-400 children live with progeria worldwide (https://www.progeriaresearch.org/prf-by-the-numbers/). This disorder was first described by Hutchinson and Gilford (Hutchinson, 1886; Gilford and Hutchinson, 1897) but it was not until 2003 when the disease-causing mutation was identified by two different laboratories (De Sandre-Giovannoli *et al.*, 2003; Eriksson *et al.*, 2003). "Classical" HGPS is caused by a heterozygous *de novo* point mutation in exon 11 of the *LMNA* gene (c.1824C>T; p.G608G) that activates an exonic cryptic splice site. The mutant pre-mRNA generated due to the use of this alternative splicing has an in-frame deletion of 150 bp in exon 11 and, consequently, it synthetizes a mutant form of lamin A with a 50 amino acids deletion called progerin (Cohen, Hernandez and Stewart, 2008; Ahmed *et al.*, 2017; Gonzalo, Kreienkamp and Askjaer, 2017).

As a result of alternative splicing, wild-type *LMNA* codes for two major lamin isoforms, lamin A (exons 1-12) and lamin C (exons 1-10). Lamin A is initially expressed as an immature form, called prelamin A, that requires various consecutive post-translational modifications (Figure 1, *Left*). First, the cysteine residue of the C-terminal *–CaaX* box (-CSIM in the case of prelamin A) is farnesylated by a farnesyltransferase (FT) (Sinensky *et al.*, 1994). Then, the last three amino acids (-SIM) are removed usually by the zinc metalloproteinase Zmspte24, a CAAX prenyl protease. Next, the exposed C-terminal cysteine is carboxymethylated by the enzyme called isoprenylcysteine carboxyl methyltransferase (ICMT) (Sinensky *et al.*, 1994; Broers *et al.*, 2006). These modifications are thought to be necessary for the translocation of prelamin A to the INM (Holtz *et al.*, 1989), where Zmpste24 removes 15 amino acids upstream the C-terminal cysteine residue to yield mature lamin A (Pendás *et al.*, 2002; Broers *et al.*, 2006). The 50 amino acids deletion in HGPS includes the target site for Zmspte24, therefore the last post-translational modification cannot take place, resulting in the accumulation of permanently farnesylated and carboxymethylated progerin (Piekarowicz *et al.*, 2019) (Figure 1, *Right*). Interestingly, the activation of this cryptic splice site has been also identified in elderly individuals who are not carriers of the HGPS mutation, suggesting that low levels of progerin expression may contribute to physiological aging (Scaffidi and Misteli, 2006; Cao, Blair, *et al.*, 2011; Dorado and Andrés, 2017; Hamczyk, del Campo and Andrés, 2018).

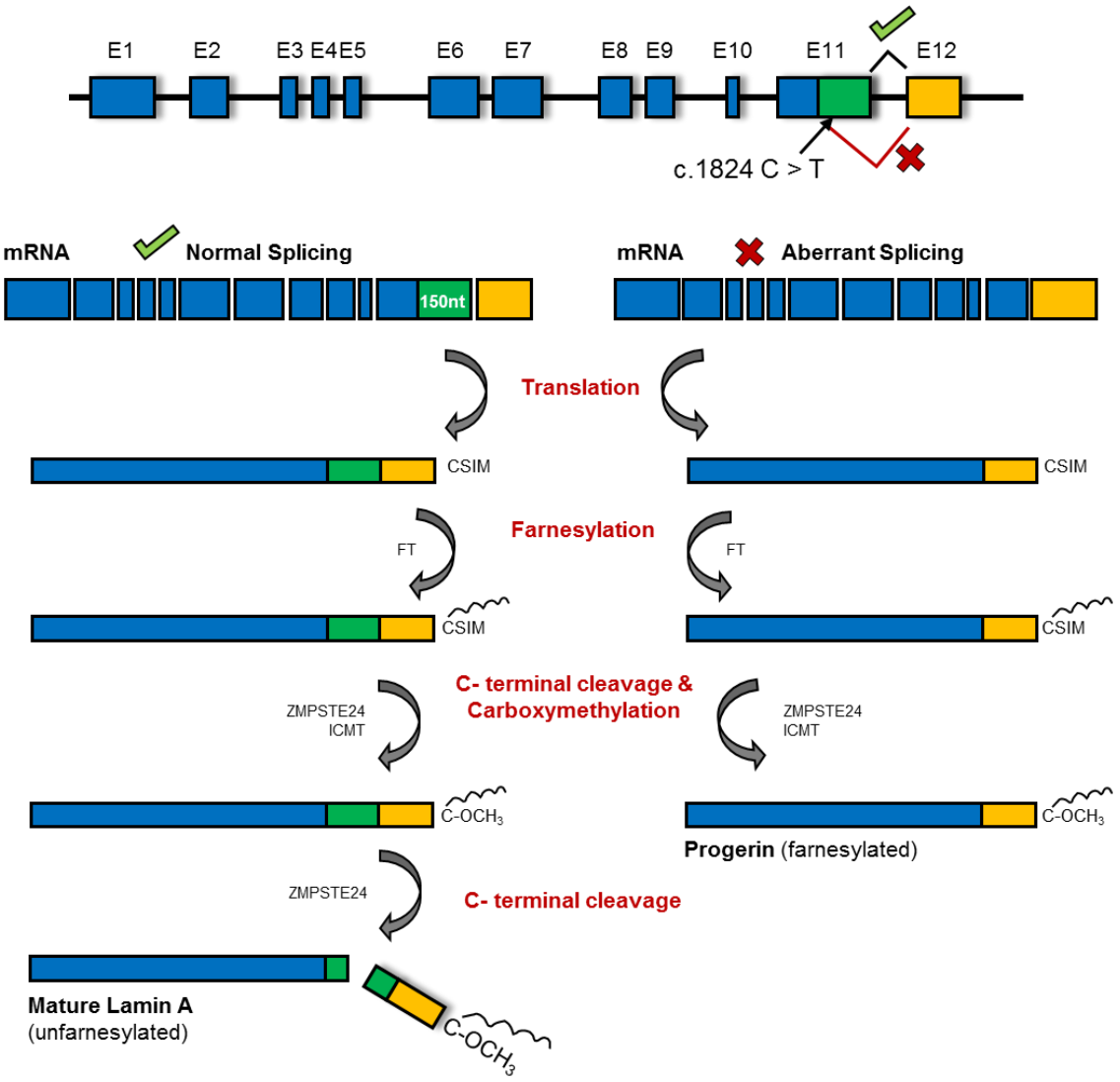

Figure 1. Inadequate post-translational processing of prelamin A caused by aberrant splicing of the *LMNA* mRNA leads to accumulation of permanently farnesylated progerin synthesis. ***Left:*** Normal splicing between exon 11 and 12 in the *LMNA* gene generates an mRNA that is translated into prelamin A, a precursor protein that undergoes several post-translational modifications. First, the cysteine residue of prelamin A C-terminus is farnesylated by a farnesyltransferase (FT). Subsequently, the three C-terminal amino acids are removed by an endonuclease (usually ZMPSTE24: zinc metallopeptidase STE24, also called FACE-1) and the newly exposed cysteine is carboxymethylated by isoprenylcysteine carboxyl methyltransferasa (ICMT). Finally, the last 15 amino acids, including the modified cysteine, are cleaved by ZMPSTE24 resulting in mature lamin A. ***Right:*** The HGPS-causing c. 1824C>T mutation in *LMNA* exon 11 activates a cryptic splice site that causes the in-frame deletion of 150 bp in exon 11, which provokes the deletion of 50 amino acids that contain the ZMSPTE24 cleavage site. As a result, the C-terminal portion cannot be removed and the cell accumulates farnesylated progerin.

HGPS is defined as a segmental premature aging disease because some features in patients are shared with physiological aging while others are unique to this rare disorder. Liver, kidneys, the gastrointestinal tracks, and the immune system are usually normal in HGPS patients. In addition, children with progeria do not manifest cancer or senility, common features in elderly people (Ullrich and Gordon, 2015; Gonzalo, Kreienkamp and Askjaer, 2017).

HGPS is a progressive disease characterized by accelerated aging. Despite some variability in signs and symptoms depending on the age and disease severity, HGPS patients strongly resemble to each other (DeBusk, 1972; Ullrich and Gordon, 2015; Gonzalo, Kreienkamp and Askjaer, 2017). In most cases, patients have a normal appearance at birth and the initial symptoms begin around the first year of life, including significant growth retardation and skin abnormalities. While the disease is progressing, HGPS patients show other characteristic features of progeria, such as bone and dental abnormalities, alopecia, progressive contractures of the joints, loss of subcutaneous fat (lipodystrophy) and prominent scalp veins (Ullrich and Gordon, 2015; Piekarowicz *et al.*, 2019). However, the most important complications of the disease are cardiovascular and cerebrovascular alterations that eventually lead to premature death predominantly due to stroke or myocardial infarction, with an average lifespan of 14.6 years old (Gordon, Massaro, *et al.*, 2014).

1.3. Cardiovascular Pathology in HGPS

Cardiovascular disease (CVD) is the primary cause of death and morbidity worldwide, and aging is the main cardiovascular risk factor (www.who.int/gho/en/) (North and Sinclair, 2012). Most of the cardiovascular alterations in HGPS are also present in the geriatric population, but CVD in progeria typically develops in the absence of common risk factors, such as hypercholesterolemia, obesity or tobacco smoking (Melissa A. Merideth *et al.*, 2008; Hamczyk, del Campo and Andrés, 2018). In addition, progerin has been detected in atherosclerotic coronary arteries from non-HGPS elderly people, more frequently at advanced ages (Olive *et al.*, 2010). HGPS therefore offers the opportunity for studying not only mechanisms of CVD in progeroid patients, but perhaps also for understanding and discovering other determinant elements in normal cardiovascular aging independently of conventional risk factors.

Endothelial dysfunction and vascular stiffness are two major age-related vascular alterations (Hamczyk, del Campo and Andrés, 2018). While endothelial function seems to be preserved in HGPS, vascular stiffness has been reported to be an early and pervasive feature in patients, which is getting increasing attention because it is thought to be an important starting point for other cardiovascular complications (Lakatta and Levy, 2003; Gerhard-Herman *et al.*, 2012; Hamczyk, del Campo and Andrés, 2018). Confirming the relevance of vessel stiffening in progeria, we recently demonstrated stiffness in both the aorta and mesenteric vessels in a mouse model of HGPS (del Campo *et al.*, 2019). In addition to other typical signs of vascular aging, such as

atherosclerosis or vascular calcification, large arteries in HGPS children exhibit an exacerbated loss of vascular smooth muscle cells (VSMCs) with replacement by collagen and extracellular matrix (ECM), as well as increased thickness and fibrosis of the adventitial layer (Varga *et al.*, 2006; Olive *et al.*, 2010; Worman and Michaelis, 2018).

Regarding cardiac alterations, HGPS patients show left ventricle (LV) hypertrophy, mitral valves (MV) calcification, interstitial fibrosis and age-related abnormalities in the electrocardiogram (ECG), such as ST depression/elevation, T-wave flattening and QT interval prolongation (Gerhard-Herman *et al.*, 2012; Rivera-Torres *et al.*, 2016; Prakash *et al.*, 2018).

1.4. Animal Models of HGPS

In order to understand any disease and be able to identify candidate therapeutic targets, it is crucial to know all the events and underlying mechanisms of the pathogenesis of the disorder. *In vitro* approaches, using stablished cell lines or patient derived cells, not only are an essential first step to develop working hypotheses, but also to provide invaluable information regarding major cellular processes. Cells derived from HGPS patients have been instrumental to improve our knowledge about the disorder and the role of lamin A or progerin in health and disease respectively. HGPS cells exhibit numerous defects, most prominently alterations in nuclear architecture and morphology as well as accumulation of DNA damage (De Sandre-Giovannoli *et al.*, 2003; Dahl *et al.*, 2006; Scaffidi and Misteli, 2006; Dorado and Andrés, 2017).

Despite the convenience of *in vitro* studies, animal models are essential to investigate systemic and cell-to-cell interactions, physiological functions, and to test candidate therapies in an *in vivo* setting. In this regard, the development of genome-editing technologies resulted in a huge opening of opportunities in biomedical research, including remarkable advances in animal model generation and in gene therapy.

Since the discovery of the HGPS mutation in 2003, several animal models have been generated that recapitulate different aspects of HGPS. Taking into account the low number of diagnosed patients worldwide (www.progeriaresearch.org), the generation of HGPS animal models is critical in order to overcome the difficulties in leading clinical trials and research on the mechanisms driving the disease, and to find effective treatments and a potential cure for these children. Moreover, since HGPS and normal aging share many common features, animal models

of HGPS could be useful to study mechanisms underlying physiological aging, including cardiovascular alterations, the main cause of mortality and morbidity in the general population.

Various mouse models of progeria have been generated that resemble many, but not all, features of human HGPS (Table 1). In addition, comparison of these mouse models reveal some phenotypic differences. Interspecies differences between mice and humans might be one of the reasons of these dissimilarities. Moreover, the diversity of strategies used for the generation of the mouse models, the target gene or even the distinct toxicity of progerin in humans and mice should be taken into account.

1.4.1. Classical HGPS Animal Models

Zmpste24-deficient mice represent the first mouse model showing a progeroid phenotype and one of the most used (Pendás *et al.*, 2002). Interestingly, this model was not developed with the aim of studying progeria, however, the characterization of the phenotype led the authors to think the afterwards demonstrated relationship between Zmpste24 protein and lamin processing and hence, the usefulness of this model in HGPS research. *Zmste24* knock-out mice show most of the alterations present in HGPS, including lipodystrophy, growth retardation, alopecia, skeletal and muscular atrophy, cardiac alterations and a premature death at an average age of 5 months (Pendás *et al.*, 2002; Varela *et al.*, 2005; Rivera-Torres *et al.*, 2016). However, the vascular phenotype has not been reported yet in *Zmste24*-null mice.

Lack of *Zmpste24* prevents the last maturation step of prelamin A, therefore *Zmste24-null* mice accumulate immature farnesylated prelamin A, but not progerin (Figure 1). To generate the first mouse model expressing progerin ($Lmna^{HG}$ mice), Yang *et al.* removed intron 10 and joined together a mutant form of exon 11 (without the last 150 bp) and wild-type exon 12, which results in the expression of progerin (Yang *et al.*, 2005; Yang, 2006). Heterozygous $Lmna^{HG/+}$ mice show several features of premature aging, such as growth retardation, body weight loss, lipodystrophy, bone abnormalities and premature death at an average age of 27 weeks. The phenotype is more severe in homozygous $Lmna^{HG/HG}$ mice, which have an average lifespan of only 3-4 weeks (Yang, 2006). However, $Lmna^{HG/+}$ and $Lmna^{HG/HG}$ mice fail to exhibit cardiovascular alterations, the most relevant feature of HGPS patients.

Table 1. **HGPS mouse models**

HGPS Mouse Model	Gene, Transgene or minigene	A-type lamin expression	Vascular alterations	Cardiac alterations	Premature aging	Reference
Zmspte24$^{-/-}$	*Zmpste24*	Prelamin A, lamin C	No	Yes	Yes	(Pendás *et al.*, 2002)
Lmna$^{HG/+}$	*Lmna*	Progerin, lamin A/C	No	NR	Yes	(Osorio *et al.*, 2011)
Lmna$^{HG/HG}$	*Lmna*	Progerin	NR	NR	Yes	(Yang *et al.*, 2005; Yang, 2006)
Lmna$^{nHG/+}$	*Lmna*	non-farnesylated progerin, lamin A/C	NR	No	Yes	(Yang, Andres, *et al.*, 2008)
Lmna$^{csmHG/+}$	*Lmna*	non-farnesylated progerin, lamin A/C	NR	No	No	(Yang *et al.*, 2011)
Lmna$^{nPLAO/nPLAO}$	*Lmna*	non-farnesylated prelamin A	NR	Yes	No	(Davies *et al.*, 2010)
Lmna$^{G609G/+}$	*Lmna*	Progerin, lamin A/C	Yes	NR	Yes	(Osorio *et al.*, 2011)
Lmna$^{G609G/G609G}$	*Lmna*	Progerin, lamin C, residual lamin A	Yes	NR	Yes	(J. M. Lee *et al.*, 2016)
Lmna$^{G609G/G609G}$	*Lmna0*	Progerin, lamin C, residual lamin A	Yes	Yes	Yes	(Osorio *et al.*, 2011)
ApoE$^{-/-}$ *Lmna*$^{G609G/G609G}$	*Lmna*	Progerin, lamin C, residual lamin A	Yes	Yes	Yes	(Hamczyk *et al.*, 2018)
BAC G608G	*Tg (LMNA G608G)*	Lamin A/C, human progerin	Yes	No	No	(Varga *et al.*, 2006)
Tetop_LA^{G608G}	*Minigene tetop_LA*^{G608G}	Lamin A/C, human progerin, human lamin A	NR	NR	Tissue-specific phenotype	(Sagelius, Rosengardten, Schmidt, *et al.*, 2008)

NR: Not reported. Adapted from: Hamczyk et al. 2018

Varga *et al.* developed a new HGPS mouse model by introducing a bacterial artificial chromosome (BAC) containing the human *LMNA* gene carrying the HGPS-causing mutation in exon 11 (Varga *et al.*, 2006). The "G608G BAC mice" is the first model showing some of the vascular alterations observed in patients, such as calcification, adventitial thickening, and progressive loss of medial VSMCs and replacement with ECM (Varga *et al.*, 2006). Unfortunately, this transgenic mouse model does not show any other feature of premature aging. Of note in this regard, the G608G BAC mice contained not only the endogenous *Lmna* gene, but also the human *LMNA* gene, and three additional genes: *UBQLN4*, *MAPBPIP*, and *RAB25* genes, whose presence could be affecting somehow the phenotype (Varga *et al.*, 2006).

Since none of these genetic modified animals neither fully recapitulates the HGPS phenotype nor the genetic-molecular scenario of the disease, Osorio *et al.* generated the *knock-in* $Lmna^{G609G}$ mouse model, which carries a 1827 C>T (p.G609G) point-mutation in the *LMNA* locus equivalent to the one present in the majority of HGPS patients (Osorio *et al.*, 2011). Like in HGPS patients, the mutant $Lmna^{G609G}$ allele provokes aberrant splicing in exon 11, leading to the expression of lamin C, progerin and small amounts of lamin A as a result of a correct splicing in spite of the cryptic donor site. $Lmna^{G609G/G609G}$ mice display several premature aging features, including growth retardation, body weight loss, bone alterations, VSMCs loss in aortic arch (but not in the thoracic aorta) and premature death at an average age of 15 weeks (Osorio *et al.*, 2011). These mice also present ECG abnormalities with normal blood pressure. Recently, we reported in these mice vascular stiffness and inward remodeling in resistance and conductance vessels and accumulation of collagen in the medial layer of thoracic aortas (del Campo *et al.*, 2019). Importantly, $Lmna^{G609G/G609G}$ mice do not exhibit atherosclerosis as a result of the extremely resistance of mice to develop this pathology (Fuster *et al.*, 2012). However, our group demonstrated exaggerated atherosclerosis in apolipoprotein E-null mice that ubiquitously express progerin ($Apoe^{-/-}Lmna^{G609G/G609G}$) (Hamczyk *et al.*, 2018), due at least in part to induction of endoplasmic reticulum stress in VSMCs (Hamczyk *et al.*, 2019). Remarkably, VSMC-specific progerin expression is sufficient to accelerate vessel stiffness and atherosclerosis, identifying this cell type as a key element in vascular disease (Hamczyk *et al.*, 2018; del Campo *et al.*, 2019). The progeroid phenotype is much milder in $Lmna^{G609G/+}$ mice, which look normal until 8 months of age, when they start to develop loss of body weight, bone alterations and die at an average age of 35 weeks (Osorio *et al.*, 2011).

Recently, Lee *et al* has developed a new *Lmna*$^{G609G/G609G}$ mouse model that exhibits a phenotype similar to former HGPS mouse models (Lee et al., 2016; Osorio et al., 2011; Varela et al., 2005; Yang et al., 2006).

1.4.2. Other Relevant HGPS Animal Models

It was hypothesized that the farnesyl group present in progerin or prelamin A is responsible, at least in part, of the toxic effect of these unprocessed proteins (Pendás *et al.*, 2002; Navarro *et al.*, 2004, 2005). To test this possibility, several mouse models expressing a non-farnesylated mutant form of lamin A were developed (Yang, Andres, *et al.*, 2008; Davies *et al.*, 2010; Yang *et al.*, 2011).

Yang *et al.* first generated *Lmna*^{nHG} mice, which express non-farnesylated progerin (Yang, Andres, *et al.*, 2008). This mouse model was identical to the original *Lmna*^{HG} but with an additional replacement of the C-terminal cysteine of the *CaaX* motif by a serine (-CSIM → -SSIM). *Lmna*^{nHG} mice exhibit the same phenotype as *Lmna*^{HG} mice, but much less severe, suggesting the possibility that permanent farnesylation is not the only cause of the toxic effect of progerin (Yang, Andres, *et al.*, 2008). However, it cannot be ruled out that the mild phenotype of *Lmna*^{nHG} mice could be due to the cytosine→serine modification itself. Hence, the same laboratory generated *Lmna*^{csmHG} mice, in which the Isoleucine amino acid from de -CSIM motif was removed. *Lmna*^{csmHG} mice, which express a non-farnesylated progerin, were undistinguishable from wild-type littermates, pointing back again to the farnesylation toxicity hypothesis (Yang *et al.*, 2011). Additionally, Davies *et al.* developed a non-farnesylated prelamin A mouse model (*Lmna*^{nPLAO}) by just changing C-terminal cysteine by a serine (-CSIM → -SSIM). These mice did not exhibit any progeroid phenotype except for the development of cardiomyopathy that could be due to the cytosine→serine modification itself (Davies *et al.*, 2010).

1.4.3. Inducible and Conditional HGPS Mouse Models

The generation of conditional and inducible models emerged because of the requirement of more sophisticated methods to control gene expression in a flexible spatio-temporal manner and, therefore, to obtain more information about the role of a specific gene at different stages of development or in different cells and tissues (Ryding, Sharp and Mullins, 2001; Bockamp *et al.*, 2008).

The Cre-lox system is one of the most common strategies used in the generation of conditional models. In this system, loxP sites are recognized by the Cre recombinase, which mediates a recombination event that removes the floxed (flanked) DNA in the tissues where Cre is expressed. Hence, tissue specificity is defined by the promoter driving Cre expression (Sternberg and Hamilton, 1981; McLellan, Rosenthal and Pinto, 2017). With the purpose of controlling not only tissue specificity but also the time of expression, Cre recombinase was fused to a ligand-binding domain of a mutated estrogen receptor. This domain allows the sequestration of the fused Cre in the cytosol, which can be activated via nuclear translocation only in presence of tamoxifen (Ryding, Sharp and Mullins, 2001).

Since HGPS is a disease that involves several organs and tissues (Gonzalo, Kreienkamp and Askjaer, 2017), there was a great interest in using conditional models in order to explore the specific contribution of progerin in different tissues and organs on the pathogenesis of the disease.

Osorio *et al.* designed the first conditional mutant allele in the mouse *Lmna* locus (*Lmna*^{LCS}, Lamin C-Stop). This allele exhibit the C > T point mutation in exon 11, however, a neomycin resistance gene flanked by two loxP sites was integrated in *Lmna* intron 10 blocking the transcription of the exons 11 and 12, and, consequently, preventing the transcription of lamin A and progerin. As a result of these manipulations, *Lmna*$^{LCS/LCS}$ mice express only lamin C (Osorio *et al.*, 2011). Interestingly, *Lmna*$^{LCS/LCS}$ mice did not exhibit any abnormal phenotype, consistent with other studies in mice showing that lamin A is dispensable in the nuclear lamina (Fong, 2006), while a complete knock-out of lamin A and lamin C (A-type lamins) causes premature death (Sullivan *et al.*, 1999; Lammerding *et al.*, 2004). Whether lamin A is also dispensable in humans remains unknown.

The generation of *Lmna*^{G609G} mice was accomplished by crossing *Lmna*^{LCS} mice with transgenic mice expressing ubiquitously the Cre recombinase (Osorio *et al.*, 2011). Using this strategy, we have recently generated and characterized mice with endothelial cell-, VSMC- and macrophage-specific progerin expression to assess the particular contribution of progerin in these cell types (Hamczyk *et al.*, 2018; del Campo *et al.*, 2019).

Other interesting mouse models were developed by Eriksson and collaborators to assess the relative importance of progerin specifically in skin, bone and teeth, tissues severely affected in HGPS patients. In a background of normal expression of the endogenous mouse *Lmna* locus,

Sagelius *et al.* designed two transgenic mouse lines, tetop-LA^{G608G} and tetop-LA^{wt}, using an inducible system that allows the expression of minigenes carrying human progerin or human lamin A protein, respectively, under the control of a tet-operon (Gossen and Bujard, 1992; Bockamp *et al.*, 2008; Sagelius, Rosengardten, Hanif, *et al.*, 2008). The system allowed the expression of human progerin or lamin A specifically in skin and osteoblasts/odontoblasts by crossbreeding tetop-LA^{G608G} and tetop-LA^{wt} mice with transgenic mice expressing K5 or Sp7 transactivators, respectively (K5tTA or Sp7tTA) (Sagelius, Rosengardten, Schmidt, *et al.*, 2008; Strandgren *et al.*, 2015). Remarkably, the skin or bone/tooth defects in these mutant mice were normalized by turning off progerin expression upon doxycycline treatment starting after the appearance of the phenotype. These studies show that the damage caused by ectopic progerin expression in skin and bone is reversible in these tissues in a context of mice with normal endogenous lamin A expression in the rest of the body (Sagelius, Rosengardten, Schmidt, *et al.*, 2008; Strandgren *et al.*, 2015). Nonetheless, in order to postulate definite conclusions, it is important to note that HGPS is a systemic disease in which progerin is expressed in many tissues, and patients express below normal levels of lamin A. Besides, the random integration of the minigenes into the mouse genome as well as the overexpression of lamin A in controls should be take into account.

All these mouse models allow to study the effect of tissue-specific expression of progerin, and some of them, the effect of removing progerin in particular tissues in a background of normal lamin A expression. However, it remains unknown whether it is possible to revert HGPS or slow down the progression of the disease at different stages by suppressing progerin ubiquitously or only in specific cell types in a context of whole-body progerin expression.

1.4.4. Large Animal Models for Progeria

HGPS mouse models allowed important advances in the understanding of the underlying mechanisms and molecular basis of progeria. Moreover, these models have also been useful for the testing of different therapeutic approaches. However, since the major complication in HGPS patients are cardiovascular alterations (Gordon, Rothman, *et al.*, 2014; Hamczyk, del Campo and Andrés, 2018), a more translational preclinical model in terms of cardiovascular pathology would be very helpful. Recently, our laboratory has reported the generation and characterization of the first minipig model for 'classical' HGPS, which was developed by somatic cell nuclear transfer using minipig skin fibroblasts that were modified to carry the heterozygous *LMNA* c.1824C>T

mutation (Dorado *et al.*, 2019). HGPS minipigs express lamin A, C and progerin and recapitulate the main features of HGPS patients, including diastolic dysfunction, MV degeneration, ECG abnormalities, growth retardation, facial and bone alterations, abnormal collagen deposition and premature death at an average age of 6 months (Dorado *et al.*, 2019). This new pig model will be very helpful in the analysis and testing of new therapeutic applications for HGPS patients.

1.5. Therapeutic Approaches In HGPS

HGPS is a fatal disease. Patients are born apparently normal and the symptoms appear gradually with time. The disease is typically diagnosed through genetic testing at 1-2 years of age, when symptoms have already manifested (Ahmed *et al.*, 2017; Gonzalo, Kreienkamp and Askjaer, 2017). In addition, HGPS is a very complex disease causing multiple alterations in many different functions that ultimately lead to premature death. For all these reasons, the development of treatments is urgently needed. Significant progress has been made since the discovery of *LMNA* mutations as the genetic mechanism causing HGPS (De Sandre-Giovannoli *et al.*, 2003; Eriksson *et al.*, 2003; Gordon, Rothman, *et al.*, 2014), which has prompted an exponential increase in research on the mechanisms underlying HGPS. All this knowledge has permitted major advances in the understanding of this disorder and in the development of advanced therapeutic approaches (Gordon, Rothman, *et al.*, 2014; Strandgren *et al.*, 2017).

Since HGPS is a genetic disorder caused by a mutant protein generated through aberrant splicing, several approaches have been therefore developed to treat HGPS at different levels: protein level (targeting protein function, turnover and post-translational modifications), RNA level (inhibition of aberrant exon 11 splicing) and DNA level (correction of the mutation).

1.5.1. Small Molecule-Based Therapies

As discussed above, cellular and animal studies strongly suggest that the toxicity of progerin and prelamin A is caused in large part by the retention of the farnesylated carboxyterminal region, which is removed in mature lamin A (Figure 1) (Pendás *et al.*, 2002; Navarro *et al.*, 2004, 2005; Young, Fong and Michaelis, 2005; Davies *et al.*, 2010; Yang *et al.*, 2011). The first therapeutic approaches have therefore focused on inhibiting prelamin A and progerin farnesylation using farnesyltransferase inhibitors (FTIs), which were originally developed for the treatment of some pediatric cancers. FTIs showed promising results in both progerin-expressing cells, reverting nuclear defects (Capell *et al.*, 2005; Mallampalli *et al.*, 2005; Toth *et al.*, 2005; Yang *et al.*, 2005),

and in animal models of HGPS, preventing cardiovascular alterations and prolonging life span (Fong, 2006; Yang, 2006; Capell *et al.*, 2008; Yang, Qiao, Fong, *et al.*, 2008).

Based on these positive results in cultured cells and animal models, the first clinical trial with HGPS patients targeted farnesylation using lonafarnib (Kieran, Gordon and Kleinman, 2007). Monotherapy with this FTI improved the rate of weight gain, vascular stiffness, bone rigidity, and sensorineural hearing, but was estimated to prolong survival only by 1.6 years (Gordon *et al.*, 2012; Gordon, Massaro, *et al.*, 2014). This limited benefit of lonafarnib may be due to an alternative geranylgeranylation of progerin occurring instead of farnesylation (Varela *et al.*, 2008). Since inhibition of prenylation (farnesylation and geranylgeranylation) using a combination of statins and aminobisphosphonates ameliorated the progeroid phenotype and extended lifespan in *Zmpste*$^{-/-}$ mice (Varela *et al.*, 2008), a 'triple-drug' clinical trial with lonafarnib, zoledronic acid and pravastatin was conducted in HGPS patients. The results of this trial revealed additional bone mineral density benefit compared with lonafarnib monotherapy, but the percentages of participants with carotid and femoral atherosclerotic plaques and extraskeletal calcifications increased (Gordon *et al.*, 2016). Because of these adverse effects, the addition of pravastatin and zoledronic acid was discontinued in HGPS clinical trials.

FTI-independent therapies have been developed in cellular and animal models. Larrieu *et al.* discovered a small-molecule compound called 'Remodelin' that inhibits the N-acetyltransferase NAT10. Treatment of HGPS cells with Remodelin restored nuclear morphology, improved chromatin organization, reduced DNA damage and senescence, and increased cell proliferation (Larrieu *et al.*, 2014). Remarkably, chemical targeting with Remodeling or genetic targeting of NAT10 improved the aging phenotype in progeric mice (Balmus *et al.*, 2018).

Other interesting strategies were based on vitamin D supplementation, blockade of ICMT-mediated methylation of progerin, and treatment with rapamacyn or retinoids to activate autophagy (Cao, Graziotto, *et al.*, 2011; Graziotto *et al.*, 2012; Ibrahim *et al.*, 2013; Kreienkamp *et al.*, 2016). Indeed, an ongoing clinical trial is testing in HGPS patients the combination of lonafarnib and everolimus, a derivative of rapamycin (Clinical trial reference number: NCT02579044).

The limited positive results in clinical trials could be due, at least in part, to differences between humans and mice. It is also important to keep in mind that all the previously described treatments were initiated in very young mice (4-5 weeks old) when disease symptoms are not

evident yet. Therefore, it is possible that the poor results in clinical trials are due to initiation of therapies in patients who already display severe symptoms, which might have caused irreversible damage. This possibility has never been tested in any mouse model with ubiquitous progerin expression.

1.5.2. RNA-Based Therapies

HGPS has a wide spectrum of symptoms and severity, from neonatal to adult-onset premature aging, which depends on the ratio of progerin-to-mature lamin A (Moulson *et al.*, 2007; Hisama *et al.*, 2011; Reunert *et al.*, 2012). Differences in the amount of progerin depend on the *LMNA* mutation, which determine the extent of the alternative splicing event that generates progerin instead of lamin A. Therefore, RNA-based therapies based on blocking this aberrant alternative splicing or modulating it towards lamin A production are promising strategies for progeria treatment (Scaffidi and Misteli, 2005; Osorio *et al.*, 2011; J. M. Lee *et al.*, 2016).

The first positive results were achieved treating HGPS patient derived-fibroblasts with morpholino antisense oligonucleotides to block the aberrant splicing in *LMNA* exon 11, which improved both nuclear morphology and mislocalization of nuclear envelope proteins (Scaffidi and Misteli, 2005; Piekarowicz *et al.*, 2019). An alternative RNA-based therapy was developed by Huang *et al.* using lentiviruses coding for a short hairpin RNA that targeted the progerin transcript variant in HGPS fibroblasts; however, the restoration of the phenotype was not complete, probably because an incomplete suppression of progerin mRNA (Huang *et al.*, 2005).

Since morpholino strategy showed promising results in *in vitro* studies, Osorio *et el.* treated knock-in *Lmna*^{G609G} mice with a combination of two different morpholinos. Injections started at 6 weeks of age and were repeated twice per week. This strategy improved most phenotypic and molecular alterations in progeroid mice, and significantly extended lifespan (Osorio *et al.*, 2011).

Lmna^{G609G} mice have been also treated with antisense oligonucleotides designed to shift alternative splicing to favor lamin C production (J. M. Lee *et al.*, 2016; Harhouri *et al.*, 2018). Treatment starting at 4 weeks of age (two injections per week) led to reduction of progerin levels and improvement in the aortic pathology, but effects on lifespan were not reported (J. M. Lee *et al.*, 2016).

1.5.3. Gene Therapy

HGPS is a very complex disease that affects multiple tissues, organs and functions. Because of this complexity, it is not surprising that drug-based strategies, either as monotherapy or in combination, are only yielding modest benefits (Gordon, Rothman, *et al.*, 2014; Gonzalo, Kreienkamp and Askjaer, 2017; Piekarowicz *et al.*, 2019). Therapies based in splicing corrections seem very promising for the treatment of muscular dystrophies, such as Duchenne Muscular Dystrophy, which has been treated effectively in preclinical models, although no successful clinical trial in humans has been reported yet (Alter *et al.*, 2006; Aoki *et al.*, 2010; Piekarowicz *et al.*, 2019). Additionally, RNA-based therapies imply the repeated administration of the therapeutic molecules throughout life. Several authors have recently started to develop and test permanent gene therapy strategies for HGPS (Strandgren *et al.*, 2017; Harhouri *et al.*, 2018). As progerin has a dominant negative effect, gene therapy should focus on blocking or removing the mutation, the primary cause of the disease (Goldman *et al.*, 2004; Scaffidi and Misteli, 2005; Gordon, Rothman, *et al.*, 2014).

The development of gene-editing technologies, together with improvements in delivery systems, have made possible *in vivo* gene therapy (Harhouri *et al.*, 2018). One of the most important and broadly used genome-editing technology nowadays is the clustered regularly interspaced short palindromic repeat/CRISPR- associated 9 (CRISPR-Cas9) system. CRISPR-Cas9 system involves a Cas9 endonuclease, and a single-guide RNA (sgRNA) consisting of a fusion on a CRISPR-RNA (crRNA) and a tran-activating crRNA (tracrRNA) (Ran *et al.*, 2013; Zarei *et al.*, 2019). The sgRNA directs the Cas9 endonuclease to the target sequence based on the specificity given by the crRNA via Watson-Crick base-pairing and the recognition of a protospacer-adjacent-motif (PAM). The cleavage generates a double strand break (DSB) that can be repaired by homologous directed repair (HDR) in the presence of a template producing a precise and defined modification in the genome (Ran *et al.*, 2013; Sander and Joung, 2014; Ahmad and Amiji, 2018; Zarei *et al.*, 2019). This technology offers significant advantages compared with other traditional methods of animal transgenesis such as higher efficiency, shorter time production or the lack of chimera formation (Zarei *et al.*, 2019).

Regarding delivery systems, the use of adeno-associated viruses (AAVs) has been gaining popularity during the last years because of their non-pathogenicity and ability to transduce a wide variety of cells, including both non-dividing and dividing cells. AAVs are also advantageous because of their capacity of inducing long-term transgene expression without transgene

integration in the host genome (Daya and Berns, 2008; Bass-Stringer *et al.*, 2018). Moreover, several AAVs serotypes (AAV 1-12) have been identified that differ in their capsid protein structures, conferring different tissue tropisms and, therefore, the possibility of implementing tissue-specific therapies. The AAV9 serotype has the broadest tissue tropism and the most robust expression compared with other serotypes (Zincarelli *et al.*, 2008; Finer and Glorioso, 2017; Bass-Stringer *et al.*, 2018).

Two recently published articles have provided proof-of-principle for *in vivo* gene therapy in HGPS mice using CRISPR-Cas9 technology (Beyret *et al.*, 2019; Santiago-Fernández *et al.*, 2019). Beyret *et al.* bred *Lmna*^{G609G} mice with mice expressing ubiquitously *S. pyogenes* Cas9. They also designed two sgRNA capable of downregulating laminA/progerin but not lamin C expression. Since HGPS is a systemic disease, AAV9s carrying these two sgRNA were systemically delivered thought intravenous facial injections into neonatal progeric mice expressing Cas9. Treated mice exhibited improved body appearance, less body weight loss, reduced VSMC degeneration, and a 25% increase in lifespan compared with untreated mice (Beyret *et al.*, 2019). Although these are promising results, caution must be taken regarding possible artefacts due to the mixed background among the mice that were used in this study (129, C57BL/6N, C57BL/6J and FVB/N) (Beyret *et al.*, 2019). Santiago-Fernandez *et al.* developed another gene-editing strategy using AAV9s carrying the *Staphylococcus aureus* Cas9 nuclease and a sgRNA capable of reducing progerin/lamin A accumulation without affecting lamin C levels. Despite the modest editing efficiency achieved, progeroid mice treated in postnatal day 3 showed a healthier appearance and other improvements, including a 26% increase in lifespan (Santiago-Fernández *et al.*, 2019). Both studies have raised hopes in the potential use of CRISPR-Cas9 as a gene therapy strategy for the treatment of HGPS patients. Nonetheless, more research is still needed regarding the possible negative effects of potential off-targets and the consequences of the elimination of lamin A in humans (Beyret *et al.*, 2019; Santiago-Fernández *et al.*, 2019).

Moreover, it is important to note that the above-mentioned gene therapy studies started the treatment in neonates, which were apparently normal. As mentioned above, this limitation also applies to other therapies based in drugs or RNA correction/elimination. Indeed, since HGPS is a progressive disease and children are diagnosed when they have prominent symptoms, all treatments in preclinical models should be tested once disease symptoms are evident in progeroid mice. In addition, taking into account that there are children affected with HGPS of all ages, defining the time-window when a therapy is more effective is extremely important.

OBJECTIVES

2. OBJECTIVES

HGPS is a fatal genetic disease characterized by accelerated aging and premature death. Patients appear normal at birth and symptoms develop gradually over time, therefore the diagnostic is typically established at 1.5-2 years of age, when patients already manifest an obvious phenotype (Ahmed *et al.*, 2017; Gonzalo, Kreienkamp and Askjaer, 2017). During the last decade, much progress has been made in understanding the mechanisms underlying progerin-induced premature aging and in the development of therapeutic approaches (Gordon, Rothman, *et al.*, 2014; Dorado and Andrés, 2017; Hamczyk, del Campo and Andrés, 2018). Indeed, several treatments have been developed that yielded positive results in cells and in animal models of HGPS (Harhouri *et al.*, 2018). Although some of these strategies have been tested in clinical trials, none is curative and the therapeutic benefits achieved have been very limited (Gordon *et al.*, 2012, 2016).

Besides, all anti-HGPS therapies tested so far in preclinical studies have used very young animals, which have not shown any obvious phenotype. Therefore, further research is needed to ascertain if the damage caused by progerin can be reverted once symptoms are already present, or if disease progression can be stopped or delayed when treatment is started late in life. It is also essential to assess whether therapies need to be ubiquitous, or whether tissue or organ specific approaches might be adequate to yield significant benefit. To address these questions, the main objectives of this Doctoral Thesis are the following:

1. To generate *Lmna*^{HGPSrev}, the first progeroid mouse model engineered to allow a controlled spatio-temporal suppression of progerin expression and restoration of wild-type lamin A expression.
2. To characterize the phenotype of *Lmna*^{HGPSrev} mice.
3. To study the progression of HGPS upon progerin elimination and lamin A restoration early and late in life in progeroid mice by:
    a. Generating a HGPS mouse model that allows tamoxifen-dependent ubiquitous progerin suppression and lamin A restoration.
    b. Using a systemic AAV-based gene therapy strategy.

MATERIAL & METHODS

3. MATERIAL & METHODS

3.1. Animal Care and Models

All mice used in this study had C57BL/6J genetic background. Both males and females were proportionally included in the experiments, except otherwise stated. *Lmna*^{G609G} (Osorio *et al.*, 2011) and *Ubc-CreERT2* (Ruzankina *et al.*, 2007) mice were kindly provided by the lab of Carlos López-Otín and Mariano Barbacid, respectively. *Lmna*^{HGPSrev} mice were generated as part of this Doctoral Thesis (see below). We crossed *Lmna*^{HGPSrev} mice with *Ubc-CreERT2 mice* to generate time-conditional Cre expressing mice with the Cre transgene in heterozygosis. With the exception of longevity studies, experiments were performed at 13-15, 15-18, 30-34, 40-43, or 50-53 weeks of age (see details in figure legends).

Mice were maintained in the animal facility of the Centro Nacional de Investigaciones Cardiovasculares Carlos III (CNIC). All animal procedures were performed conformed to EU Directive 2010/63U and Recommendation 2007/526/EC regarding the protection of animals used for experimental and other scientific purposes, enforced in Spanish law under Real Decreto 1201/2005, and were approved by the local ethics committees and the Animal Protection Area of the Comunidad Autónoma de Madrid (PROEX 051/18).

3.2. Generation of *Lmna*^{HGPSrev} Mice

We aim to generate a conditional mouse model that expresses progerin ubiquitously and that allows a controlled spatio-temporal suppression of progerin with simultaneous restoration of lamin A expression. To this end, we used the CRISPR-Cas9 system and an adequate sgRNA and a dsDNA donor template to repair by HDR the DSB generated by Cas9.

3.2.1. sgRNA Design and Validation

Using the information provided by http://crispr.mit.edu/, we designed two sgRNAs targeting the murine *Lmna* intron 10 (sgRNA_1 and sgRNA_2, See Table 2 and Figure 2A), which were purchased from ID Technologies. The pCRISPR U6 Cas92AeGFP (coding for both Cas9 and

green fluorescent protein, GFP) plasmid was kindly provided by the CNIC's Viral Vectors Unit (Figure 2B).

Table 2: crRNA sequences and data from http://crispr.mit.edu/

sgRNA	crRNA Sequence 5' → 3' + (PAM)	Score of faithfulness (over 100%)	Off-Targets
sgRNA_1	CCCATAAGTGTCTAAGATTC + (AGG)	82%	119, all with score <0.3%
sgRNA_2	GCCACAGCTCTTTATTTCGA + (AGG)	81%	141, all with score <0.3%

Digestion and ligation

The pCRISPR U6 Cas92AeGFP plasmid and sgRNA_1 and sgRNA_2 were digested at 37°C for 4 hours with *BrsGI* and *SpeI* restriction enzymes (R0575S, R0133S, New England Biolabs) using NEBbuffer 2.1 (B7202S, New England Biolabs). The DNA plasmid fragments were separated with 2% agarose gel electrophoresis and the biggest fragment was purified using Zymoclean™ Gel DNA Recovery Kit (D4007, Zymo Research). The purified plasmid fragment was incubated with Antarctic Phosphatase (M0289, New England Biolabs) for 1 hour at 37°C and then for 5 minutes at 70°C to inactivate the phosphatase.

pCRISPR U6 Cas92AeGFP plasmid was ligated to sgRNA_1 or sgRNA_2 using T4 DNA Ligase (M0202S, New England Biolabs) (16°C for 2 hours). The same preparation lacking the sgRNA was used as a negative control.

Transformation of cells and ligation validation

Each ligation product carrying sgRNA_1 or sgRNA_2 was mixed with 50 µL of ice-cold *E. coli* DH5α competent cells. The mixture was incubated for 30 min in an ice bath, then for 90 seconds at 42°C, followed by 2 minutes in an ice bath. Then, 300 µL of sterile Luria-Bertani (LB) medium was added and cell suspensions were incubated at 37°C for 60 min to induce bacterial cell growth. Cell were then spread on agar plates for overnight incubation at 37°C. Next day, single colonies were inoculated and cultured at 37°C overnight in 4 mL of LB medium supplemented with 50 mg/mL ampicillin. Part of this culture was used to isolate the plasmids and check the ligation using Wizard® Plus SV Minipreps DNA Purification System (A1330, Promega) and

digesting for 4 hours at 37°C with *MluI* restriction enzyme in NEBbuffer 3 (R0198S, New England Biolabs).

A

sgRNA_1

BsrGI

5' ccata**TGTACA**CTTACCGTAACTTGAAAGTATTTCGATTTCTTGGCTTTATATATCTTGTGGAA
AGGACGAGGTACCG**CCCATAAGTGTCTAAGATTCGTTTTAGAGCTAGAAAT**AGCAAGTT
AAAATAAGGCTAGTCCGTTATCAACTTGAAAAAGTGGCACCGAGTCGGTGCTTTTTTT
ACGCGTACTAGTcgcta **3'**

MluI *SpeI*

sgRNA_2

BsrGI

5' ccata**TGTACA**CTTACCGTAACTTGAAAGTATTTCGATTTCTTGGCTTTATATATCTTGTGGAA
AGGACGAGGTACCG**GCCACAGCTCTTTATTTCGAGTTTTAGAGCTAGAAAT**AGCAAGTT
AAAATAAGGCTAGTCCGTTATCAACTTGAAAAAGTGGCACCGAGTCGGTGCTTTTTTT
ACGCGTACTAGTcgcta **3'**

MluI *SpeI*

B

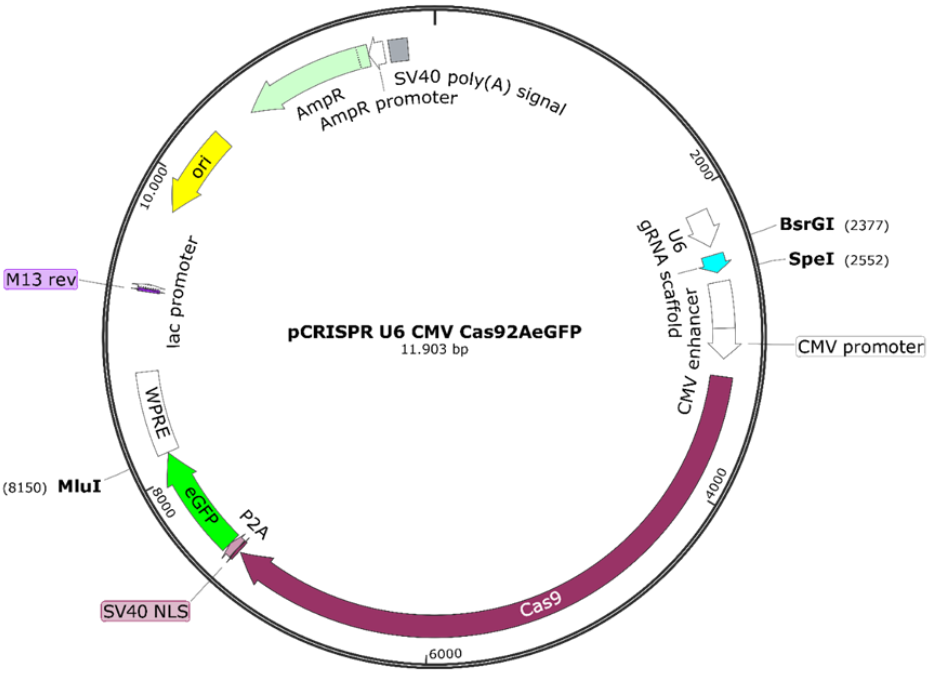

Figure 2: sgRNA sequences and pCRISPR U6 CMV Cas92AeGFP plasmid. A) Sequence of sgRNA_1 and sgRNA_2 crRNA in red/green. Nucleotides complementary to DNA target are underlined, and tracrRNA is in black. Other sequences correspond to restriction enzymes and part of the U6 promoter that is not transcribed. **B)** pCRISPR U6 CMV Cas92AeGFP plasmid showing the restriction enzyme sites used to clone sgRNA sequences. The plasmid carries a Cas9 nuclease cDNA with expression controlled by a CMV promoter, followed by a 2A self-cleaving peptide (P2A) and the DNA coding enhanced green fluorescent protein (eGFP).

The remaining culture from colonies with the correct cloned vector were transferred to 300 mL of LB medium containing 50 mg/mL ampicillin and incubated at 37°C overnight to isolate plasmidic DNA with the NucleoBond® Xtra Maxi kit (740414, Macherey-Nagel). Maxiprep products were quantified using a NanoDrop ND-1000 spectrophotometer (ThermoScientific) and were used for transfection of mouse embryonic fibroblasts (MEFs).

Transfection of MEFs

Wild-type C57BL/6J MEFs were prepared as described in Material and Methods (section 3.4 and 3.5). MEFs were seeded in 24-well plates at a density of 1 x 10^5 cells/well in 500 µL of Dulbecco's Modified Eagle Medium (DMEM, 41968-039, Sigma-Aldrich) supplemented with 10% fetal bovine serum (FBS, F7524, Sigma-Aldrich) without antibiotics. When cultures reached 90-95% confluence, cells were transfected following the manufacturer's instructions using 3 µL Lipofectamine™ 2000 (11668-027, Invitrogen) and 650 ng of each of the purified plasmids carrying either sgRNA_1 or sgRNA_2. Non-transfected MEFs were used as negative control.

Cell Sorting

Transfected and non-transfected MEFs were collected and resuspended in FACS buffer (1% FBS/PBS). Cells were sorted to >99% purity using a BD FACS AriaII cell sorter. To avoid cellular debris, cells were gated based in their relative size and complexity. Doublets were avoided using FSC and SSC width and height signals. Negative, non-transfected cells were used to determinate the gate position for GFP positive cells. GFP positive and GFP negative cells from non-transfected cultures were collected in 10% FBS/PBS and used for genomic DNA isolation.

Isolation of genomic DNA, target amplification and purification

Genomic DNA from GFP positive and negative cells was isolated using DNeasy Blood & Tissue Kit (69504 Qiagen). Cas9 DNA target (sequence of *Lmna* gene) was amplified by using the Polymerase Chain Reaction (PCR) (Mullis and Faloona, 1987). Table 3 shows the conditions and oligonucleotides used for the reaction mixture. PCR purification was performed using QIAquick PCR Purification Kit (28104 Qiagen) according to the manufacturer's instructions. PCR purification products were quantified using a NanoDrop ND-1000 spectrophotometer.

Table 3. PCR conditions and sequence of forward and reverse primers used to amplify Cas9 target.

Temperature	Time
95 °C	4 min
95 °C	35 sec
60 °C	30 sec
72 °C	60 sec
72 °C	5 min
4 °C	O/N
30 cycles	

Forward (5' → 3') CCCATTGCATGCACACTTCT
Reverse (5' → 3') AGCTTCGAGTGACTGTGACA
Amplicon size: 573 bp

Heteroduplex formation and T7 nuclease assay

Heteroduplex formation of purified PCR products (from GFP positive cells transfected with sgRNA_1 or sgRNA_2 and from non-transfected cells) was performed using the following cycles of incubation: 95°C, 10 min; 95°C–85°C, decrease 2°C/s; 85°C, 1 min 85°C–75°C, decrease 0.3°C/s; 75°C, 1 min; 75°C–65°C, decrease 0.3°C/s; 65°C, 1 min; 65°C–55°C, decrease 0.3°C/s; 55°C, 1 min; 55°C–45°C, decrease 0.3°C/s; 45°C, 1 min; 45°C–35°C, decrease 0.3°C/s; 35°C, 1 min; 35°C–25°C, decrease 0.3°C/s; 25°C, 1 min; 25°C–4°C, decrease 0.3°C/s; 4°C hold.

T7 nuclease assay with T7 endonuclease I and T7 buffer (M0302S New England Biolabs) was performed according to manufacturer's instructions using 350 ng of each sample. Purified PCR products from both GFP positive cells carrying the different sgRNAs and non-transfected cells were treated or not with T7 endonuclease. The digested products were visualized in a 1.5% agarose gel electrophoresis.

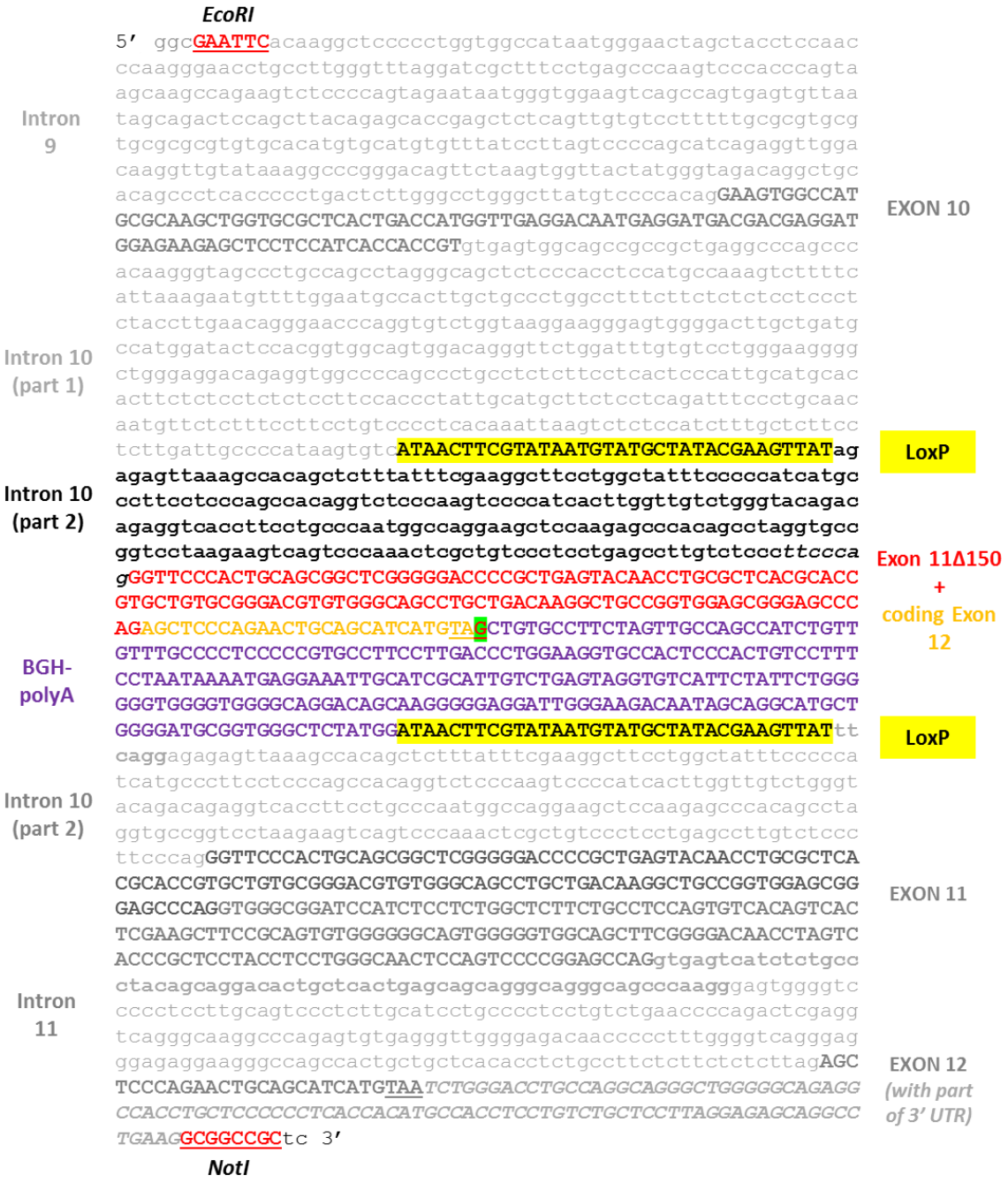

Figure 3: Sequence of the dsDNA donor template used to generate the *Lmna*^{HGPSrev} mouse model by CRISPR-Cas9 gene editing and HDR. The *Lmna* gene sequence used as a reference is the one available on the NCBI gene database (Gene ID: 16905, Chromosome 3, NC_000069.6, 88481148.88509932, complement). The 672-bp insert contains two loxP sites (highlighted in yellow), part of intron 10 (typed in black boldface), the first 117 bp of exon 11 (typed in red boldface), the coding sequence of exon 12 (typed in orange boldface), and a transcriptional stop signal (typed in purple boldface). The left (938 bp) and right (877 bp) homology arms are in light gray. Underlined red nucleotides show the restriction enzyme sites *EcoRI* (5′) and *NotI* (3′) used for cloning the dsDNA donor template in a pcDNA3.1 expression vector (GenScript). Highlighted in green is a single base change coding for a different stop codon to avoid the generation of an alternative splice site.

3.2.3. dsDNA Donor Template

As a reference, we used the murine *Lmna* genomic DNA sequence available in the NCBI gene database (Gene ID: 16905, Chromosome 3, NC_000069.6, 88481148.88509932, complement). For progerin we used the predicted mRNA sequence (*Lmna*Δ150) after aberrant splicing between exons 11 and 12 when the mouse *Lmna* c.1827C>T mutation is present. For HDR, we used a dsDNA donor template of 2494-bp that was synthetized and cloned with *EcoRI* and *NotI* restriction enzymes in a pcDNA3.1 vector (Figure 3). The dsDNA donor template contains a 938-bp left homology arm (*Lmna* intron 9, exon 10, part of intron 10), a 672-bp insert harboring a loxP-flanked cDNA of exons 11 and 12 from the *Lmna*Δ*150* (exon11Δ*150* and coding sequence of exon 12), followed by a bovine growth hormone polyadenylation (BGH-polyA) transcriptional stop signal, and an 877-bp right homology arm (part of *Lmna* intron 10, exon 11, intron 11 and part of exon 12). Additionally, the 2494-bp dsDNA donor template contained seven residual nucleotides from digested restriction enzyme sites (see section 2.4). Because the insert harbors the sequence of exon 11 and exon 12 that encodes for progerin, exon 11 lacks the last 150 nucleotides and exon 12 does not have the 3'UTR region. The endogenous wild-type sequence of the *Lmna* gene should remain intact downstream the 672-bp insertion.

3.2.4. Isolation and Purification of dsDNA Donor Template

Transformation of cells:

E. coli DH5α competent cells were transformed with 30 ng of plasmid containing donor template as previously described in section 3.2.1.

Isolation, digestion and sequencing of plasmid and dsDNA donor template:

Plasmid DNA from transformed cells was purified with NucleoBond® Xtra Maxi kit (740414, Macherey-Nagel). Plasmid DNA sequencing was done at Centro Nacional de Investigaciones Oncológicas (CNIO) using the primers shown in Table 4.

Table 4: Primers used for sequencing the dsDNA donor template cloned into pcDNA3.1 vector

Oligonucleotide (5' → 3')	
GCGAATTCACAAGGCTCCC	GTGAGGGTTGGGGAGACAA
GCATCAGAGGTTGGACAAGG	CCTTGTCCAACCTCTGATGC
CTGGTAAGGAAGGGAGTGGG	CATCCTCGTCGTCATCCTCA
TCTTCCTCTTGATTGCCCCA	GAGTGAGGAAGAGAGGCAGG
GAACTGCAGCATCATGTAGCT	GAGGGGCAAACAACAGATGG
TGGGAAGACAATAGCAGGCA	GCAGAAGAGCCAGAGGAGAT
CCATCTCCTCTGGCTCTTCT	TTCAGGCCTGCTCTCCTAAG

After sequencing, the plasmid was digested with *EcoRI* and/or *NotI* restriction enzymes (R0101S, R0189S, New England Biolabs) in NEBbuffer 3 at 37°C for 4 hours followed by 20 minutes at 65°C. Linear DNA fragments were separated in 1% agarose gel electrophoresis. The fragment containing the dsDNA donor template was isolated using Zymoclean™ Gel DNA Recovery Kit. Donor template quality, purity and concentration were assessed by separation in 0.7% agarose gel electrophoresis and by using a NanoDrop ND-1000 spectrophotometer. Purified dsDNA donor template was sequenced using the primers shown in Table 5 and was prepared for microinjection.

Table 5: Primers used for sequencing the purified dsDNA donor template

Oligonucleotide (5' → 3')	
CCATCTCCTCTGGCTCTTCT	GAGTGAGGAAGAGAGGCAGG
GTGAGGGTTGGGGAGACAA	GAGGGGCAAACAACAGATGG
CCTTGTCCAACCTCTGATGC	GCAGAAGAGCCAGAGGAGAT
CATCCTCGTCGTCATCCTCA	TTCAGGCCTGCTCTCCTAAG

3.2.5 Harvesting Donor Zygotes for Microinjection

Mice on a C57BL/6J genetic background obtained from Charles River Laboratories were used for the microinjection session. Hormonal superovulation was induced to a batch of ten immature female mice (3-5 weeks of age) by intraperitoneal injection of hormones. First, female mice received at 10:00 am an intraperitoneal injection of 0.1 mL (5 IU) of pregnant mare serum gonadotropin. Forty eight hours later, they received an intraperitoneal injection of 0.1 mL (5 IU) of human chorionic gonadotropin. Immediately after last injection, animals were mated with

appropriate stud males. Next day at 8:00 am, female mice were checked for vaginal plugs, and those positive for the plug were sacrificed. To obtain the zygotes for the microinjection session, the oviducts from sacrificed females were extracted and transferred to 2-mL Eppendorf tubes containing 1 mL of M2 culture medium (M7167, Sigma-Aldrich). The oviducts were then transferred to a 35-mm dish containing 2 mL of M2 medium and 350 µg/mL of Hyaluronidase (H3884, Sigma-Aldrich). Each ampulla was localized and torn open to release the "cumulus mass", consisting of oocytes and cumulus complexes. Oocytes were separated from surrounding cumulus cells after incubation at 37°C for 1-2 minutes, and then were transferred to fresh M2 medium for washing. Fertilized oocytes (zygotes) were incubated in culture medium Evolve-KSOM (modified embryonic culture medium KSOMaa; ZEKS-050, Zenith Biotech) at 37 °C in a 5% CO_2 / 5% O_2 atmosphere, until they were ready for pronuclear microinjection (Behringer *et al.*, 2014).

3.2.6. Microinjection of the Transgene DNA Construct into Mouse Zygotes

Microinjection Solution

Microinjection solution contained the following components at the indicated final concentrations:

- 0.61 µM sgRNA [0.61 µM crRNA and 0.61 µM tracrRNA (Integrated DNA Technologies, IDT)] (Table 6).
- *Streptococcus pyogenes* Cas9 endonuclease, with nuclear localization signal (NLS) (PNA Bio, Cat. CP01-50), 30 ng/µL.
- dsDNA donor template (2.494-pb): 4.5 ng/µL (Figure 3).
- 10x microinjection buffer: 100 mM Tris-HCl pH 7.5, 1.0 mM EDTA. Dissolved in nuclease free H_2O to a final 1x concentration.

Table 6: crRNA and tracrRNA sequences used for microinjection

	Sequence 5' → 3'
crRNA	CCCAUAAGUGUCUAAGAUUCGUUUUAGAGCUAUGCUGUUUUG
tracrRNA	AGCAUAGCAAGUUAAAAUAAGGCUAGUCCGUUAUCAACUUGAAAAAGUGGCACCGAGUCGGUGCUUU

First, sgRNA was generated by mixing and incubating crRNA and tracrRNA at room temperature for 15 minutes. Cas9-NLS was then added to the mixture and the solution was incubated at 37°C for 15 minutes to form the Cas9-sgRNA complex. Next, the dsDNA template was added to complete de microinjection solution. Finally, the solution was centrifuged at 15000 g at room temperature for 10 minutes and maintained on ice during all the microinjection protocol (Aida *et al.*, 2015).

Microinjection of Zygotes

Zygotes were microinjected with 1-2 pL of microinjection solution. Microinjection platform consisted on a 35-mm glash bottom dish containing one central drop of M2 medium with the zygotes and sterile paraffin oil (ZPOL-500, Zenith Biotech) covering the M2 medium to avoid evaporation. The microinjection chamber is under a ZEISS AxioObserver D-1 inverted optical microscope. Zygotes were manipulated and held by suction using glass holding pipettes (MPHL-30, LG uPipets Holding, LifeGlobal). Injection pressure was given and controlled by an electronic automatic microinjector (FemtoJet, Eppendorf) and was adjusted to 100-150 hPA depending on the needle opening. The micro-handling was done using an electronic system (TransferMan NK2, Eppendorf) (Behringer *et al.*, 2014) .

The microinjected zygotes were transferred to 60-mm plastic dishes containing pre-incubated Evolve-KSOM culture medium to wash them twice. Zygotes were incubated overnight at 37°C - 5% CO_2 - 5% O_2 in Evolve-KSOM medium to reach the two-cell stage (Behringer *et al.*, 2014).

3.2.7. Implantation of Microinjected Zygotes into Pseudo-Pregnant Recipient Mice

One day before the two-cell stage embryo transfer, female mice were mated with vasectomized mice, and those with a vaginal plug were used as pseudo-pregnant mice for the transfer. The two-cell stage embryo transfer was performed using a sterile glass needle through the infundibulum of female mice. Most recipient mice were pregnant and delivered a total of 34 pups after 20 days from 2 different microinjection sessions (21 pups from session #1 and 13 from session #2). Three weeks later, pups were weaned from their mothers and genotyped (see section 3.2.8). Mice positive for the transgene were called ‘founders’ and the transgenic mouse lines with the desired genetic modification were established from them (Behringer *et al.*, 2014).

3.2.8. Identification of Founders

PCR analysis

To identify mice carrying the *Lmna*^{HGPSrev} allele, we performed PCR analysis of genomic DNA from the 34 mouse pups using the primers shown in blue in Table 7.

Genomic DNA from the 8 pups carrying the mutant allele (the insert) was analyzed by PCR to verify the presence of only one copy and the proper localization of the insert in the *Lmna* locus using the primers shown in green in Table 7.

DNA extraction and Sequencing

Genomic DNA was extracted from *Lmna*^{HGPSrev} founder mice following standard Proteinase K (19131, Qiagen) protocols. DNA sequencing was performing by the CNIO using the primers listed in Table 8 (see also Figure 8).

Table 7: PCR conditions and sequence of primers used for identifying founder *Lmna*^{HGPSrev} mice

Temperature	Time
95 °C	4 min
95 °C	35 sec
62 °C	30 sec
72 °C	60 sec
72 °C	5 min
4 °C	O/N
36 cycles	

Forward (5' → 3') CCTTCCACCCTATTGCATGC
Reverse (5' → 3') TTCAGGCCTGCTCTCCTAAG
Amplicon size: **WT**: 1000 bp
Insert: 1670 bp

Temperature	Time
95 °C	4 min
95 °C	35 sec
61 °C	30 sec
72 °C	60 sec
72 °C	5 min
4 °C	O/N
36 cycles	

Reaction 1
Forward (5' → 3') CATCTGTTGTTTGCCCCTCC
Reverse (5' → 3') CTTTCCCTGGGCTCCTAGAG
Amplicon size: **WT**: -
Insert: 1337 bp

Reaction 2
Forward (5' → 3') AGAGTCGGTTGAACTCCCTG
Reverse (5' → 3') CATGATGCTGCAGTTCTGGG
Amplicon size: **WT**: 2137 bp
Insert: 1776 bp and 2821 bp

WT: Wild-type

Table 8: Primers used for sequencing part of *Lmna* gene from founder *Lmna*^{HGPSrev} mice

Oligonucleotide (5' → 3')	
CATCTGTTGTTTGCCCCTCC	AGAGTCGGTTGAACTCCCTG
GCAGAAGAGCCAGAGGAGAT	CGCTCTCATCAACTCCACTG
TTCAGGCCTGCTCTCCTAAG	GCATCAGAGGTTGGACAAGG
CTTTCCCTGGGCTCCTAGAG	TCTTCCTCTTGATTGCCCCA
TGGGAAGACAATAGCAGGCA	GAACTGCAGCATCATGTAGCT
CCATCTCCTCTGGCTCTTCT	TTGTCTTCCCAATCCTCCCC
GTGAGGGTTGGGGAGACAA	CCTTGTCCAACCTCTGATGC
GAGTGAGGAAGAGAGGCAGG	

3.3. DNA Genotyping

Genomic DNA was extracted from mouse tails following standard Proteinase K procedures. *Lmna*^{HGPSrev} mice genotyping was performed with the oligonucleotides and PCR conditions shown in Table 9.

Table 9: PCR conditions and sequence of oligonucleotides used for genotyping

Locus	Forward (5' → 3')	Reverse (5' → 3')	Amplicon size (bp)
***Lmna*^{HGPSrev}**	TCTTCCTCTTGATTGCCCCA	TAGCCAGGAAGCCTTCGAAA	**WT**: 84 **HT:** 84, 107, 750 **HM:** 107, 750
***Ubc-CreERT2*^{tg}**	CGGTCGATGCAACGAGTGATGAGG	CCAGAGACGGAAATCCATCGCTCG	**WT**: - **HT:** 700

WT: Wild-type; HT: Heterozygous; HM: Homozygous

Temperature	Time
95 °C	4 min
95 °C	35 sec
72 °C	60 sec
72 °C	5 min
4 °C	O/N
30 cycles	

Anniling temperature:	
***Lmna*^{HGPSrev}**	62 °C
***Ubc-CreERT2*^{tg}**	55 °C

3.4. Isolation of MEFs

Embryos isolated at embryonic day 13.5 (E13.5) were placed on ice-cold PBS. After removing the head (used for genotyping) and liver, embryo bodies were minced and then incubated for 20 minutes with 2x Trypsin-EDTA (0.5% Trypsin 0.53 mM EDTA•4Na) (15400-054, Invitrogen). MEFs from each embryo were plated separately into 10 cm dishes and incubated at 37°C in 5% CO_2 with DMEM supplemented with 10% heat-inactivated FBS, 5% penicillin/streptomycin (15140-122, Gibco), and 5% L-glutamine (SH30034.1 Hyclone) (complete growth medium). MEFs were then frozen at Passage 2 in 90% FBS/10% DMSO (Dimethyl sulfoxide, A3672, AppliChem).

3.5. Immortalization of MEFs

HEK293T cells were seeded at 5 x 10^6 cells per well in 100 mm dishes. Cells were transfected with pCL-Puro-SV40 LT retroviral vector for immortalization (13970, Addgene) and pCL-ECO retroviral packaging plasmid (kindly provided by Dr. Manuel Serrano) using Fugene 6 (E2692, Promega) following the manufacturer's instructions. Transfected HEK293T cells were incubated for 48 hours at 37°C / 5% CO_2 in complete growth medium. Next, supernatants containing retroviral particles were harvested each 12 hours for two days and used to infect MEFs.

For immortalization, primary MEFs were plated at 2.5 - 5 x 10^5 cells in a 100 mm dish in complete growth medium. Four rounds of infection were done sequentially during the following 48 hours. Briefly, supernatants containing retroviruses were filtered through a 0.45 µm filter, mixed with polybrene at a final concentration of 8 µg/mL (9268-5G, Sigma Aldrich), and added to each dish. Infected MEFs were serially passaged to select immortalized cells by adding 2 µg/mL puromycin (P8833, Sigma-Aldrich). All experiments using MEFs were done with immortalized cells coming from the same embryo (one of each genotype).

3.6. Transfection of MEFs

We used a *piggyBac* transposon-based expression system (Zhao *et al.*, 2016) for the generation of MEFs expressing tamoxifen-inducible Cre recombinase. Immortalized MEFs were seeded at 80% of confluence and were transfected using 18 µL of TransIT-LT1 Transfection Reagent (MIR2300, GeneFlow) mixed with 1.5 µg of pPB CAG ER-Cre-ER IRES Zeocin (transposon) (Cheetham *et al.*, 2018), and 4.5 µg of pCMV-hyPBase (transposase) (Yusa *et al.*, 2011) and

DMEM medium without any supplement. Medium was changed 6 hours post-transfection and zeocin-resistant cells were selected by incubation for at least 10 days in the presence of 400 µg/mL zeocin (R25005, Thermo Fisher).

3.7. Proliferation Assay

Lmna$^{HGPSrev/HGPSrev}$ and *Lmna*$^{+/+}$ immortalized MEFs were seeded at the same number in 24-well plates. Next day, the drugs shown in Table 10 were added to different wells, and plates were transferred into an IncuCyte microscope (Essen BioScience). Phase contrast pictures were acquired every 4 hours during 6 days in each well (9 pictures per well). Percentage of cell confluence was calculated by the Cell Player integrated software (Essen BioScience) and represented with GraphPad Prism® software. Proliferation assays were performed twice with cells treated with Camptothecin (CPT) and once with cells treated with Olaparib, Aphidicolin and 4-nitroquinoline 1-oxide (4NQO).

Table 10: Drugs and concentrations used for proliferation assays

Drugs	Concentration
Aphidicolin	0.2µM – 0.5µM
Camptothecin	35 nM - 75 nM
4-nitroquinoline 1-oxide	250 nM - 400 nM
Olaparib	7 µM - 15 µM

3.8. Protein Extraction and Western Blot

Cells were directly lysed in the cell-culture plates by scraping in SDS lysis buffer (4% SDS, 20% glycerol, and 120 mM Tris-HCl, pH 6.8). Extracts were boiled for 5 min at 95°C, and then subjected to 10 strokes through a 25-gauge needle. Absorbance at 280 nm was measured in a NanoDrop ND-1000 spectrophotometer to determine protein concentration. Protein extracts were frozen at -80°C until further use.

Mice were euthanized by CO_2 inhalation and tissues were collected, frozen in liquid nitrogen and preserved at -80°C until further use. In order to obtain a representative sample, frozen tissues were crushed and subsequently homogenized in a TissueLyser (Qiagen) using lysis buffer (50 mM Tris HCK pH 8.8, 2% SDS, 8 M Urea, 2 M Thiourea) suplemented with protease inhibitors (11836145001, Roche) and PhosSTOP phosphatase inhibitors (04906837001, Sigma-

Aldrich). Lysates were sonicated with a Bioruptor Sonication System (Diagenode) coupled to a Neslab RTE 7 Circulating Chiller (Thermo Fisher Scientific) and centrifuged at 4°C for 30 minutes. Protein concentration was determined by the Bradford method (Bradford, 1976).

Equal amounts of protein were separated by SDS-PAGE gels and transferred to an Immobilon-FL polyvinylidene fluoride membranes (IPVH00010, Millipore) using a transfer apparatus according to the manufacturer's protocols (Bio-Rad). Membranes were incubated for 60 minutes in 5% BSA in Tris-buffered saline supplemented with Tween 20 (TBS-T; 20 mM Tris-HCL at pH 7.4, 150 mM NaCl, 0.05% Tween 20). This was followed by an overnight incubation at 4°C with the following antibodies diluted in TBS-T with 2.5% BSA: anti-lamin A/C (1:200, SC-6215 and 1:1000, SC-376248, Santa Cruz Biotechnology) and anti-GAPDH (1:12000, MAB374, Millipore). Membranes were washed three times for 10 minutes each with TBS-T and then were incubated with appropriate horseradish peroxidase-conjugated secondary antibodies (Santa Cruz Biotechnology) diluted in TBS-T with 2.5% BSA. Finally, blots were washed three times with TBS-T, incubated with Luminata Forte chemiluminescent HRP substrate (Millipore) and imaged using an ImagenQuant LAS 4000 mini (GE Healthcare). Band intensity was quantified using Fiji software (ImageJ 1.51a x64).

3.9. Immunofluorescence Staining

Lmna$^{HGPSrev/HGPSrev}$ and *Lmna*$^{+/+}$ immortalized MEFs were seeded at the same number in 24-well plates. All incubations for immunofluorescence staining were performed at room temperature. Next day, cells were washed with 1x PBS and fixed with 4% paraformaldehyde for 10 minutes. Paraformaldehyde was removed and cells were washed with 1x PBS three times, followed by 5 minutes of permeabilization with PBS-0.2% Triton X-100 (9002-93-1, Sigma-Aldrich). Permeabilized cells were incubated for 30 minutes with blocking buffer (10% BSA 0.1% Tween 20 in PBS) and subsequently for 30 minutes with primary anti-γH2AX antibody (05-636, Millipore) diluted 1:500 in blocking buffer. MEFs were washed three times with 0.2% Tween 20 in PBS and then incubated for 30 minutes with Alexa Fluor-594 anti-mouse secondary antibody (1:500, A-21203, ThermoFisher). Cells were mounted with Antifade Mounting Medium with DAPI (H-1200, Vectashiel) and examined using a Leica SP5 DMI 6000B confocal microscope. The procedure for image processing and quantification of DNA damage was developed as a macro in Fiji (ImageJ 1.51a x64). Nuclei were segmented from DAPI channel by using automated thresholding with Triangle method (Zack, Rogers and Latt, 1977) after noise reduction with a

median filter (radius=3 pixels). Final cell segmentations were achieved splitting touching cells by using morphological opening (disk of radius=5 pixels as structuring element), and watershed irregular features (Brocher, 2015) (erosion=1, convexity threshold=0.5, separator size=0-50 pixels). Mean intensity of the γH2AX channel was measured in each individual cell. To allow direct comparison of different experiments, intensity values were normalized by computing Z-score in each individual batch/experiment using wild-type cells as negative control. This batch normalization procedure and aggregation of values to compute mean normalized γH2AX values in each image was performed in Matlab R2018b.

Thoracic aorta and aortic arch segments were fixed in 4% paraformaldehyde for 24 hours, embedded in paraffin, cut into 5 µm sections, deparaffinized and rehydrated. Antigen retrieval was performed using 10 mM sodium citrate buffer (pH 6). Sections were then blocked and permeabilized for 1 hour at room temperature in PBS containing 0.3% Triton X-100, 5% BSA, and 5% normal goat serum (005-000-001, Jackson ImmunoResearch). Next, samples were incubated overnight at 4°C with the following antibodies: anti-smooth muscle α-actin (SMA-Cy3, 1:200, C6198, Sigma-Aldrich) and anti-CD31 (1:100, ab28364, Abcam) diluted in PBS containing 0.3% Triton X-100, 2.5% BSA and 2.5% normal goat serum. Sections were incubated with anti-rabbit Alexa Fluor-647 secondary antibody (111-607-008, Jackson ImmunoResearch) and Hoechst 33342 for 2 hours at room temperature, and mounted in Fluoromount-G imaging medium (4958-02, Affymetrix eBioscience). Samples were examined in a Leica SP5 DMI 6000B confocal microscope and quantification was performed with Image J software. SMA positive area and number of nuclei were normalized to area of the medial layer.

3.10. Histology

Mouse organs (including thoracic aorta and aortic arch segments) were fixed in 4% paraformaldehyde. Following dehydration in an ascending ethanol series, samples were embedded in paraffin, cut into 5-µm sections, and stained with Hematoxylin & Eosin (H&E) and/or Masson's trichrome. Stained samples were imaged with OPT Scanner 3001 (OPT, Bioptonics Microscopy). H&E staining was performed to check primary tissue appearance. Five observers who were blinded to genotype examined the subcutaneous fat layer to score from 1 to 5, being 1 the lowest and 5 the highest thickness of subcutaneous fat layer. Masson´s Trichrome was used to analyze collagen content, which was measured in the medial and

adventitial layer as the green area (Fiji software; ImageJ 1.50e x64) and expressed as a percentage of the medial area layer.

3.11. RNA Extraction and cDNA Preparation

Mice were euthanized by CO_2 inhalation and tissues were collected, frozen in liquid nitrogen and preserved at -80 °C until further use. Tissue samples were homogenized by crushing and subsequently using a TissueLyser. Total RNA was extracted with TriReagent Solution (AM9738, ThermoScientific) and processed through alcohol precipitation according to the manufacturer's instructions. RNA pellets were washed in cold 75% ethanol, resuspended in nuclease-free water, and then quantified in a NanoDrop ND-1000 spectrophotometer. Total RNA (1-2 µg) was transcribed to cDNA using the High Capacity cDNA Reverse Transcription Kit (4368814, Applied Biosystems) following the manufacturer's instructions.

3.12. PCR Detection of Lamin A and Progerin

Lamin A and progerin mRNAs were detected as described (Yang, Qiao, Farber, *et al.*, 2008). The cDNA from different tissues (100 ng) was amplified by PCR and products were separated on a 1.5% agarose gel electrophoresis. Images were taken with a Molecular Imager® Gel Doc™ XR+ System (BioRad). Band intensity was quantified using Fiji software (ImageJ 1.51a x64).

3.13. Longitudinal Phenotypic Characterization of Mice

Animals were weighed and inspected for health and survival at least once every two or three weeks. Checks became more frequent when health status began to deteriorate. Animals that met humane end-point criteria (Table 11) were euthanized and the deaths recorded. Data from animals that were euthanized because of reasons unconnected to progeroid phenotype were censored.

3.14. Biochemical Analysis

Blood was extracted directly from mandibular sinus in live mice or from heart or renal artery in euthanized animals. For biochemical analysis, blood samples were collected in Microvette EDTA tubes (Sarstedt) and centrifuged at 1400 rpm for 15 min at 4°C. The plasma supernatant was stored at -80°C until samples from all experiments were collected. Biochemical variables were analyzed Unit using a Dimension RxL Max Integrated Chemistry System (Siemens Healthineers).

All protocols were performed according to manufacturer's instructions. Mice were fasted overnight for the quantification of plasma glucose level. Because of volume limitations, plasma samples for glucose measurement were pooled from 2-4 animals of the same experimental group.

Table 11: Humane End-Point Criteria for HGPS mice

Body weigh	**Value**
Loss of weight >40%	5
Loss of body weight due to progeric syndrome	1
No loss of body weight	0

Deterioration of body condition	**Value**
Condition 1 (C1): Mouse is emaciated	5
Condition 2 (C2): Mouse is underconditioned	1
Condition 3 (C3): Mouse is well-conditioned	0

C1: Skeletal structure extremely prominent; little or not flesh cover
Vertebrae distinctly segmented
C2: Segmentation of vertebral column evident
Dorsal pelvic bones are readily palpable
C3: Vertebrae and dorsal pelvis not prominent. Palpable with slight pressure

Interaction with the environment	**Value**
No interaction with the environment or littermates	5
Some lethargy, little interest for the environment	1
Normal behavior	0

Tail suspension test	
No movements or spasmodic movements	**Value**
Weak movements or slow reflexes	5
Normal behavior	1
	0

If sum of all criteria > 7 --> Euthanasia
If sum of all criteria = 5 - 6 --> Daily supervision
If sum of all criteria = 4 --> Supervision on alternate days
If sum of all criteria < 4 --> Weekly supervision

3.15. Wire Myography

Wire myography was performed as previously described (del Campo and Ferrer, 2015). Male mice were euthanized at 31-33 or 50-53 weeks of age by CO_2 inhalation. Immediately after sacrifice, the thoracic and abdominal cavities were opened. Thoracic aortas were excised and immediately placed in ice-cold Krebs Henseleit solution (KHS: 115 mM NaCl, 2.5 mM $CaCl_2$, 4.6 mM KCl, 1.2 mM KH_2PO_4, 1.2 mM $MgSO_4$, 25 mM $NaHCO_3$, 11.1 mM glucose, and 0.01 mM EDTA). The vessels were gently cleaned of fat and connective tissue and cut into 2-mm long segments, which were mounted on two tungsten wires in a wire myograph system (620M, DMT) (Figure 4A) and immersed in 37ºC KHS with constant gassing (95% O_2 and 5% CO_2). First, a normalization procedure was performed in order to determine the optimal distension of the vessels. Diameter-tension relationships were determined by artificially and stepwise stretching of the tissue, increasing its passive diameter by augmenting the distance between the wires passing through the lumen. At each step, both the force and the internal circumference (IC) of the vessel were recorded. The IC was transformed into vessel diameter in µm (del Campo and Ferrer, 2015) which is expressed in the x-axis (Figure 4B). The tension (force) experienced by the vessel wall in resisting this stretching was recorded by a force transducer connected to one of the wires, and plotted on the y-axis (Figure 4B).

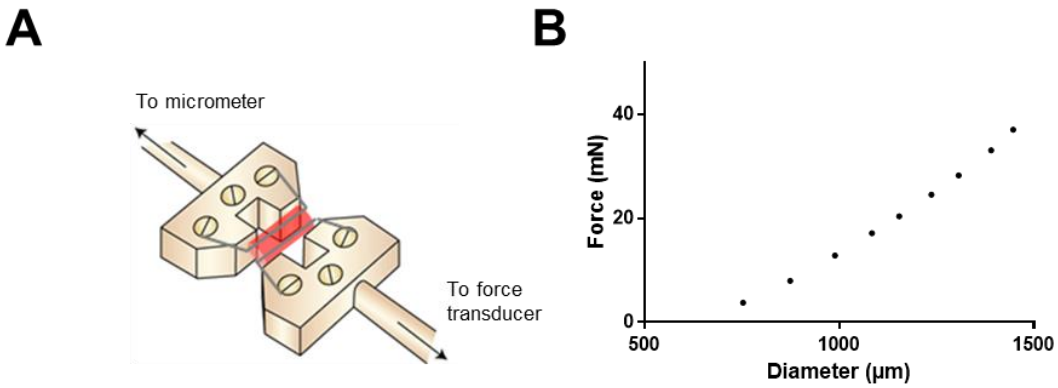

Figure 4. **Wire myography to assess vascular structure and tone. A)** Representation of a thoracic aortic ring mounted on two tungsten wires in a wire myograph system. One of the wires is connected to a micrometer screw and the other to a force transducer. **B)** Example of a diameter-force graph obtained after the normalization procedure. See details in Material & Methods section 3.15.

For each vessel segment, a linear regression was calculated from the diameter-tension relationship. Diameter-tension measurements were excluded when discalibration of the force transducer in a specific channel was detected (difference between the myograph unit and the software >5 mN). Diameter-tension relationships can be defined and compared by means of

two different parameters as previously described (del Campo *et al.*, 2019). Briefly, the slope of the regression line is calculated and compared, indicating accounting for the stiffness, while the vessel diameter at 0 pressure (Y_0 diameter) can indicate inward or outward remodeling.

The position estimated at which the tension is equivalent to an intraluminal pressure of 100 mmHg (L100) was calculated using the Laplace Equation (Tension=[pressure*radius]/thickness). After normalization, aortic segments were set up to their optimal position (physiological distension, 0.9 of L100) and let to equilibrate for 30 minutes (del Campo and Ferrer, 2015). Then, vasoconstriction was evaluated by adding 120 mM KCl. Response curves to increasing doses of phenylephrine (Phe, from 1nm to 10 µM) were also performed to assess vasoconstriction. Endothelial function was examined by recording vasodilation induced by increasing doses of acetylcholine (Ach, from 0.1 nM to 10 µM) in aortic segments previously contracted with 1 µM Phe. Finally, endothelium-independent vasodilation was assessed by a dose-dependent vasodilation induced by the nitric oxide donor DEA-NO (doses from 0.1 nM to 10 µM) in segments previously contracted with 1 µM Phe. Several washes with KHS and a stabilization period of at least 15 minutes were performed between different drug exposures. KCl, Phe, Ach and DEA-NO were obtained from Sigma-Aldrich Spain.

3.16. Pressure Myography

Animals were euthanized at 31-33 or 50-53 weeks of age by CO_2 inhalation. Immediately after sacrifice, the thoracic and abdominal cavities were opened, the mesentery and the intestines were excised and placed in ice-cold KHS, and small mesenteric resistance vessels were gently excised. Structural and mechanical properties of mesenteric resistance arteries were studied using a pressure myograph (Danish Myo Tech, Model P100, J.P. Trading I/S, Aarhus, Denmark). Vessels were placed on 2 glass micro cannulae, secured with surgical nylon suture thread and pressurized. After any small branches were tied off, vessel length was adjusted so that the vessel walls were parallel without stretching. Intraluminal pressure was then raised to 120 mm Hg and the artery was unbuckled by adjusting the cannulae. The segment was then set to 45 mm Hg and allowed to equilibrate for 30 min at 37°C in calcium-free KHS ($0Ca_2^+$; omitting calcium and adding 1 mM EGTA), applied both intravascularly and extravascularly, and gassed with a mixture of 95% O_2 and 5% CO_2. A pressure-diameter plot was obtained by performing the following procedure. Intraluminal pressure was initially reduced to 3 mm Hg. Then, the intraluminal pressure was increased in 20 mm Hg steps from 3 to 120 mm Hg. Internal and external diameters

were continuously monitored under passive conditions (Di_0Ca, De_0Ca, respectively) for 3 minutes at each intraluminal pressure. The final value used was the mean of the measurements taken during the last 30 seconds, when measurements had reached a steady state.

From internal and external diameter measurements in passive conditions, the following structural and mechanical parameters were calculated:

Wall thickness (WT) = $(De_0Ca - Di_0Ca)/2$

Wall:lumen = $(De_0Ca - Di_0Ca)/2Di_0Ca$

Incremental distensibility is the percentage of change in the arterial internal diameter for each mm Hg change in intraluminal pressure and was calculated according to this formula:

Incremental distensibility = $\Delta Di_0Ca/(Di_0Ca \times \Delta P) \times 100$

Circumferential wall strain (ε) = $(Di_0Ca - D_{00}Ca)/D_{00}Ca$, where $D_{00}Ca$ is the internal diameter at 3 mm Hg and Di_0Ca is the observed internal diameter for a given intravascular pressure, both measured in $0Ca^{2+}$ medium.

Circumferential wall stress (σ) = $(P \times Di_0Ca)/(2WT)$, where P is the intraluminal pressure (1 mm Hg = 133.4 N/m^2) and WT is wall thickness at each intraluminal pressure in $0Ca_2^+$-KHS. Arterial stiffness independent of geometry is determined by Young's elastic modulus (E=stress/strain) (Briones *et al.*, 2009; Schjørring, Carlsson and Simonsen, 2015). The stress-strain relationship is non-linear; therefore, it is more appropriate to obtain a tangential or incremental elastic modulus (Einc) by determining the slope of the stress-strain curve (Einc $=\delta\sigma/\delta\varepsilon$). Einc was obtained by fitting the stress-strain data from each animal to an exponential curve using the equation $\sigma = \sigma orige\beta\varepsilon$, where $\sigma orig$ is the stress at the original diameter (diameter at 3 mm Hg).

Taking derivatives from the equation, we determine that $Einc=\beta\sigma$. For a given σ-value, Einc is directly proportional to β. An increase in β implies an increase in Einc, which signifies an increase in stiffness.

3.17. Echocardiography

Transthoracic echocardiography was blinded performed by an expert operator using a high-frequency ultrasound system (Vevo 2100, Visualsonics Inc., Canada) with a 40-MHz linear probe. Two-dimensional (2D) and M-mode (MM) echography were performed at a frame rate above 230 frames/sec, and pulse wave Doppler (PW) was acquired with a pulse repetition frequency of 40 kHz. Mice were lightly anesthetized with 0.5-2% isoflurane in oxygen, adjusting the

isoflurane delivery trying to maintain a heart rate of 450 ± 50 bpm. Mice were placed in supine position using a heating platform and warmed ultrasound gel was used to maintain normothermia. A base apex ECG was continuously monitored. Images were transferred to a computer and were analysed off-line using the Vevo 2100 Workstation software.

Systolic function analysis

For LV systolic function assessment, parasternal standard 2D and MM, long and short axis views (LAX and SAX view, respectively) were acquired. LV ejection fraction, fractional shortening, stroke volume, cardiac output and chamber dimensions were calculated from these views. Right ventricle systolic function was indirectly estimated using the tricuspid annular plane systolic excursion (TAPSE), obtained from a MM 4-chamber apical view, measuring maximum lateral tricuspidal annulus movement.

Diastolic function analysis

The MV inflow pattern was acquired using PW Doppler echography in the 4-chamber apical view to assess diastolic function. Early and late diastolic velocity peak wave (E and A, respectively), the E/A ratio and isovolumetric relaxation time (IVRT) were measured. Pulmonary vein flow was acquired from a LAX view, orientating the transducer to optimize the visualization of flow. Diastolic and systolic wave velocities were measured as well as atrial reversed flow wave.

Pulmonary artery flow analysis

To assess pulmonary pressures, the pulmonary artery (PA) flow was measured from a 2D SAX at the level of the aorta, optimized to visualize the PA crossing the aorta and parallel to the ultrasound beams. PW Doppler was displayed just at the beginning of the PA. The PA acceleration time and ejection time were measured, and the ratio was calculated.

3.18. Electrocardiography

Mice were anesthetized with 1.5-2% isoflurane, and four ECG electrodes were inserted subcutaneously into the limbs. ECG was recorded in the morning for 2 minutes using a MP36R data acquisition workstation (Biopac Systems). ECG data were exported with AcqKnowledge software (Biopac Systems) and automatically analyzed using previously described custom R scripts developed to: *"1) Remove noise and baseline fluctuations; 2) detect heart beats, peaks and*

waves; 3) exclude artifacts; and 4) calculate HR, ECG intervals (QRS, QT, QT90,), JT gap and T-wave steepness" (Fanjul, 2019). See Section 3.23 for Statistical Analysis.

3.19. Tamoxifen Treatment

4-hydroxy-tamoxifen (4-OH TAM, H6278, Sigma Aldrich) was dissolved in ethanol (for cells) or corn oil (for mice) (C8267, Sigma Aldrich), incubated at 55°C until complete dissolution and passed through a 0.22 µm filter. For cell culture experiments, zeocin resistant MEFs were treated with 25 nM 4-OH TAM for 24h, 48h and 72h. Negative controls were treated with vehicle (ethanol) for 72h. For *in vivo* experiments, mice were randomized into treatment or control groups. Nine-week-old mice received for 10 days intraperitoneal injections of 4-OH TAM or vehicle (2 mg/day/mouse) and were sacrificed one week after finishing treatment. We also treated 53-56-week-old *Lmna*$^{HGPSrev/HGPSrev}$ *Ubc-CreERT2*$^{tg/+}$ and control mice with 4-OH TAM or vehicle (daily intraperitoneal injections, 5 days, 1mg/day/mouse) which were sacrificed when humane end-point criteria were reached (Table 11).

3.20. AAV Vector Production, Purification and Titration

Recombinant AAV of serotype 9 expressing either Cre recombinase-Tomato (pAAV9-CRE-I-TOMATO) or luciferase (pAAV9-Luciferase) were produced at CNIC's Viral Vectors Unit by double transfection in HEK293T cells (Figure 5). Briefly, HEK293T cells (~70% confluence) growing in 2 hyperflasks (corresponding to a surface area of 3440 cm^2) were co-transfected with the shuttle vector and the pDG9 helper vector encoding the AAV2 rep gene and the AAV9 capsid gene using branched poliethylenimine (average MW 25000, Sigma-Aldrich). Cells were maintained in DMEM media supplemented with 2% FBS and 1% of penicillin/streptomycin in a humidified incubator with 5% CO_2.

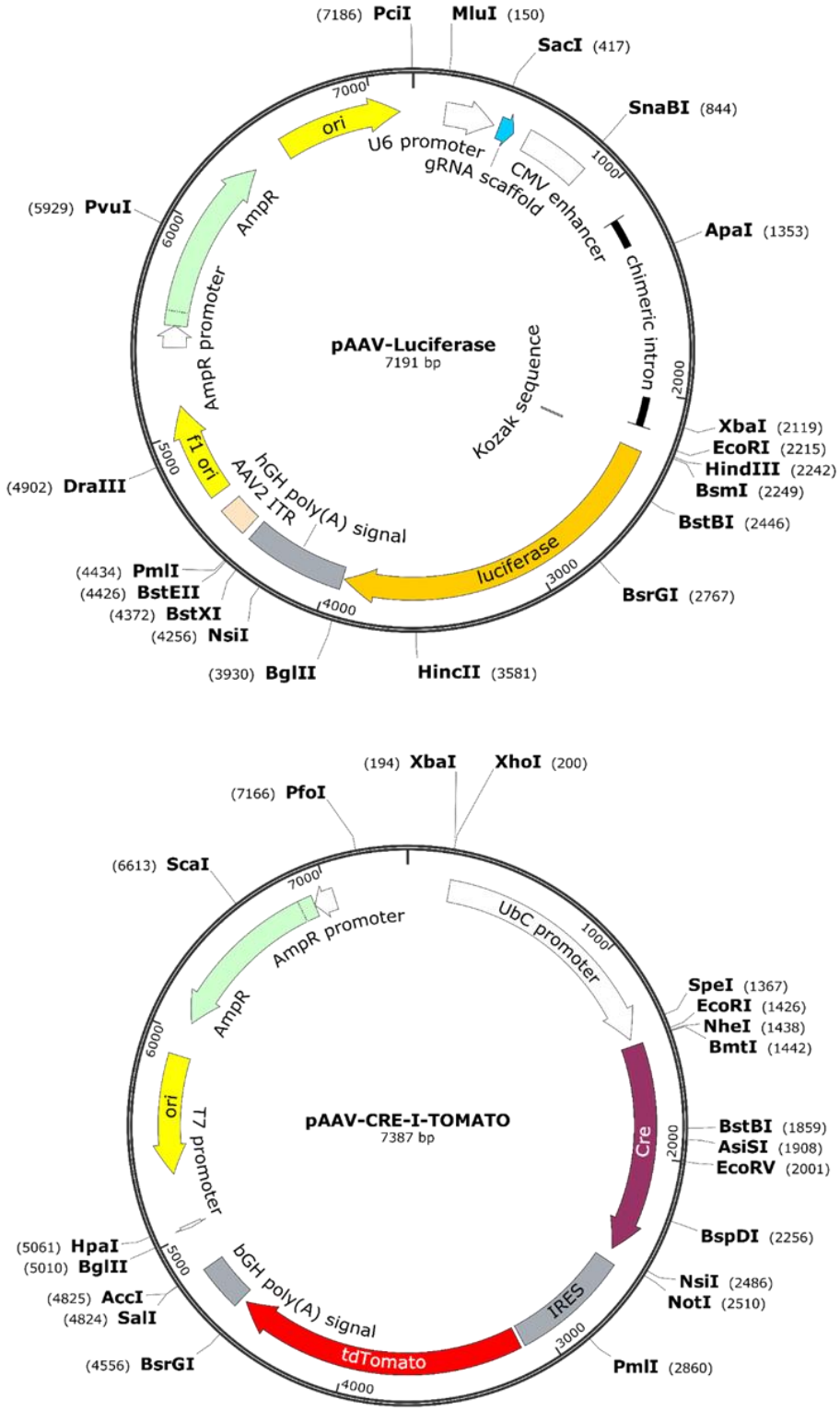

Figure 5: Map of the AAV plasmid vectors encoding Luciferase and Cre Recombinase-Tomato. Recombinant vectors encoding either Cre recombinase-Tomato (pAAV-CRE-I-TOMATO) or luciferase (pAAV-Luciferase) were produced at CNIC's Viral Vectors Unit by double transfection in HEK293T cells.

After 72 hours, transfected cells were detached by vigorous shaking, washed with PBS and subjected to 3 freeze/thaw cycles in 10 mL of lysis buffer (150 mM NaCl, 50 mM Tris pH 8.5). Once the cells were lysed, cellular and plasmidic DNA were digested with benzonase nuclease (Millipore) for 30 minutes and cell debris was eliminated by centrifugation.

For purification of AAVs, samples were subjected to isopycnic iodixanol gradient centrifugation (Optiprep, Stem-cell Technologies) and subsequent buffer exchange in Amicon Ultra-15 columns (100 kDa cutoff, Millipore). Samples were resuspended in 1 mL of 0.001% pluronic F-68 non-ionic surfactant (Thermofisher scientific) in PBS.

Titration was performed by quantitative PCR on viral genomes with primers specific for Cre (Forward: 5'-TGACGGTGGGAGAATGTTAAT-3'; Reverse: 5'-GCCGTAAATCAATCGATGAGT-3') and luciferase (Forward: 5'-CCAGGGATTTCAGTCGATGT-3'; Reverse 5'-AATCTCACGCAGGCAGTTCT-3') genes.

3.21. AAV Injection

Fifteen-to 18-week-old *Lmna*$^{+/+}$ and *Lmna*$^{HGPSrev/HGPSrev}$ mice received a single intravenous tail injection with 5×10^{11} viral genomes encoding luciferase or Cre recombinase-Tomato with expression driven by ubiquitous promoters.

3.22. Bioluminiscence Assay

Bioluminiscence assays were performed with an IVIS Spectrum In Vivo Imaging System (Perkin-Elmer). For luciferase signal detection, mice received a single intravenous injection of luciferase assay reagent (E3040, Promega, 10µL in 90µL of PBS) and were euthanized 1 minute later. Organs were extracted and bioluminescence images were taken (5 seconds exposure). Finally, samples were collected and frozen for RNA and protein extraction. The visual output represents the number of photons emitted/second/cm^2.

3.23. Statistical Analysis

Unless stated otherwise, data are shown as mean ± SEM. In all statistical analyses, differences were considered significant when $P<0.05$. Experimental conditions were randomized and comparisons in mouse studies were made between age-matched groups that included males and females. Statistical analyses were performed with Prism Graphpad Prism 7. Statistical significance

was calculated by two-tailed Student's t-test if the distribution was normal. If the compared population did not have equal standard deviations, we performed an unpaired t-test with Welch's correction. When specified, two-way ANOVA with Tukey's or Sidak's post-hoc multiple comparison test or one-way ANOVA with Sidak's post-hoc test was used. When detailed, chi-square t-test was used. A long-rank (Mantel-Cox) test was used for Kaplan-Meier survival curves.

Statistical analysis of the results from ECG was performed by custom R scripts developed to: "*1) assess the factors to be considered in each test, including both fixed and random effects; 2) evaluate normality and apply natural-logarithm transformations if convenient; 3) estimate statistical differences between each group applying a linear model with fixed or mixed effects; 4) extract and p-values*" (Fanjul, 2019). The following factors were considered as fixed effects: genotype, age group or treatment and sex. The following factors were considered as fixed effects: Subject or sample follow-up and date.

RESULTS

4. RESULTS

4.1. Generation of a New HGPS Mouse Model that Allows a Controlled Spatio-temporal Elimination of Progerin and Lamin A Restoration

4.1.1. Strategy for *Lmna*^{HGPSrev} Allele Generation

It remains to be determined whether cell, tissue and organismal damage caused by progerin is reversible upon suppression of this mutant form of lamin A, and if so, what is the time window for effective therapeutic intervention. This is in part due to the fact that none of the available HGPS-mouse models allows ubiquitous or tissue-specific suppression of progerin expression and restoration of lamin A expression in a context of whole body progerin expression, which is the situation in HGPS patients. To bypass this limitation, we sought to generate a new HGPS mouse model that allows a controlled spatio-temporal progerin elimination and lamin A restoration.

We designed a strategy to introduce in *Lmna* intron 10 a mutant cassette carrying the cDNA sequence of exons 11 and 12 coding for progerin (exon 11 lacking the last 150 nucleotides and coding sequence of wild-type exon 12), followed by a transcription stop signal (Figure 6A). To allow a controlled suppression of progerin and restoration of the wild-type lamin A protein, we flanked this insert with two loxP sites (Figure 6A). The transcriptional stop signal at the end of the insert prevents the transcription of the endogenous exons 11 and 12, therefore this mutant allele (*Lmna*^{HGPSrev}) allows the expression of progerin and lamin C. In addition, due to the presence of loxP sites, the exogenous DNA insert with the stop transcription signal can be removed upon expression of the Cre recombinase to eliminate progerin expression and restore lamin A expression (Figure 6B).

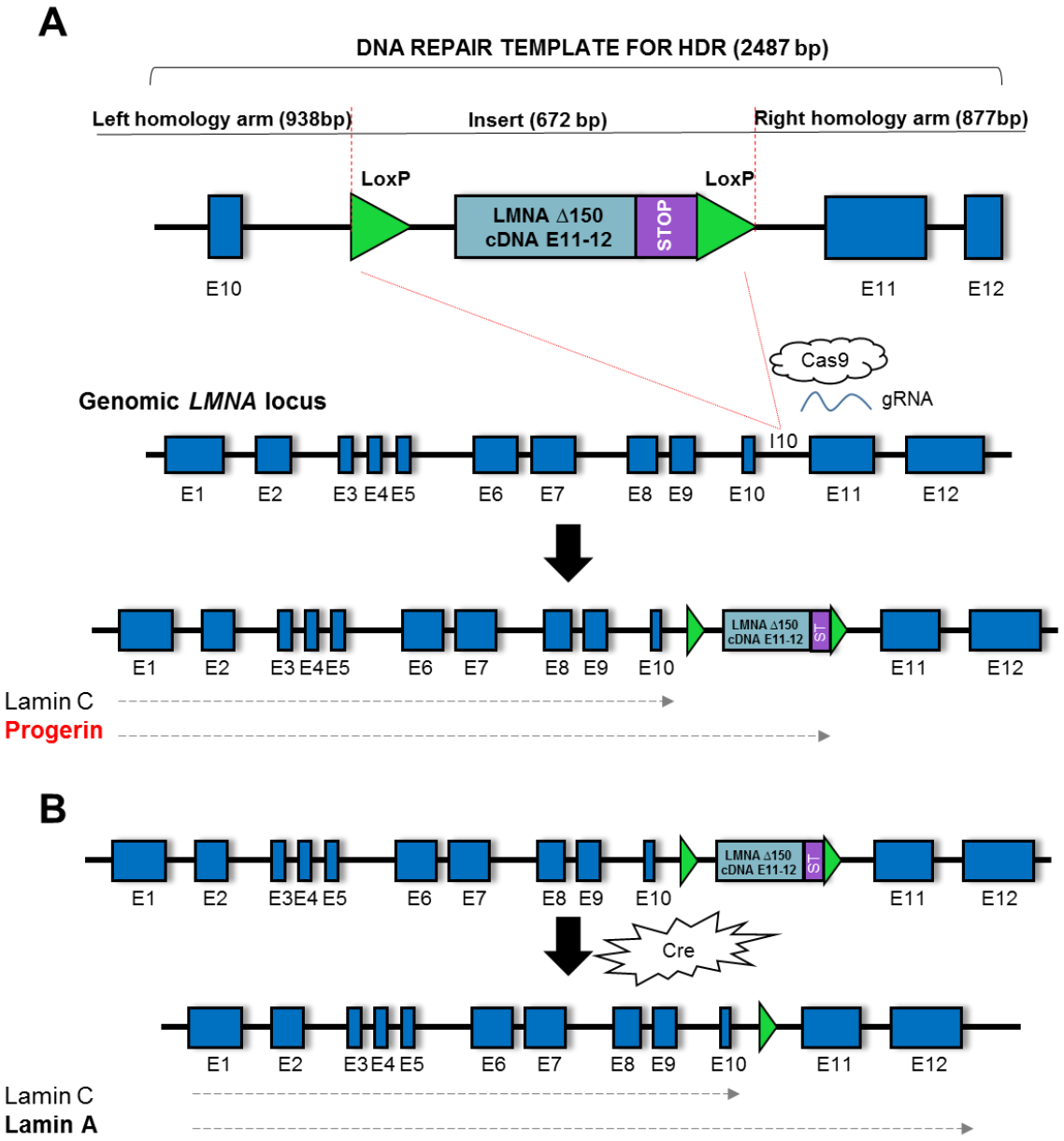

Figure 6: Strategy to generate the *Lmna*^{HGPSrev} mouse model. A) Schematic representation of the *Lmna* gene and the dsDNA donor template used to introduce the 672-bp insert into intron 10 by the CRISPR-Cas9 system and HDR. This insert is flanked by two loxP sequences and two homology arms, and contains a cDNA harboring *LmnaΔ150* exons 11-12, followed by a bovine growth hormone polyadenylation stop transcription signal. Downstream from this insert, a right homology arm contains the endogenous wild-type exon 11/intron/exon 12 of the *Lmna* gene, which are not transcribed into mRNA due to the stop transcription signal included at the 3' end of the 672-bp insert. **B)** Cre recombinase activity removes the floxed insert to generate a modified *Lmna* allele with a residual loxP site and the endogenous exon 11/intron/exon 12 sequence. The presence of this modified allele allows expression of wild-type Lamin A and Lamin C. I: intron; E: exon.

4.1.2. Single-guide RNA Design and Validation

We decided to generate the new mouse model using CRISPR-Cas9 technology and zygote microinjections, which allows higher efficiency and shorter production time compared with traditional embryonic stem cell technology (Ran *et al.*, 2013; Zarei *et al.*, 2019). We designed two different sgRNAs with the 5'-NGG PAM sequence of *Streptococcus pyogenes* Cas9 to target *Lmna* intron 10 efficiently and with low off-target score (Table 2 and Figure 2A). The targeting efficiency of these sgRNAs was evaluated based on the generation of insertions and/or deletions (indels) by non-homologous end joining (NHEJ) repair pathway after Cas9 cleavage. Figure 7 schematizes the protocol we used to validate both sgRNAs. Briefly, each sgRNA was cloned into the pCRISPR U6 CMV Cas92AeGFP plasmid (Figure 2B). Immortalized wild-type MEFs (see Materials & Methods, section 3.5) were transfected with the amplified and purified cloned vector, then the genomic DNA from GFP positive clones was isolated. Next, the target DNA sequence was amplified and, after heteroduplex formation, a T7 endonuclease assay was performed. The digested products were visualized in an agarose gel. These experiments revealed more efficient cleavage with sgRNA_1 compared with sgRNA_2, as revealed by higher percentage of PCR product cleaved ($\%PCR_{cut}$). We therefore used sgRNA_1 for the microinjection sessions.

4.1.3. dsDNA Donor Template Design and Purification

We next designed a dsDNA donor template, which is needed to repair by HDR pathway the DSB generated by the nuclease activity of Cas9 (Ran *et al.*, 2013; Karimian *et al.*, 2019).

The dsDNA donor template was composed by two homology arms flanking the genetic alteration that we wanted to introduce (see section 4.1.1 and Figure 3, 6). Before zygote microinjections, the dsDNA donor template was purified and sequenced in order to ensure the insertion of a high quality and well-defined cassette into the *Lmna* locus (see Materials & Methods, section 3.2.4).

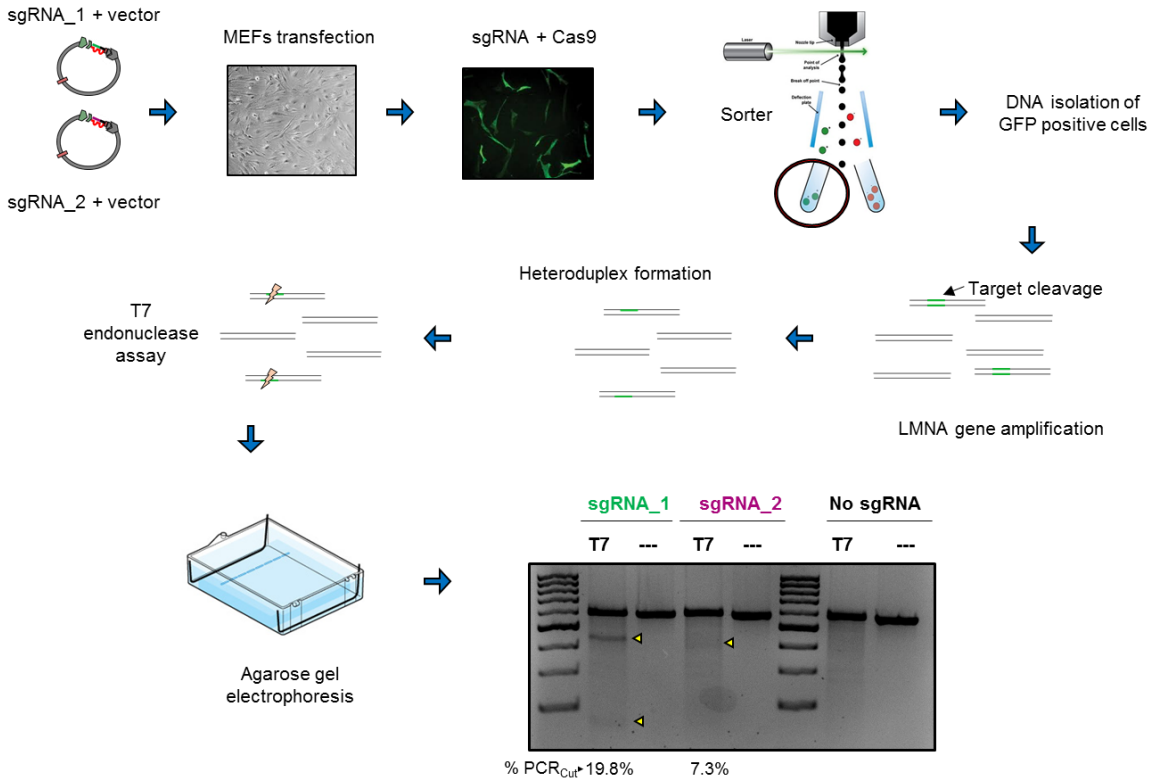

Figure 7: *In vitro* validation of sgRNAs. Two different sgRNAs to target *Lmna* intron 10 were designed and cloned into the pCRISPR U6 CMV Cas92AcGFP plasmid (see Figure 2B), which contains the cDNA to drive Cas9 and eGFP expression. Vectors were transfected into wild-type MEFs and transfected cells were selected by sorting green fluorescent cells to extract genomic DNA. The target DNA sequence of each sgRNA was amplified by PCR and a T7 nuclease assay was performed after heteroduplex formation. The resulting DNA products were separated by agarose gel electrophoresis, which revealed that sgRNA_1 is more efficient than sgRNA_2 *in vitro*.

4.1.4. Identification of Founder *Lmna*$^{HGPSrev/HGPSrev}$ Mice

After two microinjection sessions (see Material and Methods, section 3.2.6 – 3.2.8), 34 pups were weaned and genotyped. To identify mice carrying the insertion in the genome, we designed two oligonucleotides that would differentiate between wild-type and mutant mice by hybridizing inside the homology arms (Figure 8A). PCR using these primers identified eight mice positive for the insert, which were analyzed to assess if only one copy of the cassette was integrated in the correct position in the *Lmna* locus. We therefore designed two pairs of primers inside and outside the homology arms, which allowed us to identify 4 mice carrying only one copy of the insert in the correct place (Figure 8B). The correct genotype of these 4 founder mice of the new *Lmna*^{HGPSrev} HGPS mouse line was confirmed by sequencing of genomic DNA (Figure 8C).

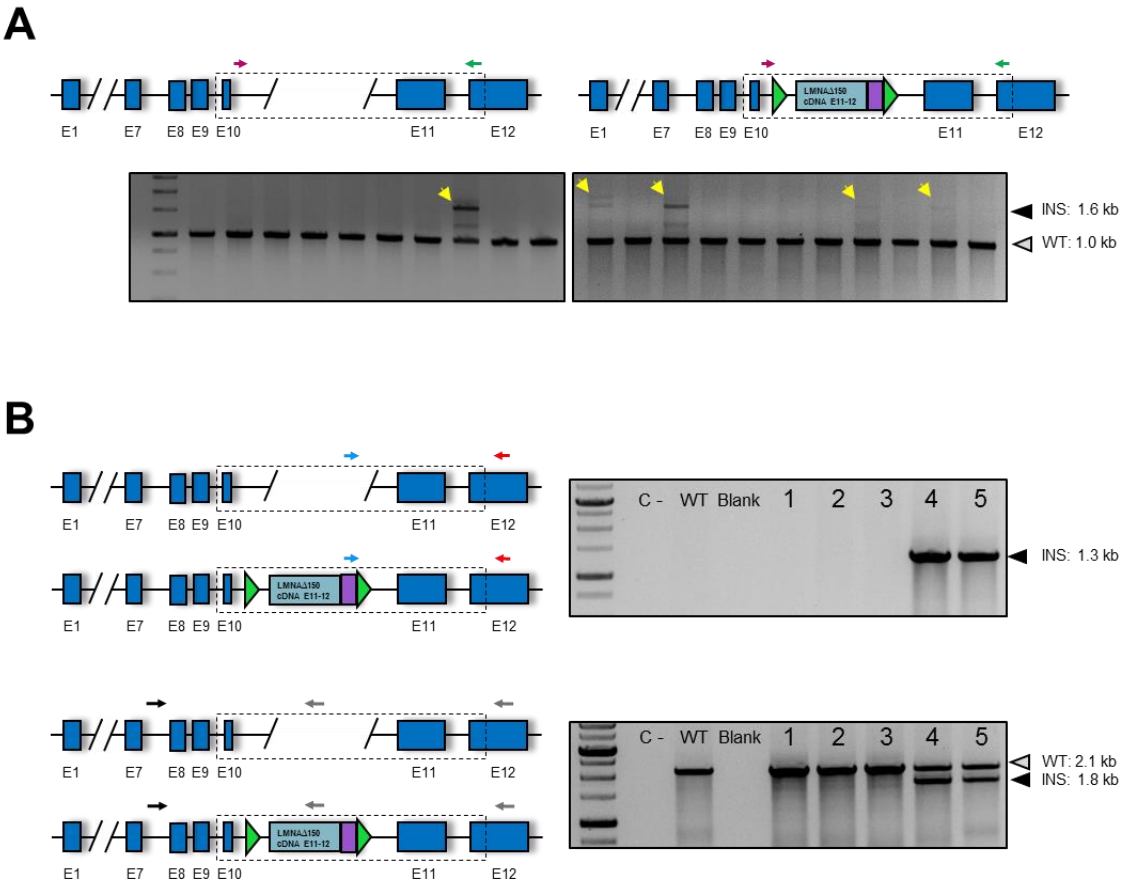

Figure 8: Design of primers for identification of founder *Lmna*^{HGPSrev} mice. **A)** Schematic representation of the *Lmna* gene showing a pair of primers hybridizing inside the homology arms. PCR using these primers generate a 1,000-bp fragment for the wild-type (WT) allele and a 1,670-bp fragment for the mutant *Lmna*^{HGPSrev} allele. The agarose gels show the PCR reaction using these primers to analyze the first 21 pups that were born after the first microinjection session. Yellow arrowheads show 5 positive mice. **B)** Schematic representation of the *Lmna* gene and two pairs of primers hybridizing outside the homology arms, which were used to analyze the 5 positive mice identified in **A**. PCR product size using blue and red primers: insertion (INS) → 1,337 bp; WT → No hybridization. PCR product size using grey and black primers: insertion → 1,776-bp and 2,821 bp; WT → 2,137 bp. The agarose gels show the PCR reaction using these primers. Only mice 4 and 5 had the insert in the desired genomic locus. **C)** Representative genomic sequencing of the *Lmna* gene showing the fusion between exon 11Δ150 and exon 12 without intron 11 from one of the identified *Lmna*^{HGPSrev} founders.

.

To ensure the correct translation of the mutant allele, we analyzed tail protein extracts from two of the identified founders. We observed progerin and lamin C expression as well as lamin A expression due to the mosaicism of founders (Figure 9A). We next analyzed tail protein extracts from the first mice obtained by breeding the founders. As expected, mice from this first generation expressed both progerin and lamin C and lamin A expression was undetectable (Figure 9B).

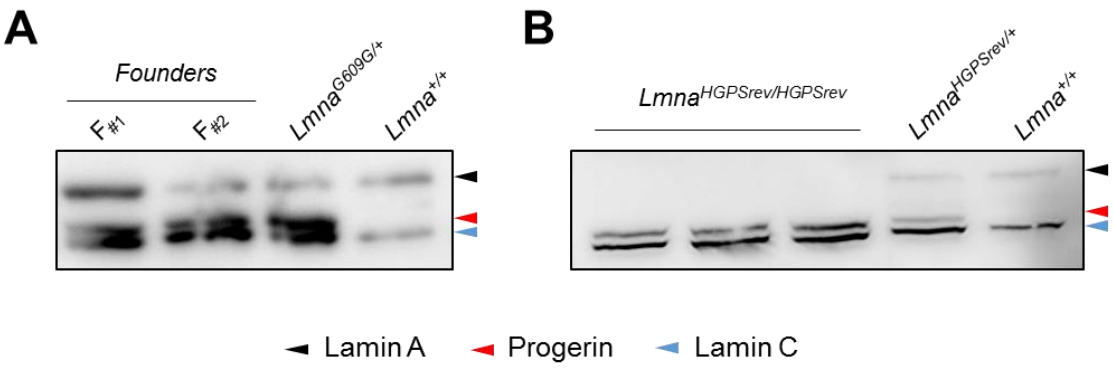

Figure 9: Founder *Lmna*^{HGPSrev} mice express progerin. A monoclonal antibody that recognizes a common region in lamin A, lamin C and progerin was used for western blot analysis of protein lysates prepared from tails from the two first identified *Lmna*^{HGPSrev} founders ($F_{\#1}$ and $F_{\#2}$) and controls **(A)** and from the first mice obtained after colony expansion **(B)**, demonstrating establishment of the insertion in the germline of the founders.

4.1.5. In Vitro Verification of DNA Damage, Progerin Suppression and Lamin A Restoration in MEFs from *Lmna*$^{HGPSrev/HGPSrev}$ Mice

Before the *in vivo* characterization of the new *Lmna*$^{HGPSrev/HGPSrev}$ mouse line, we sought to perform *in vitro* studies to verify the presence of cellular symptoms of HGPS. Among the multiple cellular defects reported in HGPS fibroblasts, nuclear morphology abnormalities and accumulation of DNA damage are the most remarkable alterations (Liu *et al.*, 2005; Dahl *et al.*, 2006; Scaffidi and Misteli, 2006). Additionally, we aimed to examine if the removal of the exogenous DNA cassette from the mutant allele lead to progerin suppression and the restoration of lamin A expression.

Upon DNA damage, histone H2AX is phosphorylated at sites of DNA lesions, therefore the presence of γ-H2AX foci is used as a marker of increased DNA damage (Liu *et al.*, 2005; Podhorecka, Skladanowski and Bozko, 2010). To examine *in vitro* the levels of DNA damage induced by progerin, we generated immortalized MEFs from *Lmna*$^{HGPSrev/HGPSrev}$ and control *Lmna*$^{+/+}$ mice. Western blot analysis confirmed the expression of progerin and lamin C in mutant MEFs, whereas *Lmna*$^{+/+}$ cells expressed lamin A and C (Figure 10A). Immunofluorescence analysis

revealed increased levels of γH2AX foci in nuclei in *Lmna*$^{HGPSrev/HGPSrev}$ MEFs compared with controls, indicating greater DNA damage in HGPS cells (Figure 10B).

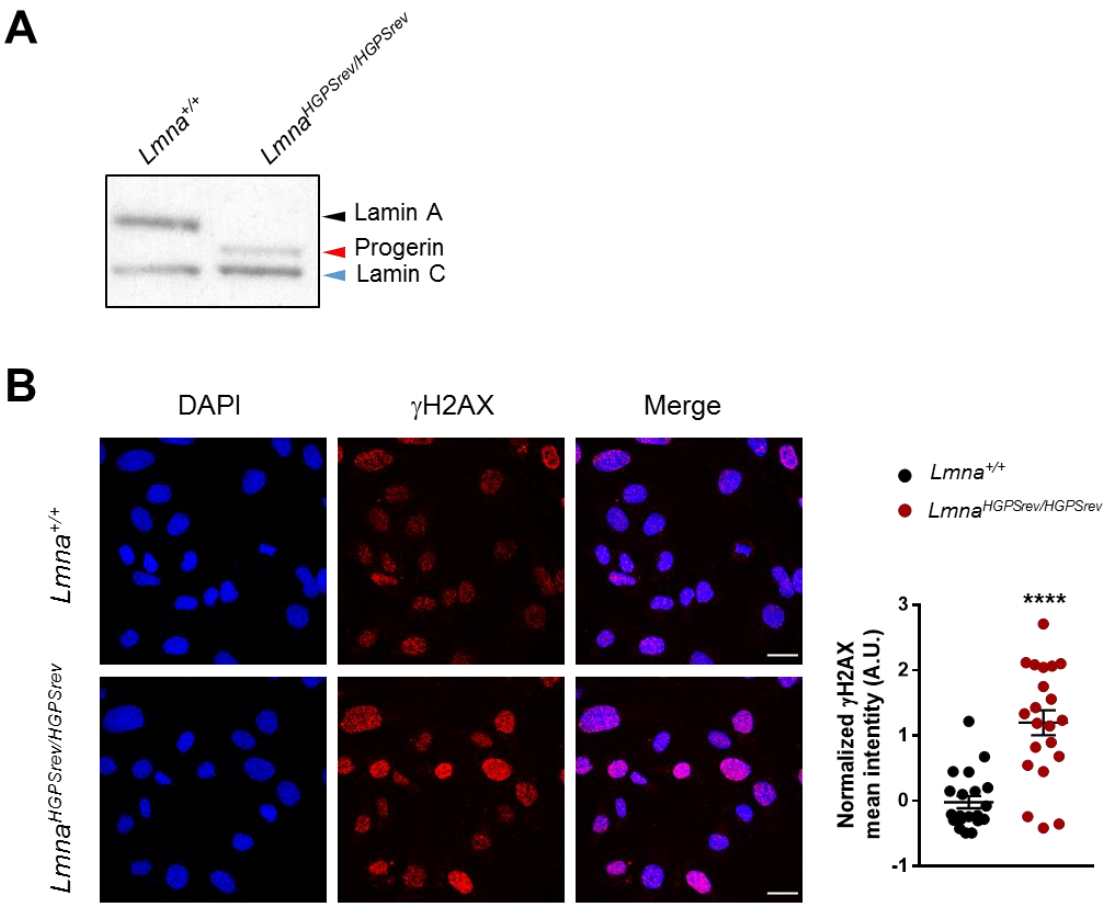

Figure 10: Higher level of DNA damage in *Lmna*$^{HGPSrev/HGPSrev}$ MEFs. Western blot analysis **(A)** and immunofluorescence microscopy **(B)** of MEFs obtained from *Lmna*$^{HGPSrev/HGPSrev}$ and *Lmna*$^{+/+}$ mice. Western blot was performed with a monoclonal anti-lamin A/C antibody that also recognizes progerin. Cells for immunofluorescence were stained with DAPI (blue signal) and with an antibody against γH2AX (red signal). Mean intensity of γH2AX channel from five independent experiments was measured in each individual cell and was normalized by Z-score in each experiment using WT cells as negative control. Scale bar: 25 µm. Statistical differences were analyzed by two-tailed Welch's t-test. ****, P<0.0001.

We next analyzed how progerin-expressing cells respond to different types of DNA damage in terms of cell sensitivity by studying cell proliferation upon stimulation with the following DNA damage-inducing agents: 1) CPT, a topoisomerase I poison whose toxicity is a result of conversion of single-strand breaks into DSBs in S-phase cells, hence, this damage can be repaired only by the HDR pathway (Podhorecka, Skladanowski and Bozko, 2010); 2) Olaparib, an inhibitor of poly ADP ribose polymerase that causes the accumulation of unrepaired single strand breaks that eventually collide with replication forks, generating one-ended DSBs that must be repaired specifically by HDR (Kötter *et al.*, 2014); 3) Aphidicolin, a DNA replication inhibitor that generates replication stress (Vesela *et al.*, 2017); and 4NQO, an ultraviolet radiation-mimetic chemical that induces DNA lesions usually corrected by nucleotide excision repair (Wang *et al.*, 2016).

CPT and Olaparib inhibited in a dose-dependent manner the proliferative capacity of *Lmna*$^{HGPSrev/HGPSrev}$ MEFs compared with controls (Figure 11A). From 40 hours of treatment and up to the end of the assay, *Lmna*$^{HGPSrev/HGPSrev}$ MEFs treated with both concentrations of CPT had significantly less confluence than controls ($p<0.05$). Likewise, *Lmna*$^{HGPSrev/HGPSrev}$ MEFs treated with both concentrations of Olaparib had significantly less confluence ($p<0.05$) from 40 hours of treatment up to the end of the experiment (Figure 11A). These results suggest a defective HDR pathway in *Lmna*$^{HGPSrev/HGPSrev}$ MEFs compared with controls. Proliferation assays with Aphidicolin and 4NQO showed differences in progeroid cells compared with controls in the middle times, however *Lmna*$^{HGPSrev/HGPSrev}$ MEFs finally recovered at the end of the experiment (Figure 11B). These results suggest a possible delay in the resolution of replicative stress and nucleotide excision repair in progerin-expressing MEFs.

To test whether Cre recombinase could suppress progerin expression and restore lamin A expression *in vitro*, we used a *piggyBac* transposon-based system to generate *Lmna*$^{HGPSrev/HGPSrev}$ and *Lmna*$^{+/+}$ MEFs expressing Cre recombinase and a zeocin resistant gene under the control of a tamoxifen-inducible and ubiquitous promoter (Figure 12A). Zeocin resistant cells of both genotypes were selected, tamoxifen was added to the culture media and protein lysates were prepared 24, 48 and 72 hours after tamoxifen induction. As expected, untreated *Lmna*$^{+/+}$ MEFs expressed both lamin A and lamin C and *Lmna*$^{HGPSrev/HGPSrev}$ MEFs expressed progerin and lamin C (Figure 12B, ln. 1 and 2, respectively). Tamoxifen treatment did not change the pattern of expression in *Lmna*$^{+/+}$ cells (Figure 12B, ln. 3, 5 and 7), but *Lmna*$^{HGPSrev/HGPSrev}$ MEFs treated with tamoxifen progressively suppressed progerin and restored lamin A expression, with progerin

levels being undetectable at 3 days after tamoxifen induction (Figure 12B, compare ln. 2 with 4, 6 and 8). These results confirm *in vitro* the efficacy of the strategy followed to generate this new model to induce progerin suppression and lamin A restoration.

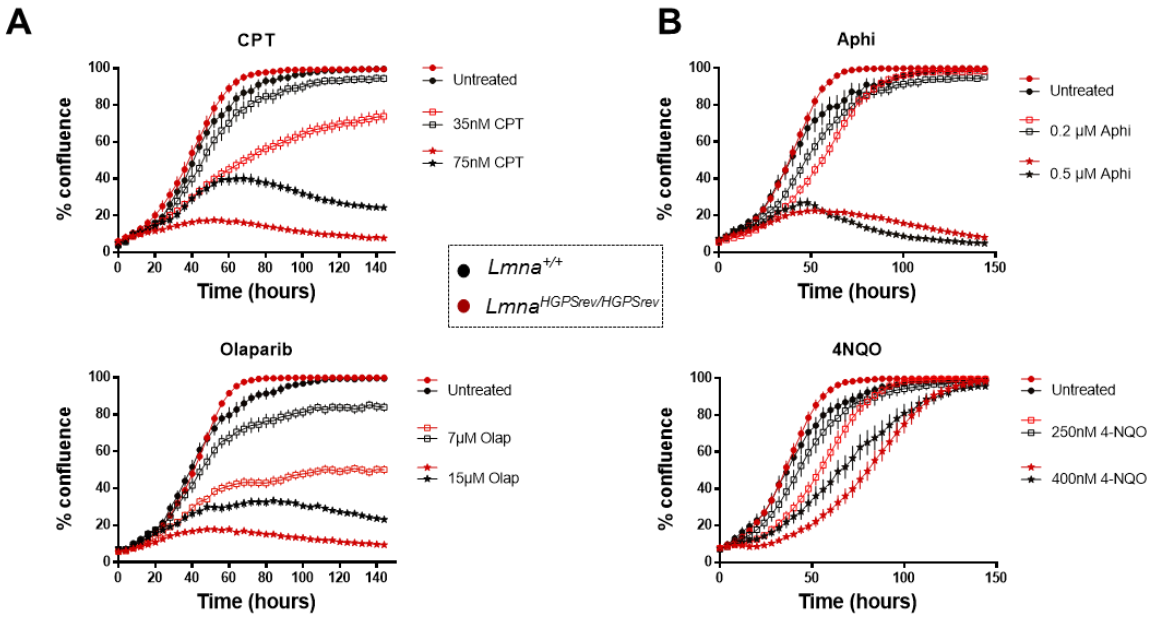

Figure 11: MEFs from *Lmna*$^{HGPSrev/HGPSrev}$ mice are more sensitive to CPT and Olaparib than wild-type controls. MEFs from wild-type and progeroid mice (*Lmna*$^{+/+}$ and *Lmna*$^{HGPSrev/HGPSrev}$, respectively) were seeded in 24-mm plates and treated with the indicated concentrations of CPT, Olaparib (Olap), Aphidicolin (Aphi) and 4NQO. Cells were then maintained at 37°C 5% CO_2 in the IncuCyte imaging system for 6 days. Cell confluence was calculated by dynamic imaging taking 9 pictures every 4-hours. Statistical differences were analyzed by two-way ANOVA with Tukey's post hoc test between wild-type and progeroid mice in each condition. 35 nM and 75 nM CPT: $P<0.05$ after 40h of incubation. 7 µM and 15 µM Olap: $P<0.05$ after 40h of incubation. 0.2 µM Aphi: $P<0.05$ from 40 – 60 hours. 250 nM 4NQO: $P<0.05$ from 36-60h; 400 nM 4NQO: $P<0.05$ from 48-84h.

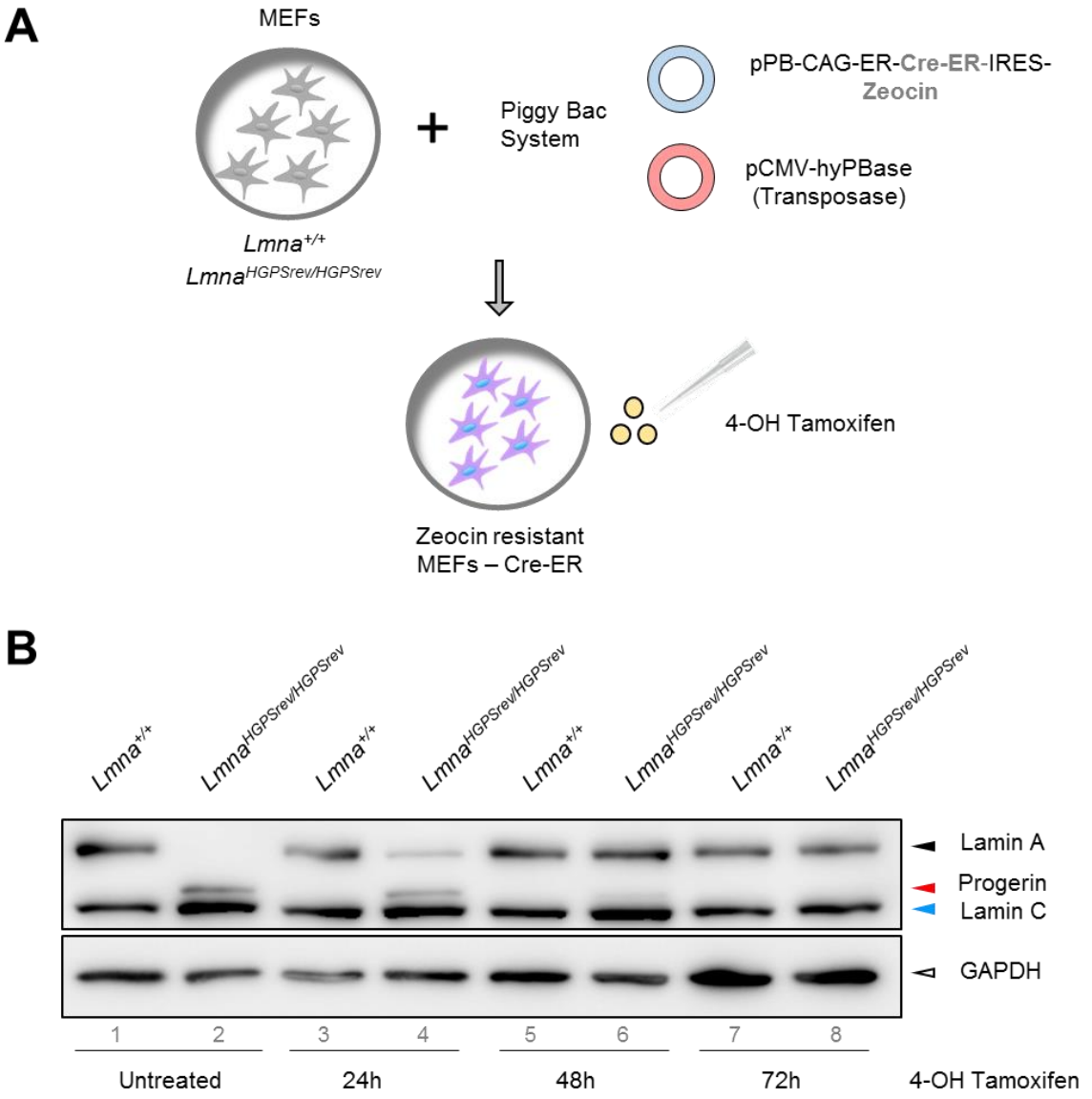

Figure 12: *In vitro* progerin elimination and lamin A restoration in *Lmna*$^{HGPSrev/HGPSrev}$ MEFs upon Cre activation. A) Schematic representation of the *piggyBac* transposon-based system used for the generation of *Lmna*$^{HGPSrev/HGPSrev}$ and *Lmna*$^{+/+}$ MEFs expressing a tamoxifen-inducible Cre recombinase with expression controlled by a ubiquitous CAG promoter. MEFs were transfected with the pCMV-hyPBase plasmid encoding a transposase and the transposon pPB-CAG-ER-Cre-ER-IRES-Zeocin that contains both the inducible Cre and a gene to confer resistance to zeocin. Transfected MEFs will be resistant to zeocin and will express the tamoxifen-inducible Cre recombinase protein. **B)** Western blot analysis to examine lamin A/C and progerin expression in transfected MEFS of both genotypes. Cells were cultured with vehicle (ethanol) (Untreated) or with 25 nM 4-OH tamoxifen for the indicated periods of time. A representative image of one of the three western blots is shown.

4.2. Phenotype Characterization of the New HGPS Model

4.2.1. *Lmna*$^{HGPSrev/HGPSrev}$ Mice Express Lamin C and Progerin but Exhibit Undetectable Lamin A

Having demonstrated *in vitro* the feasibility of our restoration strategy upon loxP sites recombination, we started the *in vivo* characterization of the *Lmna*^{HGPSrev} mouse model. Reverse transcription PCR (Figure 13) and western blot (Figure 14) demonstrated expression of both progerin and lamin C in all liver, kidney, heart, aorta, skeletal muscle and spleen from *Lmna*$^{HGPSrev/HGPSrev}$. We used in these experiments tissues from *Lmna*$^{G609G/+}$ and *Lmna*$^{G609G/G609G}$ mice as positive controls for progerin expression. Note that lamin A was detected in *Lmna*$^{+/+}$, *Lmna*$^{G609G/+}$ and *Lmna*$^{G609G/G609G}$ mice but was undetectable or negligible in all organs of *Lmna*$^{HGPSrev/HGPSrev}$ mice. Moreover, compared with *Lmna*$^{G609G/G609G}$ mice, heart, skeletal muscle and aorta of *Lmna*$^{HGPSrev/HGPSrev}$ mice express significantly lower levels of progerin protein (Figure 14).

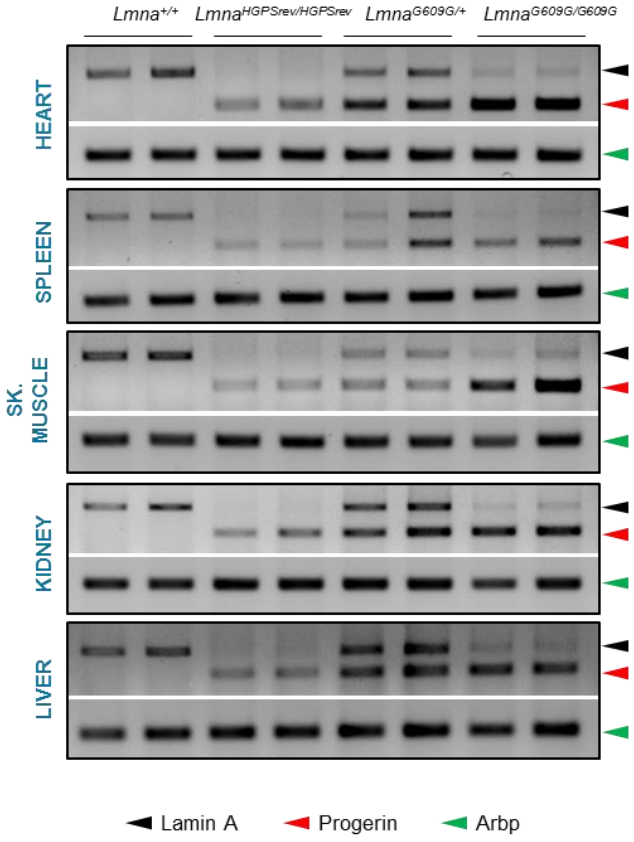

Figure 13: Progerin expression in different organs of progeroid mice. Representative images of PCR products showing lamin A and progerin mRNA expression in heart, spleen, skeletal muscle (Sk. muscle), kidney and liver of 9-week-old mice of the indicated genotypes (n=6 for each genotype). Progerin was expressed in all organs from *Lmna*$^{HGPSrev/HGPSrev}$ mice, and in *Lmna*$^{G609G/+}$ and *Lmna*$^{G609G/G609G}$ mice (used as positive controls). Lamin A was expressed in *Lmna*$^{+/+}$, *Lmna*$^{G609G/+}$ and *Lmna*$^{G609G/G609G}$ mice, but was undetectable or negligible in all organs of *Lmna*$^{HGPSrev/HGPSrev}$ mice. Arbp was used as an endogenous control.

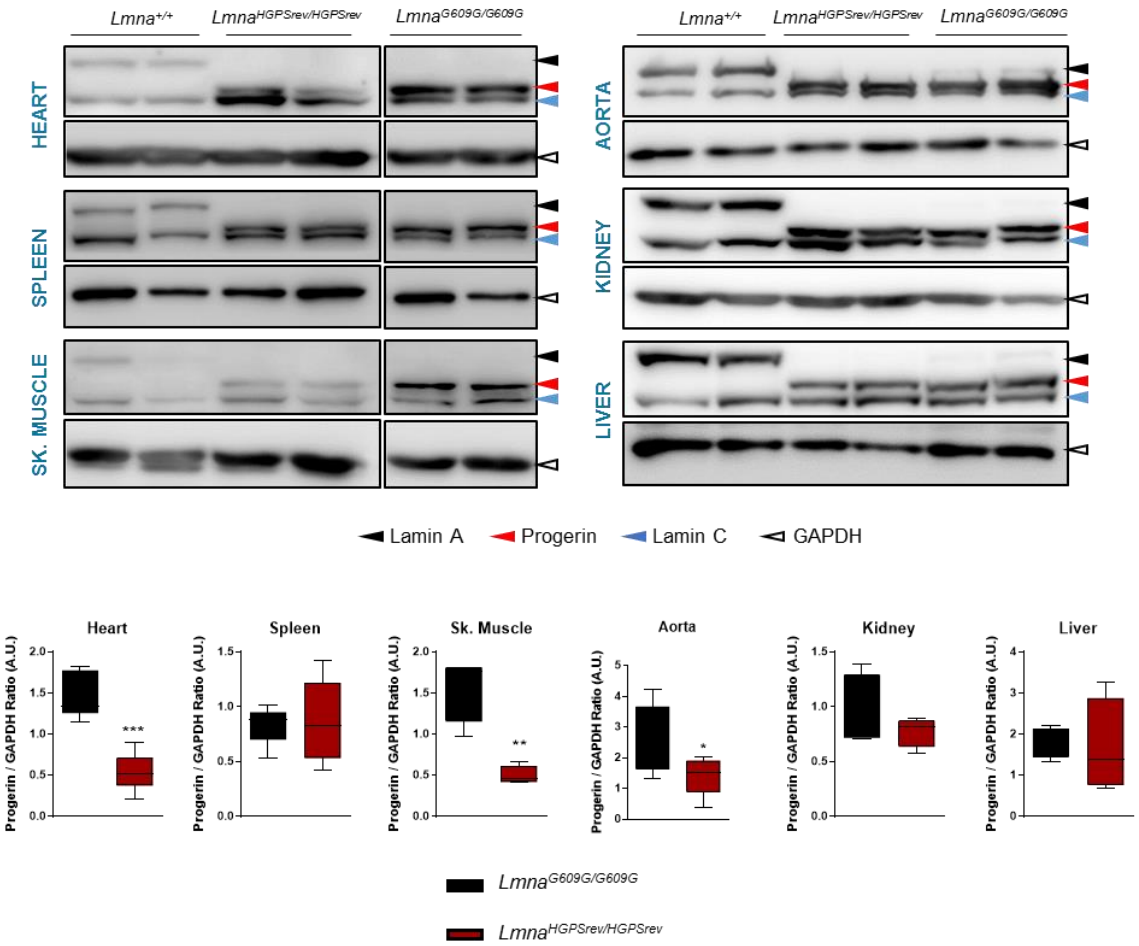

Figure 14: Progerin protein expression in different organs of progeroid mice. Representative images of western blot analysis showing lamin A/C and progerin expression in heart, spleen, skeletal muscle (Sk. muscle), aorta, kidney and liver of 9-week-old mice of the indicated genotypes (n=6 for each genotype). Progerin was expressed in all organs from *Lmna*$^{HGPSrev/HGPSrev}$ and *Lmna*$^{G609G/G609G}$ mice (used as positive controls). Lamin A was expressed in *Lmna*$^{+/+}$ mice but was undetectable or negligible in all organs of *Lmna*$^{HGPSrev/HGPSrev}$ and *Lmna*$^{G609G/G609G}$ mice. Quantification of the relative abundance of protein bands was performed using Fiji software. Progerin signal intensities were normalized to GADPH. Statistical differences were analyzed by two-tailed t-test. *, P<0.05; **, P<0.01; ***, P<0.001.

We next examined the external phenotype of our new mouse model. At birth, homozygous *Lmna*$^{HGPSrev/HGPSrev}$ mice were indistinguishable from their *Lmna*$^{+/+}$ littermate controls, and maintained a normal appearance until approximately 20 weeks of age. Then, both male and female *Lmna*$^{HGPSrev/HGPSrev}$ mice started showing a severe reduction in the rate of weight gain and eventually began to lose weight at approximately 50 weeks of age (Figure 15A). Like in previous progeroid mouse models, homozygous mice died prematurely, with a median survival of 59 weeks in this case (Figure 15B). In contrast, heterozygous *Lmna*$^{HGPSrev/+}$ mice displayed normal body size and weight and their survival was undistinguishable from *Lmna*$^{+/+}$ littermate controls (Figure 15A, 15B). This gross examination indicates that, like human HGPS patients, our new mouse model develops disease symptoms progressively. We therefore decided to perform a

more thorough phenotypic characterization of *Lmna*$^{HGPSrev/HGPSrev}$ mice to measure different disease parameters at ≈30 weeks and at ≈50 weeks of age too, when mice already display a severe phenotype but before their maximum lifespan.

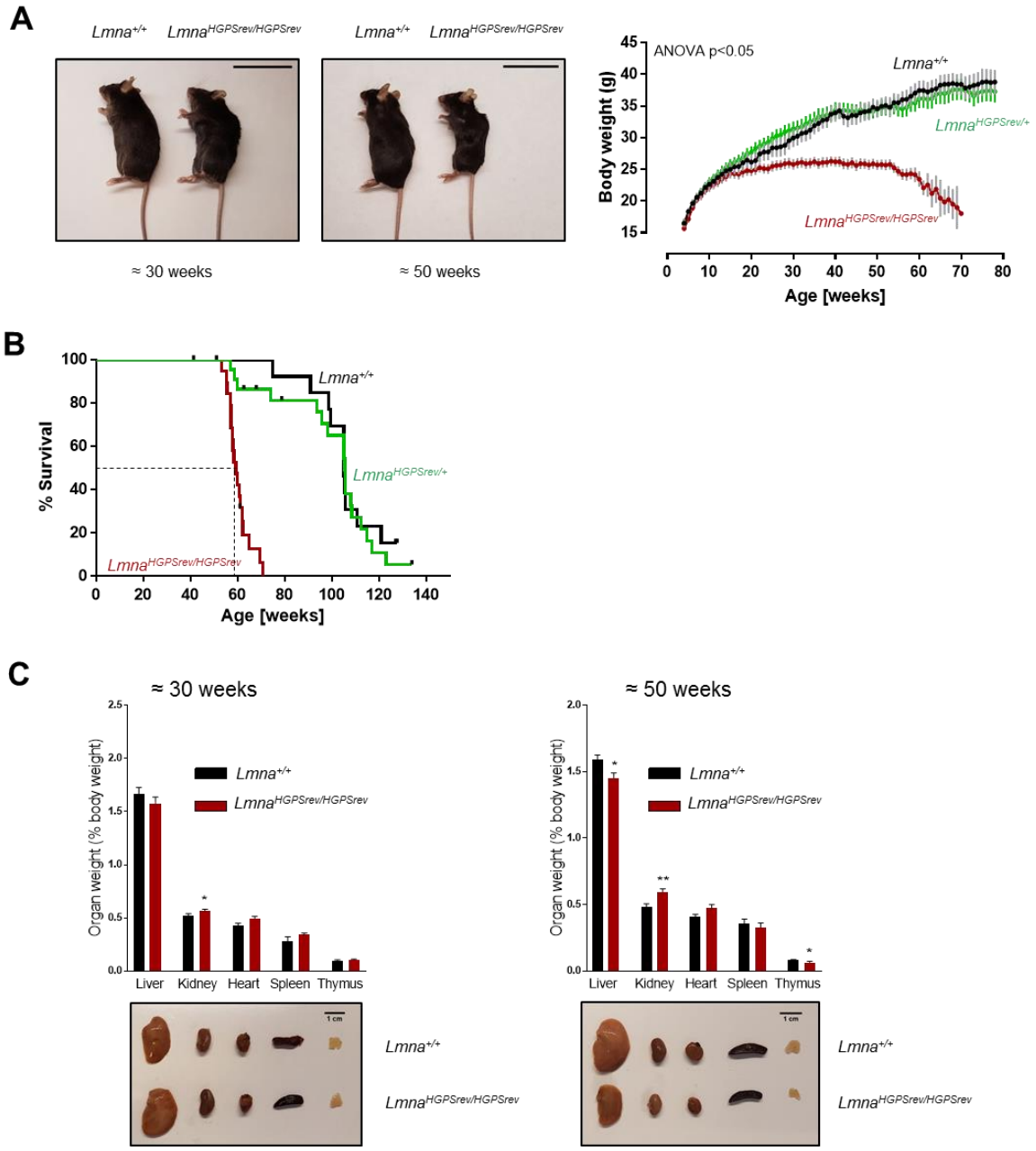

Figure 15: Defective post-natal growth and reduced life span in progeroid homozygous *Lmna*$^{HGPSrev/HGPSrev}$ mice. A) Representative images of ≈30 and ≈50-week-old mice of the indicated genotypes. The graph show postnatal body weight curves (n=22 *Lmna*$^{HGPSrev/HGPSrev}$, n=25 *Lmna*$^{HGPSrev/+}$, and n=14 *Lmna*$^{+/+}$ mice). Statistical differences were analyzed by two-way ANOVA with Tukey's post hoc test. Scale bar: 5 cm. **B)** Kaplan-Meier survival plot. Median survival was 59.3 weeks for *Lmna*$^{HGPSrev/HGPSrev}$ mice (n=22), 105.5 weeks for *Lmna*$^{HGPSrev/+}$ mice (n=22), and 105 weeks for *Lmna*$^{+/+}$ mice (n=13) (P<0.001 for *Lmna*$^{HGPSrev/HGPSrev}$ versus *Lmna*$^{+/+}$ mice, log-rank test). **C)** Representative images and quantification of the weight of liver, kidney, heart, spleen and thymus of ≈30 and ≈50-week-old mice of the indicated genotype. Scale bar: 1 cm. Statistical differences were analyzed by two-tailed t-test with Welch's correction when necessary. *, P<0.05; **, P<0.01.

The relative size of most organs in ≈30-week-old and ≈50-week-old *Lmna*$^{HGPSrev/HGPSrev}$ mice remains proportional to their body weight, with the exception of the kidney, which had a significantly higher relative weight in progeroid mice than in controls at both ages (Figure 15C). In addition, the relative weight of the thymus was also smaller in progeroid mice than in control *Lmna*$^{+/+}$ mice at ≈50-week-old (Figure 15C).

We also examined several biochemical parameters in the plasma of homozygous *Lmna*$^{HGPSrev/HGPSrev}$ mice and controls. At ≈30 weeks of age, we found no significant differences in plasma parameters except that plasmatic levels of low-density-lipoproteins (LDL) were lower in progeroid mice (Figure 16A, top graphs). At ≈50 weeks of age, *Lmna*$^{HGPSrev/HGPSrev}$ mice had lower levels of plasmatic triglycerides, total cholesterol, and high-density-lipoproteins (HDL) (Figure 16A, bottom graphs), similar to HGPS patients (Melissa A Merideth *et al.*, 2008). Moreover, like in the *Lmna*$^{G609G/G609G}$ mouse model, *Lmna*$^{HGPSrev/HGPSrev}$ mice displayed lower levels of glucose in plasma compared with *Lmna*$^{+/+}$ controls (Figure 16B).

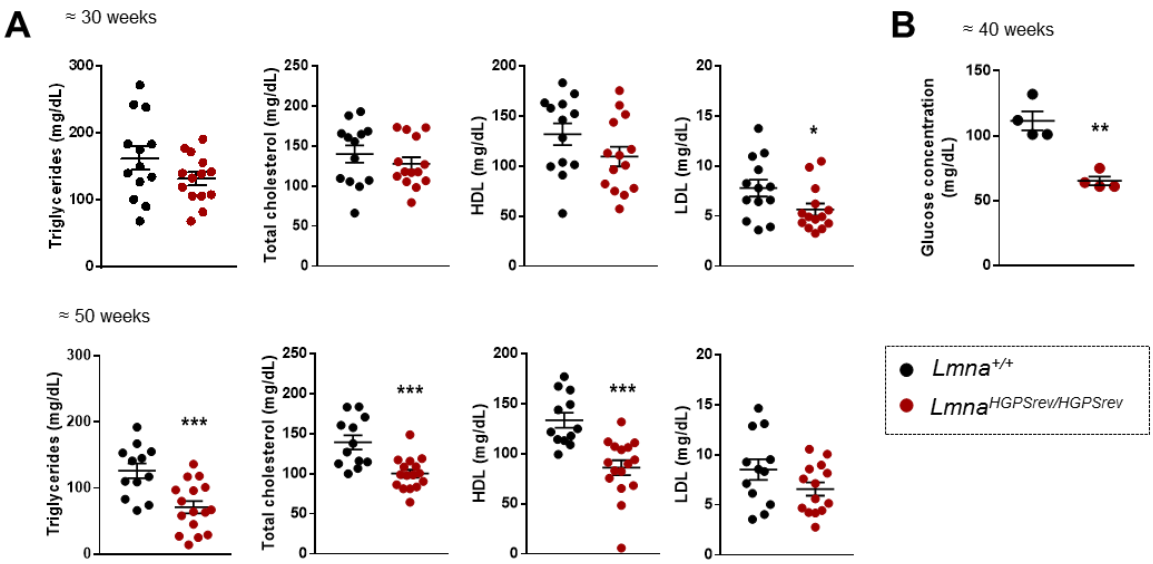

Figure 16: Biochemical analysis of plasma from *Lmna*$^{+/+}$ and progeroid *Lmna*$^{HGPSrev/HGPSrev}$ mice. A) Plasma lipid levels in ≈30- (top) ≈50-week-old mice (bottom) (n=12-16 per genotype). **B)** Plasma glucose levels in ≈40-week-old mice (n=4 pools of 2-4 mice per genotype). HDL: high-density lipoprotein, LDL: low-density lipoprotein. Statistical differences were analyzed by two-tailed t-test. *, P<0.05; **, P<0.01; ***, P<0.001.

.

We next performed histological studies in paraffin-embedded tissue sections. We found a significant loss of subcutaneous fat in the skin of *Lmna*$^{HGPSrev/HGPSrev}$ mice at both ≈30 weeks and ≈50 weeks of age (Figure 17A). In contrast, no between-genotype differences were observed in heart structure (Figure 17B) and spleen (Figure 17C, top images). In addition, we noted higher number of *Lmna*$^{+/+}$ mice with hepatic steatosis compared with *Lmna*$^{HGPSrev/HGPSrev}$ mice (Figure 17C, bottom images).

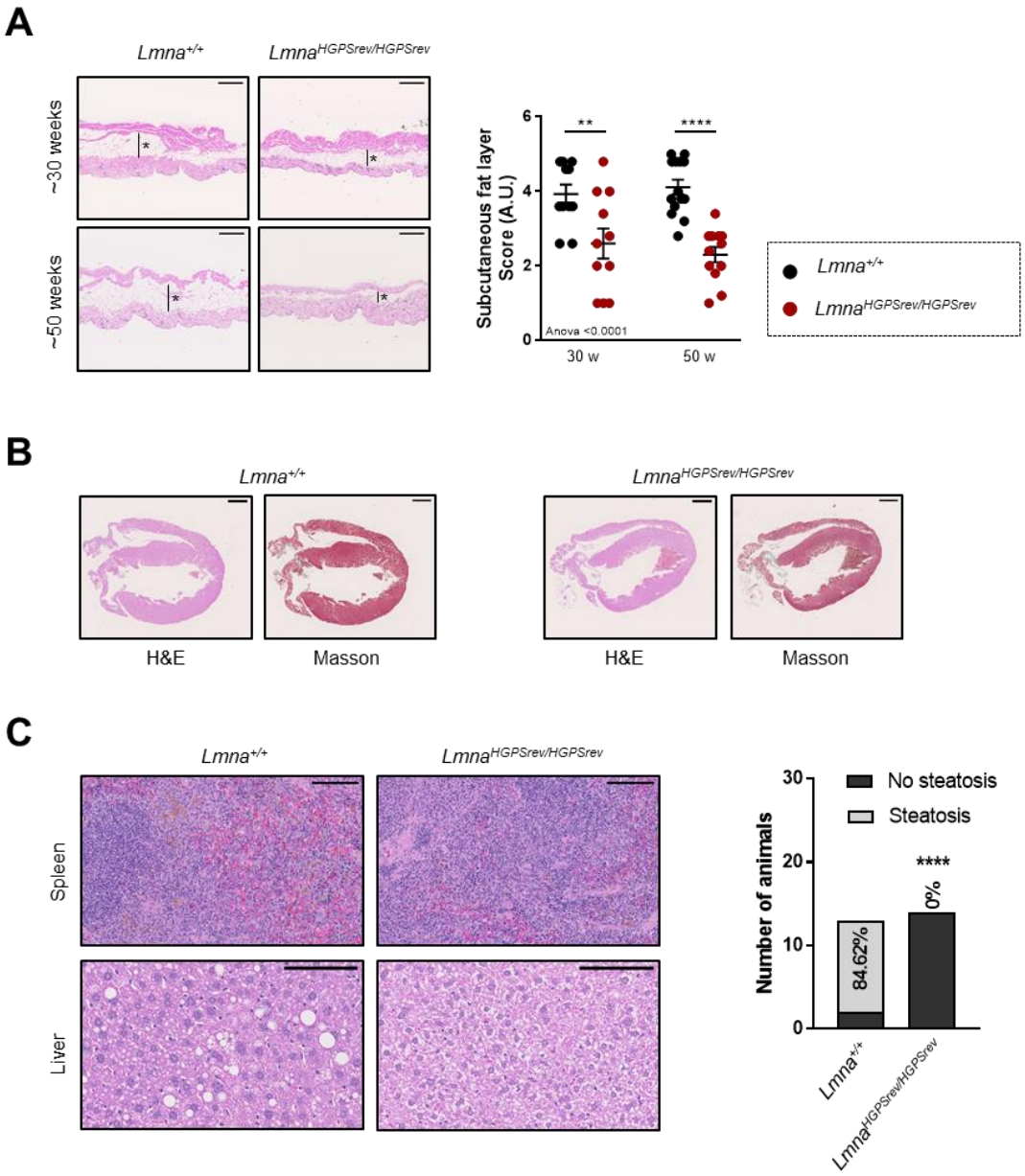

Figure 17: Histological examination of organs from progeroid *Lmna*$^{HGPSrev/HGPSrev}$ mice. Tissue cross-sections from ≈30- and ≈50-week-old *Lmna*$^{+/+}$ (n=11-13) and *Lmna*$^{HGPSrev/HGPSrev}$ mice (n=11-12). **A)** Representative images of skin stained with hematoxylin-eosin (H&E), with asterisks indicating the subcutaneous fat layer. Five independent observers who were blinded to genotype scored the thickness of the subcutaneous fat layer, being 1 the lowest and 5 the highest thickness. Scale bar: 500 µm. **B)** Representative images of heart sections staining with H&E and Masson's trichrome stain. Scale bar: 1 mm. **C)** Representative images of spleen and liver sections stained with H&E, and quantification of the number of mice with liver steatosis. Scale bar: 100 µm. Statistical differences were analyzed by one-way ANOVA with Sidak's post-hoc test **(A)** and chi-square t-test **(C)**. **, P<0.01; ****, P<0.0001.

With the aim of evaluating if increased amount of progerin results in a more aggressive phenotype, we crossbred *Lmna*$^{HGPSrev/+}$ with *Lmna*$^{G609G/+}$ mice to generate *Lmna*$^{HGPSrev/G609G}$ mice. Based on our western blot and PCR analysis (Figure 14, 15) and in the existing alleles of the different mouse strains, the amount of progerin produced by these strains is expected to be higher in *Lmna*$^{HGPSrev/G609G}$ mice, intermediate in *Lmna*$^{G609G/+}$ mice, and lower in *Lmna*$^{HGPSrev/+}$ mice. Accordingly, post-natal body weight (Figure 18A) and average survival (Figure 18B) were more severely affected in *Lmna*$^{HGPSrev/G609G}$ mice, *Lmna*$^{G609G/+}$ mice had an intermediate phenotype, and *Lmna*$^{HGPSrev/+}$ were the less affected.

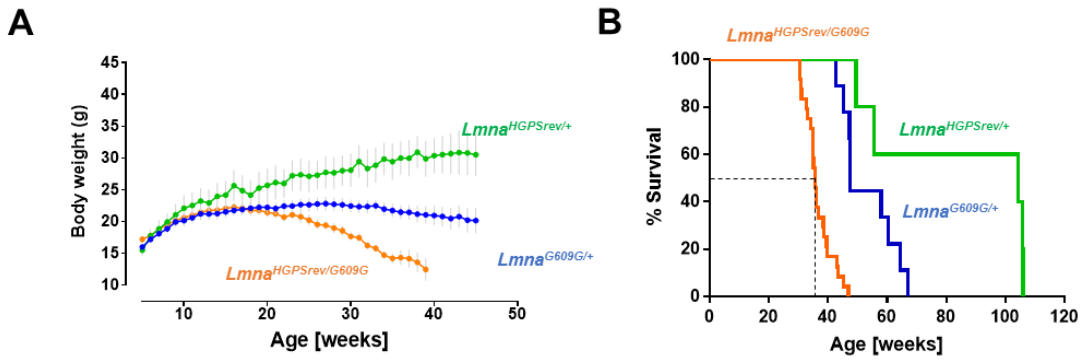

Figure 18: *Lmna*$^{HGPSrev/G609G}$ mice exhibit more severe phenotype than *Lmna*$^{G609G/+}$ and *Lmna*$^{HGPSrev/+}$ mice. **A)** Postnatal body weight curves (n=24 *Lmna*$^{HGPSrev/G609G}$, n=5 *Lmna*$^{HGPSrev/+}$, and n=13 *Lmna*$^{G609G/+}$ mice). **B)** Kaplan-Meier survival plot. Median survival was 35.7 weeks for *Lmna*$^{HGPSrev/G609G}$ mice (n=24), 104.4 weeks for *Lmna*$^{HGPSrev/+}$ mice (n=5), and 47.6 weeks for *Lmna*$^{G609G/+}$ mice (n=9). P<0.0001 for all comparisons, log-rank test.

4.2.2. Vascular Characterization of *Lmna*$^{HGPSrev/HGPSrev}$ Mice

Structural and functional alterations in the vascular system are a hallmark of human HGPS patients, but some available progeroid mouse models do not recapitulate the full spectrum of vascular defects. We therefore sought to carefully assess vascular structure and function in *Lmna*$^{HGPSrev/HGPSrev}$ mice. We first examined collagen content in cross sections of aortic arch and thoracic aorta stained with Masson's trichrome. In aortic arch, collagen deposition was significantly higher in the medial layer in both ≈30- and ≈50-week-old *Lmna*$^{HGPSrev/HGPSrev}$ mice compared with age-matched controls (Figure 19A). There were no differences in collagen amount in the adventitial layer from aortic arch sections when comparing ≈30-week-old mice of both genotypes, but was significantly higher in ≈50-week-old *Lmna*$^{HGPSrev/HGPSrev}$ mice (Figure 19A). In thoracic aorta, the only significant change we observed was higher deposition of collagen in the media in ≈50-week-old *Lmna*$^{HGPSrev/HGPSrev}$ mice (Figure 19B). These findings are consistent with the reported accumulation of collagen in vessels of HGPS patients (Stehbens *et al.*, 2001;

Olive *et al.*, 2010) and other progeroid mouse models (Varga *et al.*, 2006; del Campo *et al.*, 2019).

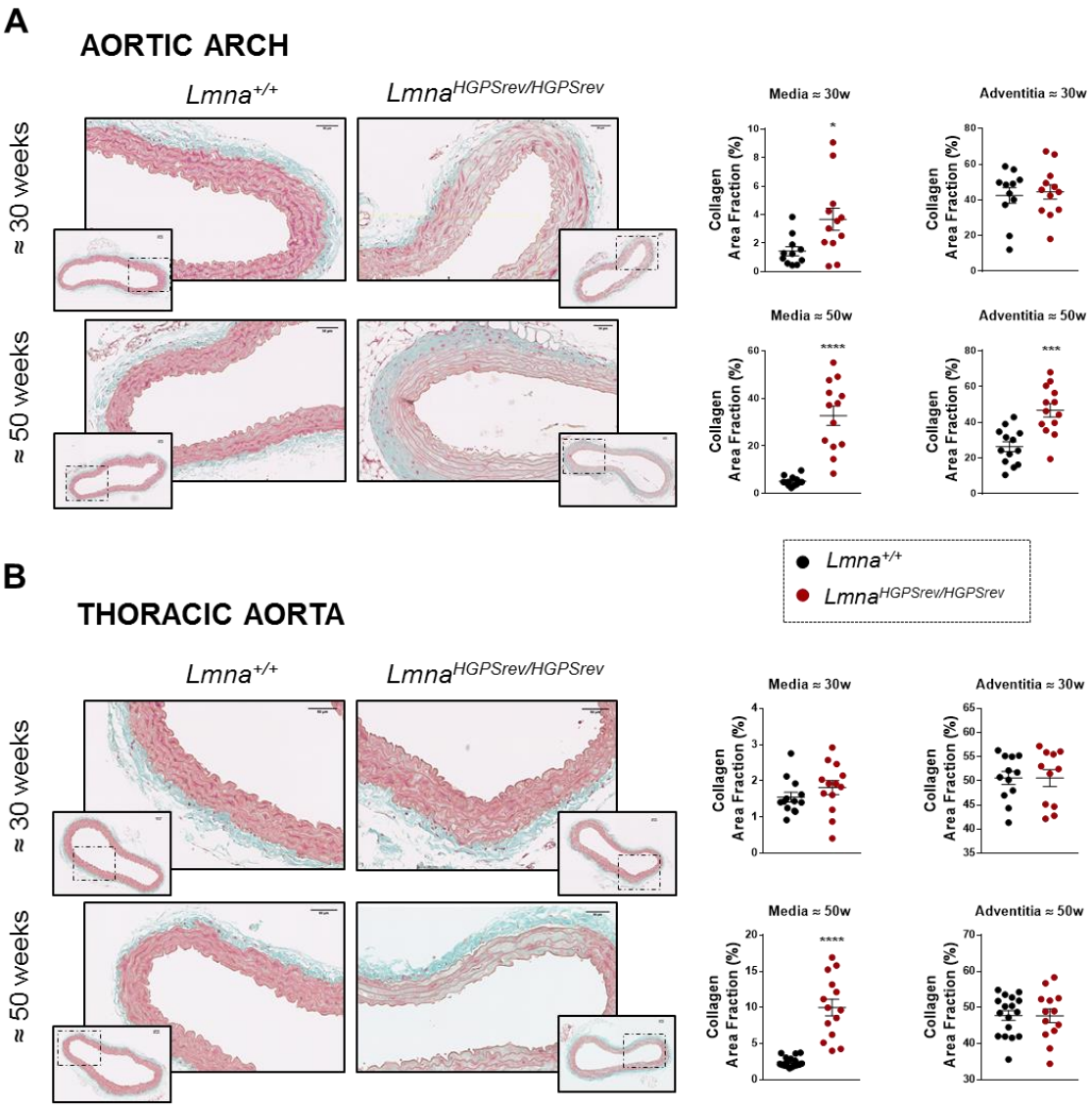

Figure 19: Higher collagen deposition in vessels from *Lmna*$^{HGPSrev/HGPSrev}$ mice. Aortic cross-sections from mice of the indicated ages and genotypes were stained with Masson's trichrome to visualize and quantify collagen deposition in the medial and adventitial layers. **A)** Representative images and quantification of collagen content in aortic arch (n=11-13 *Lmna*$^{HGPSrev/HGPSrev}$ mice; n=12-13 *Lmna*$^{+/+}$ mice). **B)** Representative images and quantification of collagen content in thoracic aorta (n=13-14 *Lmna*$^{HGPSrev/HGPSrev}$ mice; n=13-17 *Lmna*$^{+/+}$ mice). Statistical differences were analyzed by two-tailed t-test with Welch's correction. *, P<0.05; ***, P<0.001; ****, P<0.0001.

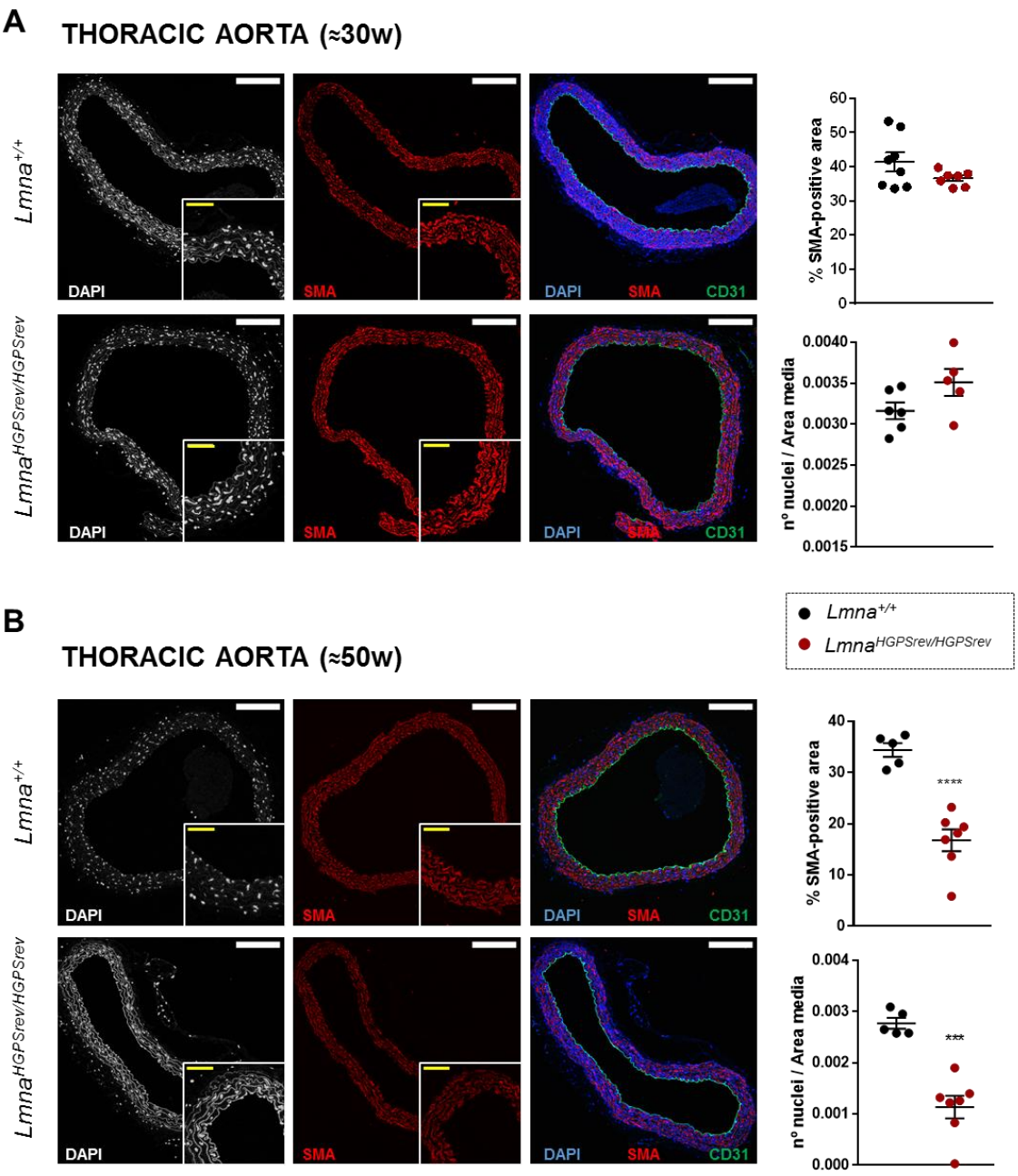

Figure 20: *Lmna*$^{HGPSrev/HGPSrev}$ mice exhibit VSMC loss in thoracic aorta. Representative immunofluorescence images of thoracic aortas from ≈30-week-old mice (n=5-8) **(A)** and ≈50-week-old mice (n=5-7) **(B)** stained with anti-smooth muscle actin (SMA) antibody (red signal), anti-CD31 antibody (green signal) and Hoechst3442 (blue signal) to visualize VSMCs, endothelial cells and nuclei, respectively. Graphs show quantification of VSMC content in the media as either % of SMA-positive area or nuclear density. Scale bar: white 150 µm, yellow 50 µm. Statistical differences were analyzed by two-tailed t-test. ***, P<0.001; ****, P<0.0001.

VSMC depletion is another feature of HGPS patients (Stehbens *et al.*, 2001) and mouse HGPS models (Varga *et al.*, 2006; Osorio *et al.*, 2011; J. M. Lee *et al.*, 2016; Hamczyk *et al.*, 2018). To examine whether collagen deposition is accompanied by loss of VSMC content in our model, we performed immunofluorescence studies to quantify smooth muscle actin (SMA) expression and nuclear density (Hoechst3442 staining) in the media in aortic arch and thoracic aorta

sections from *Lmna*$^{+/+}$ and *Lmna*$^{HGPSrev/HGPSrev}$ mice of different ages. Analysis in ≈30 week-old mice revealed no between-genotype differences in thoracic aorta (Figure 20A) and aortic arch (Figure 21A), but VSMC loss was very severe in both regions in ≈50-week-old *Lmna*$^{HGPSrev/HGPSrev}$ mice (Figure 20B, 21B).

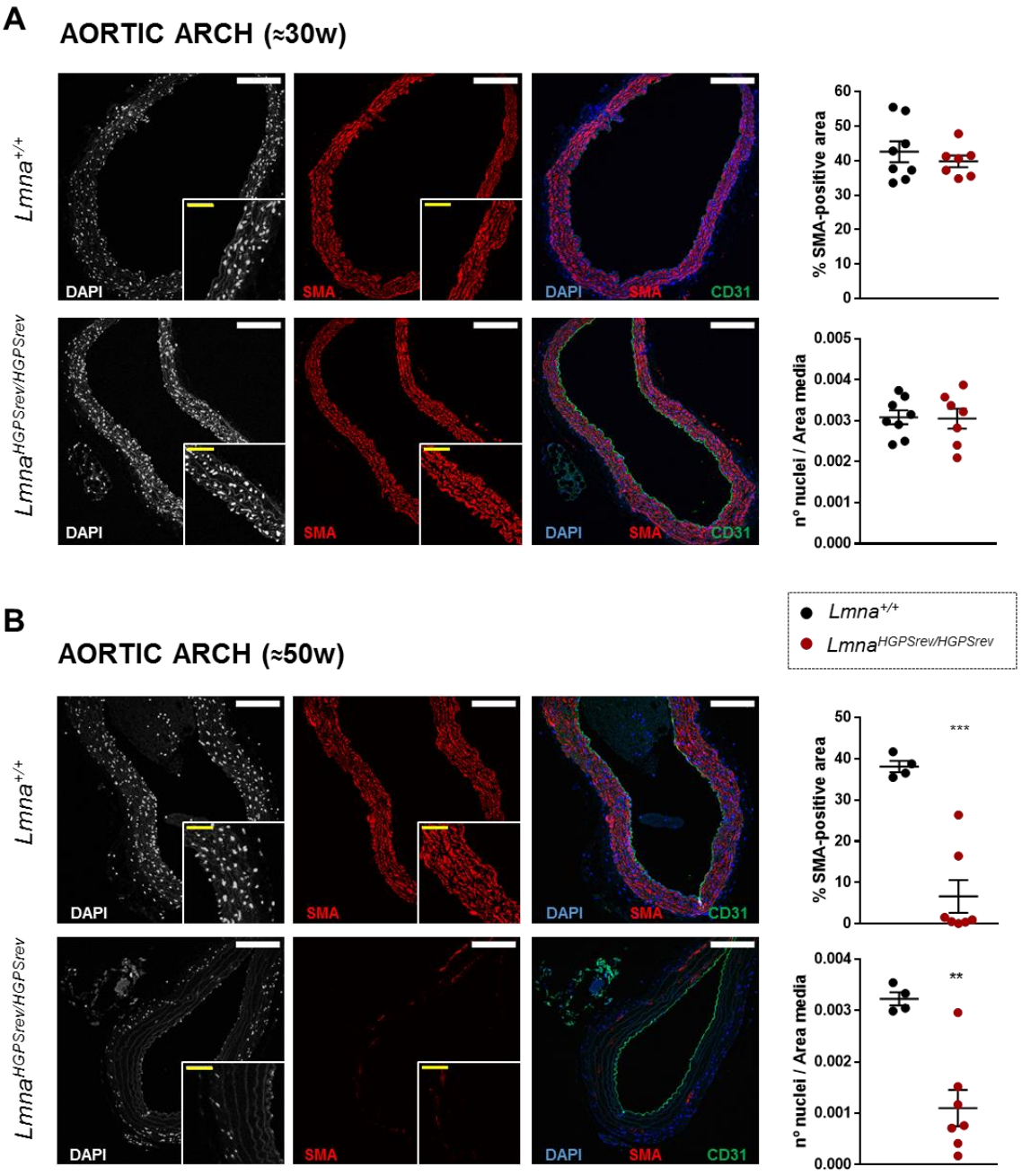

Figure 21: *Lmna*$^{HGPSrev/HGPSrev}$ mice exhibit VSMC loss in aortic arch. Representative immunofluorescence images of aortic arch from ≈30-week-old mice (n=7-8) **(A)** and ≈50-week-old mice (n=4-7) **(B)** stained with anti-smooth muscle actin (SMA) antibody (red signal), anti-CD31 antibody (green signal) and Hoechst3442 (blue signal) to visualize VSMCs, endothelial cells and nuclei, respectively. Graphs show quantification of VSMC content in the media as either % of SMA-positive area or nuclear density. Scale bar: white 150 µm, yellow 50 µm. Statistical differences were analyzed by two-tailed t-test. **, P<0.01; ***, P<0.001.

Vessel stiffness is a very early and pervasive feature in HGPS patients (Lakatta and Levy, 2003; Gerhard-Herman *et al.*, 2012; Hamczyk, del Campo and Andrés, 2018), and our recent studies suggest that collagen is involved in vascular stiffness in progeroid *Lmna*$^{G609G/G609G}$ mice (del Campo *et al.*, 2019). We therefore performed wire and pressure myography studies to evaluate the mechanical properties of vessels from ≈30- and ≈50-week-old *Lmna*$^{HGPSrev/HGPSrev}$ mice and age-matched controls. Diameter-force relations in wire myography experiments can be related by comparing the parameters that describe the regression lines calculated for each of the diameter-force measurements, i.e, the slope, which accounts for the stiffness, and the x-axis intercept (the diameter at 0 force). We observed significant differences in the diameter-force relations, with aortic segments from *Lmna*$^{HGPSrev/HGPSrev}$ mice exhibiting higher slopes at both ages, indicating increased aortic stiffness compared to their littermate controls (Figure 22).

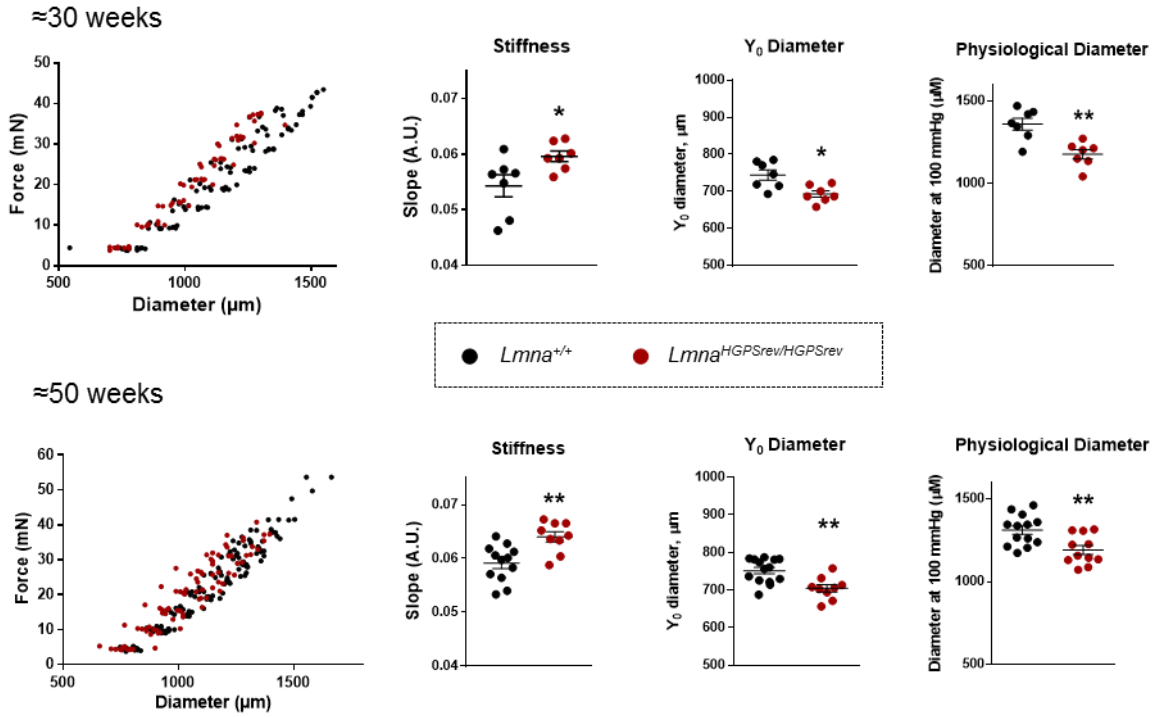

Figure 22: Aortas from progeroid *Lmna*$^{HGPSrev/HGPSrev}$ mice exhibit stiffness and inward remodeling. Aortic rings from ≈30- and ≈50-week-old male mice of the indicated genotypes (n=7-12) were mounted on a wire myograph to analyze diameter-tension relationships, linear regression slope, and diameter at 0 mmHg and estimated at 100 mHg. A.U.: Arbitrary Units. Statistical differences were analyzed by two-tailed t-test. *, P<0.05; **, P<0.01.

These results reinforce the conception of aortic stiffness as one of the earliest features in HGPS, both in humans and mice. In addition, the diameter at 0 force and the estimated physiological diameter at 100 mmHg (diameter when the force is equivalent to an intraluminal pressure of 100 mmHg) were decreased in *Lmna*$^{HGPSrev/HGPSrev}$ aortas at both ages, indicating inwardy remodeled aortas (Figure 22).

We also assessed mechanical and structural properties of small mesenteric arteries by analyzing pressure-diameter properties using a pressure myograph. Outer (vessel) and inner (lumen) diameters were smaller in *Lmna*$^{HGPSrev/HGPSrev}$ vessels at both ages, thus confirming inward remodeling in resistance vessels. Moreover, mesenteric arteries from ≈50 week-old *Lmna*$^{HGPSrev/HGPSrev}$ mice showed a tendency to vascular stiffness, as suggested by a higher slope (BETA) in the stress-strain curve (Figure 23).

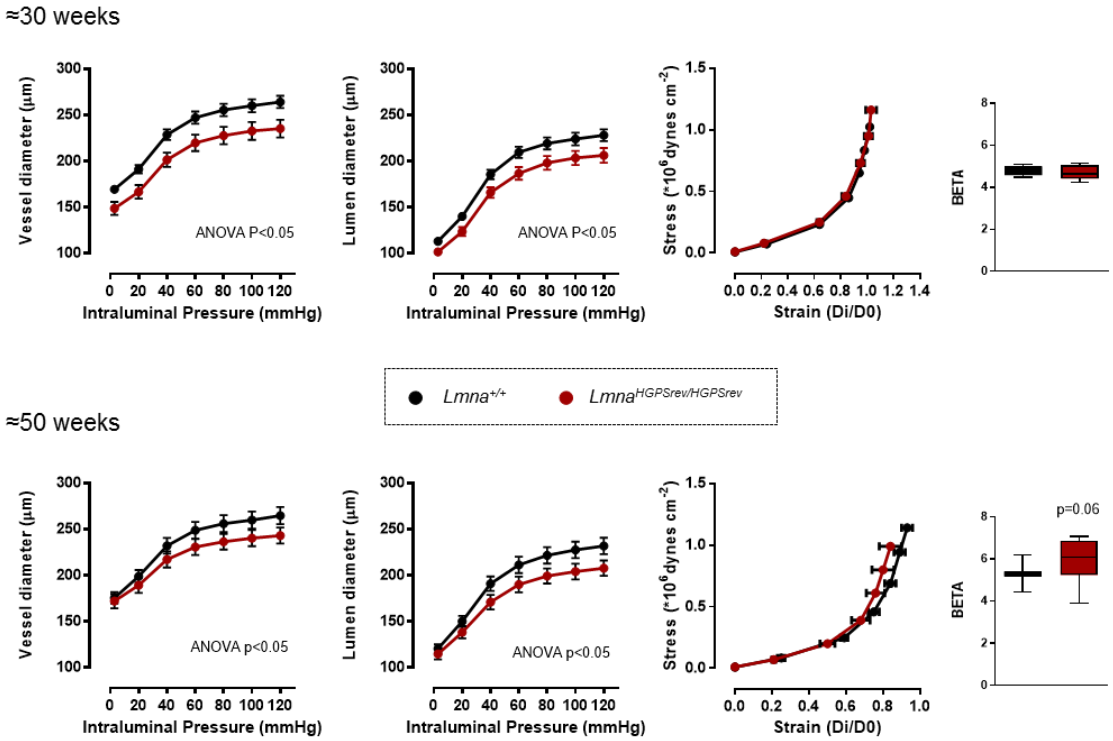

Figure 23: Small mesenteric arteries from *Lmna*$^{HGPSrev/HGPSrev}$ mice exhibit inward remodeling. Mesenteric arteries from ≈30- and ≈50-week-old male *Lmna*$^{+/+}$ mice (n=7-8) and *Lmna*$^{HGPSrev/HGPSrev}$ mice (n=7-9) were mounted on a pressure myograph to analyze pressure-diameter curves for the vessel (outer) and lumen (inner) diameters, and the corresponding stress-strain curves. Statistical differences were analyzed by two-tailed t-test and two-way ANOVA. Data are shown as mean ± SEM (vessel diameter, lumen diameter, and stress-strain curve) and as median with interquartile range and minima and maxima (BETA).

VSMCs are essential for proper regulation of vascular tone, which can be altered by the presence of a stiffer ECM (Lacolley *et al.*, 2017) and for the lack of VSMCs. Taking into account these concerns, we performed wire miography studies to analyze vascular tone in aortic segments from ≈30- and ≈50-week-old *Lmna*$^{HGPSrev/HGPSrev}$ mice and controls. Whereas comparing the younger wild-type and progeroid mice revealed no differences in endothelial-dependent vasodilation (induced by acetylcholine) in ≈30-week-old mice, both endothelium-independent (induced by DEA-NO) and -dependent vasodilation were significantly reduced in ≈50-week-old *Lmna*$^{HGPSrev/HGPSrev}$ mice (Figure 24A).

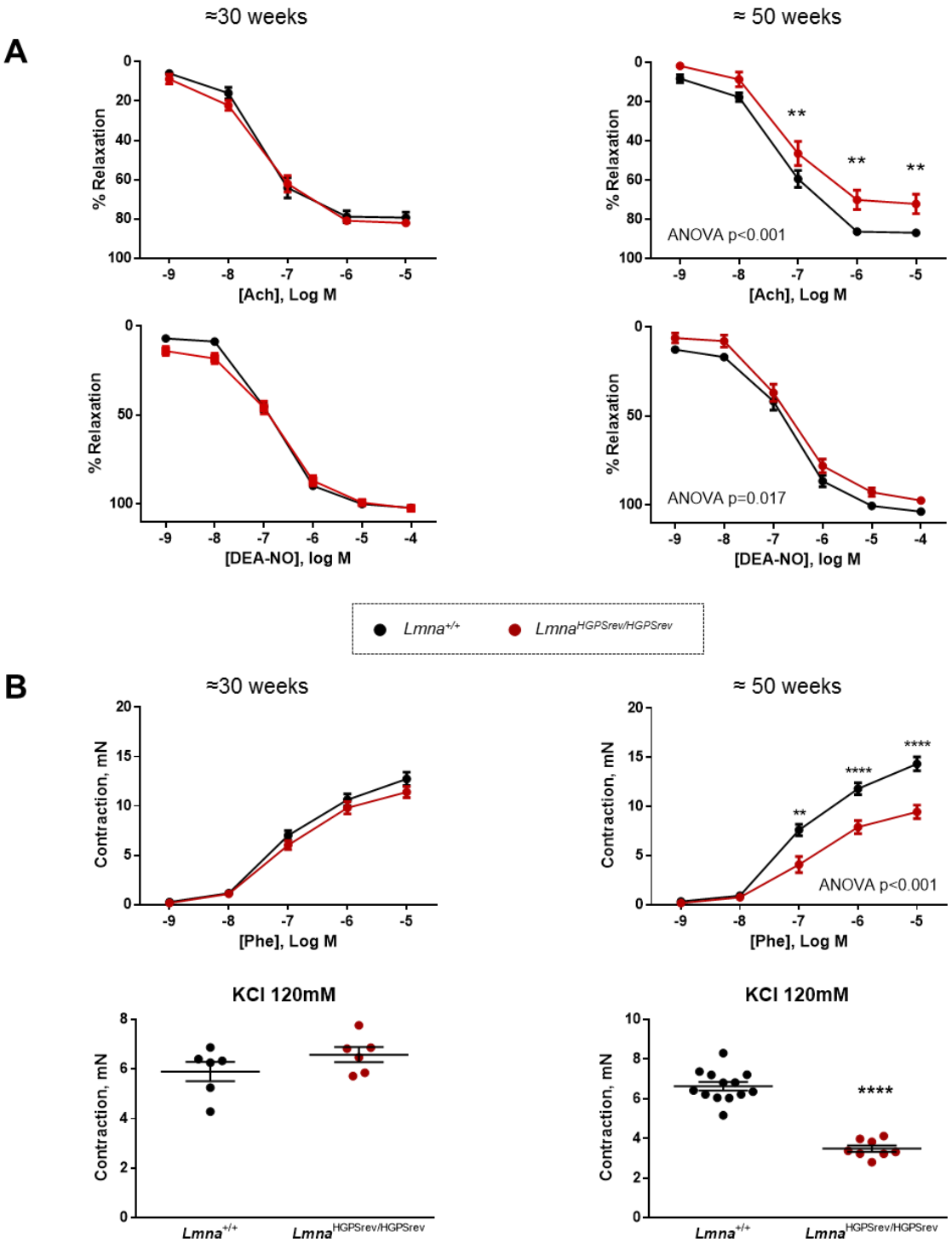

Figure 24: Defective contraction and endothelium-dependent and -independent dilation in thoracic aorta from *Lmna*$^{HGPSrev/HGPSrev}$ mice. Thoracic aortas from ≈30- (n=6) and ≈50-week-old (n=8-13) progeroid mice and aged-matched *Lmna*$^{+/+}$ mice were mounted on a wire myograph to analyze vessel dilation and contraction. **A)** Endothelium-dependent vasodilation induced by acetylcholine (Ach) and endothelium-independent vasodilation induced by DEA-NO. **B)** Contraction induced by phenylephrine (Phe) and KCl. Statistical differences were analyzed by two-way ANOVA with Sidak's post-hoc test in Ach, DEA-NO and Phe graphs, and by two-tailed t-test in KCL graphs. **, P<0.01; ****, P<0.0001. KCL: potassium chloride.

Likewise, we found no between-genotype differences in phenylephrine-induced and KCl-induced contraction in ≈30-week-old mice, but aortic segments from ≈50 week-old *Lmna*$^{HGPSrev/HGPSrev}$ mice exhibited a clear impairment of the contractile responses to both vasoconstrictors (Figure 24B).

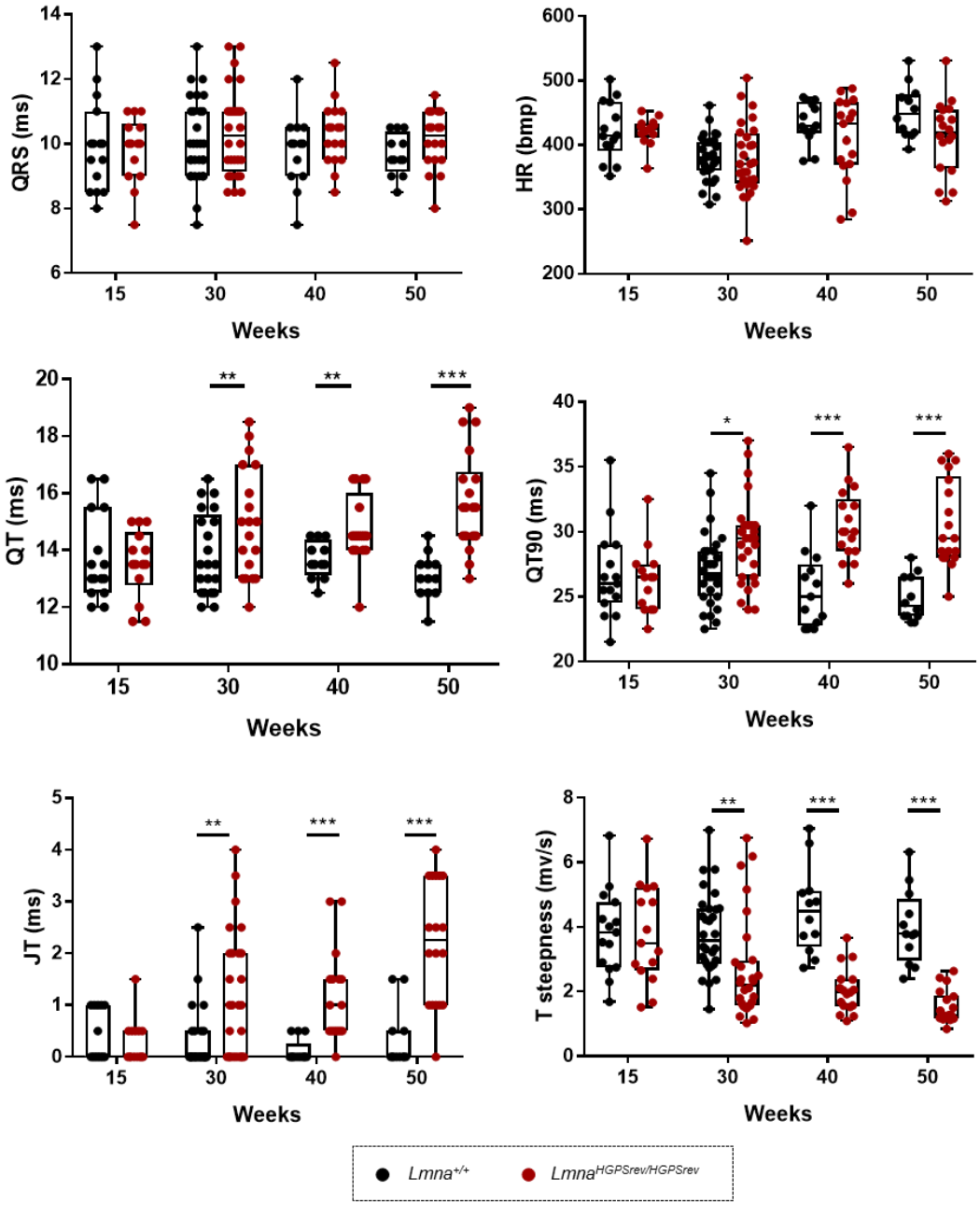

Figure 25: Repolarization abnormalities in *Lmna*$^{HGPSrev/HGPSrev}$ mice. Results of ECG assessment of ≈15-, ≈30-, ≈40-, and ≈50-week-old *Lmna*$^{HGPSrev/HGPSrev}$ mice (n=13-28) and aged-matched *Lmna*$^{+/+}$ mice (n=14-30). Data is show as dot blots and median with interquartile range and minima and maxima. Statistical analysis was performed by custom R scripts. *, P<0.05; **, P<0.01; ***, P<0.001. HR: Heart rate.

4.2.3. Characterization of Cardiac Function in *Lmna*$^{HGPSrev/HGPSrev}$ Mice

To analyze the cardiac phenotype in the *Lmna*^{HGPSrev} strain, we first performed ECG experiments at ages ranging from 15 to 50 weeks. We did not observe any significant change in QRS complex duration at any ages (Figure 25). Importantly, we did not observe bradycardia in *Lmna*$^{HGPSrev/HGPSrev}$ mice (Figure 25), consistent with previous observations in humans (Rivera-Torres *et al.*, 2016; Prakash *et al.*, 2018). Also consistent with previous findings in HGPS patients and in progeroid Zmpste24$^{-/-}$ mice (Rivera-Torres *et al.*, 2016), *Lmna*$^{HGPSrev/HGPSrev}$ mice exhibited age-dependent QT and QT_{90} interval prolongation as well as T-wave flattening and retardation (expressed as a gap between J and T waves), which were normal at early stages but became severe with disease progression (Figure 25).

We next performed echocardiographic studies in ≈50 week-old *Lmna*$^{+/+}$ and *Lmna*$^{HGPSrev/HGPSrev}$ mice. Analysis of systolic function in the LV revealed no between-genotype differences as indicated by ejection fraction (EF) values (Figure 26A). TAPSE, an indirect measurement of systolic function in the right ventricle, was also similar in both genotypes (Figure 26A). Likewise, pulmonary acceleration time (PAT) and pulmonary ejection time (PET) ratio were similar when comparing mice of both genotypes (Figure 26B), indicating that *Lmna*$^{HGPSrev/HGPSrev}$ mice do not develop pulmonary hypertension.

Regarding diastolic function, we observed no between-genotype differences in the IVRT and E/A wave ratio (Figure 26C). However, the percentage of mice with ratios under 1.35 value, which is considered an abnormal LV relaxation pattern (Villalba-Orero *et al.*, 2017), was 30.77% in *Lmna*$^{+/+}$ mice and 53.35% in *Lmna*$^{HGPSrev/HGPSrev}$ mice (Figure 26C). Furthermore, flow velocity from one of the pulmonary veins that drain into the left atrium (pulmonary vein d1 velocity) was significantly lower in progeroid mice (Figure 26C), a typical feature found in diastolic dysfunction (Figure 27C). Interestingly, impaired diastolic function is one of the human pathological alterations that is present both in human aging and HGPS (North and Sinclair, 2012; Prakash *et al.*, 2018).

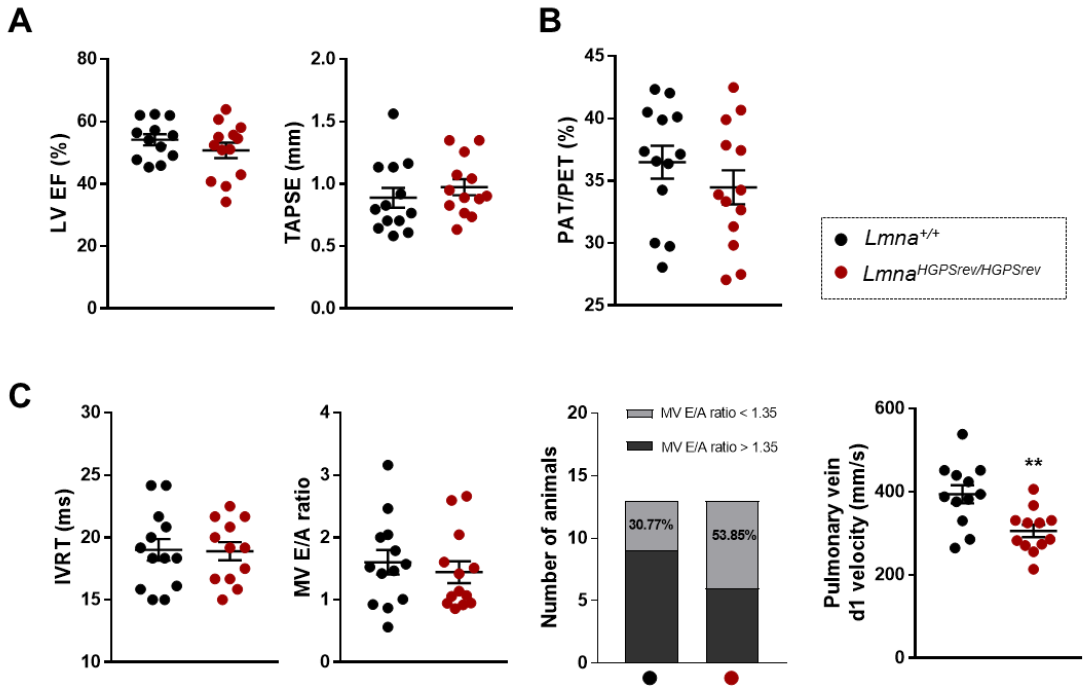

Figure 26: Echocardiographic assessment of *Lmna*$^{HGPSrev/HGPSrev}$ mice. Echocardiographic assessment of ≈50-week-old mice of the indicated genotypes (n=12-13) to quantify parameters related to left ventricle (LV) contractility (EF: ejection fraction), systolic function in the right ventricle (TAPSE) **(A)**, pulmonary hypertension **(B)**, and diastolic function **(C)**. The pulmonary vein velocity, the isovolumetric relaxation time (IVRT), and the number of animals with mitral valve (MV) early and late diastolic velocity peak wave (E and A respectively) ratio below or above 1.35 was quantified in **C**. PAT: Pulmonary artery acceleration time. PET: pulmonary artery ejection time. Statistical differences were analyzed by two-tailed t-test or chi-square t-test. **, P<0.01.

Progeroid mice also exhibited significantly lower cardiac output (CO) (Figure 27A), which is unlikely to result from a reduced heart rate (Figure 25 and 27A), and was associated with lower LV stroke volume (LVSV) (Figure 27A). Nevertheless, it is important to consider that the smaller size of *Lmna*$^{HGPSrev/HGPSrev}$ mice compared with *Lmna*$^{+/+}$ controls (Figure 15A) could affect the results. Indeed, LV mass and LV internal diameter (ID) were significantly lower in *Lmna*$^{HGPSrev/HGPSrev}$ mice (Figure 27B), although no between-genotype differences were observed in either the intraventricular septum (IVS) measurement or LV posterior wall thickness (PW), indicating that *Lmna*$^{HGPSrev/HGPSrev}$ mice do not develop cardiac hypertrophy (Figure 27C).

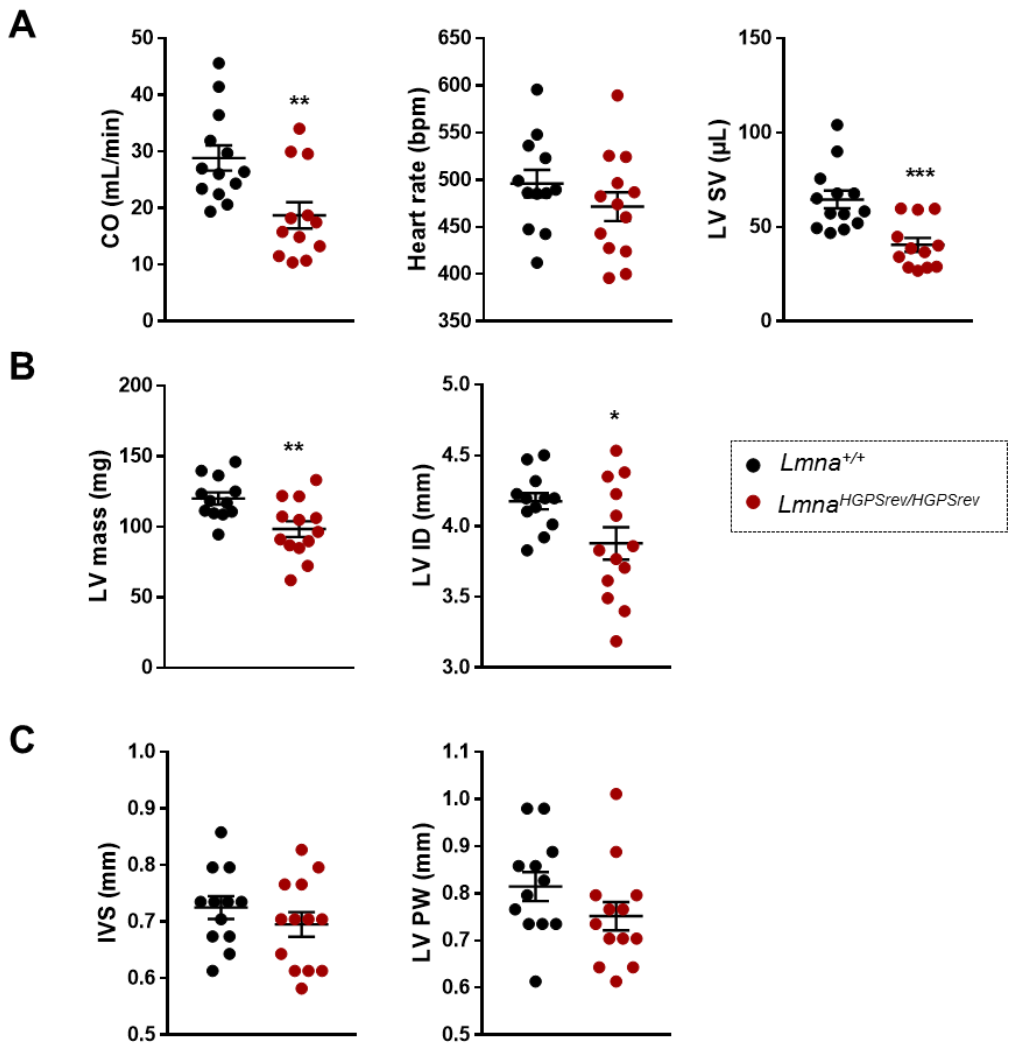

Figure 27: Cardiac function characterization in *Lmna*$^{HGPSrev/HGPSrev}$ mice. Echocardiography study of ≈50-week-old mice of the indicated genotypes (n = 12-13) to measure LV cardiac output (CO), heart rate and LV stroke volume (SV) **(A)**, left ventricle (LV) mass and internal diameter (ID) **(B)**, and intraventricular septum (IVS) and LV posterior (PW) wall dimension **(C)**. Statistical differences were analyzed by two-tailed t-test with Welch's correction when necessary. *, P<0.05; **, P<0.01; ***, P<0.001.

4.3. Study of the Effect of Progerin Suppression and Lamin A Restoration Early and Late in Time in the Development of HGPS

4.3.1. *In Vivo* Validation of Progerin Expression Suppression and Lamin A Restoration

We have generated a new mouse model of HGPS that reproduces the main phenotypic features of human progeria. Remarkably, our progeroid mouse model is the first one allowing a controlled suppression of progerin and, at the same time, restoration of lamin A expression. We sought to use these mice to assess whether progerin elimination and lamin A restoration can slow down the progression of HGPS or even revert some symptoms. To this end, we crossbred our model with transgenic mice carrying a tamoxifen-inducible Cre recombinase with expression driven by a ubiquitous promoter (Ubq-CreERT2). This mouse line ubiquitously expresses the CreERT2 recombinase, which is activated upon treatment with tamoxifen, thus allowing a temporal control of progerin suppression and lamin A restoration by removing the inserted cassette (Figure 28).

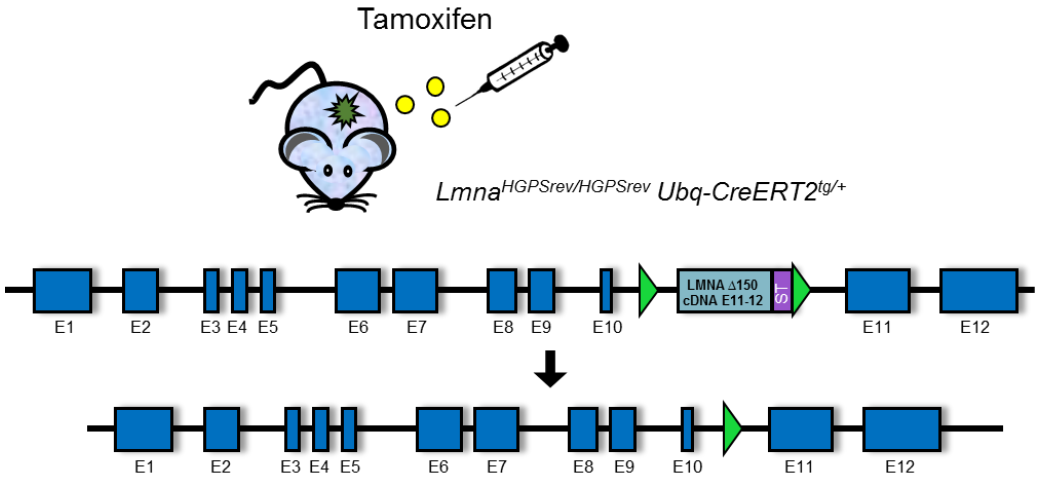

Figure 28: Progerin suppression and lamin A restoration in *Lmna*$^{HGPSrev/HGPSrev}$ *Ubq-CreERT2*$^{tg/+}$ mice treated with tamoxifen. Schematic representation illustrating tamoxifen-induced activation of the Cre recombinase protein in *Lmna*$^{HGPSrev/HGPSrev}$ *Ubq-CreERT2*$^{tg/+}$ mice, which removes the floxed DNA sequence in the mutant *Lmna* allele to suppress progerin expression and restore lamin A expression. E: exon.

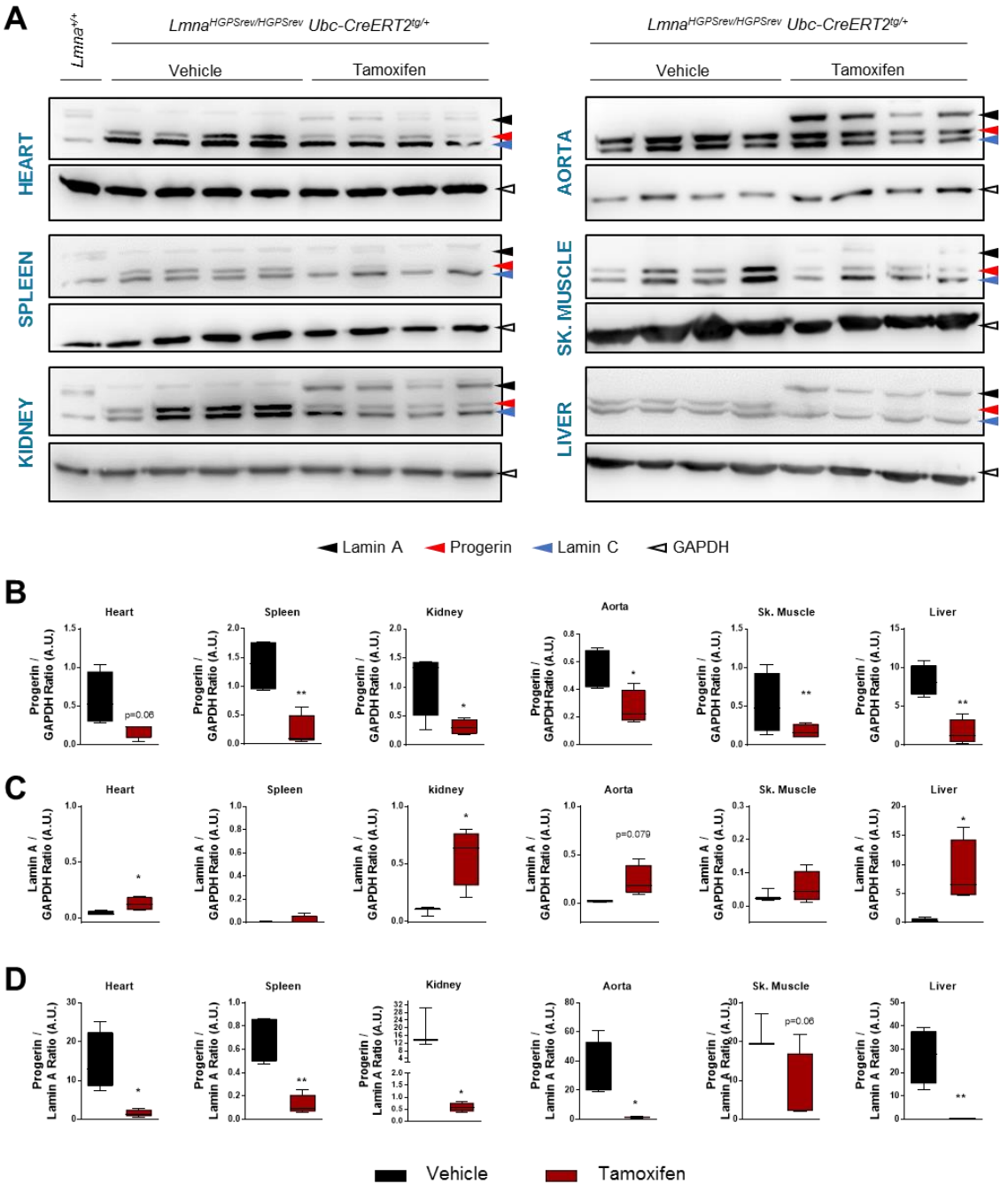

Figure 29: Progerin suppression and lamin A restoration in organs of progeroid *Lmna$^{HGPSrev/HGPSrev}$ Ubq-CreERT2$^{tg/+}$* mice treated with tamoxifen. Nine-week-old *Lmna$^{HGPSrev/HGPSrev}$ Ubq-CreERT2$^{tg/+}$* mice treated with tamoxifen or vehicle (n=4 each condition) were sacrificed to prepare protein extracts from the indicated organs for western blot analysis using a monoclonal antibody that recognizes lamin A, lamin C and progerin. **A)** Representative western blots. **B-D)** The relative abundance of protein bands was quantified using Fiji software. Progerin and lamin A signal intensities were normalized to GADPH. In some blots, there is a non-specific band above the lamin A band. Data are shown as median with interquartile range and minima and maxima. Statistical differences were analyzed by two-tailed t-test. *, P<0.05; **, P<0.01.

Western blot demonstrated tamoxifen-induced reduction in progerin levels in all tested organs, which reached statistically significant differences in spleen, kidney, aorta, skeletal muscle and liver, and a tendency in the heart (Figure 29A and B). Progerin suppression in tamoxifen-treated mice was accompanied by increased lamin A protein level in most of the tested organs (Figure 29A and C). Importantly, the progerin/lamin A ratio in tamoxifen-treated mice was significantly reduced in heart, spleen, kidney, aorta and liver, except for skeletal muscle, where it almost reached statistical significance (Figure 29D).

It has been reported that the Ubc-CreERT2 recombinase shows some spontaneous activity that induces recombination *in vivo* in the absence of tamoxifen (Kristianto *et al.*, 2017). Although our western blot did not show detectable levels of lamin A in vehicle-treated mice (Figure 29A), we wanted to analyze the effect of the possible spontaneous Cre activity in a longitudinal experiment where we measured weight, ECG parameters and survival in untreated *Lmna*$^{HGPSrev/HGPSrev}$, *Lmna*$^{HGPSrev/HGPSrev}$ *Ubc-CreERT2*$^{tg/+}$ and *Lmna*$^{+/+}$ mice. Importantly, Kaplan-Meier survival curves were identical in untreated *Lmna*$^{HGPSrev/HGPSrev}$ *Ubc-CreERT2*$^{tg/+}$ and *Lmna*$^{HGPSrev/HGPSrev}$ mice (Figure 30A). In addition, although *Lmna*$^{HGPSrev/HGPSrev}$ *Ubc-CreERT2*$^{tg/+}$ mice showed slightly but not significant increment in body weight compared with *Lmna*$^{HGPSrev/HGPSrev}$, it was still significantly lower than in *Lmna*$^{+/+}$ controls (Figure 30B).

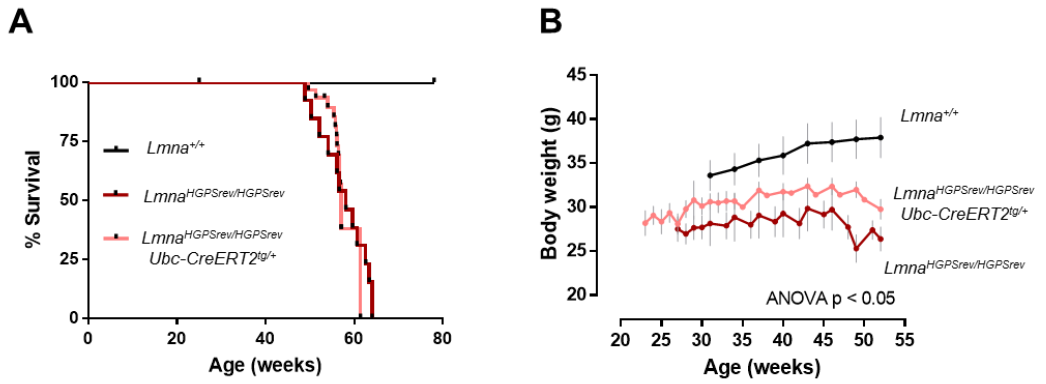

Figure 30: *Lmna*$^{HGPSrev/HGPSrev}$ *Ubc-CreERT2*$^{tg/+}$ mice and *Lmna*$^{HGPSrev/HGPSrev}$ mice have identical survival. A) Kaplan-Meier survival plot. Median survival is 58.1 weeks for *Lmna*$^{HGPSrev/HGPSrev}$ mice (n=13), and 57 weeks for *Lmna*$^{HGPSrev/HGPSrev}$ *Ubc-CreERT2*$^{tg/+}$ mice (n=14). **B)** Body weight curves for *Lmna*$^{HGPSrev/HGPSrev}$ mice (n=13), *Lmna*$^{HGPSrev/HGPSrev}$ *Ubc-CreERT2*$^{tg/+}$ mice (n=28), and *Lmna*$^{+/+}$ mice (n=14). Statistical analysis was performed using log-rank test **(A)** and two-way ANOVA with Tukey's post-hoc test **(B)**.

Regarding ECG parameters, we did not observe significant differences between *Lmna*$^{HGPSrev/HGPSrev}$ *Ubc-CreERT2*$^{tg/+}$ and *Lmna*$^{+/+}$ mice at ≈30 weeks (Figure 31A), and T-wave steepness was the only affected ECG parameter in ≈50-week-old *Lmna*$^{HGPSrev/HGPSrev}$ *Ubc-CreERT2*$^{tg/+}$ mice (Figure 31B). *Lmna*$^{HGPSrev/HGPSrev}$ mice were used as controls in these experiments, which showed ECG alterations that were consistent with our previous results (Figure 25).

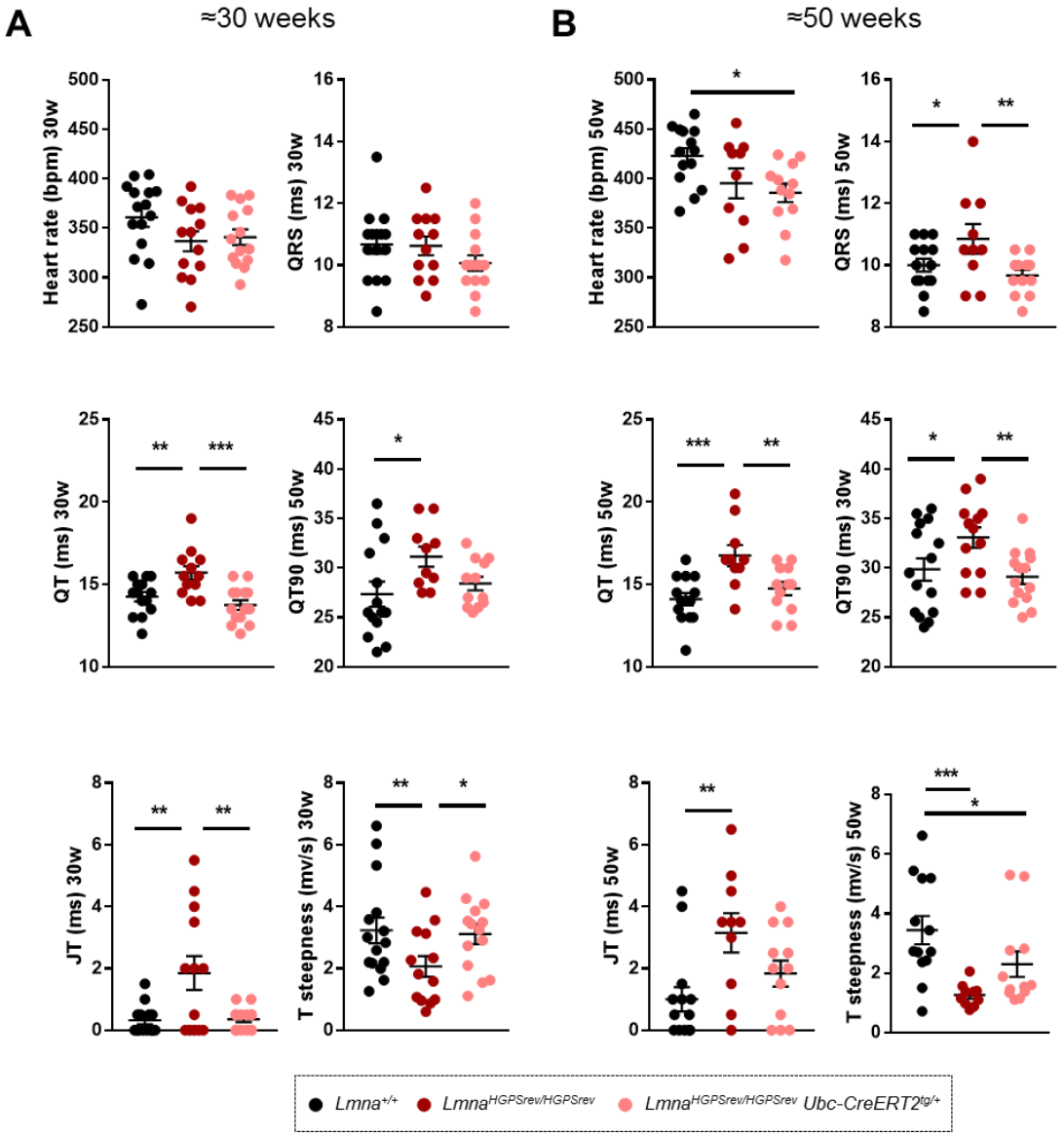

Figure 31: Mild electrocardiographic abnormalities in *Lmna*$^{HGPSrev/HGPSrev}$ *Ubc-CreERT2*$^{tg/+}$ mice. ECG assessment of ≈30- **(A)** and ≈50-week-old **(B)** *Lmna*$^{HGPSrev/HGPSrev}$ *Ubc-CreERT2*$^{tg/+}$ mice (n=13-28) and aged matched *Lmna*$^{+/+}$ and *Lmna*$^{HGPSrev/HGPSrev}$ mice used as controls (n=13-15). Statistical analysis was performed by custom R scripts. *, P<0.05; **, P<0.01; ***, P<0.001.

Although *Lmna*$^{HGPSrev/HGPSrev}$ *Ubc-CreERT2*$^{tg/+}$ mice showed milder cardiac phenotype than *Lmna*$^{HGPSrev/HGPSrev}$ mice, we decided to use this inducible Cre-loxP system to check the effect of progerin suppression and lamin A restoration on the progression of the disease because lifespan in *Lmna*$^{HGPSrev/HGPSrev}$ *Ubc-CreERT2*$^{tg/+}$ mice is shortened in the same extent than in *Lmna*$^{HGPSrev/HGPSrev}$ mice, both mouse lines have reduced body weight compared with *Lmna*$^{+/+}$ controls, and *Lmna*$^{HGPSrev/HGPSrev}$ *Ubc-CreERT2*$^{tg/+}$ mice exhibit some ECG alterations at advanced ages.

4.3.2. Lifespan Extension in Progeroid Mice after Progerin Suppression and Lamin A Restoration

With the aim of assessing whether the suppression of progerin and restoration of lamin A in late stages of HGPS disease could have a therapeutic effect, we treated with tamoxifen a group of 53-56-week-old *Lmna*$^{HGPSrev/HGPSrev}$ *Ubc-CreERT2*$^{tg/+}$ mice, an age close to their maximum life span. Remarkably, although tamoxifen treatment did not improve body weight in these mice (Figure 32A), it significantly increased survival compared with vehicle-treated controls (Figure 32B).

To check the efficiency of tamoxifen at inducing progerin suppression and lamin A restoration, we analyzed by western blot the liver and heart of 6 untreated and 6 treated mice. Five treated animals which exhibited a prolongation in life span compared with untreated controls showed progerin suppression and restoration of lamin A expression (Figure 32C). Moreover, one mouse which died 2 days after tamoxifen treatment did not show progerin suppression and lamin A restoration (marked with arrowhead in Figure 32C). Quantification of protein bands in the western blots showed reduced progerin expression, increased lamin A expression and lower progerin-to-lamin A ratio in liver and heart of tamoxifen- *versus* vehicle-treated mice (Figure 32D).

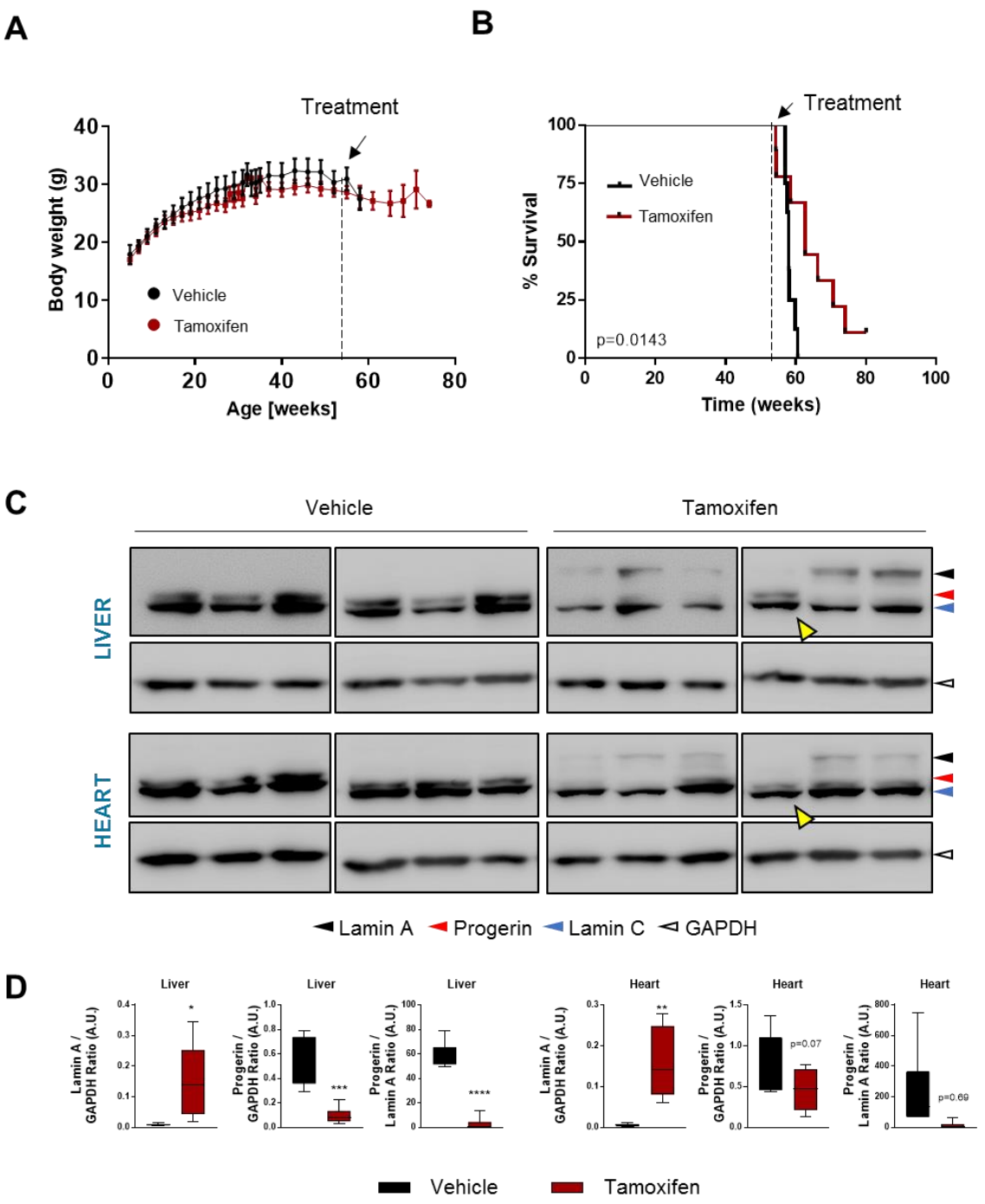

Figure 32: Tamoxifen-dependent reduction of progerin expression and induction of lamin A expression late in life of *Lmna*$^{HGPSrev/HGPSrev}$ *Ubc-CreERT2*$^{tg/+}$ mice extends their lifespan. Mice were treated with tamoxifen (n=9) or vehicle (corn oil) (n=8) starting at 53-56 weeks of age. **A)** Body weight curves. **(B)** Kaplan-Meier survival plot. **C)** Representative western blot analysis showing lamin A and progerin expression in heart and liver of mice treated with vehicle or tamoxifen that were sacrificed because of human-end point criteria. The yellow arrow points to an animal that died two days after the end of tamoxifen treatment. **D)** The relative amount of protein bands was quantified using Fiji software. Progerin and lamin A signal intensities were normalized with GADPH. Data are shown as median with interquartile range and minima and maxima. Statistical differences were analyzed by two-tailed t-test *, P<0.05; **, P<0.01; ***, P<0.001; ****, P<0.0001.

4.3.3. *In Vivo* Gene Therapy Delays HGPS Progression in Progeroid *Lmna*$^{HGPSrev/HGPSrev}$ Mice

Due to the encouraging results obtained in old progeroid *Lmna*$^{HGPSrev/HGPSrev}$ *Ubc-CreERT2*$^{tg/+}$ mice treated with tamoxifen, we sougth to develop a more translational strategy to treat *Lmna*$^{HGPSrev/HGPSrev}$ mice based on ectopic expression of Cre recombinase. We decided to try *in vivo* gene therapy with serotype 9 AAVs delivery vector because of its safety and its success in other studies (Beyret *et al.*, 2019; Santiago-Fernández *et al.*, 2019).

We generated AAVs expressing either Cre (AAV9-Cre) or luciferase (AAV9-luciferase), which were injected intraperitoneally into 15-18-week-old *Lmna*$^{HGPSrev/HGPSrev}$ mice. *Ex vivo* bioluminescence assays showed high level of luciferase in the liver of mice injected with AAV9-luciferase compared with non-injected mice (Figure 33A), consistent with previous studies showing that the liver is one of the most preferred targets of AAVs (Kattenhorn *et al.*, 2016). As expected, semi-quantitative reverse transcription PCR analysis confirmed luciferase and Cre recombinase mRNA expression in the liver of mice infected with AAV9-luciferase and AAV9-Cre, respectively (Figure 33B). In addition, although the decrease in progerin expression was too low for detection by semi-quantitative reverse transcription PCR, we detected a significant induction of lamin A expression in the liver of *Lmna*$^{HGPSrev/HGPSrev}$ mice injected with AAV9-Cre compared with controls injected with AAV9-luciferase (Figure 33B).

Body weight before AAV-injection in 15-18-week-old *Lmna*$^{HGPSrev/HGPSrev}$ mice, was significantly reduced compared with *Lmna*$^{+/+}$ controls (Figure 33C). Follow-up during 24 weeks after injection revealed normal body weight gain in *Lmna*$^{+/+}$ mice infected with AAV9-Cre compared with controls injected with AAV9-Luciferase (Figure 33D). As expected, *Lmna*$^{HGPSrev/HGPSrev}$ mice infected with AAVs-luciferase exhibited a reduction in body weight gain, which was remarkably less pronounced in *Lmna*$^{HGPSrev/HGPSrev}$ mice infected with AAVs-Cre Luciferase (Figure 33D). Follow up of these mice is ongoing to assess the long-term effect of AAV9-Cre on body weight and other progeroid alterations that develop at older ages, and also to ascertain the impact of these gene therapy strategy on survival.

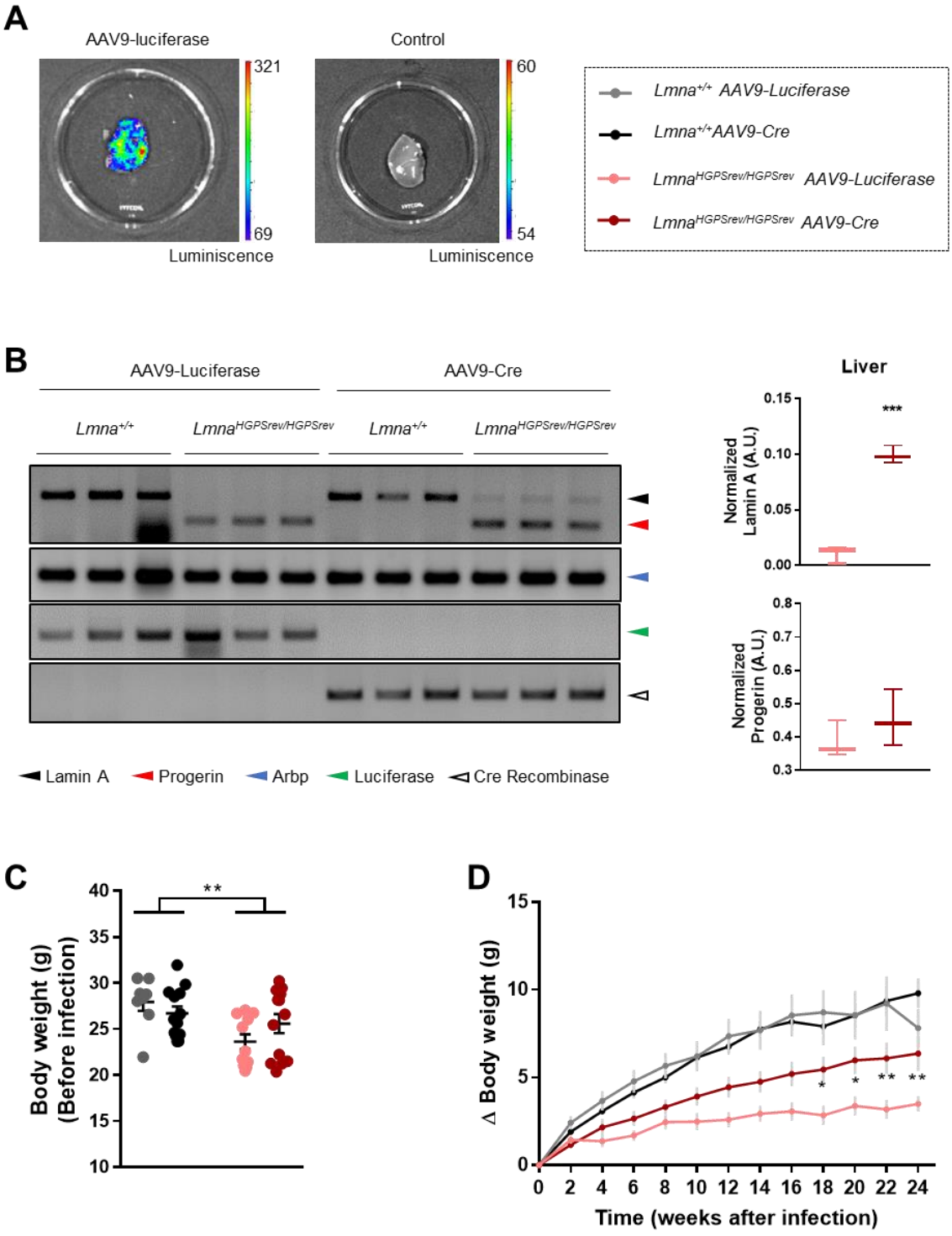

Figure 33: Gene therapy with AAV9-Cre ameliorates post-natal growth of progeroid *Lmna*$^{HGPSrev/HGPSrev}$ mice. 15-18-week-old *Lmna*$^{HGPSrev/HGPSrev}$ and *Lmna*$^{+/+}$ mice received intravenously (tail vein) 1 injection of AAV9 vectors driving the expression of luciferase (AAV9-Luciferase) or Cre recombinase (AAV9-Cre) (dose: 5 x 10^{11} viral genomes). **A)** Representative *ex vivo* bioluminescence images of luciferase expression in liver from mice injected with AAV9-luciferase, and from non-infected mice (control). **B)** Semi-quantitative PCR analysis of lamin A, progerin, luciferase, and Cre recombinase mRNA expression in liver of 30-week-old mice infected with AAV9-Luciferase or AAV9-Cre. Relative quantification of PCR products was performed using Fiji software. Progerin and lamin A signal intensities were normalized relative to Arbp (A.U.: arbitrary units). **C)** Body weight of *Lmna*$^{HGPSrev/HGPSrev}$ and *Lmna*$^{+/+}$ mice one week before infection. **D)** Body weight gain after injection of AAVs. Statistical differences were analyzed by unpaired t-test in **B**, by two-way ANOVA (P<0.01) in **C** and by two-way ANOVA (P<0.0001) with Tukey's post hoc test in **D**. *, P<0.05; **, P<0.01; ***, P<0.001.

DISCUSSION

5. DISCUSSION

CVD is the main cause of death and morbidity worldwide, and aging is the primary cardiovascular risk factor (Lakatta and Levy, 2003; North and Sinclair, 2012). Strikingly, aging is not only restricted to old people since it is estimated that there are hundreds of children worldwide suffering from a premature aging disease called HGPS (https://www.progeriaresearch.org/prf-by-the-numbers/). "Classical" HGPS is an autosomal dominant ultrarare genetic disease caused by a heterozygous *de novo* point mutation in the *LMNA* gene (c.1824C>T; p.G608G) that activates a cryptic splice site leading to the synthesis of progerin, a mutant form of lamin A (Ahmed *et al.*, 2017; Dorado and Andrés, 2017; Gonzalo, Kreienkamp and Askjaer, 2017; Hamczyk, del Campo and Andrés, 2018). HGPS patients display several premature aging features, such as alopecia, contractures of the joints, lipodystrophy and bone and dental problems. They also exhibit accelerated atherosclerosis and associated cerebro- and cardiovascular abnormalities, which eventually lead to premature death by stroke or myocardial infarction at an average age of 14.6 years (Gordon, Massaro, *et al.*, 2014).

Currently, there is no cure for HGPS patients (Kieran, Gordon and Kleinman, 2007; Beyret *et al.*, 2019). Taking into account the extremely low number of patients worldwide and the severity of the disease, it is critical to generate animal models to understand the underlying mechanisms to establish the basis for future therapeutic strategies. Several HGPS mouse models have been generated that resemble many features of this disease. Some of these models express ubiquitously progerin or its immature form prelamin A (Pendás *et al.*, 2002; Varga *et al.*, 2006; Yang, 2006; Osorio *et al.*, 2011; J. M. Lee *et al.*, 2016; Hamczyk *et al.*, 2018). Moreover, some models allow to explore the role of tissue-specific progerin expression (Sagelius, Rosengardten, Schmidt, *et al.*, 2008; Osorio *et al.*, 2011; Strandgren *et al.*, 2015) and the reversibility of progerin-induced phenotypes when expressed specifically in epidermal keratinocytes or bone (Sagelius et al., 2008; Strandgren et al., 2015). However, there are no available mouse models exhibiting ubiquitous progerin expression to study the effects of suppressing its expression either globally or in a cell type-specific manner in early or advanced states of the disease.

Based on results in cellular and animal models of the disease, different therapeutic approaches have been proposed to treat HGPS. However, their efficacy in preclinical models has been very limited. Currently, the only strategy that has been tested in clinical trials is treatment with lonafarnib, alone or in combination with pravastatin and zolenodrate, to inhibit progerin farnesylation, but the benefit for HGPS patients has been very modest (Gordon *et al.*, 2012, 2016). As the cause of HGPS is a *LMNA* gene mutation, a definitive gene therapy targeting the mutation is the most promising strategy to cure the disease. Indeed, two recent studies using newborn *Lmna*$^{G609G/G609G}$ *mice* have reported ameliorated symptoms of HGPS and increased lifespan after an *in vivo* gene therapy strategy designed to correct the disease-causing mutation (Beyret *et al.*, 2019; Santiago-Fernández *et al.*, 2019). However, these studies started gene therapy in neonates, which do not exhibit any apparent symptom of disease. Importantly, in order to develop an effective therapy for HGPS, it should be taken into account that HGPS patients appear normal at birth, and symptoms begin to appear during the first 2 years of life and become increasingly noticeable over time (Ullrich and Gordon, 2015). Hence, HGPS patients are diagnosed once they have a clear symptomatology, when part of the biological damage caused by progerin has already occurred. Therefore, therapies should be tested in animals with disease symptoms already present. To date, no therapy based on progerin suppression and lamin A restoration has been tested in preclinical models with noticeable signs of HGPS. Thus, it remains unknown whether disease progression can be halted or delayed once the symptoms are clearly established.

This Doctoral Thesis aims to generate and characterize *Lmna*^{HGPSrev} mice, the first animal model that allows a controlled spatio-temporal suppression of ubiquitously-expressed progerin while simultaneously restoring lamin A expression (Figure 6). The Tetop LA^{G609G} mouse model allows a controlled expression and suppression of progerin in a tissue-specific manner (Sagelius, Rosengardten, Schmidt, *et al.*, 2008; Strandgren *et al.*, 2015); however our new model shows clear advantages compared with this and other previous models. Indeed, the unique features of *Lmna*^{HGPSrev} mice allow to address very relevant questions in progeria research: 1) Can we prevent or slow down HGPS progression by ubiquitously suppressing progerin and restoring lamin A expression at early stages of the disease when symptoms begin to develop?; 2) How late can we stop progerin expression and restore lamin A to achieve beneficial effects?; and 3) Can we revert or slow down HGPS progression by suppressing progerin expression in a given specific cell type, or do systemic factors resulting from progerin expression in other tissues contribute significantly

to HGPS? If proven effective, cell type-specific therapies would likely be less challenging than whole-body progerin suppression. Furthermore, the ability to restore the expression of lamin A upon progerin suppression is also a key feature of *Lmna*^{HGPSrev} mice, because although lamin A appears to be dispensable in mice (Fong, 2006; López-Mejía *et al.*, 2014), the consequences of its elimination in humans remain unknown.

One of the most remarkable cellular alterations in HGPS is the accumulation of DNA damage (De Sandre-Giovannoli *et al.*, 2003; Dahl *et al.*, 2006; Scaffidi and Misteli, 2006; Dorado and Andrés, 2017). Therefore, we investigated whether cells derived from progeroid *Lmna*^{HGPSrev} mice exhibit DNA damage. Our results showed increased DNA damage in *Lmna*$^{HGPrev/HGPSrev}$ MEFs compared to controls, and suggested more sensitivity to DNA damage-inducing drugs that require specifically HDR for repair (Figure 10, 11). Future studies are warranted to investigate the NHEJ repair pathway and DNA damage response to other types of DNA lesions in *Lmna*$^{HGPrev/HGPSrev}$ MEFs.

We have also performed a thorough *in vivo* characterization of the new model. Firstly, we verified that *Lmna*$^{HGPrev/HGPSrev}$ mice express progerin mRNA and protein in all organs tested (Figure 13, 14). Moreover, our longitudinal study revealed that *Lmna*$^{HGPrev/HGPSrev}$ mice display important features of HGPS patients, such us body weight reduction (Figure 15A), loss of subcutaneous fat (Figure 17A), and premature death (Figure 15B). Regarding biochemical blood parameters, we observed reduced plasma HDL levels (Figure 16A), a common feature in HGPS patients. Of note, in contrast to HGPS patients, plasma triglyceride and cholesterol levels are reduced in *Lmna*$^{HGPrev/HGPSrev}$ mice compared to *Lmna*$^{+/+}$ controls (Figure 16A), suggesting some metabolic problems. These differences between progeroid mice and HGPS patients could be attributed to interspecies differences. Indeed, these abnormalities, together with low glucose levels in plasma (Figure 16B), have been also observed in other mouse models of progeria (Pendás *et al.*, 2002; Bárcena *et al.*, 2018).

Lmna$^{HGPrev/HGPSrev}$ mice exhibit a delayed phenotype compared to *Lmna*$^{G609G/G609G}$ mice (Osorio *et al.*, 2011). Since HGPS severity seems to be dependent on the amount of progerin or the ratio of progerin-to-mature lamin A (Moulson *et al.*, 2007; Hisama *et al.*, 2011; Reunert *et al.*, 2012), we hypothesized that this delayed phenotype could be due to the fact that *Lmna*$^{HGPSrev/HGPSrev}$ mice express lower levels of progerin than *Lmna*$^{G609G/G609G}$ mice (Figure 14). This hypothesis is consistent with our experiments showing that *Lmna*$^{HGPSrev/G609G}$ mice (Figure 18) exhibit a more

severe phenotype than *Lmna*$^{G609G/+}$ and *Lmna*$^{HGPSrev/HGPSrev}$ mice, but less acute than *Lmna*$^{G609G/G609G}$ mice (Osorio *et al.*, 2011).

It is unclear why *Lmna*$^{HGPSrev/HGPSrev}$ mice express lower progerin level than *Lmna*$^{G609G/G609G}$ mice. Since we already observed differences in progerin mRNA levels (Figure 13), defects in progerin translation are not likely the cause. Thus, defective DNA transcription, increased mRNA degradation or enhanced alternative splicing towards lamin C production in *Lmna*$^{HGPSrev/HGPSrev}$ mice seem to be more plausible causes. On the other hand, it has been suggested that specific interaction between lamin A and progerin has a detrimental effect and *in vivo* blockade of this interaction ameliorates the HGPS phenotype (S.-J. Lee *et al.*, 2016). Since lamin A levels are undetectable or negligible in *Lmna*$^{HGPSrev/HGPSrev}$ mice, we cannot rule out that the delayed phenotype in this model could be due to the lack of interaction between progerin and lamin A.

Phenotype differences have been reported among previous HGPS mouse models. For example, G608G BAC mice do not resemble any HGPS physical alteration but they display many of the vascular alterations observed in patients (Varga *et al.*, 2006). In contrast, *Lmna*^{HG} mice do not show vascular abnormalities but exhibit other premature aging features, such as growth retardation, lipodystrophy and premature death (Yang, 2006). One reason for these differences among HGPS mouse models could be the diversity of strategies used for their generation. *Lmna*$^{HGPrev/HGPSrev}$ mice resemble not only some of the premature aging features, such as failure to thrive, loss of subcutaneous fat (Figure 15A, 17A) or lifespan shortening (Figure 15B), but also cardiac abnormalities (Figure 25) and vascular alterations (Figure 19-24). Importantly, cardiovascular dysfunction is the main complication of human HGPS that leads to premature death.

Although autopsy data on HGPS patients are very limited, loss of VSMCs in the medial layer of vessels and its replacement by collagen have been reported in the arterial system in HGPS patients (Stehbens *et al.*, 2001; Olive *et al.*, 2010; Worman and Michaelis, 2018). In our work, we have observed loss of VSMCs both in the thoracic aorta and in the aortic arch in ≈50-week-old *Lmna*$^{HGPSrev/HGPSrev}$ mice (Figure 20B, 21B). This loss of VSMCs is associated with increased collagen deposition (Figure 19) as was also observed in HGPS patients and mouse models (Varga *et al.*, 2006; Hamczyk *et al.*, 2018, 2019; del Campo *et al.*, 2019). Importantly, the presence of excessive collagen in the aortic arch before VSMC depletion at early stages in *Lmna*$^{HGPSrev/HGPSrev}$

mice (Figure 19A, 21A) suggests for the first time that collagen deposition precedes loss of VSMCs.

Lmna$^{HGPSrev/HGPSrev}$ mice offer some advantages compared to other HGPS mouse models. The thoracic aorta does not show significant VSMCs loss in *Lmna*$^{G609G/G609G}$ mice, one of the most used progeroid models (Osorio *et al.*, 2011; del Campo *et al.*, 2019), probably because they die before vascular pathology has been completely developed, since a tendency for this loss has been reported (Osorio *et al.*, 2011). Although BAC G608G mice exhibit vascular pathology, they do not display any other HGPS features (Varga *et al.*, 2006). Thus, the *Lmna*^{HGPSrev} mouse model offers the possibility of studying the role of progerin suppression specifically in VSMCs, and testing whether this suppression prevents the loss of medial VSMC loss and collagen deposition.

Vascular stiffness is an early and pervasive feature in HGPS patients, as well as one major age-related vascular alteration that promotes many cardiovascular complications (Lakatta and Levy, 2003; Gerhard-Herman *et al.*, 2012; Hamczyk, del Campo and Andrés, 2018). We therefore performed wire and pressure myography experiments to determine whether *Lmna*$^{HGPSrev/HGPSrev}$ mice develop vessel stiffening. Consistent with previous observations in *Lmna*$^{G609G/G609G}$ mice (del Campo *et al.*, 2019), *Lmna*$^{HGPSrev/HGPSrev}$ mice exhibit vascular stiffness and inward remodeling in the thoracic aorta, both at medium and late stages of disease progression (Figure 22), strengthening the concept that aortic stiffness is main feature of HGPS. Analysis of small mesenteric vessels in *Lmna*$^{HGPSrev/HGPSrev}$ mice also revealed statistically significant inward remodeling at both medium and late stages, and a tendency to vascular stiffness in old *Lmna*$^{HGPSrev/HGPSrev}$ mice (Figure 23).

Since VSMCs are the major contributors to vascular contraction, that, indeed, can be impaired by the presence of a stiff ECM (Lacolley *et al.*, 2017), we analyzed the mechanisms regulating vascular tone in thoracic aortas from *Lmna*$^{HGPSrev/HGPSrev}$ mice. We observed both endothelial dysfunction (Figure 24A) and decreased contractility (Figure 24B) in the aorta of ≈50-week-old *Lmna*$^{HGPSrev/HGPSrev}$ mice. Interestingly, whereas endothelial function is compromised during aging, normal flow mediated dilation measurements have suggested a preserved endothelial function in HGPS patients (Melissa A Merideth *et al.*, 2008). However, since HGPS patients develop atherosclerosis (Olive *et al.*, 2010), the endothelium -a key player in atherosclerosis development- (Choudhury, Fuster and Fayad, 2004), should be altered at some point. Remarkably, vascular contractility and endothelial function are preserved in ≈30-week-old *Lmna*$^{HGPSrev/HGPSrev}$ mice, which exhibit vascular stiffness at the same age (Figure 22, 24). We

therefore suggest that vascular tone alterations (i.e, impaired contractility and impaired endothelial dependent and independent vasodilation) might be a consequence, but it is not the cause of vascular stiffness.

Regarding electrographic alterations, *Lmna*$^{HGPSrev/HGPSrev}$ mice exhibit significant T-wave flattening and QT, QT_{90} and JT interval prolongation, which were exacerbated as disease progressed compared with age-matched controls (Figure 25). These findings are consistent with repolarization abnormalities previously described in *Zmste24*-deficient mice and HGPS patients (Melissa A. Merideth *et al.*, 2008; Rivera-Torres *et al.*, 2016; Fanjul, 2019). Importantly, while *Zmste24*-deficient and *Lmna*$^{G609G/G609G}$ mice develop bradycardia (Rivera-Torres *et al.*, 2016; Fanjul, 2019), we did not observe this alteration in *Lmna*$^{HGPSrev/HGPSrev}$ mice (Figure 25), in agreement with the results of two studies in HGPS patients (Rivera-Torres *et al.*, 2016; Prakash *et al.*, 2018).

We wanted to explore in detail the cardiac alterations in *Lmna*$^{HGPSrev/HGPSrev}$ mice and their similarities with those found in HGPS patients. Diastolic dysfunction seems to be a common abnormality in HGPS patients, with increasing prevalence at older ages (Prakash *et al.*, 2018), mirroring findings seen during normal aging (Hamczyk, del Campo and Andrés, 2018). One of the proposed mechanisms leading to diastolic dysfunction is reduced compliance, resulting from diffuse myocardial fibrosis and concomitant increased stiffness of the LV (Villalba-Orero *et al.*, 2017; Hamczyk, del Campo and Andrés, 2018; Prakash *et al.*, 2018). Although our echocardiographic analysis did not reveal statistically significant differences in the E/A ratio when comparing *Lmna*$^{HGPSrev/HGPSrev}$ mice and *Lmna*$^{+/+}$ controls (Figure 26C), our progeroid mice showed reduced flow velocity from one of the pulmonary veins that drain into the left atrium (Figure 26C), indicating possible diastolic dysfunction. Hence, future analysis of diffuse myocardial fibrosis are warranted to conclusively asses if the diastolic dysfunction observed in HGPS patients also occur in *Lmna*$^{HGPSrev/HGPSrev}$ mice. Additionally, consistent with HGPS patients, neither systolic function nor pulmonary tension were altered in *Lmna*$^{HGPSrev/HGPSrev}$ mice compared with age-matched controls (Figure 26A, 26B).

After characterizing our new mouse model and confirming its progeroid phenotype, we sought to determine the potential therapeutic benefit of suppressing progerin expression and restoring lamin A levels once the HGPS phenotype has developed. To this end, we generated *Lmna*$^{HGPSrev/HGPSrev}$ *Ubc-CreERT2*$^{tg/+}$ mice by crossing *Lmna*^{HGPSrev} mice with transgenic *Ubq-CreERT2*$^{tg/+}$ mice, which carry a tamoxifen-inducible Cre recombinase controlled by a ubiquitous promoter

(Figure 28). Of note, although survival was undistinguishable between *Lmna*$^{HGPSrev/HGPSrev}$ *Ubc-CreERT2*$^{tg/+}$ and *Lmna*$^{HGPSrev/HGPSrev}$ mice (Figure 30A), cardiac symptoms were milder in *Lmna*$^{HGPSrev/HGPSrev}$ *Ubc-CreERT2*$^{tg/+}$ mice (Figure 31). Although we did not observe detectable levels of lamin A in *Lmna*$^{HGPSrev/HGPSrev}$ *Ubc-CreERT2*$^{tg/+}$ mice treated with vehicle (Figure 29, 32C), we cannot rule out a residual spontaneuous Cre activity (Kristianto *et al.*, 2017) as a cause of the observed milder phenotype in these animals. Moreover, it has been previously described that *Zmspte24*-deficient mosaic mice did not display progeroid phenotype (de la Rosa *et al.*, 2013). Therefore, a milder phenotype in *Lmna*$^{HGPSrev/HGPSrev}$ *Ubc-CreERT2*$^{tg/+}$ mice with spontaneous recombination would not be surprising.

Tamoxifen treatment of *Lmna*$^{HGPSrev/HGPSrev}$ *Ubc-CreERT2*$^{tg/+}$ mice removed the progerin cassette inserted in the *Lmna* locus and restored lamin A protein expression (Figure 29). These results verified the feasibility of our strategy at the genetic and protein level. Notably, we have demonstrated that it is possible to enhance significantly the survival of progeroid mice even when treatment starts at very advanced stages of disease progression (Figure 32A). Although we have shown that tamoxifen-treated animals exhibit progerin suppression or reduction and restoration of lamin A expression (Figure 32C), more organs need to be analyzed. Interestingly, one of the animals that died 2 days after tamoxifen administration did not show changes in progerin and lamin A protein expression (Figure 32C, yellow arrowhead). These results are very encouraging because they give great hope for patients with advanced symptomatology, so we can claim that *'it´s never too late'* to start anti-HGPS treatments. However, it seems there is a point where the damage generated by progerin is irreversible, since prolongation of life span in tamoxifen-treated *Lmna*$^{HGPSrev/HGPSrev}$ *Ubc-CreERT2*$^{tg/+}$ mice die prematurely compared to the life span of *Lmna*$^{+/+}$ animals (Figure 32A). Furthermore, these mice did not improve body weight after tamoxifen administration (Figure 32B), suggesting irreversible processes at the very last stages of disease progression. However, we cannot rule out that the lack of a complete reversion of the HGPS phenotype may be due to incomplete progerin removal and lamin A restoration.

Two recently published studies provided proof-of-concept for CRISPR-Cas9 system-based *in vivo* gene therapy in newborn HGPS mice (Beyret *et al.*, 2019; Santiago-Fernández *et al.*, 2019). However, none of these therapies has tested its efficiency in adult mice with an established progeroid phenotype. In our work, we have observed a significant improvement of the body weight in 15-18-week-old *Lmna*$^{HGPSrev/HGPSrev}$ mice infected with AAV9 expressing Cre recombinase (Figure 33D). Thus, we have demonstrated for the first time that *in vivo* gene therapy slows

down the progression of the disease. Ongoing follow up of these mice will ascertain the impact of our gene therapy on survival.

Our mouse model also allows progerin suppression and lamin A restoration in specific cell types using transgenic mice with cell type-specific Cre expression. Our laboratory has recently demonstrated that expressing progerin specifically in VSMCs induces inward remodeling and vascular stiffness (del Campo *et al.*, 2019). In addition progerin expression in VSMCs is sufficient to provoke vascular pathology and to shorten significantly the life span of Apolipoprotein E deficient mice, suggesting that these cells are a major contributors to HGPS vascular pathology (Hamczyk *et al.*, 2018, 2019; Hamczyk and Andrés, 2019). We have therefore generated *Lmna*$^{HGPSrev/HGPSre}$ *SM22aCre*$^{+/tg}$ mice, in which progerin is suppressed and lamin A restored in VSMCs. Characterization of these mice will allow us to ascertain if we can prevent or slow down vascular alterations and augment survival by suppressing progerin expression in VSMCs. Future studies will include other cell types to identify the key organs that determine life- and health-span in progeria, which should be targeted for therapeutic purposes.

Collectively, this Doctoral Thesis aimed at generating, characterizing and validating *Lmna*$^{HGPSrev/HGPSrev}$ mice, a new mouse model of HGPS to study the effect of progerin elimination and lamin A restoration either ubiquitously or from specific tissues in a background of whole-body progerin expression. Using these mice, we have addressed a fundamental question concerning the real possibilities of stopping or slowing down the progression of HGPS by removing progerin once the disease phenotype is established, something that had remained unknown so far. Our results constitute an important advance for the progeria field and give hope for the development of new therapies to treat or cure HGPS. Ongoing studies are examining the benefit of suppressing progerin and restoring lamin A starting at earlier stages of HGPS using both the tamoxifen-inducible Cre mouse model and AAV-Cre strategy. Our model will also address whether cardiovascular alterations and HGPS progression can be prevented or delayed by suppressing progerin expression only in specific cell types that are relevant to CVD such as VSMCs, endothelial cells and cardiomyocytes.

CONCLUSSIONS

6. CONCLUSIONS

In this Doctoral Thesis, we have used the CRISPR-Cas9 system to generate a new conditional mouse model of HGPS to assess disease progression upon progerin suppression and lamin A restoration. This model also allows to evaluate the relative contribution of systemic and tissue-specific factors to the development of HGPS to assess the effectiveness of potential future therapies designed to eliminate progerin ubiquitously or in a tissue-specific manner. The main conclusions derived from this Doctoral Thesis are the following:

1. *Lmna*$^{HGPSrev/HGPSrev}$ mice express progerin ubiquitously and recapitulate the features of human HGPS such as failure to thrive, loss of subcutaneous fat, premature death and cardiovascular alterations, including collagen deposition, VSMC depletion, impaired vessel contraction, arterial endothelial dysfunction, vessel stiffness and inward remodeling and cardiac repolarization abnormalities.

2. The *Lmna*^{HGPSrev} conditional allele allows the suppression of progerin expression with simultaneous restoration of lamin A expression upon activation of the Cre recombinase both *in vitro* and *in vivo*.

3. Suppression of progerin expression and lamin A restoration upon tamoxifen activation of the Cre recombinase at late stages of HGPS prolongs the survival of *Lmna*$^{HGPSrev/HGPSrev}$ *Ubc-CreERT*$^{tg/+}$ mice.

4. Gene therapy with a single injection of adeno-associated virus overexpressing the Cre recombinase starting in *Lmna*$^{HGPSrev/HGPSrev}$ mice exhibiting initial symptoms of HPGS improves body weight gain.

6. CONCLUSIONES

En esta Tesis Doctoral hemos generado mediante el sistema CRISPR-Cas9 un nuevo modelo de ratón condicional de HGPS para analizar el efecto de la eliminación de la progerina y la restauración de la lamina A en el desarrollo de la progeria. Este modelo también permite investigar la contribución relativa de factores sistémicos y específicos de tejido al desarrollo de la progeria para evaluar la eficacia de posibles terapias futuras dirigidas a la eliminación ubicua o tejido-específica de la progerina. Las principales conclusiones derivadas de este trabajo son:

1. Los ratones *Lmna*$^{HGPSrev/HGPSrev}$ expresan progerina y recapitulan gran parte de las características de HGPS en humanos como muerte prematura, peso corporal reducido, perdida de grasa subcutánea y alteraciones cardiovasculares incluyendo acumulación de colágeno, pérdida de células del músculo liso vascular, contracción vascular defectuosa, disfunción endotelial, rigidez y remodelado vascular hacia dentro, y alteraciones electrocardiográficas.

2. El alelo condicional *Lmna*^{HGPSrev} permite la eliminación de la expresión de la progerina y la restauración simultánea de la lamina A inducida por la activación de la recombinasa Cre tanto *in vitro* como *in vivo*.

3. La eliminación de la progerina y la restauración de la lamina A en estadios avanzados de la enfermedad provocada por la activación de la recombinasa Cre inducida por tratamiento con tamoxifeno aumenta la supervivencia de los ratones *Lmna*$^{HGPSrev/HGPSrev}$ *Ubc-CreERT*$^{tg/+}$.

4. La terapia génica basada en una única inyección sistémica de virus adeno-asociados que sobreexpresan la recombinasa Cre mejora la ganancia de peso de ratones *Lmna*$^{HGPSrev/HGPSrev}$ adultos en los que el tratamiento se inicia cuando ya presentan síntomas de HGPS.

BIBLIOGRAPHY

Ahmad, G. and Amiji, M. (2018) 'Use of CRISPR/ Cas9 gene-editing tools for developing models in drug discovery', *Drug Discovery Today*, 23(3), pp. 519–533.

Ahmed, M. S. *et al.* (2017) 'Hutchinson–Gilford Progeria Syndrome: A premature aging disease', *Molecular Neurobiology*, 55(5), pp. 4417–4427.

Aida, T. *et al.* (2015) 'Cloning-free CRISPR/Cas system facilitates functional cassette knock-in in mice.', *Genome biology*, 16(1), p. 87.

Alter, J. *et al.* (2006) 'Systemic delivery of morpholino oligonucleotide restores dystrophin expression bodywide and improves dystrophic pathology', *Nature Medicine*, 12(2), pp. 175–177.

Andrés, V. and González-Granado, J. M. (2009) 'Role of A-type lamins in signaling, transcription, and chromatin organization.', *The Journal of cell biology*, 187(7), pp. 945–57.

Aoki, Y. *et al.* (2010) 'In-frame dystrophin following exon 51-skipping improves muscle pathology and function in the exon 52–deficient mdx mouse', *Molecular Therapy*, 18(11), pp. 1995–2005.

Balmus, G. *et al.* (2018) 'Targeting of NAT10 enhances healthspan in a mouse model of human accelerated aging syndrome', *Nature Communications*, 9(1), p. 1700.

Bárcena, C. *et al.* (2018) 'Methionine restriction extends lifespan in progeroid mice and alters lipid and bile acid metabolism.', *Cell reports*, 24(9), pp. 2392–2403.

Bass-Stringer, S. *et al.* (2018) 'Adeno-Associated Virus gene therapy: Translational progress and future prospects in the treatment of heart failure.', *Heart, lung & circulation*, 27(11), pp. 1285–1300.

Behringer, R. *et al.* (2014) *Manipulating the mouse embryo: a laboratory manual*. Fourth Edi. Cold Spring Harbor Laboratory Press.

Beyret, E. *et al.* (2019) 'Single-dose CRISPR–Cas9 therapy extends lifespan of mice with Hutchinson–Gilford progeria syndrome', *Nature Medicine*, 25(3), pp. 419–422.

Bockamp, E. *et al.* (2008) 'Conditional transgenic mouse models: from the basics to genome-wide sets of knockouts and current studies of tissue regeneration', *Regenerative Medicine*, 3(2), pp. 217–235.

Bradford, M. M. (1976) 'A rapid and sensitive method for the quantitation of microgram quantities of protein utilizing the principle of protein-dye binding.', *Analytical biochemistry*, 72, pp. 248–54.

Briones, A. M. *et al.* (2009) 'Atorvastatin prevents angiotensin II–induced vascular remodeling and oxidative stress', *Hypertension*, 54(1), pp. 142–149.

Brocher, J. (2015) 'The BioVoxxel Image Processing and Analysis Toolbox', in *European BioImage Analysis Symposium*. Paris, France.

Broers, J. L. V. *et al.* (2006) 'Nuclear Lamins: Laminopathies and their role in premature ageing', *Physiological Reviews*, 86(3), pp. 967–1008.

del Campo, L. *et al.* (2019) 'Vascular smooth muscle cell specific progerin expression in a mouse model of Hutchinson–Gilford progeria syndrome promotes arterial stiffness: Therapeutic effect of dietary nitrite', *Aging Cell*, 18(3), p. e12936.

del Campo, L. and Ferrer, M. (2015) 'Wire myography to study vascular tone and vascular structure of isolated mouse arteries', in *Methods in molecular biology*, pp. 255–276.

Cao, K., Blair, C. D., *et al.* (2011) 'Progerin and telomere dysfunction collaborate to trigger cellular senescence in normal human fibroblasts.', *The Journal of clinical investigation*, 121(7), pp. 2833–44.

Cao, K., Graziotto, J. J., *et al.* (2011) 'Rapamycin reverses cellular phenotypes and enhances mutant protein clearance in Hutchinson-Gilford progeria syndrome cells.', *Science Translational Medicine*, 3(89), p. 89ra58.

Capell, B. C. *et al.* (2005) 'Inhibiting farnesylation of progerin prevents the characteristic nuclear blebbing of Hutchinson-Gilford progeria syndrome', *Proceedings of the National Academy of Sciences*, 102(36), pp. 12879–12884.

Capell, B. C. *et al.* (2008) 'A farnesyltransferase inhibitor prevents both the onset and late progression of cardiovascular disease in a progeria mouse model', *Proceedings of the National Academy of Sciences*, 105(41), pp. 15902–15907.

Cheetham, S. W. *et al.* (2018) 'Targeted DamID reveals differential binding of mammalian pluripotency factors', *Development*, 145(20), p. dev170209.

Choudhury, R. P., Fuster, V. and Fayad, Z. A. (2004) 'Molecular, cellular and functional imaging of atherothrombosis', *Nature Reviews Drug Discovery*, 3(11), pp. 913–925.

Cohen, T. V., Hernandez, L. and Stewart, C. L. (2008) 'Functions of the nuclear envelope and lamina in development and disease.', *Biochemical Society transactions*, 36(Pt 6), pp. 1329–34.

Dahl, K. N. *et al.* (2006) 'Distinct structural and mechanical properties of the nuclear lamina in Hutchinson-Gilford progeria syndrome', *Proceedings of the National Academy of Sciences*, 103(27), pp. 10271–10276.

Davies, B. S. J. *et al.* (2010) 'An accumulation of non-farnesylated prelamin A causes cardiomyopathy but not progeria.', *Human molecular genetics*, 19(13), pp. 2682–94.

Daya, S. and Berns, K. I. (2008) 'Gene therapy using Adeno-Associated Virus vectors', *Clinical Microbiology Reviews*, 21(4), pp. 583–593.

DeBusk, F. L. (1972) 'The Hutchinson-Gilford progeria syndrome', *The Journal of Pediatrics*, 80(4), pp. 697–724.

Dechat, T. *et al.* (2008) 'Nuclear lamins: major factors in the structural organization and function of the nucleus and chromatin.', *Genes & development*, 22(7), pp. 832–53.

Dechat, T. *et al.* (2010) 'Nuclear lamins.', *Cold Spring Harbor perspectives in biology*, 2(11), p. a000547.

Dorado, B. *et al.* (2019) 'Generation and characterization of a novel knockin minipig model of

Hutchinson-Gilford progeria syndrome', *Cell Discovery*, 5(1), p. 16.

Dorado, B. and Andrés, V. (2017) 'A-type lamins and cardiovascular disease in premature aging syndromes', *Current Opinion in Cell Biology*, 46, pp. 17–25.

Eriksson, M. *et al.* (2003) 'Recurrent de novo point mutations in lamin A cause Hutchinson-Gilford progeria syndrome', *Nature*, 423(6937), pp. 293–298.

Fanjul, V. (2019) *Molecular mechanisms underlying cardiometabolic disease in aging*. Universidad Autónoma de Madrid. Doctoral Thesis.

Finer, M. and Glorioso, J. (2017) 'A brief account of viral vectors and their promise for gene therapy', *Gene Therapy*, 24(1), pp. 1–2.

Fong, L. G. (2006) 'Prelamin A and lamin A appear to be dispensable in the nuclear lamina', *Journal of Clinical Investigation*, 116(3), pp. 743–752.

Fuster, J. J. *et al.* (2012) 'Animal Models of Atherosclerosis', in *Progress in Molecular Biology and Translational Science*, pp. 1–23.

Gerhard-Herman, M. *et al.* (2012) 'Mechanisms of premature vascular aging in children with Hutchinson-Gilford progeria syndrome.', *Hypertension*, 59(1), pp. 92–7.

Gilford, H. and Hutchinson, J. (1897) 'On a condition of mixed premature and immature development', *Journal of the Royal Society of Medicine*, MCT-80(1), pp. 17–45.

Goldman, R. D. *et al.* (2004) 'Accumulation of mutant lamin A causes progressive changes in nuclear architecture in Hutchinson-Gilford progeria syndrome.', *Proceedings of the National Academy of Sciences of the United States of America*, 101(24), pp. 8963–8.

Gonzalo, S., Kreienkamp, R. and Askjaer, P. (2017) 'Hutchinson-Gilford Progeria Syndrome: A premature aging disease caused by LMNA gene mutations', *Ageing Research Reviews*, 33, pp. 18–29.

Gordon, L. B. *et al.* (2012) 'Clinical trial of a farnesyltransferase inhibitor in children with Hutchinson-Gilford progeria syndrome.', *Proceedings of the National Academy of Sciences of the United States of America*, 109(41), pp. 16666–71.

Gordon, L. B., Massaro, J., *et al.* (2014) 'Impact of farnesylation inhibitors on survival in Hutchinson-Gilford Progeria Syndrome', *Circulation*, 130(1), pp. 27–34.

Gordon, L. B., Rothman, F. G., *et al.* (2014) 'Progeria: A Paradigm for Translational Medicine', *Cell*, 156(3), pp. 400–407.

Gordon, L. B. *et al.* (2016) 'Clinical trial of the protein farnesylation inhibitors Lonafarnib, Pravastatin, and Zoledronic Acid in children with Hutchinson-Gilford Progeria Syndrome', *Circulation*, 134(2), pp. 114–25.

Gossen, M. and Bujard, H. (1992) 'Tight control of gene expression in mammalian cells by tetracycline-responsive promoters.', *Proceedings of the National Academy of Sciences of the United States of America*, 89(12), pp. 5547–51.

Graziotto, J. J. *et al.* (2012) 'Rapamycin activates autophagy in Hutchinson-Gilford progeria syndrome: implications for normal aging and age-dependent neurodegenerative disorders.', *Autophagy*, 8(1), pp. 147–51.

Hamczyk, M. R. *et al.* (2018) 'Vascular smooth muscle-specific progerin expression accelerates atherosclerosis and death in a mouse model of Hutchinson-Gilford Progeria Syndrome.', *Circulation*, 138(3), pp. 266–282.

Hamczyk, M. R. *et al.* (2019) 'Progerin accelerates atherosclerosis by inducing endoplasmic reticulum stress in vascular smooth muscle cells.', *EMBO molecular medicine*, 11(4).

Hamczyk, M. R. and Andrés, V. (2019) 'Vascular smooth muscle cell loss underpins the accelerated atherosclerosis in Hutchinson-Gilford progeria syndrome', *Nucleus*, 10(1), pp. 48–54.

Hamczyk, M. R., del Campo, L. and Andrés, V. (2018) 'Aging in the Cardiovascular System: Lessons from Hutchinson-Gilford Progeria Syndrome', *Annual Review of Physiology*, 80(1), pp. 27–48.

Harhouri, K. *et al.* (2018) 'An overview of treatment strategies for Hutchinson-Gilford Progeria syndrome', *Nucleus*, 9(1), pp. 265–276.

Hetzer, M. W. (2010) 'The Nuclear Envelope', *Cold Spring Harbor Perspectives in Biology*, 2(3), pp. a000539–a000539.

Hisama, F. M. *et al.* (2011) 'Coronary artery disease in a Werner syndrome-like form of progeria characterized by low levels of progerin, a splice variant of lamin A', *American Journal of Medical Genetics Part A*, 155(12), pp. 3002–3006.

Holtz, D. *et al.* (1989) 'The CaaX motif of lamin A functions in conjunction with the nuclear localization signal to target assembly to the nuclear envelope', *Cell*, 59(6), pp. 969–977.

Huang, S. *et al.* (2005) 'Correction of cellular phenotypes of Hutchinson-Gilford Progeria cells by RNA interference', *Human Genetics*, 118(3–4), pp. 444–450.

Hutchinson, J. (1886) 'Congenital absence of hair and mammary glands with atrophic condition of the skin and its appendages', *Trans Med Chir Soc Edinburgh*.

Ibrahim, M. X. *et al.* (2013) 'Targeting isoprenylcysteine methylation ameliorates disease in a mouse model of progeria', *Science*, 340(6138), pp. 1330–3.

Karimian, A. *et al.* (2019) 'CRISPR/Cas9 technology as a potent molecular tool for gene therapy', *Journal of Cellular Physiology*, 234(8), pp. 12267–12277.

Kattenhorn, L. M. *et al.* (2016) 'Adeno-Associated Virus Gene Therapy for Liver Disease', *Human gene therapy*, 27(12), pp. 947–961.

Kieran, M. W., Gordon, L. and Kleinman, M. (2007) 'New approaches to progeria', *Pediatrics*, 120(4), pp. 834–841.

Kötter, A. *et al.* (2014) 'Inhibition of PARP1-dependent end-joining contributes to Olaparib-mediated radiosensitization in tumor cells', *Molecular Oncology*, 8(8), pp. 1616–1625.

Kreienkamp, R. *et al.* (2016) 'Vitamin D receptor signaling improves Hutchinson-Gilford progeria syndrome cellular phenotypes', *Oncotarget*, 7(21).

Kristianto, J. *et al.* (2017) 'Spontaneous recombinase activity of Cre–ERT2 in vivo', *Transgenic Research*, 26(3), pp. 411–417.

de la Rosa, J. *et al.* (2013) 'Prelamin A causes progeria through cell-extrinsic mechanisms and

prevents cancer invasion', *Nature Communications*, 4(1), p. 2268.

Lacolley, P. *et al.* (2017) 'Vascular smooth muscle cells and arterial stiffening: Relevance in development, aging, and disease', *Physiological Reviews*, 97(4), pp. 1555–1617.

Lakatta, E. G. and Levy, D. (2003) 'Arterial and cardiac aging: Major shareholders in cardiovascular disease enterprises', *Circulation*, 107(1), pp. 139–146.

Lammerding, J. *et al.* (2004) 'Lamin A/C deficiency causes defective nuclear mechanics and mechanotransduction.', *The Journal of clinical investigation*, 113(3), pp. 370–8.

Larrieu, D. *et al.* (2014) 'Chemical inhibition of NAT10 corrects defects of laminopathic cells', *Science*, 344(6183), pp. 527–532.

Lee, J. M. *et al.* (2016) 'Modulation of LMNA splicing as a strategy to treat prelamin A diseases.', *The Journal of clinical investigation*, 126(4), pp. 1592–602.

Lee, S.-J. *et al.* (2016) 'Interruption of progerin–lamin A/C binding ameliorates Hutchinson-Gilford progeria syndrome phenotype', *The Journal of Clinical Investigation*, 126(10), pp. 3879–3893.

Liu, B. *et al.* (2005) 'Genomic instability in laminopathy-based premature aging', *Nature Medicine*, 11(7), pp. 780–785.

López-Mejía, I. C. *et al.* (2014) 'Antagonistic functions of LMNA isoforms in energy expenditure and lifespan.', *EMBO reports*, 15(5), pp. 529–39.

Mallampalli, M. P. *et al.* (2005) 'Inhibiting farnesylation reverses the nuclear morphology defect in a HeLa cell model for Hutchinson-Gilford progeria syndrome', *Proceedings of the National Academy of Sciences*, 102(40), pp. 14416–14421.

McLellan, M. A., Rosenthal, N. A. and Pinto, A. R. (2017) 'Cre- lox P-mediated recombination: General principles and experimental considerations', *Current Protocols in Mouse Biology*, 7(1), pp. 1–12.

Merideth, M. A. *et al.* (2008) 'Phenotype and course of Hutchinson–Gilford Progeria Syndrome', *New England Journal of Medicine*, 358(6), pp. 592–604.

Moulson, C. L. *et al.* (2007) 'Increased progerin expression associated with unusual LMNA mutations causes severe progeroid syndromes', *Human Mutation*, 28(9), pp. 882–9.

Mullis, K. B. and Faloona, F. A. (1987) 'Specific synthesis of DNA in vitro via a polymerase-catalyzed chain reaction.', *Methods in enzymology*, 155, pp. 335–50.

Navarro, C. L. *et al.* (2004) 'Lamin A and ZMPSTE24 (FACE-1) defects cause nuclear disorganization and identify restrictive dermopathy as a lethal neonatal laminopathy', *Human Molecular Genetics*, 13(20), pp. 2493–2503.

Navarro, C. L. *et al.* (2005) 'Loss of ZMPSTE24 (FACE-1) causes autosomal recessive restrictive dermopathy and accumulation of Lamin A precursors', *Human Molecular Genetics*, 14(11), pp. 1503–1513.

North, B. J. and Sinclair, D. A. (2012) 'The intersection between aging and cardiovascular disease', *Circulation Research*, 110(8), pp. 1097–1108.

Olive, M. *et al.* (2010) 'Cardiovascular pathology in Hutchinson-Gilford progeria: correlation

with the vascular pathology of aging.', *Arteriosclerosis, thrombosis, and vascular biology*, 30(11), pp. 2301–9.

Osorio, F. G. *et al.* (2011) 'Splicing-directed therapy in a new mouse model of human accelerated aging.', *Science translational medicine*, 3(106), p. 106ra107.

Pendás, A. M. *et al.* (2002) 'Defective prelamin A processing and muscular and adipocyte alterations in Zmpste24 metalloproteinase-deficient mice.', *Nature genetics*, 31(1), pp. 94–9.

Piekarowicz, K. *et al.* (2019) 'Hutchinson-Gilford Progeria Syndrome—Current status and prospects for gene therapy treatment', *Cells*, 8(2), p. 88.

Podhorecka, M., Skladanowski, A. and Bozko, P. (2010) 'H2AX phosphorylation: Its role in DNA damage response and cancer therapy', *Journal of Nucleic Acids*, 2010, pp. 1–9.

Prakash, A. *et al.* (2018) 'Cardiac Abnormalities in Patients With Hutchinson-Gilford Progeria Syndrome.', *JAMA cardiology*, 3(4), pp. 326–334.

Progeria Research Fundation (2019). Retrieved from www.progeriaresearch.org

Ran, F. A. *et al.* (2013) 'Genome engineering using the CRISPR-Cas9 system.', *Nature protocols*, 8(11), pp. 2281–308.

Reunert, J. *et al.* (2012) 'Neonatal progeria: increased ratio of progerin to lamin A leads to progeria of the newborn.', *European journal of human genetics : EJHG*, 20(9), pp. 933–7.

Rivera-Torres, J. *et al.* (2016) 'Cardiac electrical defects in progeroid mice and Hutchinson-Gilford progeria syndrome patients with nuclear lamina alterations', *Proceedings of the National Academy of Sciences of the United States of America*, 113(46), p. E7250.

Ruzankina, Y. *et al.* (2007) 'Deletion of the developmentally essential gene ATR in adult mice leads to age-related phenotypes and stem cell loss.', *Cell stem cell*, 1(1), pp. 113–26.

Ryding, A. D. S., Sharp, M. G. F. and Mullins, J. J. (2001) 'Conditional transgenic technologies', *Journal of Endocrinology*, 171(1), pp. 1–14.

Sagelius, H., Rosengardten, Y., Schmidt, E., *et al.* (2008) 'Reversible phenotype in a mouse model of Hutchinson-Gilford progeria syndrome.', *Journal of medical genetics*, 45(12), pp. 794–801.

Sagelius, H., Rosengardten, Y., Hanif, M., *et al.* (2008) 'Targeted transgenic expression of the mutation causing Hutchinson-Gilford progeria syndrome leads to proliferative and degenerative epidermal disease.', *Journal of cell science*, 121(Pt 7), pp. 969–78.

Sander, J. D. and Joung, J. K. (2014) 'CRISPR-Cas systems for editing, regulating and targeting genomes.', *Nature biotechnology*, 32(4), pp. 347–55.

De Sandre-Giovannoli, A. *et al.* (2003) 'Lamin a truncation in Hutchinson-Gilford progeria.', *Science*, 300(5628), p. 2055.

Santiago-Fernández, O. *et al.* (2019) 'Development of a CRISPR/Cas9-based therapy for Hutchinson–Gilford progeria syndrome', *Nature Medicine*, 25(3), pp. 423–426.

Scaffidi, P. and Misteli, T. (2005) 'Reversal of the cellular phenotype in the premature aging disease Hutchinson-Gilford progeria syndrome.', *Nature medicine*, 11(4), pp. 440–5.

Scaffidi, P. and Misteli, T. (2006) 'Lamin A-dependent nuclear defects in human aging.', *Science*,

312(5776), pp. 1059–63.

Schjørring, O. L., Carlsson, R. and Simonsen, U. (2015) 'Pressure myography to study the function and structure of isolated small arteries.', *Methods in molecular biology*, 1339, pp. 277–95.

Sinensky, M. *et al.* (1994) 'The processing pathway of prelamin A', *Journal of Cell Science*, 107(1), pp. 61–67.

Stehbens, W. E. *et al.* (2001) 'Smooth muscle cell depletion and collagen types in progeric arteries', *Cardiovascular Pathology*, 10(3), pp. 133–136.

Sternberg, N. and Hamilton, D. (1981) 'Bacteriophage P1 site-specific recombination', *Journal of Molecular Biology*, 150(4), pp. 467–486.

Strandgren, C. *et al.* (2015) 'Transgene silencing of the Hutchinson-Gilford progeria syndrome mutation results in a reversible bone phenotype, whereas resveratrol treatment does not show overall beneficial effects', *The FASEB Journal*, 29(8), pp. 3193–3205.

Strandgren, C. *et al.* (2017) 'Emerging candidate treatment strategies for Hutchinson-Gilford progeria syndrome.', *Biochemical Society transactions*, 45(6), pp. 1279–1293.

Sullivan, T. *et al.* (1999) 'Loss of a-Type Lamin Expression Compromises Nuclear Envelope Integrity Leading to Muscular Dystrophy', *The Journal of Cell Biology*, 147(5), pp. 913–920.

Toth, J. I. *et al.* (2005) 'Blocking protein farnesyltransferase improves nuclear shape in fibroblasts from humans with progeroid syndromes', *Proceedings of the National Academy of Sciences*, 102(36), pp. 12873–12878.

Ullrich, N. J. and Gordon, L. B. (2015) 'Hutchinson–Gilford progeria syndrome', in *Handbook of Clinical Neurology*. Elservier B.V., pp. 249–264.

The Universal Mutation Database. *LMNA* mutation data base. Retrieved from: www.umd.be/*LMNA*/.

Varela, I. *et al.* (2005) 'Accelerated ageing in mice deficient in Zmpste24 protease is linked to p53 signalling activation.', *Nature*, 437(7058), pp. 564–8.

Varela, I. *et al.* (2008) 'Combined treatment with statins and aminobisphosphonates extends longevity in a mouse model of human premature aging', *Nature Medicine*, 14(7), pp. 767–772.

Varga, R. *et al.* (2006) 'Progressive vascular smooth muscle cell defects in a mouse model of Hutchinson-Gilford progeria syndrome.', *Proceedings of the National Academy of Sciences of the United States of America*, 103(9), pp. 3250–5.

Vesela, E. *et al.* (2017) 'Common chemical inductors of replication stress: Focus on cell-based studies', *Biomolecules*, 7(4), p. 19.

Villalba-Orero, M. *et al.* (2017) 'Lung ultrasound as a translational approach for non-invasive assessment of heart failure with reduced or preserved ejection fraction in mice', *Cardiovascular Research*, 113(10), pp. 1113–1123.

Wang, L.-E. *et al.* (2016) '4-Nitroquinoline-1-oxide-induced mutagen sensitivity and risk of cutaneous melanoma', *Melanoma Research*, 26(2), pp. 181–187.

World Helath Organization (2017). Global health observatory. Retrieved from

https:/www.who.int/gho/en/

Worman, H. J. and Michaelis, S. (2018) 'Permanently farnesylated prelamin A, progeria, and atherosclerosis', *Circulation*, 138(3), pp. 283–286.

Yang, S. H. *et al.* (2005) 'Blocking protein farnesyltransferase improves nuclear blebbing in mouse fibroblasts with a targeted Hutchinson-Gilford progeria syndrome mutation.', *Proceedings of the National Academy of Sciences of the United States of America*, 102(29), pp. 10291–6.

Yang, S. H. (2006) 'A farnesyltransferase inhibitor improves disease phenotypes in mice with a Hutchinson-Gilford progeria syndrome mutation', *Journal of Clinical Investigation*, 116(8), pp. 2115–2121.

Yang, S. H., Qiao, X., Farber, E. A., *et al.* (2008) 'Eliminating the synthesis of mature lamin A reduces disease phenotypes in mice carrying a Hutchinson-Gilford progeria syndrome allele.', *The Journal of biological chemistry*, 283(11), pp. 7094–7099.

Yang, S. H., Andres, D. A., *et al.* (2008) 'Progerin elicits disease phenotypes of progeria in mice whether or not it is farnesylated', *Journal of Clinical Investigation*, 118(10), pp. 3291–3300.

Yang, S. H., Qiao, X., Fong, L. G., *et al.* (2008) 'Treatment with a farnesyltransferase inhibitor improves survival in mice with a Hutchinson-Gilford progeria syndrome mutation', *Biochimica et Biophysica Acta - Molecular and Cell Biology of Lipids*, 1781(1–2), pp. 36–39.

Yang, S. H. *et al.* (2011) 'Absence of progeria-like disease phenotypes in knock-in mice expressing a non-farnesylated version of progerin.', *Human molecular genetics*, 20(3), pp. 436–44.

Young, S. G., Fong, L. G. and Michaelis, S. (2005) 'Prelamin A, Zmpste24, misshapen cell nuclei, and progeria--new evidence suggesting that protein farnesylation could be important for disease pathogenesis.', *Journal of lipid research*, 46(12), pp. 2531–58.

Yusa, K. *et al.* (2011) 'A hyperactive piggyBac transposase for mammalian applications.', *Proceedings of the National Academy of Sciences of the United States of America*, 108(4), pp. 1531–6.

Zack, G. W., Rogers, W. E. and Latt, S. A. (1977) 'Automatic measurement of sister chromatid exchange frequency.', *Journal of Histochemistry & Cytochemistry*, 25(7), pp. 741–753.

Zarei, A. *et al.* (2019) 'Creating cell and animal models of human disease by genome editing using CRISPR/Cas9', *The Journal of Gene Medicine*, 21(4), p. e3082.

Zhao, S. *et al.* (2016) 'PiggyBac transposon vectors: the tools of the human gene encoding.', *Translational lung cancer research*, 5(1), pp. 120–5.

Zincarelli, C. *et al.* (2008) 'Analysis of AAV Serotypes 1–9 Mediated Gene Expression and Tropism in Mice After Systemic Injection', *Molecular Therapy*, 16(6), pp. 1073–1080.

ANNEXES

Publications prepared during the thesis:

Lara del Campo*, **Amanda Sánchez-López***, Mercedes Salaices, Elba Expósito, Cristina González-Gómez, Lorena Cussó, Gabriela Guzmán-Martínez, Jesús Ruiz-Cabello, Manuel Desco, Ana M. Briones, and Vicente Andrés. Vascular smooth muscle cell-specific progerin expression in a mouse model of Hutchinson-Gilford progeria syndrome promotes arterial stiffness. Therapeutic effect of dietary nitrite**.** 2019, *Aging Cell.* 18:e12936 doi.org/10.111

* These authors contributed equally to this work.

Received: 5 July 2018 | Revised: 23 January 2019 | Accepted: 3 February 2019

DOI: 10.1111/acel.12936

ORIGINAL ARTICLE

WILEY Aging Cell

Vascular smooth muscle cell-specific progerin expression in a mouse model of Hutchinson–Gilford progeria syndrome promotes arterial stiffness: Therapeutic effect of dietary nitrite

Lara del Campo[1,2*] | Amanda Sánchez-López[1,2*] | Mercedes Salaices[2,3] | Ryan A. von Kleeck[4] | Elba Expósito[1,2] | Cristina González-Gómez[1,2] | Lorena Cussó[1,5,6,7] | Gabriela Guzmán-Martínez[1,8] | Jesús Ruiz-Cabello[1,9] | Manuel Desco[1,5,6,7] | Richard K. Assoian[4] | Ana M. Briones[2,3] | Vicente Andrés[1,2]

[1]Centro Nacional de Investigaciones Cardiovasculares (CNIC), Madrid, Spain

[2]CIBER de Enfermedades Cardiovasculares (CIBERCV), Spain

[3]Departamento de Farmacología y Terapéutica, Facultad de Medicina, Instituto de Investigación Hospital La Paz (IdiPaz), Universidad Autónoma de Madrid, Madrid, Spain

[4]Center for Engineering Mechanobiology and Department of Systems Pharmacology and Translational Therapeutics, University of Pennsylvania, Philadelphia, Pennsylvania

[5]Departamento de Bioingeniería e Ingeniería Aeroespacial, Universidad Carlos III de Madrid, Madrid, Spain

[6]Instituto de Investigación Sanitaria Gregorio Marañón, Madrid, Spain

[7]Centro de Investigación Biomédica en Red de Salud Mental (CIBERSAM), Spain

[8]Cardiac Imaging Unit, Cardiology Department, Hospital Universitario La Paz, Madrid, Spain

[9]CIBER de Enfermedades Respiratorias (CIBERES), Spain

Correspondence
Vicente Andrés, CNIC, Madrid, Spain.
Email: vandres@cnic.es

Present address
Jesús Ruiz-Cabello, CIC biomaGUNE and Ikerbasque- Basque Foundation for Science, San Sebastián, Spain; Universidad Complutense Madrid, Madrid, Spain.

Abstract

Vascular stiffness is a major cause of cardiovascular disease during normal aging and in Hutchinson–Gilford progeria syndrome (HGPS), a rare genetic disorder caused by ubiquitous progerin expression. This mutant form of lamin A causes premature aging associated with cardiovascular alterations that lead to death at an average age of 14.6 years. We investigated the mechanisms underlying vessel stiffness in $Lmna^{G609G/G609G}$ mice with ubiquitous progerin expression, and tested the effect of treatment with nitrites. We also bred $Lmna^{LCS/LCS}Tie2Cre^{+/tg}$ and $Lmna^{LCS/LCS}SM22\alpha Cre^{+/tg}$ mice, which express progerin specifically in endothelial cells (ECs) and in vascular smooth muscle cells (VSMCs), respectively, to determine the specific contribution of each cell type to vascular pathology. We found vessel stiffness and inward remodeling in arteries of $Lmna^{G609G/G609G}$ and $Lmna^{LCS/LCS}SM22\alpha Cre^{+/tg}$, but not in those from $Lmna^{LCS/LCS}Tie2Cre^{+/tg}$ *mice*. Structural alterations in aortas of progeroid mice were associated with decreased smooth muscle tissue content, increased collagen deposition, and decreased transverse waving of elastin layers in the media. Functional studies identified collagen (unlike elastin and the cytoskeleton) as an underlying cause of aortic stiffness in progeroid mice. Consistent with this, we found increased deposition of collagens III, IV, V, and XII in the media of progeroid aortas. Vessel stiffness and inward remodeling in progeroid mice were prevented by adding sodium nitrite in drinking water. In conclusion, $Lmna^{G609G/G609G}$ arteries exhibit stiffness and inward remodeling, mainly due to progerin-induced damage to VSMCs, which causes increased deposition of medial collagen and a secondary alteration in elastin structure. Treatment with nitrites prevents vascular stiffness in progeria.

*These authors contributed equally to this study.

Funding information
Ministerio Ciencia, Innovación y Universidades, Grant/Award Number: SAF2016-79490-R, SAF2016-8035-P, SEV-2015-0505, SVP-2014-068334; European Regional Development Fund; NIH grants, Grant/Award Number: AG047373, T32-GM008076, F31HL142160; NSF grant, Grant/Award Number: CMMI 1548571; Red de Investigación Cardiovascular (RETIC Program, Instituto de Salud Carlos III; Pro-CNIC Foundation

KEYWORDS
aging, dietary nitrite, progeria, smooth muscle cells, vascular stiffness

1 | INTRODUCTION

Cardiovascular disease (CVD) is the leading cause of death and morbidity worldwide (World Health Organization, 2017). Most of the classical risk factors associated with CVD development are modifiable, for example, dyslipidemia, high blood pressure, smoking, and diabetes (D'Agostino et al., 2008). However, the most important CVD risk factor is aging, an ostensibly unmodifiable risk factor that is a defining demographic phenomenon of our times, with a high sanitary and socio-economic impact (Population Division, 2002). It is therefore of utmost importance to gain a thorough knowledge of the mechanisms through which aging alone, independently of other modifiable cardiovascular risk factors, induces changes in the cardiovascular structure and function, in order to provide sustainable and accessible therapies to a rapidly aging population.

In addition to the characterization of risk factors epidemiologically associated and contributing to CVD development (D'Agostino et al., 2008), great advances have been made in the definition of tissue and cellular properties underlying age-induced cardiovascular decline (Lakatta, 2003; Lakatta & Levy, 2003a, 2003b). Among them, vascular stiffness is attracting increasing attention due to evidence that this alteration is a key starting point for other cardiovascular complications, especially during aging (Hamczyk, del Campo, & Andrés, 2018; Lakatta & Levy, 2003a). Age-related arterial stiffness triggers and promotes endothelial dysfunction and permeability (Huveneers, Daemen, & Hordijk, 2015), increased blood pressure, cardiac and vascular fibrosis and inflammation, inducing both vessel and cardiac overload, finally leading to atherosclerosis and heart failure (Kohn, Lampi, & Reinhart-King, 2015; Mitchell, 2008; Wang, Monticone, & Lakatta, 2014). Furthermore, epidemiological studies indicate that vessel stiffness is a strong independent predictor of clinical cardiovascular events, especially during aging (Vlachopoulos, Aznaouridis, & Stefanadis, 2010). Therefore, targeting vessel stiffening has great potential to prevent age-related cardiovascular disorders (Adji, O'Rourke, & Namasivayam, 2011; Boutouyrie, Laurent, & Briet, 2008; Safar, 2018).

Hutchinson–Gilford progeria syndrome (HGPS, OMIM 176670) is an ultra-rare human genetic disease (estimated prevalence, 1 in 20 million) characterized by several signs of premature aging, including accelerated CVD (Hennekam, 2006). The disease is caused by a heterozygous de novo point mutation in the *LMNA* gene, most frequently c.1824C>T (p.G608G) (Eriksson et al., 2003; De Sandre-Giovannoli et al., 2003). This synonymous mutation activates a cryptic splice donor site that removes 150 nucleotides from exon 11, generating a truncated form of lamin A, known as progerin, a protein that cannot undergo complete maturation and remains permanently carboxymethylated and farnesylated. As a result, progerin accumulates within the nuclear lamina and disrupts normal nuclear architecture, leading to DNA damage and many other nuclear and cell defects (Dorado & Andres, 2017; Goldman et al., 2004). The most important clinical manifestations of HGPS patients are cardiovascular complications, with patients typically dying at an average age of 14.6 years (Gordon et al., 2014). The pattern of cardiovascular deterioration is broadly similar in progeria and normal aging, although HGPS patients typically lack or are mildly affected by traditional cardiovascular risk factors (Hamczyk, del Campo & Andrés, 2018). HGPS therefore offers a unique opportunity to study mechanisms that cause age-associated vascular dysfunction independently of other risk factors (Gerhard-Herman et al., 2012; Hamczyk, Campo et al., 2018). Vessel stiffness is also a key player in CVD associated with HGPS, which appears very early and pervasively (Gerhard-Herman et al., 2012; Gordon et al., 2012), and is an important cardiovascular outcome measure in HGPS clinical trials (Gordon et al., 2012, 2016). Despite the importance of vessel stiffness in the cardiovascular pathophysiology of both HGPS and normal aging, the underlying mechanisms and specific contribution of different cell types have yet to be defined.

The present study aims to investigate the mechanisms underlying vessel stiffness in HGPS by analyzing vascular structure and mechanics in mutant $Lmna^{G609G/G609G}$ mice, which express progerin ubiquitously and recapitulate the main clinical manifestations of human HGPS (reduced lifespan, lipodystrophy, and bone and cardiovascular abnormalities; Hamczyk, Villa-Bellosta et al., 2018; Osorio et al., 2011; Villa-Bellosta et al., 2013). In order to analyze the specific contribution of different cell types to the vascular pathology of progeria, we bred $Lmna^{LCS/LCS}Tie2Cre^{+/tg}$ and $Lmna^{LCS/LCS}SM22\alpha Cre^{+/tg}$ mice, which respectively express progerin specifically in endothelial cells (ECs) and vascular smooth muscle cells (VSMCs).

Many different therapeutic approaches for HGPS have been proposed in the last years, but clinical trials have demonstrated only very

limited benefit for patients (Harhouri et al., 2018). New therapies for HGPS should be safe to permit long-term use and should preferably target CVD, the main cause of death in HGPS (Harhouri et al., 2018). Vessel stiffness is an important determinant of CVD and is measured in HGPS clinical trials (Gordon et al., 2016, 2012; Ullrich et al., 2013). We therefore tested the effects of dietary supplementation with sodium nitrite on vascular stiffness in *Lmna*$^{G609G/G609G}$ mice, a treatment that has been shown to prevent large elastic artery stiffness during normal aging in both mouse and humans, without reported side effects (Rammos et al., 2014; Sindler et al., 2011).

2 | RESULTS

2.1 | *Lmna*$^{G609G/G609G}$ mice ubiquitously expressing progerin show aortic stiffness and inward remodeling that are reproduced in mice with VSMC-specific progerin expression

The mean survival of *Lmna*$^{G609G/G609G}$ mice in our animal facility is 21.71 ± 0.82 weeks. All studies were carried out with 13- to 15-week-old male mice, which showed evident symptoms of disease but were not yet in the last stages of their lifespan. Mechanical properties of aortas were analyzed by ex vivo analysis with wire myography. These assays showed that diameter–tension relationships in aortas from *Lmna*$^{G609G/G609G}$ are left-shifted compared to *Lmna*$^{+/+}$ controls (Figure 1a, left). Regression lines were calculated for these relations and compared. The slopes of regression lines were significantly steeper in *Lmna*$^{G609G/G609G}$ aortas, indicating increased aortic stiffness (Figure 1a, middle). Moreover, the estimated physiological diameter (diameter at 100 mmHg, Figure 1a, right) and the diameter at 0 force (Supporting Information Figure S1, left) were both decreased in aortas of *Lmna*$^{G609G/G609G}$, indicating inward remodeling.

Since systolic and diastolic pressures are unaltered in *Lmna*$^{G609G/G609G}$ mice (Osorio et al., 2011), magnetic resonance imaging (MRI) was used to measure the stroke change in lumen area of the thoracic aorta as an in vivo measure of distensibility and stiffness (Laurent et al., 2006). We found smaller systolic and diastolic aortic diameters in *Lmna*$^{G609G/G609G}$ mice (Figure 1b, left). Moreover, the distensibility of the vessel was significantly lower in progeroid mice, as evidenced by the decreased slope of the ascending part of the cross-sectional area–time curve (Figure 1b, right).

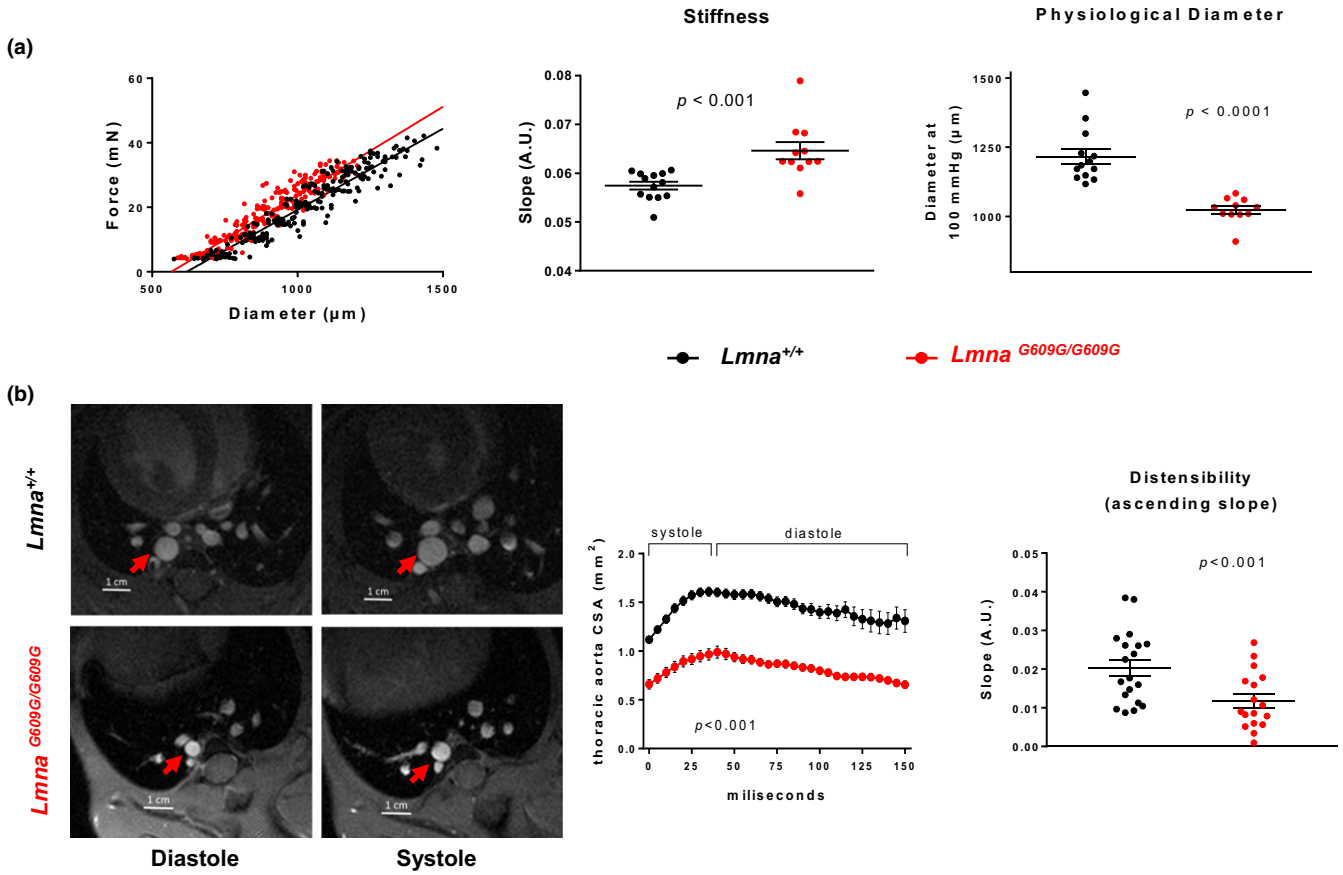

FIGURE 1 The aortas of progeroid mice exhibit arterial stiffness and inward remodeling. (a) Wire myography analysis of diameter–tension relationships, linear regression slope, and diameter estimated at 100 mmHg for aortic rings (n = 11 *Lmna*$^{G609G/G609G}$ mice and n = 13 *Lmna*$^{+/+}$ littermate controls). (b) Magnetic resonance imaging (MRI) of the thoracic aorta in *Lmna*$^{+/+}$ mice (n = 19) and *Lmna*$^{G609G/G609G}$ mice (n = 17) and quantification of aortic size in area units (mm^2) over a complete cardiac cycle. Distensibility is expressed as the slope of the ascending part of the aortic size–time curve

To determine the relative contribution of VSMCs and ECs to the alterations observed in progeroid mouse aortas, we analyzed mice expressing progerin only in VSMCs (*Lmna*$^{LCS/LCS}$*SM22αCre*$^{+/tg}$) or only in ECs (*Lmna*$^{LCS/LCS}$*Tie2αCre*$^{+/tg}$). Littermate *Lmna*$^{LCS/LCS}$ mice were used as controls. Cell-type-specific progerin expression was confirmed by immunofluorescence on aortic sections (Supporting Information Figure S2). Wire myography revealed a steeper slope of the diameter–tension relationships and a decreased physiological diameter in the aortas of *Lmna*$^{LCS/LCS}$*SM22αCre*$^{+/tg}$ mice (Figure 2a), whereas values were unaltered in aortas from *Lmna*$^{LCS/LCS}$*Tie2Cre*$^{+/tg}$ mice (Figure 2b). These data indicate that VSMC-specific progerin expression, but not EC-specific expression, is sufficient to induce aortic stiffness and inward remodeling.

Pulse wave velocity (PWV) is the gold standard method for non-invasive measurement of arterial stiffness in humans (Laurent et al., 2006). Attempts to measure PWV in progeroid *Lmna*$^{G609G/G609G}$ mice were impeded by the presence of aortic regurgitation (data not shown), which interfered with PWV measurement. Nevertheless, we were able to measure PWV in *Lmna*$^{LCS/LCS}$*SM22αCre*$^{+/tg}$ mice, since they do not develop aortic regurgitation. This analysis confirmed increased arterial stiffness in these mice relative to *Lmna*$^{LCS/LCS}$ controls (Supporting Information Figure S3), validating the MRI and wire myography results.

2.2 | *Lmna*$^{G609G/G609G}$ mice and *Lmna*$^{LCS/LCS}$*SM22αCre*$^{+/tg}$ mice show stiffness and inward remodeling in small mesenteric vessels

The structural and mechanical properties of small mesenteric arteries were studied by pressure myography, which reveals pressure–diameter properties. Vessels from *Lmna*$^{G609G/G609G}$ mice had smaller inner and outer diameters than controls, indicating inward remodeling, as well as left-shifted stress–strain curves, indicating vessel stiffness (Figure 3a). These alterations were also observed in small mesenteric arteries from the VSMC-specific *Lmna*$^{LCS/LCS}$*SM22αCre*$^{+/tg}$ mice (Figure 3b), reinforcing the important role of VSMCs in the remodeling and stiffness of progeroid mouse arteries.

2.3 | Collagen is an important mediator of aortic stiffness in *Lmna*$^{G609G/G609G}$ mice

We explored the involvement of structural components of the vessel wall that could play a role in aortic stiffness in progeroid mice, that is, collagen, elastin, and the cytoskeleton. Thus, we analyzed aortic diameter–tension relationships by wire myography in the absence and presence of specific disrupting agents: collagenase type II to degrade collagen, elastase to degrade elastin fibers, and mycalolide B

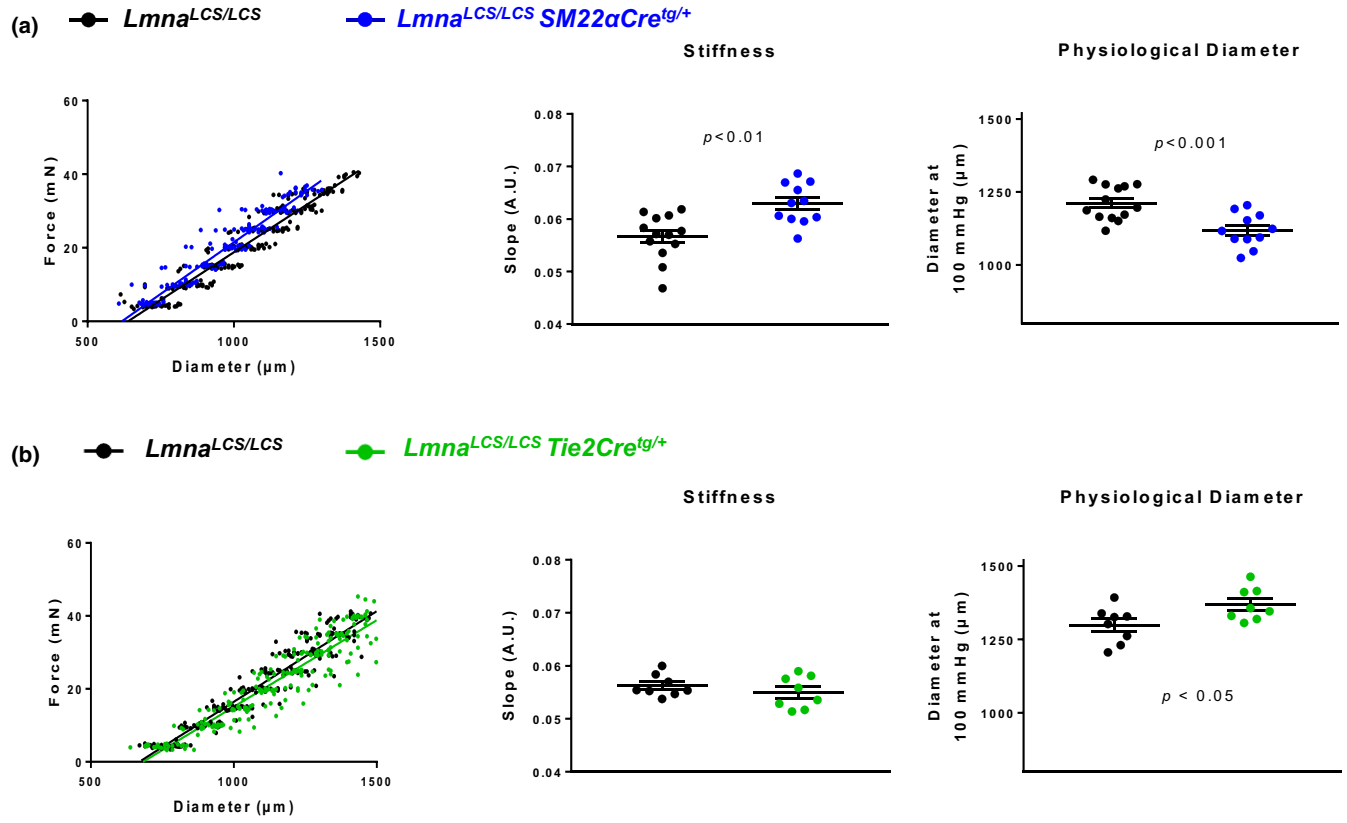

FIGURE 2 Mice with VSMC-specific progerin expression display arterial stiffness and inward remodeling, whereas mice with EC-specific progerin expression do not. (a, b) Wire myography analysis of diameter–tension relationships, linear regression slope, and diameter estimated at 100 mmHg for each vessel segment in aortic rings from *Lmna*$^{LCS/LCS}$*SM22αCre*$^{tg/+}$ mice (n = 11) (a) and *Lmna*$^{LCS/LCS}$*Tie2Cre*$^{tg/+}$ mice (n = 8) (b). Mice of both genotypes are compared with *Lmna*$^{LCS/LCS}$ littermate controls (n = 13 and 8, respectively)

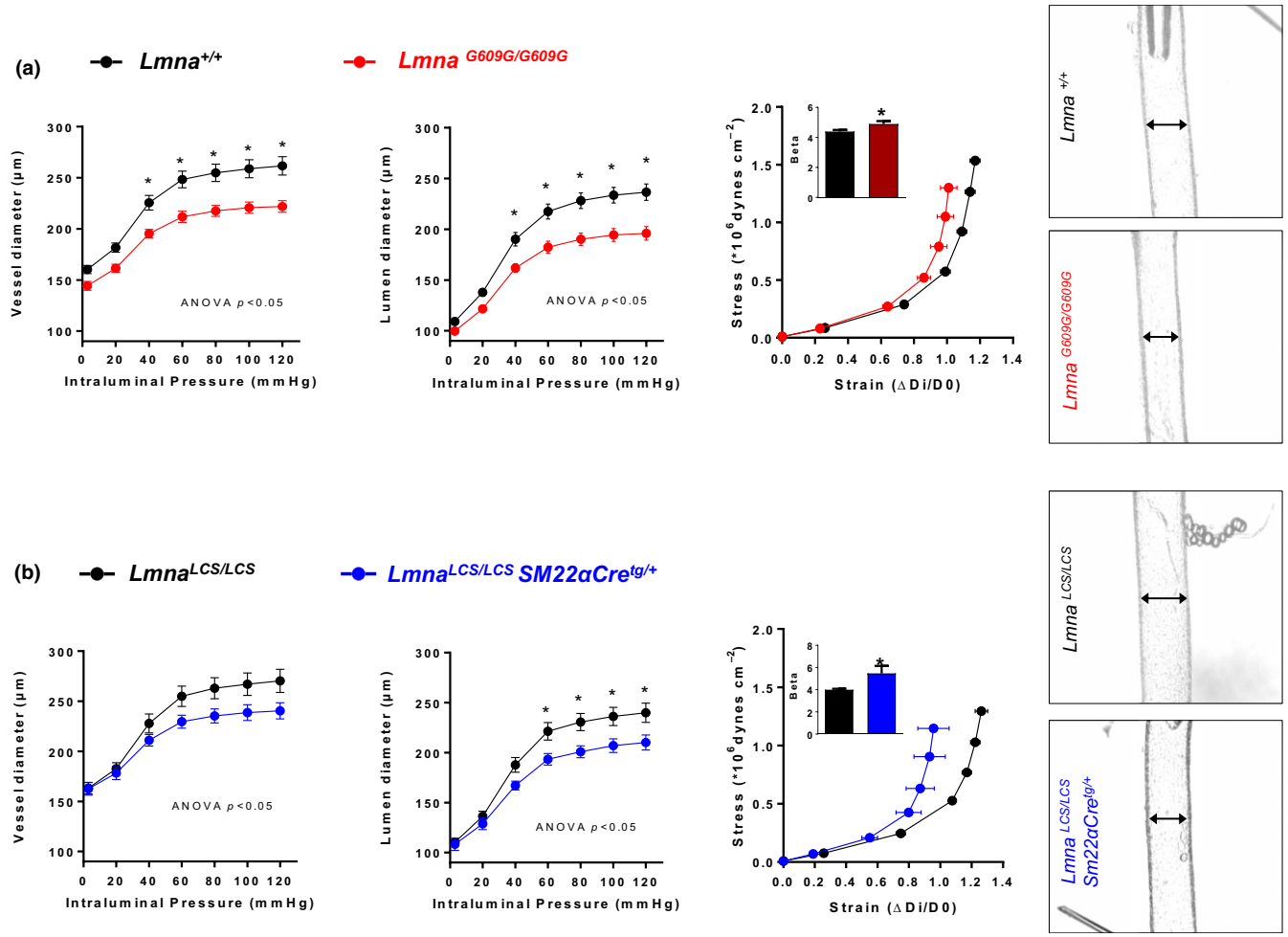

FIGURE 3 Small mesenteric vessels from ubiquitous and VSMC-specific progeroid mice exhibit arterial stiffness and inward remodeling. Pressure–diameter curves for the vessel (outer) and lumen (inner) diameters, corresponding stress–strain curves, and representative images of the pressurized arteries at 60 mmHg. (a) Arteries from *Lmna*$^{G609G/G609G}$ mice (n = 10), compared with *Lmna*$^{+/+}$ littermate controls (n = 9). (b) Arterioles from *Lmna*$^{LCS/LCS}$*SM22αCre*$^{tg/+}$ mice (n = 6), compared with *Lmna*$^{LCS/LCS}$ littermate controls (n = 6)

to depolymerize cytoskeletal F-actin to G-actin. These agents can induce substantial changes in the diameter–tension relationships in control aortas, but we were particularly interested in possible differences between *Lmna*$^{+/+}$ and *Lmna*$^{G609G/G609G}$, which could indicate a different contribution of the corresponding structure to vessel wall mechanical properties. Collagenase significantly reduced the slope of the diameter–tension relationships in *Lmna*$^{G609G/G609G}$ aortas, but had no effect on aortas from control *Lmna*$^{+/+}$ mice (Figure 4a). These results suggest that collagen is involved in the increased slope in progeroid mice and therefore in aortic stiffness. Collagenase revealed no between-genotype differences in the estimated diameter at 100 mmHg (Supporting Information Figure S4A).

Elastase and mycalolide B had similar effects in *Lmna*$^{+/+}$ and *Lmna*$^{G609G/G609G}$ mouse aortas (Figure 4b,c), indicating that alterations in elastin and the cytoskeleton are not involved in the development of stiffness or inward remodeling in the aortas of *Lmna*$^{G609G/G609G}$ mice.

2.4 | Aortas from *Lmna*$^{G609G/G609G}$ mice show increased collagen deposition and smooth muscle degeneration in the medial layer

Histological analysis of aortic sections stained with hematoxylin–eosin (H&E) and Masson's trichrome revealed decreased smooth muscle area and increased collagen area in the medial layer of *Lmna*$^{G609G/G609G}$ aortas (Figure 5a). Fluorescent imaging of DAPI-stained nuclei revealed no significant between-genotype differences in cell number in the medial layer (Figure 5b), suggesting that the decrease in muscle tissue in progeroid mice is due to loss of smooth muscle mass, and not to increased cell death.

Collagen density and cross-linking were evaluated in *Lmna*$^{+/+}$ and *Lmna*$^{G609G/G609G}$ aortas by visualizing picrosirius-red-stained aortic sections under polarized light. This technique detected collagen bundles only in the adventitial layer, showing no between-genotype differences in the total amount of adventitial collagen nor in the

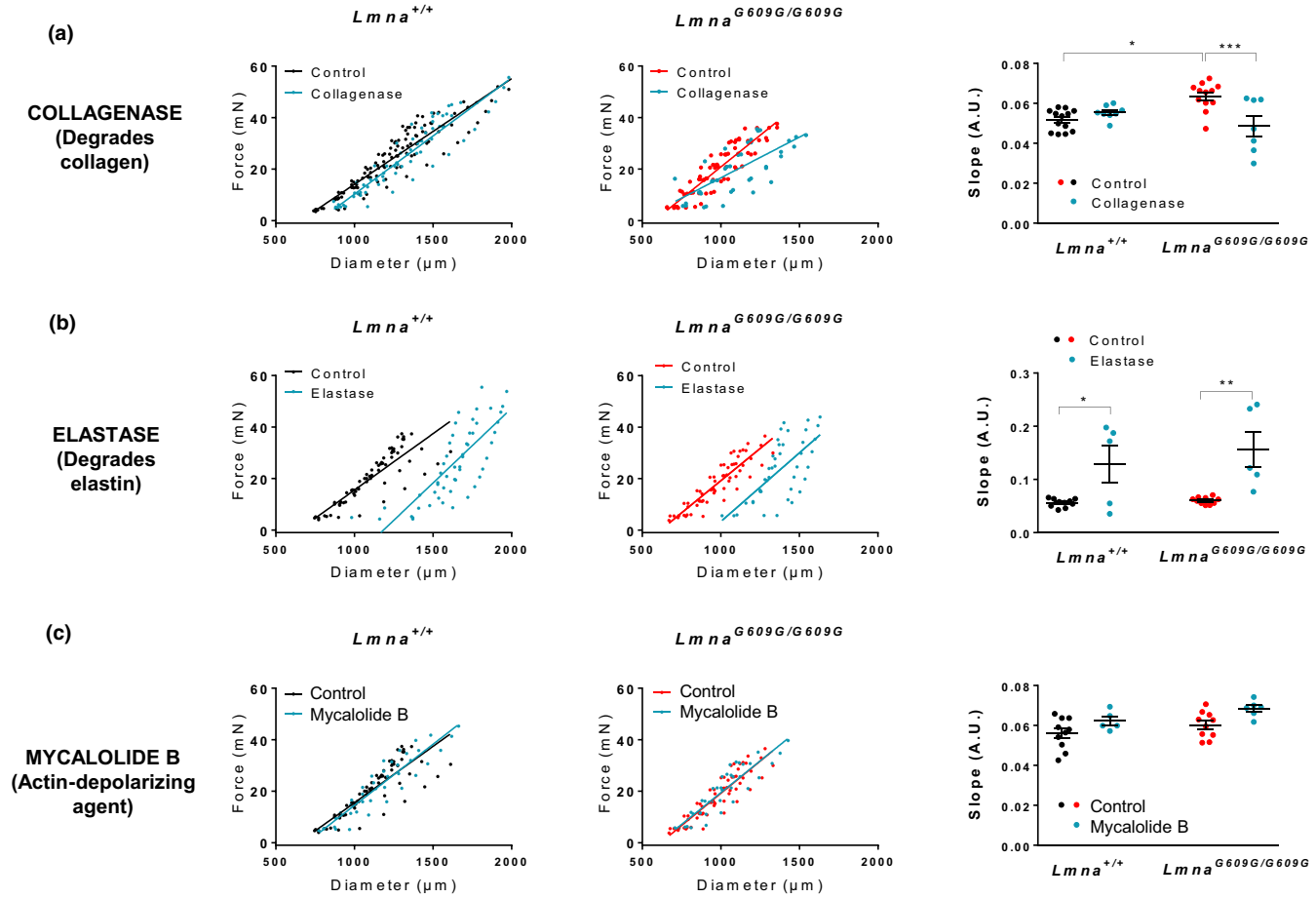

FIGURE 4 Collagen disruption prevents stiffness in aortas of *Lmna*$^{G609G/G609G}$ mice. Diameter–tension relationships and corresponding linear regression slopes in aortic rings from *Lmna*$^{+/+}$ mice (n = 5–10) and *Lmna*$^{G609G/G609G}$ mice (n = 5–10) after incubation with drugs affecting vessel structure: collagenase (collagen degradation), elastase (elastin–fiber degradation), and mycalolide B (depolymerization of F-actin to G-actin). Vehicle was used as control

relative amount of orange (thick) or green (thin) collagen fibers (Supporting Information Figure S5). Second-harmonic generation microscopy was also performed to evaluate the structure of fibrous collagen. We detected collagen fibrils in the adventitial layer, but not in the media; quantification showed no differences in the structure, distribution, or amount of collagen fibers in the adventitial layer (Supporting Information Figure S6).

Morphological analysis of elastin layers, visualized as green autofluorescence, showed significant loss of elastin fiber ondulations in *Lmna*$^{G609G/G609G}$ aortas, quantified as an increase in elastin linearization (Figure 5b). We also measured the lumen perimeter and calculated media thickness in aortic histological sections. Media thickness is unaltered, while lumen perimeter is decreased in aortas from *Lmna*$^{G609G/G609G}$ mice (Figure 5c). These data agree with those obtained by wire myography, showing a decreased lumen diameter even in unloaded conditions (arteries not subjected to intraluminal force; Supporting Information Figure S1A). These results thus reinforce the idea that progeroid arteries are not only stiffer but also exhibit inward remodeling.

2.5 | Aortas from *Lmna*$^{G609G/G609G}$ mice show increased expression of collagens III, IV, V, and XII in the medial layer

We performed immunofluorescence experiments to examine the amount and localization of collagens in aortas from *Lmna*$^{+/+}$ and *Lmna*$^{G609G/G609G}$ *mice* (Figure 6). We focused on collagens typically present in the vessel wall that are expressed in HGPS (Stehbens, Delahunt, Shozawa, & Gilbert-Barness, 2001), that is, collagens I, III, IV, and V. We also analyzed collagen XII since it cross-links and organizes other collagen fibers (Chiquet, Birk, Bonnemann, & Koch, 2014). Moreover, mutations in the collagen XII gene cause Ehlers–Danlos myopathy, a very rare disease with connective tissue and vascular phenotype opposite to that seen in HGPS patients, including joint hypermobility, soft highly elastic skin, and vascular fragility (Malfait, 2018). We found that collagen I is mainly present in the adventitial layer, and no significant differences in its expression were detected in the adventitial and medial layers (Figure 6). In contrast, collagens III, IV, V, and XII were mainly expressed in the media, with

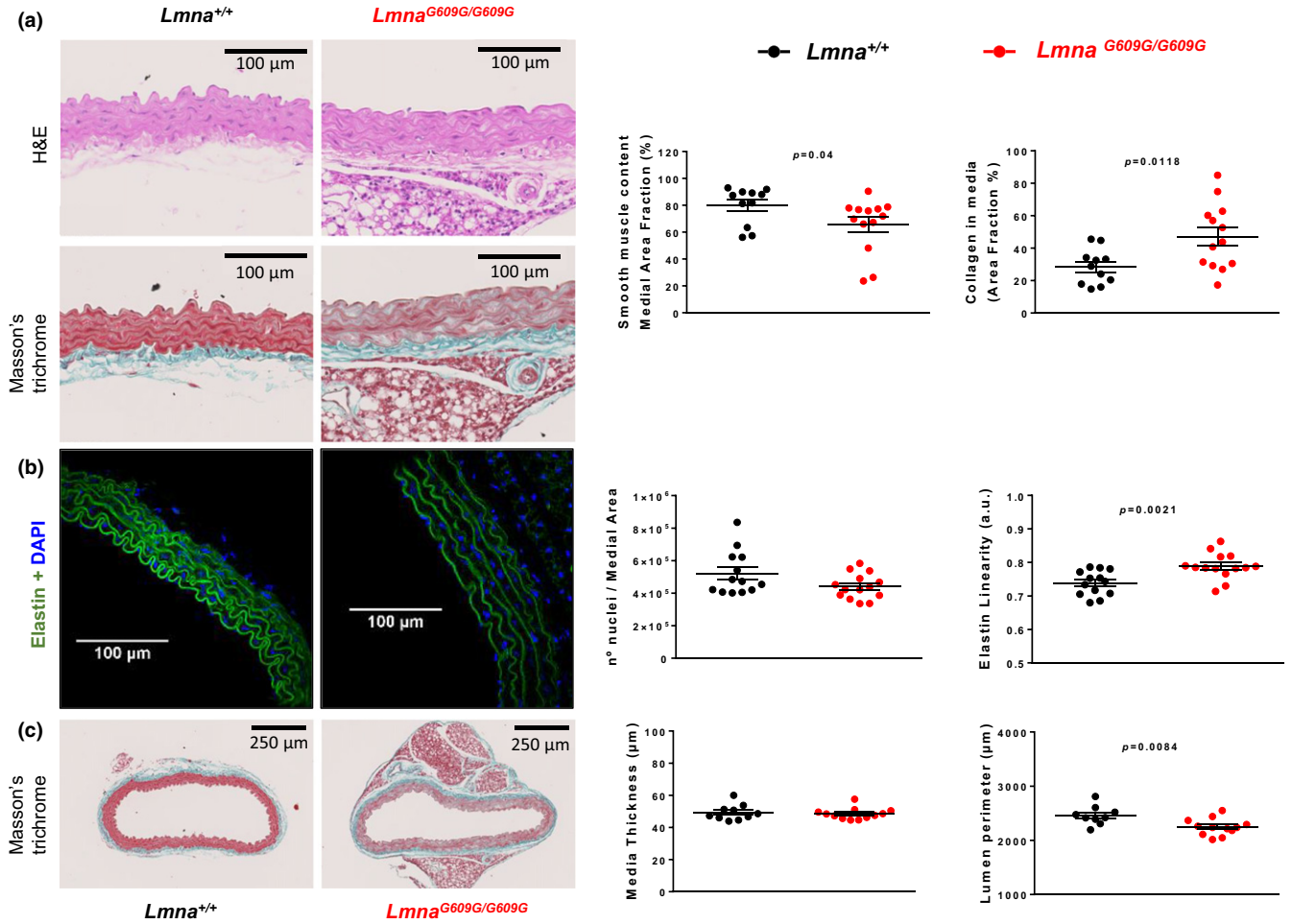

FIGURE 5 Aortic media of *Lmna*$^{G609G/G609G}$ mice shows increased collagen deposition, a decreased amount of smooth muscle tissue, and altered elastin waving. (a) Histological analysis of aortic sections from *Lmna*$^{G609G/G609G}$ mice (n = 13) and *Lmna*$^{+/+}$ mice (n = 11) stained with H&E and Masson's trichrome, showing increased collagen deposition and decreased smooth muscle area in the aortic medial layer of progeroid mice. (b) Confocal microscopy images of elastin autofluorescence and DAPI nuclear staining (n = 13–14), showing increased elastin wave linearity in aortic sections from *Lmna*$^{G609G/G609G}$ mice unaccompanied by significant changes in nuclear number. (c) Morphological analysis of whole aortic sections (n = 9–12), showing no change in medial layer thickness and a decreased lumen perimeter relative to controls, indicating inward remodeling in the *Lmna*$^{G609G/G609G}$ aorta

significantly more deposition in the medial layer of *Lmna*$^{G609G/G609G}$ aortas (Figure 6).

2.6 | Dietary nitrite supplementation protects against inward remodeling and stiffness in small mesenteric arteries of progeroid mice

We treated control *Lmna*$^{+/+}$ and progeroid *Lmna*$^{G609G/G609G}$ mice with nitrites to explore the effect of this treatment on the observed alterations in *Lmna*$^{G609G/G609G}$ aortas (Figure 7a). Dietary nitrite supplementation at 50 mg/L prevented inward remodeling and vessel stiffness in small mesenteric arteries (Figure 7b). This dose was ineffective in aorta, but increasing the dose to 500 mg/L improved aortic vessel stiffness and inward remodeling (Figure 7c).

3 | DISCUSSION

The present study provides insight into the mechanisms underlying vessel stiffness and vascular dysfunction in aging by studying the *Lmna*$^{G609G/G609G}$ *knock-in* mouse model of HGPS. Like HGPS patients, these mice express progerin ubiquitously and age prematurely, and they display the main clinical manifestations of the human disease, including lipodystrophy, bone and cardiovascular abnormalities, and reduced lifespan (Hamczyk, Villa-Bellosta et al., 2018; Osorio et al., 2011; Villa-Bellosta et al., 2013).

We observed arterial stiffness and inward remodeling (smaller inner and outer diameters) in both the aorta and small mesenteric vessels of *Lmna*$^{G609G/G609G}$ mice. Future studies are warranted to assess whether prelamin A accumulation in progeroid *Zmpste24*$^{-/-}$ mice also causes vessel stiffening. The observed alterations in vessels of *Lmna*$^{G609G/G609G}$ mice are reproduced in arteries of *Lmna*$^{LCS/}$

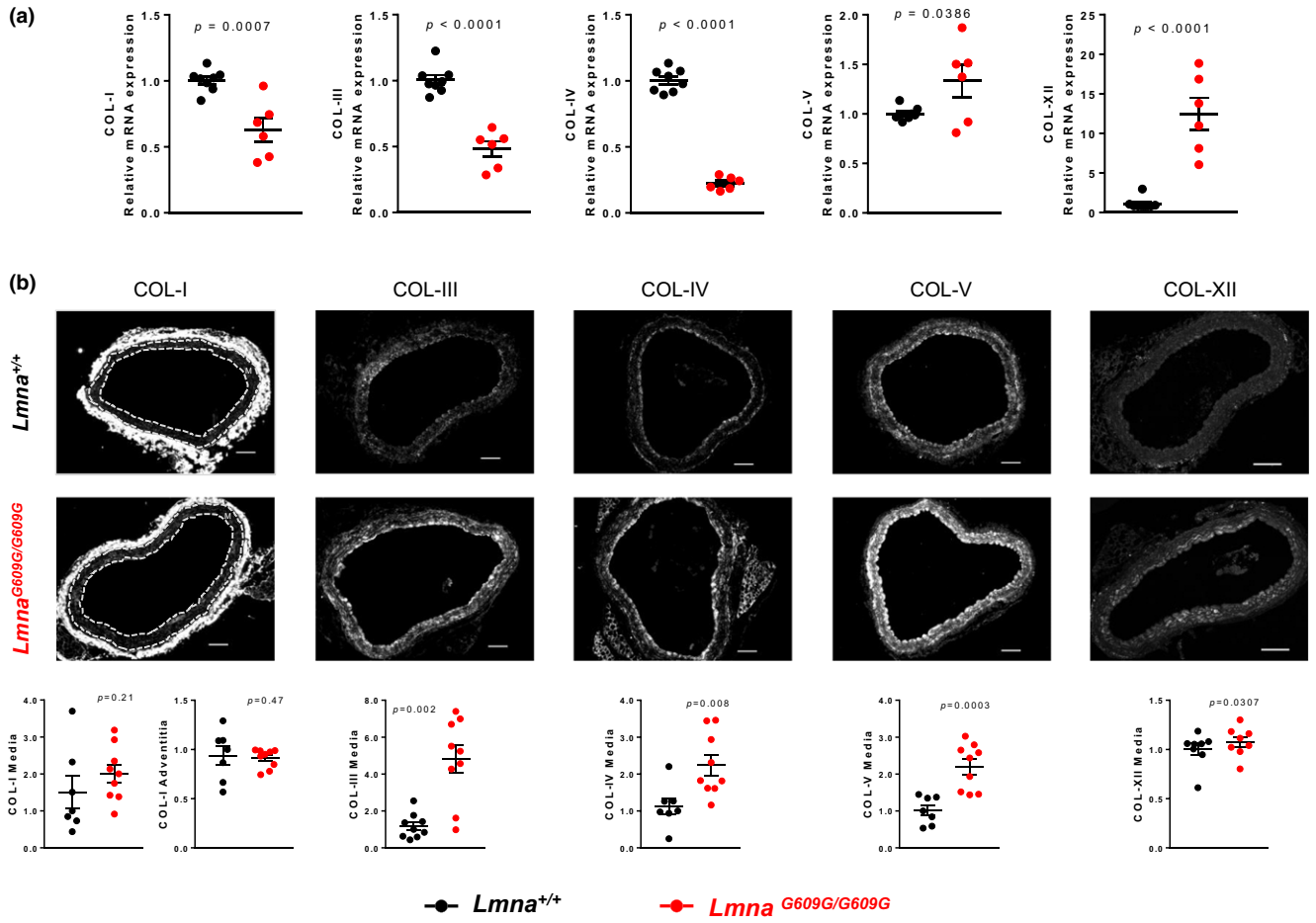

FIGURE 6 Increased deposition of collagens III, IV, V and XII in aortic media of *Lmna*$^{G609G/G609G}$ mice. Representative images of immunofluorescence staining of collagens I, III, IV, V, and XII in *Lmna*$^{+/+}$ and *Lmna*$^{G609G/G609G}$ aortic sections (n = 7-10) and quantification of the normalized mean signal intensities. Media (M) layer is denoted in collagen I images between dashed lines. Scale bar 100 μm

^{LCS}*SM22αCre*$^{+/tg}$ mice, with VSMC-specific progerin expression, indicating that VSMCs contribute significantly to vessel stiffness in progeria. The presence of remodeling and stiffness we observed in small resistance vessels of progeroid mice should be noted as an important newly described feature in progeria, since evidence exists suggesting that associations between aortic stiffness and cardiovascular events are mediated by pathways that include microvascular damage and remodeling (Cooper et al., 2016). Vessel stiffness might therefore be a key target to threat progeria, since reversing it could improve or restore vascular and cardiac function, but also improve the function of other organs that are compromised by impaired perfusion associated with microvascular dysfunction (Chirinos, 2016; Mitchell, 2008).

Aortas from mice expressing progerin specifically in ECs (*Lmna*$^{LCS/LCS}$*Tie2Cre*$^{+/tg}$ mice) showed none of these structural alterations, suggesting that ECs play no role in vascular stiffness in progeria. However, ECs appear to be critical effector cells of other progerin-induced cardiovascular alterations, since transgenic mice overexpressing progerin only in ECs develop perivascular fibrosis in coronary arteries and interstitial myocardial fibrosis, advance to left ventricular hypertrophy associated with diastolic dysfunction, and die prematurely (Osmanagic-Myers et al., 2018). Further studies with ubiquitous and cell-type-specific progerin expression mouse models are warranted to identify systemic and cell-intrinsic mechanisms underlying primary and secondary cardiovascular anomalies in progeria. We hypothesize that early VSMC dysfunction precedes and possibly can trigger endothelial dysfunction associated with the development of atherosclerosis in HGPS consistent with our recent studies showing that VSMC-specific progerin expression is sufficient to aggravate atherosclerosis and to cause atherosclerosis-related premature death in *apolipoprotein E*-null mice (Hamczyk, Villa-Bellosta et al., 2018). However, VSMC-specific progerin expression in atherosclerosis-resistant mice with an intact *apolipoprotein E* gene does not affect lifespan (Hamczyk, Villa-Bellosta et al., 2018), despite the development of vessel stiffening in aorta and small resistance vessels (Figures 2b and 3b). Further efforts are warranted to assess whether EC-specific progerin expression is sufficient to aggravate atheroma formation in atherosclerosis-prone mouse models (e.g., *apolipoprotein E*-null mice and low-density lipoprotein receptor-null mice).

The here described new parameters to measure vessel stiffness using the wire myograph allowed us to identify the tissue and

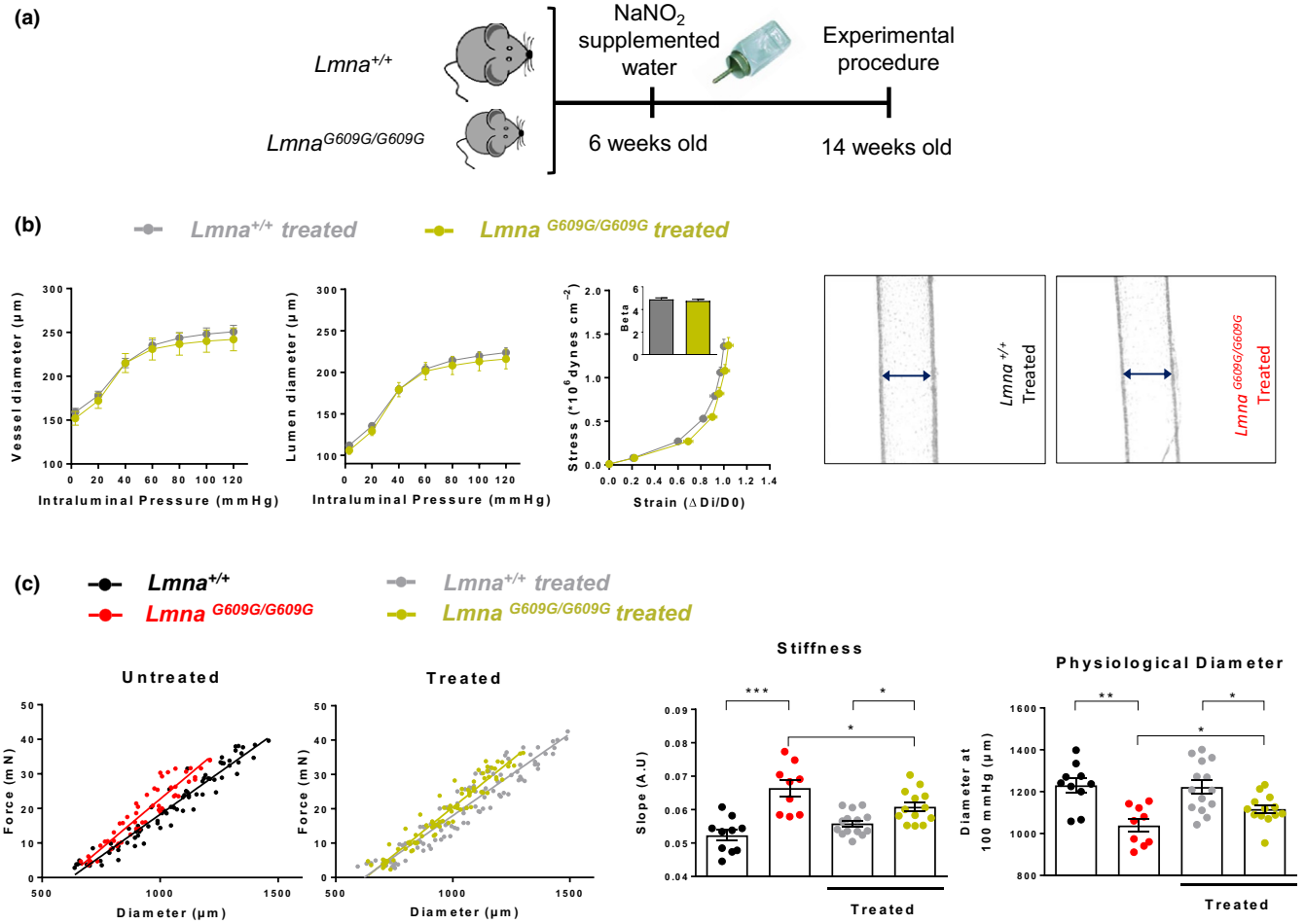

FIGURE 7 Dietary nitrite supplementation protects *Lmna*$^{G609G/G609G}$ mice against vascular stiffness and inward remodeling. (a) Study design. (b) Pressure–diameter curves for vessel (outer) and lumen (inner) diameters, corresponding stress–strain curves, and representative images of the pressurized arteries at 60 mmHg in nitrite-treated *Lmna*$^{G609G/G609G+/+}$ (n = 7) and *Lmna*$^{+/+}$ (n = 6) mice. (c) Effect of dietary nitrite supplementation on diameter–tension relationships, slope, and physiological diameter in aortic rings from *Lmna*$^{+/+}$ mice (n = 10–14) and *Lmna*$^{G609G/G609G}$ mice (n = 9–13). Nitrites attenuate arterial stiffness, as evidenced by increases in the force–diameter slope and the physiological diameter in aortic rings of treated *Lmna*$^{G609G/G609G}$ mice

cellular mechanisms underlying structural alterations in the aortas of progeroid mice. These functional studies in which we disrupted individual vessel wall components identified collagen as an underlying cause of stiffness in the aorta of *Lmna*$^{G609G/G609G}$ mice, with no evidence for a significant contribution from elastin or the cytoskeleton. Further imaging of vessel wall components showed that arteries from progeroid animals have increased collagen deposition and decreased area of smooth muscle tissue, unaccompanied by significant decreases in cell number. VSMCs thus degenerate in the vessels of progeroid mice, and their space within the vessel wall is progressively replaced by collagen, which accounts for the increased stiffness. The change in elastin–fiber conformation to a more linear layer arrangement in *Lmna*$^{G609G/G609G}$ mice might be an indirect consequence of the alterations in collagen, and not a cause of the stiffness, since the elastase experiments showed that differences in diameter–tension relationships between control and progeroid aortas were maintained after elastin disruption. This fibrotic process caused by progerin expression in VSMCs mimics the well-known medial degeneration and sclerosis process associated with physiological aging which promotes atherosclerosis in the long term (Sawabe, 2010). Of note, vascular stiffness in normal aging has been attributed not only to collagen accumulation, but also to elastin degradation and increased collagen cross-linking (Kohn et al., 2015). Although our mechanistic experiment suggests collagen and not elastin as a causing agent of stiffness, we cannot rule out the involvement of increased medial collagen cross-linking in vascular stiffness in progeria. Hence, the analysis of collagen organization and packaging by picrosirius red staining or by second-harmonic generation imaging did not have enough resolution to detect collagen in the medial layer, but showed no between-genotype differences in the organization and amount of collagen in the adventitia. The analysis of individual collagen types by immunofluorescence confirmed no changes in the amount of collagen in the adventitia (collagen I), and increased expression of collagens III, IV, V, and XII in the medial layer of the aorta. Further studies are required to identify the specific mechanisms by which progerin induces increased expression of different

collagens, and well as to assess the relative contribution of each collagen to the stiffening of progeroid vessels.

Our findings also establish *Lmna*$^{G609G/G609G}$ and *Lmna*$^{LCS/LCS}$*SM22αCre*$^{+/tg}$ mice as animal models for the study of age-related vascular stiffness without the interference from other cardiovascular risk factors. The *Lmna*$^{LCS/LCS}$*SM22αCre*$^{+/tg}$ mice will be especially useful, since they are free of other specific progeroid disease symptoms.

Nitrite supplementation of drinking water prevents vessel stiffness associated with normal aging (Rammos et al., 2014; Sindler et al., 2011), and our analysis in progeroid mice establishes that dietary nitrite protects against inward remodeling and stiffness in small mesenteric arteries and aortas in progeria. Nitrites are inorganic ions (NO_2^-) usually obtained through the diet from green leafy vegetables. They have become attractive candidates for restoring physiological nitric oxide (NO) signaling in states of NO insufficiency such as aging, since they have the ability to generate NO in hypoxia or low pH conditions (in highly energy demanding tissues) through the nitrite reductase activity of a wide variety of enzymes (e.g., myoglobin or hemoglobin) (Sindler, Devan, Fleenor, & Seals, 2014). The observed protective effects of nitrites can be explained by their ability to increase NO bioavailability (Lundberg & Weitzberg, 2008; Totzeck et al., 2012), resulting in NO-mediated protection against fibrosis (Chen et al., 2017; Kaikita et al., 2001, 2002), oxidative stress, inflammation, and mitochondrial dysfunction (Liu & Huang, 2008; Wink et al., 2001), which may protect VSMCs from progerin-induced degeneration. Since HGPS patients die mainly of atherosclerosis and associated ischemic events, and no cure has been found yet, any therapeutic approach aiming to retard the key pathophysiological alterations that trigger their cardiovascular decline such as vessel stiffness may have a beneficial impact on the patients. Consistent with this view, clinical trials have demonstrated reduced vessel stiffness in HGPS patients treated with the farnesyltransferase inhibitor lonafarnib, which has been estimated to prolong lifespan by 1.6 years (Gordon et al., 2012, 2018; Ullrich et al., 2013). Therefore, both HGPS patients and the general aging population may benefit from the vasoprotective effects of nitrites.

4 | EXPERIMENTAL PROCEDURES

4.1 | Mice

Lmna$^{G609G/G609G}$ knock-in mice ubiquitously express progerin (Osorio et al., 2011). Controls for these mice were *Lmna*$^{+/+}$ littermates. We crossed *Lmna*$^{LCS/LCS}$ mice (Osorio et al., 2011) with *SM22αCre* mice (The Jackson Laboratory) or with *Tie2-Cre* mice (Kisanuki et al., 2001) to target progerin expression to VSMCs (*Lmna*$^{LCS/LCS}$*SM22α-Cre*$^{tg/+}$) or to ECs (*Lmna*$^{LCS/LCS}$*Tie2Cre*$^{tg/+}$). Controls used were *Lmna*$^{LCS/LCS}$*Tie2Cre*$^{+/+}$ or *Lmna*$^{LCS/LCS}$*SM22αCre*$^{+/+}$ littermates, respectively. All studies were carried out with 13- to 15-week-old male mice on the C57BL/6 background, and analyses were performed by researchers blinded to genotype and treatment.

Mice were maintained in the animal facility of the Centro Nacional de Investigaciones Cardiovasculares Carlos III (CNIC) under specific-pathogen-free conditions. All animal procedures conformed to EU Directive 2010/63EU and Recommendation 2007/526/EC regarding the protection of animals used for experimental and other scientific purposes, enforced in Spanish law under Real Decreto 1201/2005, and were approved by the local ethics committees and the Animal Protection Area of the Comunidad Autónoma de Madrid (PROEX 135/14).

4.2 | Sample preparation

Animals were euthanized by CO_2 inhalation. Immediately after sacrifice, the thoracic and abdominal cavities were opened. Blood samples were collected from the inferior vena cava, placed in 500 µl EDTA collecting tubes (Microvette), and maintained at 4°C for no more than 1 hr before processing to obtain plasma. Thoracic and mesenteric arteries were excised and used for different protocols.

4.3 | Nitrite treatment

Lmna$^{G609G/G609G}$ and *Lmna*$^{+/+}$ mice received treatment with sodium nitrite ($NaNO_2$, 50 mg/L or 500 mg/L in drinking water) over the 8 weeks before sacrifice (from 6 to 14 weeks of age) (Figure 7a) The doses used have been reported to be safe in mice, showing no evidence of toxicological or carcinogenic effects and no changes in water consumption (National Toxicology Program, 2001). Consistent with this, we observed no adverse effects or changes in water consumption in treated animals.

4.4 | Wire myography

Thoracic aortas were placed in ice-cold Krebs–Henseleit solution (KHS: 115 mM NaCl, 2.5 mM $CaCl_2$, 4.6 mM KCl, 1.2 mM KH_2PO_4, 1.2 mM $MgSO_4$, 25 mM $NaHCO_3$, 11.1 mM glucose, and 0.01 mM EDTA) immediately after sacrifice. The vessels were gently cleaned of fat and connective tissue and cut into 2-mm-long segments. Wire myography was performed as previously described (del Campo & Ferrer, 2015). Aortic segments were mounted on two tungsten wires in a wire myograph system (620M, DMT) and immersed in KHS at 37°C with constant gassing (95% O_2 and 5% CO_2). Diameter–tension relationships were determined by artificial, stepwise stretching of the tissue, increasing its passive diameter by augmenting the distance between the wires passing through the lumen. At each step, we recorded both the force and the internal circumference of the vessel, which was transformed into vessel diameter in µm (del Campo & Ferrer, 2015). The tension experienced by the vessel wall in resisting this stretching was recorded by a force transducer connected to one of the wires, and plotted on the *y*-axis. The estimated diameter at 100 mmHg was calculated from the diameter–tension relationship and the Laplace equation (Tension = [pressure * radius]/thickness) using the DMT normalization module (LabChart software, ADInstruments; del Campo & Ferrer, 2015). For each vessel segment, a linear regression was calculated from the diameter–tension relationship. Diameter–tension measurements were excluded when discalibration

of the force transducer in a specific channel was detected (difference between the myograph unit and the software >5 mM). Diameter–tension relationships can be defined and compared with two parameters. First, the slope of the linear regression quantifies the change in tension per unit change in vessel diameter, so that a steeper slope indicates greater stiffness. Second, the extrapolated value of diameter when the force is equal to 0 represents the vessel diameter at 0 pressure (Y_0 diameter), which, together with the estimated diameter at 100 mmHg (third), can indicate inward or outward remodeling.

The contribution of different vessel wall components to vessel stiffness was assessed by analyzing the diameter–tension relationships upon degradation of collagen with collagenase type II (0.2% w/v; Thermo Fisher Scientific), elastin with elastase (28 μg/μl; Sigma), or the cytoskeleton with the selective F-actin depolymerizer mycalolide B (4 μM; Enzo Life Sciences). Aortic rings incubated with collagenase for 15 min in KHS were compared with vessels directly mounted on the wire myograph in KHS (vehicle). Incubations with elastase or mycalolide B were maintained for 3 hr at 37°C in HEPES buffer (119 mM NaCl, 20 mM HEPES, 4.6 mM KCl, 1 mM $MgSO_4{\cdot}7H_2O$, 0.15 mM $Na_2HPO_4{\cdot}12\ H_2O$, 0.4 mM KH_2PO_4, 5 mM $NaHCO_3$, 1.2 mM $CaCl_2{\cdot}2H_2O$, 5.5 mM glucose, pH 7.4). Diameter–tension relationships from these incubations were compared with data from control aortic rings incubated for 3 hr in HEPES at 37°C (vehicle). Note that diameter–tension relationships and corresponding slopes for aortic rings incubated with elastase or mycalolide B share the same control data, although they are plotted separately for clarity (Figure 4).

4.5 | Pressure myography

Structural and mechanical properties of mesenteric resistance arteries were studied with a pressure myograph (Danish Myo Tech, Model P100, J.P. Trading I/S, Aarhus, Denmark). Vessels were placed on two glass microcannulae and secured with surgical nylon suture thread. After any small branches were tied off, vessel length was adjusted so that the vessel walls were parallel without stretching. Intraluminal pressure was then raised to 120 mmHg, and the artery was unbuckled by adjusting the cannulae. The segment was then set to 45 mmHg and allowed to equilibrate for 30 min at 37°C in calcium-free KHS ($0Ca^{2+}$; omitting calcium and adding 1 mM EGTA), perfused intravascularly and extravascularly, and gassed with a mixture of 95% O_2 and 5% CO_2. Intraluminal pressure was reduced to 3 mmHg. A pressure–diameter plot was obtained by increasing intraluminal pressure in 20 mmHg steps from 3 to 120 mmHg. Internal and external diameters were continuously measured under passive conditions (D_{i0Ca}, D_{e0Ca}, respectively) for 3 min at each intraluminal pressure. The final value used was the mean of the measurements taken during the last 30 s, when measurements had reached a steady state.

From internal and external diameter measurements in passive conditions, the following structural and mechanical parameters were calculated:

$$\text{Wall thickness (WT)} = (D_{e0Ca} - D_{i0Ca})/2$$

$$\text{Wall:lumen} = (D_{e0Ca} - D_{i0Ca})/2D_{i0Ca}$$

Incremental distensibility is the percentage of change in the arterial internal diameter for each mmHg change in intraluminal pressure and was calculated according to this formula:

$$\text{Incremental distensibility} = \Delta D_{i0Ca}/(D_{i0Ca} \times \Delta P) \times 100$$

Circumferential wall strain (ε) = $(D_{i0Ca} - D_{00Ca})/D_{00Ca}$, where D_{00Ca} is the internal diameter at 3 mmHg, and D_{i0Ca} is the observed internal diameter for a given intravascular pressure, both measured in $0Ca^{2+}$ medium.

Circumferential wall stress (σ) = $(P \times D_{i0Ca})/(2WT)$, where P is the intraluminal pressure (1 mmHg = 133.4×10^3 dynes·cm^{-2}), and WT is wall thickness at each intraluminal pressure in $0Ca^{2+}$-KHS.

Arterial stiffness independent of geometry is determined by Young's elastic modulus (E = stress/strain) (Briones et al., 2009; Schjorring, Carlsson, & Simonsen, 2015). The stress–strain relationship is nonlinear; therefore, it is more appropriate to obtain a tangential or incremental elastic modulus (E_{inc}) by determining the slope of the stress–strain curve ($E_{inc} = \delta\sigma/\delta\varepsilon$). E_{inc} was obtained by fitting the stress–strain data from each animal to an exponential curve using the equation $\sigma = \sigma_{orig}e^{\beta\varepsilon}$, where σ_{orig} is the stress at the original diameter (diameter at 3 mmHg).

Taking derivatives from the equation, we determine that $E_{inc} = \beta\sigma$. For a given σ-value, E_{inc} is directly proportional to β. An increase in β implies an increase in E_{inc}, which signifies an increase in stiffness.

4.6 | Histological analysis

Thoracic aorta segments were fixed in 4% paraformaldehyde. Following dehydration in an ascending ethanol series, samples were embedded in paraffin, cut into 5-μm sections, and stained with H&E, Masson's trichrome, or picrosirius red. H&E staining was performed to check primary tissue appearance. Samples stained with H&E and Masson's trichrome were imaged with OPT Scanner 3001 (OPT, Bioptonics Microscopy). Medial thickness and lumen perimeter length were measured in Masson's trichrome-stained specimens. Collagen and VSMC content were measured in the medial layer as the green or red area, respectively, in Masson's trichrome-stained specimens (Fiji software; ImageJ 1.50e x64) and expressed as a percentage of the medial area.

Picrosirius-red-stained slices were imaged under a Nikon Eclipse 90i microscope both in bright field and under polarized light in order to visualize collagen bundles with different thickness and packaging (Rittie, 2017). Under polarized light, denser collagen bundles are seen as yellow-orange, whereas the less dense or thinner collagen bundles appear green (Lattouf et al., 2014). Under polarized light, we observed green or yellow-orange collagen bundles only in the adventitial layer, and quantified them with ImageJ software.

To analyze elastin lamellae and nuclei, 5-μm aortic sections were stained with DAPI (1:500; Invitrogen), mounted in Eukitt®

mounting medium (Sigma-Aldrich), and imaged with a confocal microscope (Leica SP5 DMI 6000B) taking advantage of the intrinsic autofluorescence of elastin fibers. The semiautomatic image processing and quantification of elastin "rectilinearity" were developed as a toolbox in Fiji (ImageJ 1.50e 64-bit for Windows). Rectilinearity measures the length and waviness of each elastin fiber. Thus, a region of interest with elastin fibers and a threshold to segment them are selected. A skeletonization of the segmented objects (Lee, Kashyap, & Chu, 1994), after removing small connected components, extracts the center lines of each lamellae independently of their intensity or thickness; these are later analyzed to measure the length ("fiber length") of each resulting branch and the corresponding Euclidean distance between starting and final points ("fiber distance"; Arganda-Carreras, Fernandez-Gonzalez, Munoz-Barrutia, & Ortiz-De-Solorzano, 2010). The final output is the ratio between the accumulative sum of fiber distance and fiber length for all branches. A first preprocessing step was applied to remove noise from the original image by applying a median filtering followed by background subtraction using the "rolling ball" algorithm (Sternberg, 1983).

4.7 | In vivo magnetic resonance imaging

For the MRI acquisition, mice were anesthetized with 2% isoflurane and a 1.8 L/min oxygen flow. Ophthalmic gel was placed on the eyes to prevent drying. Thoracic aorta cine MR studies were acquired using a 7-T Agilent/Varian scanner (Agilent, Santa Clara, CA, USA) equipped with a DD2 console, an actively shielded 115/60 gradient set, and a microstrip helmet coil used for both RF transmission and reception. MRI sequences were based on an ECG-triggered fast gradient echo cine sequence with the following imaging parameters: 181.82/2.07 ms (minimum repetition time TR, minimum echo time TE); field of view, 3.0 cm^2; acquisition matrix, 256 x 256; flip angle, 40°; 8 averages; 20 cardiac phases; 2 slices; slice thickness, 0.2-0.4 mm; and slice gap, 0.6 mm.

To determine the descending aorta cross section, we acquired two transverse images perpendicular to the long axis of the aorta and spinal cord, located slightly above the heart apex level, set on three orthogonal planes (transverse, coronal, and sagittal) used to localize the thoracic aorta, spinal cord, lungs, and heart.

For image quantification, aortic lumen area was measured on the cine MR images by manual segmentation by a trained operator, using the freely available Segment software v1.9 R3819 (http://segment.heiberg.se) (Heiberg et al., 2010). In some images, the area could not be determined, and therefore, we used the upper section data, with data from the lower section used to fill in missing values when necessary. Since the time sampling was different for each animal (depending on heart rate), a time linear interpolation was applied to all curves in order to obtain equivalent points throughout the cardiac cycle. For curve plotting purposes, the mean and standard deviation at each time point was determined for both animal groups. All time curves were cut at 150 ms, as the different cycle duration for each animal prevented a proper time alignment beyond that point. From the original area raw data in mm^2, the following derived parameters were calculated: distensibility or initial ascending slope (estimated by linear fitting over the first 20 ms at systole); incremental area (measured as area difference from the first point); strain (measured as the aortic radius increase divided by initial radius). Total strain was defined as the integral of the strain curve.

4.8 | Immunofluorescence staining

Thoracic aorta segments were fixed for 24 hr in 4% paraformaldehyde, embedded in paraffin, cut into 5-μm sections, deparaffinized, and rehydrated. Sections were antigen-unmasked, permeabilized, and incubated with blocking solution. Primary antibodies were incubated overnight at 4°C in blocking buffer. Sections were washed and incubated with appropriate secondary antibodies for 1-2 hr at room temperature and with DAPI/Hoechst, mounted with Fluoromount™ (Sigma) or Thermo Fisher SlowFade Gold antifade reagent (S36936), and visualized in a confocal microscope (Leica SP5 DMI 6000B for collagen XII and Lamin A; Nikon Eclipse 80i for collagens I, III, IV, V).

For lamin A staining, antigen retrieval was performed with 0.37 g/L EDTA buffer (pH 8) for 30 min, permeabilization with 0.5% Triton X-100 for 10 min, and blocking with 5% BSA. For collagen XII staining, antigen retrieval was performed with citrate buffer (pH 6) for 20 min in the microwave, and blocking and permeabilization with 0.3% Triton X-100, 5% normal goat serum, and 5% BSA in PBS. For the rest of collagens, permeabilization was not necessary and antigen retrieval was performed with Antigen Unmasking Solution (H3300, Vector Labs). Blocking was performed with 2% BSA solution in PBS for 15 min.

Antibodies used were as follows: antilamin A H-102 antibody (1:100; Santa Cruz Biotechnology); anticollagen XII antibody (1:100, courtesy of Manuel Koch, Germany); COL-I (Southern Biotech 1310-01, 1:400); COL-III (Proteintech 22734-1-AP, 1:250 in PBS); COL-IV (Abcam ab6586, 1:250); COL-V (Abcam ab7046, 1:250).

Collagen signal was quantified using ImageJ. Mean fluorescence intensity was obtained for the selected area of the medial layer (and the adventitial layer, in the case of Collagen I). Intensity values were then normalized to the median of the controls. For collagen XII, due to background, maximum entropy threshold was used to select collagen XII-positive pixels, and integrated density was obtained and normalized to the median of the control mice.

4.9 | Second-harmonic generation microscopy

Second-harmonic generation microscopy was used to visualize the three dimensional organization of collagen throughout the arotic wall and to examine structural differences. H&E-stained thoracic aorta sections were used for the quantification of backward second-harmonic generation signal from collagen fibrils, which was obtained by multiphoton excitation at 860 nm using a tunable femtosecond pulsed laser (MaiTai DeepSee, Spectra-Physics) coupled to a Zeiss LSM780 upright system and a water-dipping Plan-Apochromat 10x/NA 0,45 objective (Carl Zeiss Jena GmbH). Quantification was

performed by ImageJ to obtain the amount and density of the collagen signal, as well as kurtosis and skewness parameters. Kurtosis measures the degree to which a distribution is more or less peaked than a normal distribution, and skewness measures the degree of asymmetry of a distribution (Mostaco-Guidolin et al., 2013). Since second-harmonic generation imaging detected collagen bundles only in the adventitia, the results obtained from the quantification of these images refer only to the adventitial layer.

4.10 | Pulse wave velocity

PWV is the velocity at which the arterial wave propagates through the circulatory system. Aortic-femoral PWV was measured by Doppler ultrasound using the transient time (TT) system (Laurent et al., 2006). Animals were anesthetized (1.5% isoflurane in oxygen) and maintained in supine position on a temperature-controlled surface to maintain body temperature at 37°C with continuous electrocardiographic (EKG) recording. The pulse wave was recorded using a pulsed wave Doppler ultrasound in a VEVO 2100 system (VisualSonic). The ascending aorta was located in 2D mode, and the wave Doppler flow was then recorded simultaneously with EKG. The process was repeated on the femoral artery at the level of the thigh. The time from the QRS R wave to the foot of the pulse waveform was measured in both the ascending aorta and femoral artery. The TT is the difference between these times measured at the two measurement points. PWV is calculated as the distance between the two measurement points divided by the pulse wave TT.

4.11 | Statistical analysis

Results are represented as mean ± standard error of the media (*SEM*). The Student *t* test was used to compare univariable data between the two groups. Single-variable comparisons between more than two groups were performed with one-way ANOVA followed by the Sidak multiple comparisons tests. Outliers identified using the maximum normalized residual test (Grubbs' test) were excluded. Diameter–tension relationships were analyzed by calculating the linear regression lines and their corresponding slopes and diameter at force 0 (Y_0), which were then compared among groups using the Student *t* test or one-way ANOVA. Diameter–pressure curves were compared with two-way ANOVA followed by the Sidak multiple comparisons tests. Stress–strain curves were analyzed by extracting the β value for each curve (see Section 2.6, Pressure myography), which we compared among groups using the Student *t* test. Aortic cross-sectional area curves obtained by MRI and collagen immunofluorescence measurements were compared by the Mann–Whitney *U* test. Results were considered statistically significant at *p*-values <0.05. Statistical analysis was performed with GraphPad Prism 7 software.

ACKNOWLEDGMENTS

We thank Carlos López-Otín for providing *Lmna*^{G609G} and *Lmna*^{LCS} mice, Yeny Rojas for acquiring MR images, David Sanz-Rosa and Jose Luis de la Pompa for providing *Tie2-Cre* mice, Simon Bartlett for English editing, Fátima Sánchez-Cabo for help with statistical analysis, Daniel Jiménez Carretero for help with image analysis, Manuel Koch for providing collagen XII antibody, the CNIC Microscopy and Dynamic Imaging Unit for support on optical microscopy, the CNIC Animal Facility for animal care, and the CNIC Histology Service for technical support. This study was supported by the Spanish Ministerio de Ciencia, Innovación y Universidades (MCIU, grants SAF2016-79490-R and SAF2016-80305-P), with co-funding from the European Regional Development Fund (ERDF, "Una manera de hacer Europa"). RvK and RKA are supported by NIH grants AG047373, T32-GM008076, F31HL142160 and NSF grant CMMI 1548571. L.d.C. was supported by a Jordi Soler postdoctoral grant from the Red de Investigación Cardiovascular (RETIC Program, Instituto de Salud Carlos III), and A.S.-L. was supported by a Severo Ochoa predoctoral grant from the MCIU (SVP-2014-068334) and by a grant from Asociación Apadrina la Ciencia-Ford España-Ford Motor Company Fund. The CNIC is supported by the MCIU and the Pro-CNIC Foundation, and is a Severo Ochoa Center of Excellence (SEV-2015-0505).

CONFLICT OF INTEREST

None declared.

AUTHOR'S CONTRIBUTION

L.d.C and V.A. conceived and designed the study, and wrote the manuscript; L.d.C. performed experiments, and analyzed and interpreted results; A.S.-L. was involved in the design of the study, performed experiments, analyzed and interpreted results, and participated in manuscript writing; A.M.B. carried out, analyzed, and interpreted pressure myography experiments; R.A.K and R.K.A. carried out, analyzed, and interpreted collagen immunofluorescence studies; C.G.-G. and E.E. provided technical support in the laboratory experiments; L.C., J.R.-C., and M.D. analyzed and interpreted MRI data; G.G.-M. revised and interpreted PWV experiments; M.S. revised and interpreted pressure myography experiments; V.A. interpreted results and supervised the study. All authors discussed the results and made a critical revision of the manuscript.

REFERENCES

Adji, A., O'Rourke, M. F., & Namasivayam, M. (2011). Arterial stiffness, its assessment, prognostic value, and implications for treatment. *American Journal of Hypertension*, *24*(1), 5–17. https://doi.org/10.1038/ajh.2010.192

Arganda-Carreras, I., Fernandez-Gonzalez, R., Munoz-Barrutia, A., & Ortiz-De-Solorzano, C. (2010). 3D reconstruction of histological sections: Application to mammary gland tissue. *Microscopy Research and Technique*, *73*(11), 1019–1029. https://doi.org/10.1002/jemt.20829

Boutouyrie, P., Laurent, S., & Briet, M. (2008). Importance of arterial stiffness as cardiovascular risk factor for future development of new type of drugs. *Fundamental & Clinical Pharmacology*, *22*(3), 241–246. https://doi.org/10.1111/j.1472-8206.2008.00584.x

Briones, A. M., Rodriguez-Criado, N., Hernanz, R., Garcia-Redondo, A. B., Rodrigues-Diez, R. R., Alonso, M. J., … Salaices, M. (2009). Atorvastatin prevents angiotensin II-induced vascular remodeling and oxidative stress. *Hypertension*, *54*(1), 142–149. https://doi.org/10.1161/hypertensionaha.109.133710

Chen, C., Yun, X. J., Liu, L. Z., Guo, H., Liu, L. F., & Chen, X. L. (2017). Exogenous nitric oxide enhances the prophylactic effect of aminoguanidine, a preferred iNOS inhibitor, on bleomycin-induced fibrosis in the lung: Implications for the direct roles of the NO molecule in vivo. *Nitric Oxide*, *70*, 31–41. https://doi.org/10.1016/j.niox.2017.07.005

Chiquet, M., Birk, D. E., Bonnemann, C. G., & Koch, M. (2014). Collagen XII: Protecting bone and muscle integrity by organizing collagen fibrils. *International Journal of Biochemistry & Cell Biology*, *53*, 51–54. https://doi.org/10.1016/j.biocel.2014.04.020

Chirinos, J. A. (2016). Large artery stiffness, microvascular function, and cardiovascular risk. *Circulation: Cardiovascular Imaging*, *9*(12), e005903. https://doi.org/10.1161/circimaging.116.005903

Cooper, L. L., Palmisano, J. N., Benjamin, E. J., Larson, M. G., Vasan, R. S., Mitchell, G. F., & Hamburg, N. M. (2016). Microvascular function contributes to the relation between aortic stiffness and cardiovascular events: The Framingham Heart Study. *Circulation: Cardiovascular Imaging*, *9*(12), e004979. https://doi.org/10.1161/CIRCIMAGING.116.004979

D'Agostino, R. B. Sr, Vasan, R. S., Pencina, M. J., Wolf, P. A., Cobain, M., Massaro, J. M., & Kannel, W. B. (2008). General cardiovascular risk profile for use in primary care: The Framingham Heart Study. *Circulation*, *117*(6), 743–753. https://doi.org/10.1161/circulationaha.107.699579

De Sandre-Giovannoli, A., Bernard, R., Cau, P., Navarro, C., Amiel, J., Boccaccio, I., … Levy, N. (2003). Lamin a truncation in Hutchinson-Gilford progeria. *Science*, *300*(5628), 2055. https://doi.org/10.1126/science.1084125

del Campo, L., & Ferrer, M. (2015). Wire myography to study vascular tone and vascular structure of isolated mouse arteries. *Methods in Molecular Biology*, *1339*, 255–276. https://doi.org/10.1007/978-1-4939-2929-0_18

Dorado, B., & Andrés, V. (2017). A-type lamins and cardiovascular disease in premature aging syndromes. *Current Opinion in Cell Biology*, *46*, 17–25. https://doi.org/10.1016/j.ceb.2016.12.005

Eriksson, M., Brown, W. T., Gordon, L. B., Glynn, M. W., Singer, J., Scott, L., … Collins, F. S. (2003). Recurrent de novo point mutations in lamin A cause Hutchinson-Gilford progeria syndrome. *Nature*, *423*(6937), 293–298. https://doi.org/10.1038/nature01629

Gerhard-Herman, M., Smoot, L. B., Wake, N., Kieran, M. W., Kleinman, M. E., Miller, D. T., … Gordon, L. B. (2012). Mechanisms of premature vascular aging in children with Hutchinson-Gilford progeria syndrome. *Hypertension*, *59*(1), 92–97. https://doi.org/10.1161/hypertensionaha.111.180919

Goldman, R. D., Shumaker, D. K., Erdos, M. R., Eriksson, M., Goldman, A. E., Gordon, L. B., … Collins, F. S. (2004). Accumulation of mutant lamin A causes progressive changes in nuclear architecture in Hutchinson-Gilford progeria syndrome. *Proceedings of the National Academy of Sciences USA*, *101*(24), 8963–8968. https://doi.org/10.1073/pnas.0402943101

Gordon, L. B., Kleinman, M. E., Massaro, J., D'Agostino, R. B., Shappell, H., Gerhard-Herman, M., … Kieran, M. W. (2016). Clinical trial of the protein farnesylation inhibitors lonafarnib, pravastatin, and zoledronic acid in children with Hutchinson-Gilford progeria syndrome. *Circulation*, *134*(2), 114–125. https://doi.org/10.1161/circulationaha.116.022188

Gordon, L. b., Kleinman, M. e., Miller, D. t., Neuberg, D. s., Giobbie-Hurder, A., Gerhard-Herman, M., … Kieran, M. w. (2012). Clinical trial of a farnesyltransferase inhibitor in children with Hutchinson-Gilford progeria syndrome. *Proceedings of the National Academy of Sciences USA*, *109*(41), 16666–16671. https://doi.org/10.1073/pnas.1202529109

Gordon, L. B., Massaro, J., D'Agostino, R. B., Campbell, S. E., Brazier, J., Brown, W. T., … Kieran, M. W. (2014). Impact of farnesylation inhibitors on survival in Hutchinson-Gilford progeria syndrome. *Circulation*, *130*(1), 27–34. https://doi.org/10.1161/circulationaha.113.008285

Gordon, L. B., Shappell, H., Massaro, J., D'Agostino, R. B., Brazier, J., Campbell, S. E., … Kieran, M. W. (2018). Association of Lonafarnib treatment vs no treatment with mortality rate in patients with Hutchinson-Gilford progeria syndrome. *JAMA*, *319*(16), 1687–1695. https://doi.org/10.1001/jama.2018.3264

Hamczyk, M. R., del Campo, L. D., & Andrés, V. (2018). Aging in the cardiovascular system: Lessons from Hutchinson-Gilford progeria syndrome. *Annual Review of Physiology*, *80*, 27–48. https://doi.org/10.1146/annurev-physiol-021317-121454

Hamczyk, M. R., Villa-Bellosta, R., Gonzalo, P., Andrés-Manzano, M. J., Nogales, P., Bentzon, J. F., … Andrés, V. (2018). Vascular smooth muscle-specific progerin expression accelerates atherosclerosis and death in a mouse model of Hutchinson-Gilford progeria syndrome. *Circulation*, *138*(3), 266–282. https://doi.org/10.1161/circulationaha.117.030856

Harhouri, K., Frankel, D., Bartoli, C., Roll, P., De Sandre-Giovannoli, A., & Levy, N. (2018). An overview of treatment strategies for Hutchinson-Gilford progeria syndrome. *Nucleus*, *9*(1), 246–257. https://doi.org/10.1080/19491034.2018.1460045

Heiberg, E., Sjogren, J., Ugander, M., Carlsson, M., Engblom, H., & Arheden, H. (2010). Design and validation of segment–freely available software for cardiovascular image analysis. *BMC Medical Imaging*, *10*, 1. https://doi.org/10.1186/1471-2342-10-1

Hennekam, R. C. (2006). Hutchinson-Gilford progeria syndrome: Review of the phenotype. *American Journal of Medical Genetics. Part A*, *140*(23), 2603–2624. https://doi.org/10.1002/ajmg.a.31346

Huveneers, S., Daemen, M. J., & Hordijk, P. L. (2015). Between Rho(k) and a hard place: The relation between vessel wall stiffness, endothelial contractility, and cardiovascular disease. *Circulation Research*, *116*(5), 895–908. https://doi.org/10.1161/circresaha.116.305720

Kaikita, K., Fogo, A. B., Ma, L., Schoenhard, J. A., Brown, N. J., & Vaughan, D. E. (2001). Plasminogen activator inhibitor-1 deficiency prevents hypertension and vascular fibrosis in response to long-term nitric oxide synthase inhibition. *Circulation*, *104*(7), 839–844. https://doi.org/10.1161/hc3301.092803

Kaikita, K., Schoenhard, J. A., Painter, C. A., Ripley, R. T., Brown, N. J., Fogo, A. B., & Vaughan, D. E. (2002). Potential roles of plasminogen activator system in coronary vascular remodeling induced by long-term nitric oxide synthase inhibition. *Journal of Molecular and Cellular Cardiology*, *34*(6), 617–627. https://doi.org/10.1006/jmcc.2002.2001

Kisanuki, Y. Y., Hammer, R. E., Miyazaki, J., Williams, S. C., Richardson, J. A., & Yanagisawa, M. (2001). Tie2-Cre transgenic mice: A new model for endothelial cell-lineage analysis in vivo. *Developmental Biology*, *230*(2), 230–242. https://doi.org/10.1006/dbio.2000.0106

Kohn, J. C., Lampi, M. C., & Reinhart-King, C. A. (2015). Age-related vascular stiffening: Causes and consequences. *Frontiers in Genetics*, *6*, 112. https://doi.org/10.3389/fgene.2015.00112

Lakatta, E. G. (2003). Arterial and cardiac aging: Major shareholders in cardiovascular disease enterprises: Part III: Cellular and molecular clues to heart and arterial aging. *Circulation*, *107*(3), 490–497. https://doi.org/10.1161/01.CIR.0000048894.99865.02

Lakatta, E. G., & Levy, D. (2003a). Arterial and cardiac aging: Major shareholders in cardiovascular disease enterprises: Part I: Aging arteries: A "set up" for vascular disease. *Circulation*, *107*(1), 139–146.

Lakatta, E. G., & Levy, D. (2003b). Arterial and cardiac aging: Major shareholders in cardiovascular disease enterprises: Part II: The aging heart in health: Links to heart disease. *Circulation*, *107*(2), 346–354.

Lattouf, R., Younes, R., Lutomski, D., Naaman, N., Godeau, G., Senni, K., & Changotade, S. (2014). Picrosirius red staining: A useful tool to

appraise collagen networks in normal and pathological tissues. *Journal of Histochemistry and Cytochemistry*, *62*(10), 751–758. https://doi.org/10.1369/0022155414545787

Laurent, S., Cockcroft, J., Van Bortel, L., Boutouyrie, P., Giannattasio, C., Hayoz, D., … Struijker-Boudier, H. (2006). Expert consensus document on arterial stiffness: Methodological issues and clinical applications. *European Heart Journal*, *27*(21), 2588–2605. https://doi.org/10.1093/eurheartj/ehl254

Lee, T. C., Kashyap, R. L., & Chu, C. N. (1994). Building skeleton Models via 3-D medial surface axis thinning algorithms. *CVGIP: Graphical Models and Image Processing*, *56*(6), 462–478. https://doi.org/10.1006/cgip.1994.1042

Liu, V. W., & Huang, P. L. (2008). Cardiovascular roles of nitric oxide: A review of insights from nitric oxide synthase gene disrupted mice. *Cardiovascular Research*, *77*(1), 19–29. https://doi.org/10.1016/j.cardiores.2007.06.024

Lundberg, J. O., & Weitzberg, E. (2008). Nitrite reduction to nitric oxide in the vasculature. *American Journal of Physiology. Heart and Circulatory Physiology*, *295*(2), H477–478. https://doi.org/10.1152/ajpheart.00611.2008

Malfait, F. (2018). Vascular aspects of the Ehlers-Danlos Syndromes. *Matrix Biology*, *71–72*, 380–395. https://doi.org/10.1016/j.matbio.2018.04.013

Mitchell, G. F. (2008). Effects of central arterial aging on the structure and function of the peripheral vasculature: implications for end-organ damage. *Journal of Applied Physiology*, *105*(5), 1652–1660. https://doi.org/10.1152/japplphysiol.90549.2008

Mostaço-Guidolin, L. B., Ko, A.-T., Wang, F., Xiang, B. o., Hewko, M., Tian, G., … Sowa, M. G. (2013). Collagen morphology and texture analysis: From statistics to classification. *Scientific Reports*, *3*, 2190. https://doi.org/10.1038/srep02190

National Toxicology Program (2001). Toxicology and carcinogenesis studies of sodium nitrite (CAS NO. 7632–00-0) in F344/N rats and B6C3F1 mice (drinking water studies). *Natlional Toxicological Program Technical Report Series*, *495*, 7–273.

Osmanagic-Myers, S., Kiss, A., Manakanatas, C., Hamza, O., Sedlmayer, F., Szabo, P. L., … Foisner, R. (2018). Endothelial progerin expression causes cardiovascular pathology through an impaired mechanoresponse. *Journal of Clinical Investigation*, *129*(2), 531–545. https://doi.org/10.1172/JCI121297

Osorio, F. g., Navarro, C. l., Cadinanos, J., Lopez-Mejia, I. c., Quiros, P. m., Bartoli, C., … Lopez-Otin, C. (2011). Splicing-directed therapy in a new mouse model of human accelerated aging. *Science Translational Medicine*, *3*(106), 106ra107. https://doi.org/10.1126/scitranslmed.3002847

Population Division, D., United Nations. (2002). World Population Ageing 1950–2050.

Rammos, C., Hendgen-Cotta, U. B., Sobierajski, J., Bernard, A., Kelm, M., & Rassaf, T. (2014). Dietary nitrate reverses vascular dysfunction in older adults with moderately increased cardiovascular risk. *Journal of the American College of Cardiology*, *63*(15), 1584–1585. https://doi.org/10.1016/j.jacc.2013.08.691

Rittie, L. (2017). Method for picrosirius red-polarization detection of collagen fibers in tissue sections. *Methods in Molecular Biology*, *1627*, 395–407. https://doi.org/10.1007/978-1-4939-7113-8_26

Safar, M. E. (2018). Arterial stiffness as a risk factor for clinical hypertension. *Nature Reviews Cardiology*, *15*(2), 97–105. https://doi.org/10.1038/nrcardio.2017.155

Sawabe, M. (2010). Vascular aging: From molecular mechanism to clinical significance. *Geriatrics & Gerontology International*, *10*(Suppl 1), S213–S220. https://doi.org/10.1111/j.1447-0594.2010.00603.x

Schjorring, O. L., Carlsson, R., & Simonsen, U. (2015). Pressure myography to study the function and structure of isolated small arteries. *Methods in Molecular Biology*, *1339*, 277–295. https://doi.org/10.1007/978-1-4939-2929-0_19

Sindler, A. L., Devan, A. E., Fleenor, B. S., & Seals, D. R. (2014). Inorganic nitrite supplementation for healthy arterial aging. *Journal of Applied Physiology*, *116*(5), 463–477. https://doi.org/10.1152/japplphysiol.01100.2013

Sindler, A. L., Fleenor, B. S., Calvert, J. W., Marshall, K. D., Zigler, M. L., Lefer, D. J., & Seals, D. R. (2011). Nitrite supplementation reverses vascular endothelial dysfunction and large elastic artery stiffness with aging. *Aging Cell*, *10*(3), 429–437. https://doi.org/10.1111/j.1474-9726.2011.00679.x

Stehbens, W. E., Delahunt, B., Shozawa, T., & Gilbert-Barness, E. (2001). Smooth muscle cell depletion and collagen types in progeric arteries. *Cardiovasc Pathol*, *10*(3), 133–136. https://doi.org/10.1016/S1054-8807(01)00069-2

Sternberg, S. R. (1983). Biomedical image processing. *Computer*, *16*(1), 22–34. https://doi.org/10.1109/MC.1983.1654163

Totzeck, M., Hendgen-Cotta, U. B., Luedike, P., Berenbrink, M., Klare, J. P., Steinhoff, H.-J., … Rassaf, T. (2012). Nitrite regulates hypoxic vasodilation via myoglobin-dependent nitric oxide generation. *Circulation*, *126*(3), 325–334. https://doi.org/10.1161/circulationaha.111.087155

Ullrich, N. J., Kieran, M. W., Miller, D. T., Gordon, L. B., Cho, Y.-J., Silvera, V. M., … Kleinman, M. E. (2013). Neurologic features of Hutchinson-Gilford progeria syndrome after lonafarnib treatment. *Neurology*, *81*(5), 427–430. https://doi.org/10.1212/WNL.0b013e31829d85c0

Villa-Bellosta, R., Rivera-Torres, J., Osorio, F. G., Acin-Perez, R., Enriquez, J. A., Lopez-Otin, C., & Andres, V. (2013). Defective extracellular pyrophosphate metabolism promotes vascular calcification in a mouse model of Hutchinson-Gilford progeria syndrome that is ameliorated on pyrophosphate treatment. *Circulation*, *127*(24), 2442–2451. https://doi.org/10.1161/circulationaha.112.000571

Vlachopoulos, C., Aznaouridis, K., & Stefanadis, C. (2010). Prediction of cardiovascular events and all-cause mortality with arterial stiffness: A systematic review and meta-analysis. *Journal of the American College of Cardiology*, *55*(13), 1318–1327. https://doi.org/10.1016/j.jacc.2009.10.061

Wang, M., Monticone, R. E., & Lakatta, E. G. (2014). Proinflammation of aging central arteries: A mini-review. *Gerontology*, *60*(6), 519–529. https://doi.org/10.1159/000362548

Wink, D. A., Miranda, K. M., Espey, M. G., Pluta, R. M., Hewett, S. J., Colton, C., … Grisham, M. B. (2001). Mechanisms of the antioxidant effects of nitric oxide. *Antioxidants & Redox Signaling*, *3*(2), 203–213. https://doi.org/10.1089/152308601300185179

World Health Organization. (2017). Global health observatory. Retrieved from http://www.who.int/gho

SUPPORTING INFORMATION

Additional supporting information may be found online in the Supporting Information section at the end of the article.

How to cite this article: del Campo L, Sánchez-López A, Salaices M, et al. Vascular smooth muscle cell-specific progerin expression in a mouse model of Hutchinson–Gilford progeria syndrome promotes arterial stiffness: Therapeutic effect of dietary nitrite. *Aging Cell*. 2019;18:e12936. https://doi.org/10.1111/acel.12936

Supporting information

Vascular smooth muscle cell-specific progerin expression in a mouse model of Hutchinson-Gilford progeria syndrome promotes arterial stiffness: Therapeutic effect of dietary nitrite

Running title: VSMCs and arterial stiffness in progeria

Lara del Campo, PhD[1,2,*], Amanda Sánchez-López, MSc[1,2,*], Mercedes Salaices, PhD [2,3], Ryan A. von Kleeck [9],Elba Expósito[1,2], Cristina González-Gómez[1,2], Lorena Cussó, PhD[1,4,5,6], Gabriela Guzmán-Martínez, MD, PhD[1,7], Jesús Ruiz-Cabello, PhD[1,8,**], Manuel Desco, PhD[1,4,5,6], Richard K. Assoian [9], Ana M. Briones, PhD [2,3] and Vicente Andrés, PhD [1,2,‡]

[1] Centro Nacional de Investigaciones Cardiovasculares (CNIC), Madrid, Spain

[2] CIBER de Enfermedades Cardiovasculares (CIBERCV), Spain

[3] Departamento de Farmacología y Terapéutica, Facultad de Medicina, Universidad Autónoma de Madrid, Instituto de Investigación Hospital La Paz (IdiPaz), Madrid, Spain

[4] Departamento de Bioingeniería e Ingeniería Aeroespacial, Universidad Carlos III de Madrid, Madrid, Spain

[5] Instituto de Investigación Sanitaria Gregorio Marañón, Madrid, Spain

[6] Centro de Investigación Biomédica en Red de Salud Mental (CIBERSAM), Spain

[7] Cardiac Imaging Unit, Cardiology Department, Hospital Universitario La Paz, IdiPaz, 28046 Madrid, Spain.

[8] CIBER de Enfermedades Respiratorias (CIBERES), Spain

[9] Center for Engineering Mechanobiology and Department of Systems Pharmacology and Translational Therapeutics, University of Pennsylvania, Philadelphia, PA 19104.

* These authors contributed equally to this study

** Current affiliation and address: CIC biomaGUNE and Ikerbasque- Basque Foundation for Science, Paseo Miramón 182, 20014 San Sebastián (Spain), and Universidad Complutense Madrid.

‡ Corresponding author:

Vicente Andrés
CNIC, Melchor Fernández Almagro 3, 28029 Madrid (Spain)
Phone: +34-91 453 12 00 (Ext. 1502)
E-mail: vandres@cnic.es

KEY WORDS: aging, progeria, vascular stiffness, smooth muscle cells, dietary nitrite

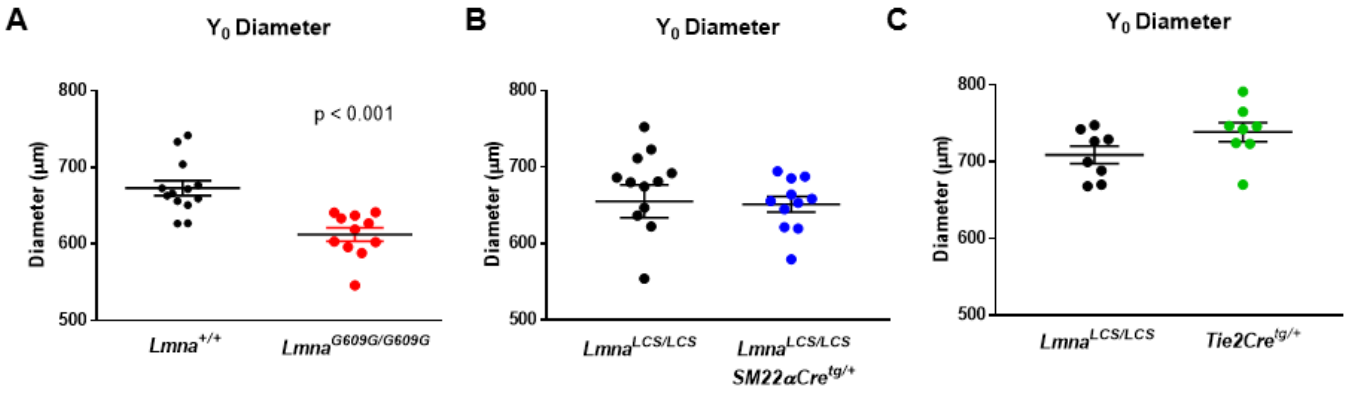

Supplementary Figure S1. Aortic diameter at unloaded conditions (no distension). Y_0 diameter was obtained from diameter-force relations by wire myography in aortic rings from *Lmna*$^{G609G/G609G}$ mice (A), *Lmna*$^{LCS/LCS}$*SM22αCre*$^{tg/+}$ (n=11) (B) and *Lmna*$^{LCS/LCS}$*Tie2Cre*$^{tg/+}$ (n=8) (C) mice, which are compared with corresponding littermate controls *Lmna*$^{+/+}$ and *Lmna*$^{LCS/LCS}$ respectively (n=13 and 8, respectively).

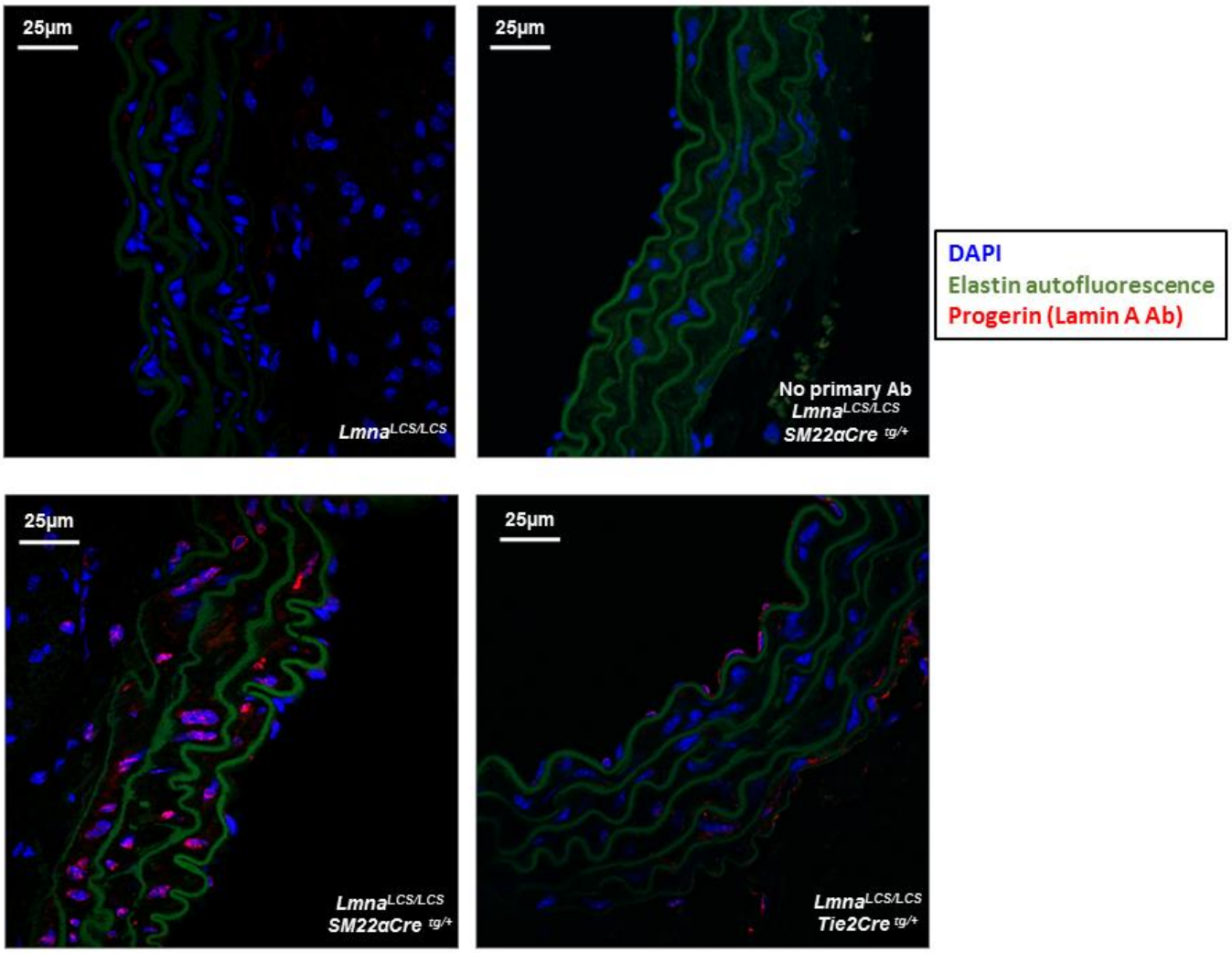

Supplementary Figure S2. Cell-specific progerin expression in aorta from *Lmna*$^{LCS/LCS}$*SM22αCre* $^{tg/+}$ and *Lmna*$^{LCS/LCS}$*Tie2Cre* $^{tg/+}$ mice. Immunofluorescence imaging of thoracic aortic sections from *Lmna*$^{LCS/LCS}$, *Lmna*$^{LCS/LCS}$*SM22αCre* $^{tg/+}$ and *Lmna*$^{LCS/LCS}$*Tie2Cre* $^{tg/+}$ mice stained with DAPI for nuclei and an anti-Lamin A antibody that recognizes progerin but not Lamin C. Elastin is also visualized due to its green autofluorescence. Negative control without primary antibody (No primary Ab) was performed in an aortic section of *Lmna*$^{LCS/LCS}$*SM22αCre*$^{tg/+}$ mice incubated with vehicle instead of primary Anti-Lamin A antibody.

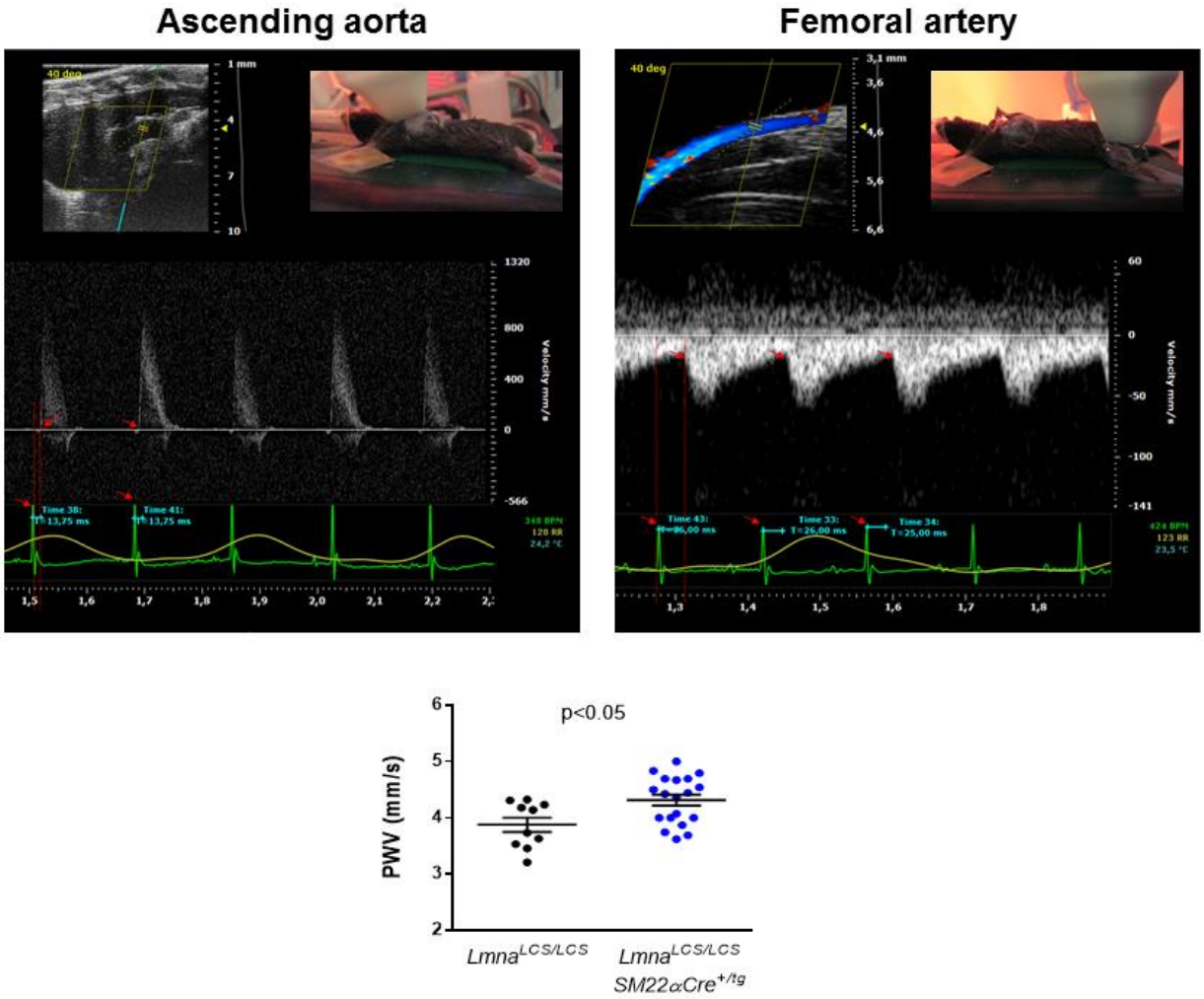

Supplementary Figure S3. Aortic-femoral aorta stiffness measured by pulse wave velocity (PWV) in *Lmna*$^{LCS/LCS}$ and *Lmna*$^{LCS/LCS}$ *SM22αCre*$^{tg/+}$ mice. PWV was measured in control *Lmna*$^{LCS/LCS}$ mice and in *Lmna*$^{LCS/LCS}$ *SM22αCre*$^{tg/+}$ mice with VSMC-specific progerin expression (PWV could not be measured in *Lmna*$^{G609G/G609G}$ mice because they presented aortic regurgitation).Stiffness of the artery is directly proportional to the velocity of the pulse wave. The velocity of the pulse wave is calculated by measuring the time from the R wave of QRS to the foot of the pulse waveform in both the aorta and the femoral arteries. The distance from the aortic arch to the femoral artery is divided by the transit time (TT) to get the velocity of the pulse wave.

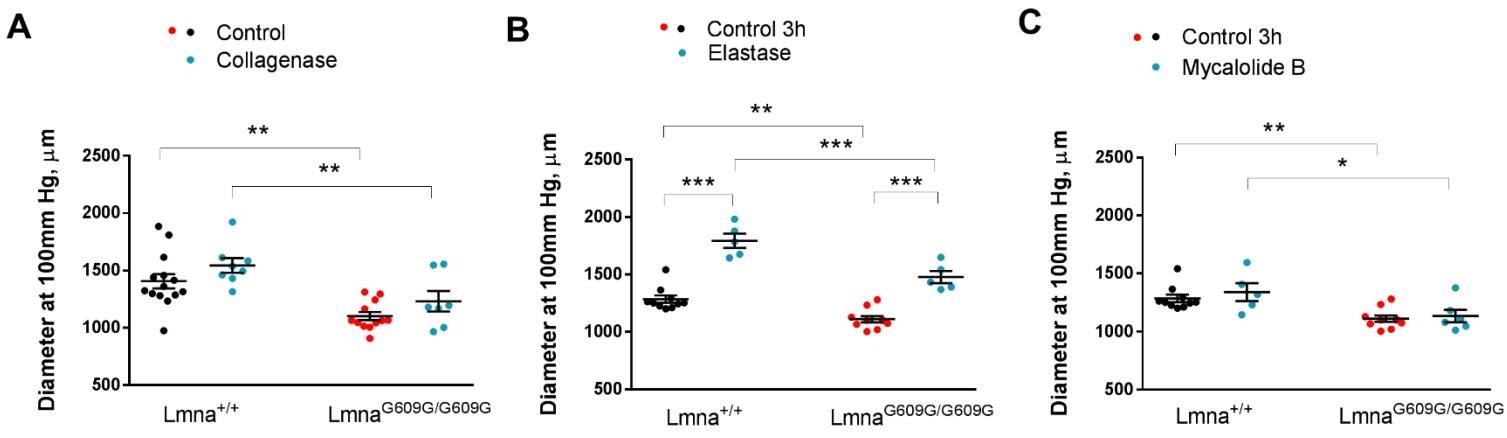

Supplementary figure S4. Effect of collagenase, elastase, and mycalolide B on physiological diameter. Diameter was estimated at 100 mmHg obtained from diameter-force relations by wire myography in aortic rings from *Lmna*$^{+/+}$ and *Lmna*$^{G609G/G609G}$ mice. Collagenase (A) and elastase (B) degrade collagen and elastin respectively, and mycalolide B (C) depolymerizes F actin to G actin, thus disrupting the cytosqueleton.

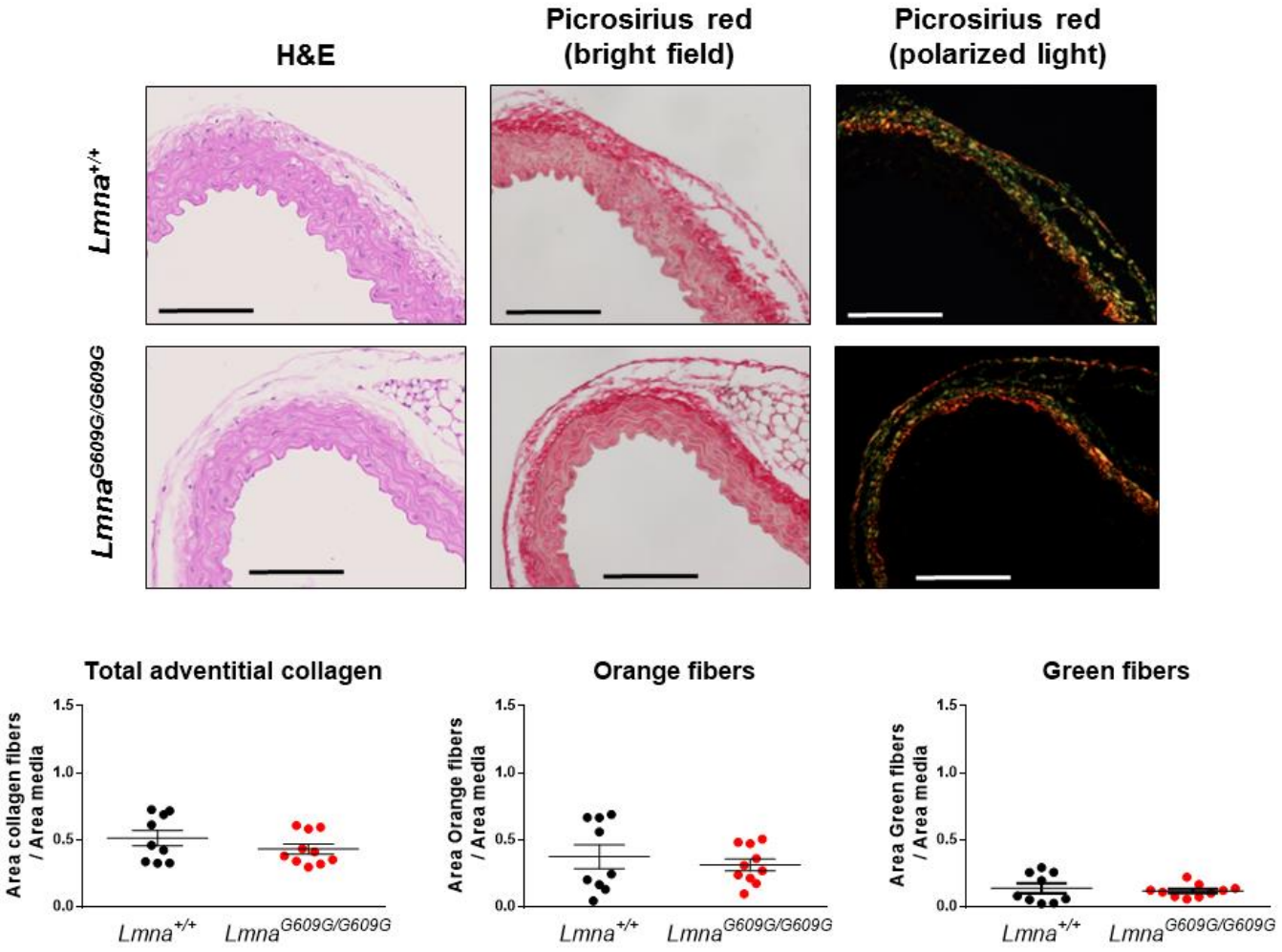

Supplementary Figure S5. Adventitial collagen is not altered in progeroid mice. Histologic analysis of aorta from *Lmna*$^{G609G/G609G}$ mice (n=9) and *Lmna*$^{+/+}$ (n=10) mice stained with Haematoxylin/Eosin (H&E), and Picrosirius Red. Picrosirius red-stained specimens were visualized both under bright field or polarized light, the latter of which allows visualizing collagen bundles, being the green ones the less compacted and the orange ones the more dense, compacted or crosslinked collagen fibers. Under polarized light, collagen bundles were only detected in the adventitia. Quantification of this adventitial collagen bundles shows no changes in the total amount of detected collagen nor in the relative amount of the thicker (Orange) of the thinner (Green) fibers between *Lmna*$^{G609G/G609G}$ and *Lmna*$^{+/+}$ aortic sections. Scale bar 100µm.

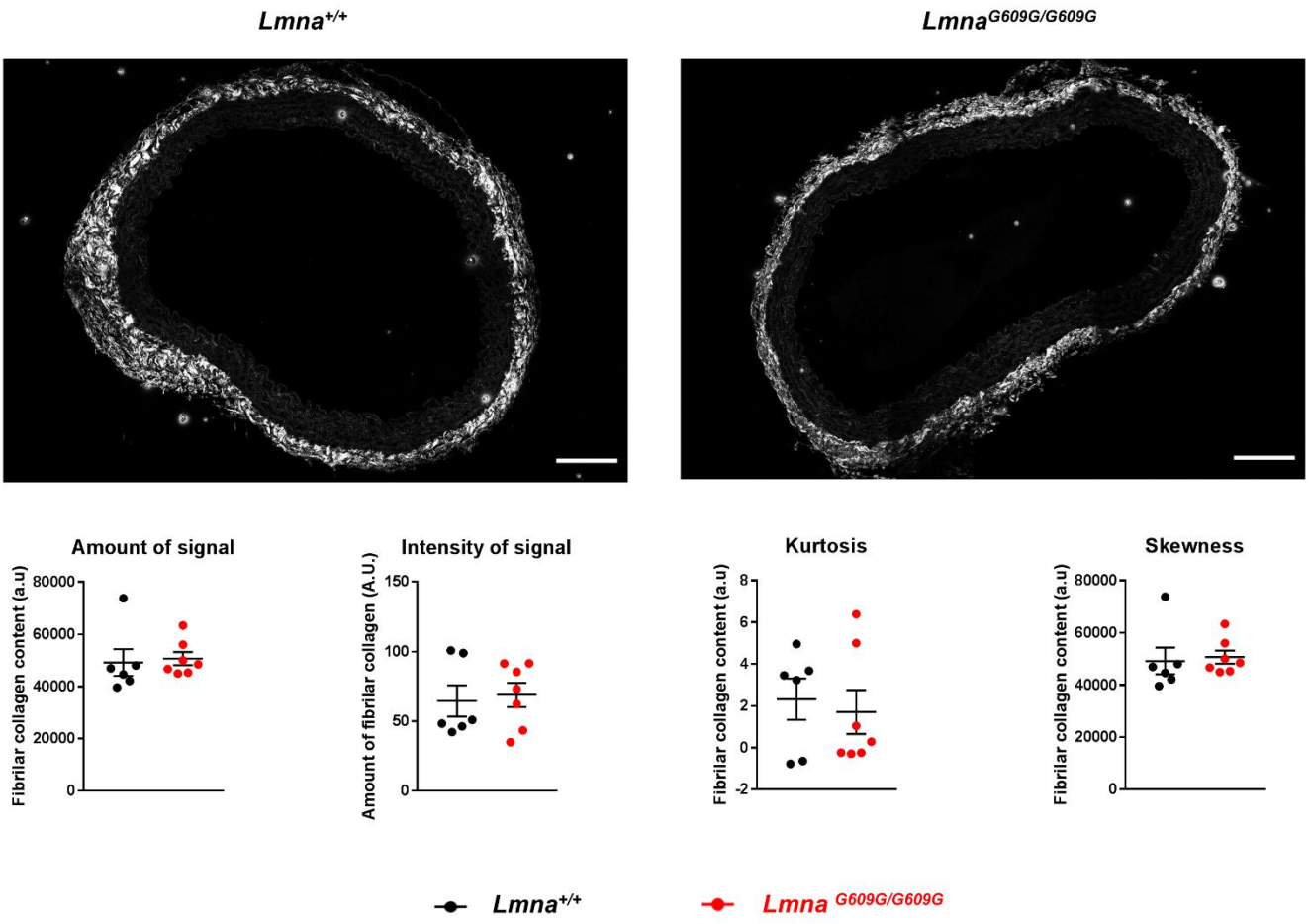

Supplementary Figure S6. Second Harmonic Generation (SHG) imaging in the adventitia layer in thoracic aortas from *Lmna*$^{+/+}$ and *Lmna*$^{G609G/G609G}$ mice. SHG imaging of thoracic aortas from *Lmna*$^{G609G/G609G}$ (n=7) and *Lmna*$^{+/+}$ mice (n=6) detected collagen bundles only in the adventitial layer. Quantification showed no differences in the collagen amount, organization or distribution in the adventitia layer. Scale bar 100µm.

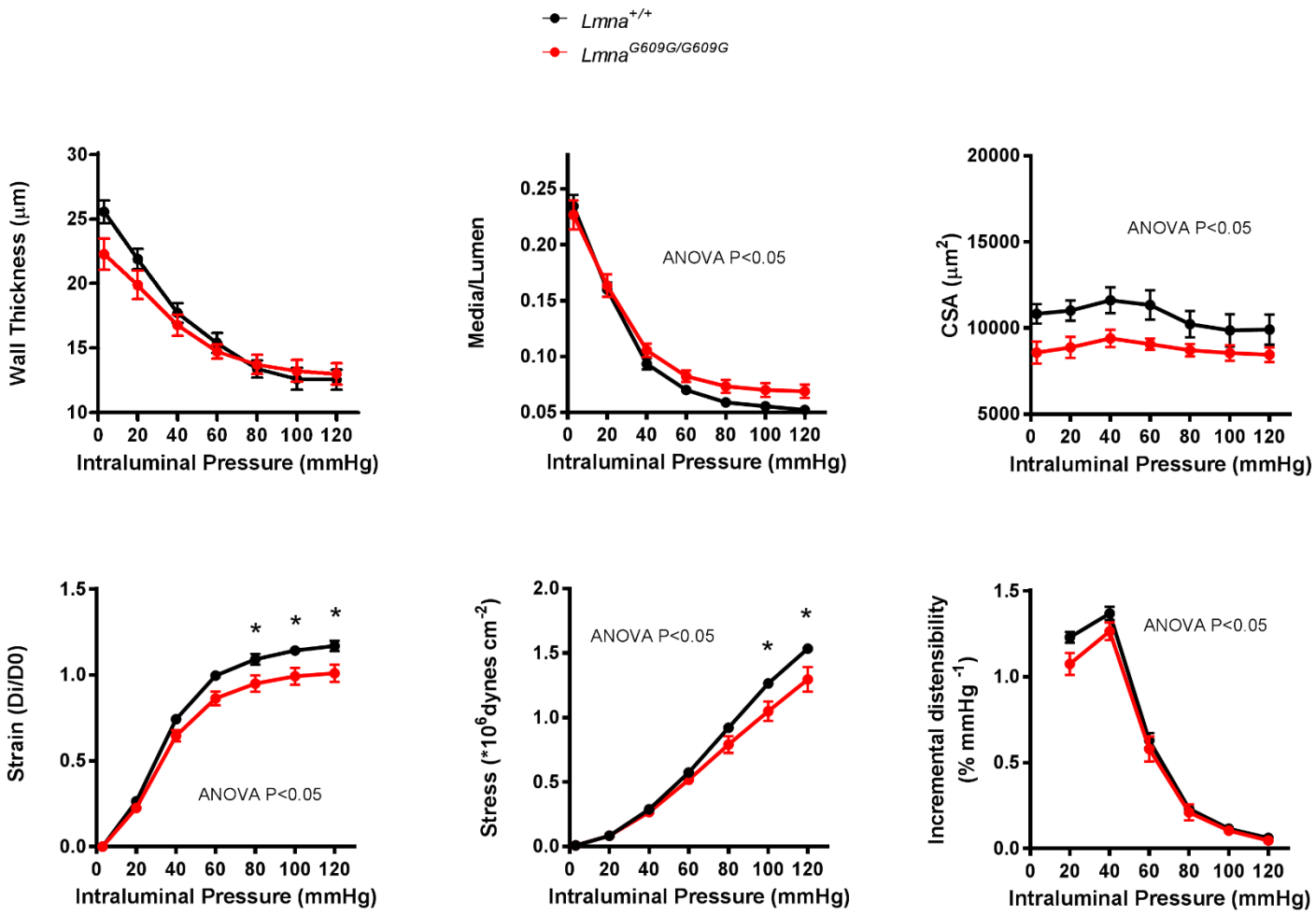

Supplementary Figure S7. Comparison of different parameters obtained from pressure-diameter curves with the pressure myograph in small mesenteric arteries from *Lmna*$^{+/+}$ and *Lmna*$^{G609G/G609G}$ mice. Wall thickness and Media/Lumen ratio are maintained, while cross sectional area of the vessel wall is decreased in small mesenteric arteries from *Lmna*$^{G609G/G609G}$ mice (n=9) compared with control *Lmna*$^{+/+}$ mice (n=9).